



University of HUDDERSFIELD

University of Huddersfield Repository

Chasti, Basit Shafi

Novel Machine Tool Feed Drive Design for High Dynamic Stiffness and Ultra-Low Vibration

Original Citation

Chasti, Basit Shafi (2021) Novel Machine Tool Feed Drive Design for High Dynamic Stiffness and Ultra-Low Vibration. Masters thesis, University of Huddersfield.

This version is available at <http://eprints.hud.ac.uk/id/eprint/35476/>

The University Repository is a digital collection of the research output of the University, available on Open Access. Copyright and Moral Rights for the items on this site are retained by the individual author and/or other copyright owners. Users may access full items free of charge; copies of full text items generally can be reproduced, displayed or performed and given to third parties in any format or medium for personal research or study, educational or not-for-profit purposes without prior permission or charge, provided:

- The authors, title and full bibliographic details is credited in any copy;
- A hyperlink and/or URL is included for the original metadata page; and
- The content is not changed in any way.

For more information, including our policy and submission procedure, please contact the Repository Team at: E.mailbox@hud.ac.uk.

<http://eprints.hud.ac.uk/>

NOVEL MACHINE TOOL FEED DRIVE DESIGN FOR HIGH DYNAMIC STIFFNESS AND ULTRA-LOW VIBRATION

(M.sc By Research Mechanical Engineering)

UNIVERSITY OF HUDDERSFIELD

Name: Basit Shafi Chasti

Student ID: u1372125

Main Supervisor: Dr. Simon Fletcher

Co-Supervisor: Prof. Andrew Peter
Longstaff

Date: 09/02/2021

ABSTRACT

Increasing demand for highly efficient production systems has been one of the primary subjects in the 21st century, this has led to the development of complex and flexible manufacturing systems and in-process measurement tools. The tasks performed on a CNC are complex than ever with an expectation to perform machine dimensional measurement with the help of retrofit probing systems. However, high power requirements of machining operations are the prime attributes that their feed drive system must possess this gives rise to high levels of vibration consequently causing high dynamic errors. This leads to less accuracy during measurement operations hence posing a need to have vibration-free measurement machines or commonly known as Coordinate measuring machines (CMM'S). To solve this problem, there is a need for a novel feed drive system that can help in the reduction of vibration during measurement, this can lead to more accurate machining operations as well as efficient use of scanning probes.

In this thesis, various solutions of high dynamically stiff novel feed drive solutions capable of Nano positioning have been studied in detail. Since the goal of the project is based on feed drive systems two major areas were explored including, Bearings Design and Drive Train Design. Other miscellaneous options were also studied which fall in either of the groups or are just a combination of them. Two parameters are at the core of the research problem, 1) High Stiffness capability of Machining operations and 2.) Precision measurement.

Studies reveal that many possible solutions exist but many of them are not economically viable while others provide Nano positioning but are incapable of having high stiffness required in the machining centre. Also, the Integration of Air bearings in Medium to large-sized machine tool CNC is missing. This results in a gap knowledge, in terms of Bearings Design which was studied thoroughly to result in a novel hybrid feed drive. The study was focused more on the bearing design as it offered many promising solutions. It is deduced in the section 2.5 that the magnetic bearings and air bearing provide an alternative solution.

The problem was understood and further explored by carrying out market research followed by a critical review of various technical papers. Most of the breadth, as well as depth in the field of Feed drive design, was covered and documented in detail for further research. Various Novel Ideas were generated and rated based on their viability leading to novel hybrid bearing design.

All the preliminary Analysis necessary for the validation and verification of Novel hybrid bearing original as well as the prototype design has been set for further validation, including the Finite element modelling of the original feed drive its validation with experimental modal analysis and detailed design and analysis of the Novel Hybrid bearing design and the prototype.

A prototype that can replicate the physics of the Novel hybrid bearing solution has been Designed and Manufactured with all the plans of experimental Analysis carried out for further research and development.

ACKNOWLEDGEMENTS

This dissertation has provided a great platform for me not only in terms of developing my Research and technical engineering skills but also in the progression of my personal development plan; the project was stringent in terms of the level of expertise and has been a great boon to add to my skillset. Firstly, I Would like to Thank God for providing me with patience and perseverance to meet such technically demanding challenges that were carried out independently. This Project also has a contribution of a few honourable people and academia that I would like to mention. I would like to pass my deep gratitude to the University of Huddersfield for providing me with such an excellent opportunity to synthesize and nourish my engineering skills through such a practical and impeccable approach-based project.

To my Supervisors Dr Simon Fletcher and Prof Andrew Longstaff, I am greatly thankful to them for providing me with such a constructive and methodological feedback throughout my project timescale. It has been an honour to work with them and gain technical report writing skills carried systematically in this report. To my acknowledgements, I would also like to add Mr Andrew Bell for supporting and assisting me with Manufacturing operations and their related knowledge.

Finally, I would like to thank my parents for their consistent support and encouragement throughout my research degree.

TABLE OF CONTENTS

| | |
|---------------------------------------------------------------------------------------------------------------------|----|
| ABSTRACT | 1 |
| ACKNOWLEDGEMENTS | 2 |
| LIST OF FIGURES | 7 |
| LIST OF TABLES | 11 |
| CHAPTER 1: INTRODUCTION AND BACKGROUND | 12 |
| 1 .1 INTRODUCTION | 12 |
| 1 .2 BACKGROUND | 13 |
| 1.2.1 History of CNC | 13 |
| 1.2.2 Existing Technology | 16 |
| 1.3 PROJECT AIM/SCOPE: | 24 |
| 1.4 OBJECTIVES: | 24 |
| 1.5 STRUCTURE OF THE THESIS | 25 |
| CHAPTER 2: LITERATURE/CRITICAL REVIEW | 26 |
| 2.1 BEARING DESIGN: | 26 |
| 2.1.1: Friction reduction Based Bearing | 26 |
| 2.1.2: Flexural Design | 28 |
| 2.1.3: Magnetic Guide for Photolithography | 29 |
| 2.1.4: Machine Tool With Active Magnetic Guides | 29 |
| 2.1.5: Magnetic levitation | 32 |
| 2.1.6: Dynamic characteristics of a direct-drive air-bearing slide system with squeeze film damping: | 34 |
| 2.1.7: Porous Ceramic Water Hydrostatic Bearings for Improved for Accuracy Performance | 37 |
| 2.1.8: Cage Speed of Hydrodynamic Rolling Hybrid Bearings | 39 |
| 2.1.9: Investigations on a permanent magnetic–hydrodynamic hybrid journal bearing: | 40 |
| 2.1.10: Hybrid bearings for turbopumps | 42 |
| 2.1.11: WJRM hybrid linear bearing | 43 |
| 2.2 DRIVE TRAIN DESIGN: | 44 |
| 2.2.1: New Slide with Friction Drive | 44 |
| 2.2.2: A Twist-Roller Friction Drive for Nanometre Positioning - Simplified Design Using Ball Bearings | 47 |
| 2.2.3: Ultra precision Feed System Based on Walking Drive: | 47 |
| 2.2.4: Electrohydraulic actuator | 51 |
| 2.2.5: Voice coil motor infer meter and ball screw sub nanometre drive | 51 |
| 2.2.6: Using 3 Ball Screws for high Thrust with a Coupling. | 53 |

| | |
|----------------------------------------------------------------------------------------------------------------------|----|
| 2.2.7: Concept design with rack and roller pinion: | 53 |
| 2.3 MISCELLANEOUS TECHNOLOGY AND HYBRID FEED DRIVES | 54 |
| 2.3.1: Main Points from Drive centre gravity | 54 |
| 2.3.2: Energy optimized jerk-decoupling technology for translator feed axes | 56 |
| 2.3.3: Magnetically Levitated six degree of freedom rotary table | 57 |
| 2.3.4: Control of a dual stage magneto strictive actuator and linear motor ed drive system | 58 |
| 2.3.5: Linear motor and ball screw hybrid feed drive system | 59 |
| 2.3.6: Incorporating active damping control technique: | 61 |
| 2.3.7: Structure optimisation of longitudinal feed system design of cnc spinning machine. | 63 |
| 2.3.8: Dual stage feed drive using piezo electric actuators: | 64 |
| 2. 4 CRITICAL APPRAISALS | 67 |
| 2.4.1 Friction reduction Based Bearing | 67 |
| 2.4.2 Flexural Design | 67 |
| 2.4.3 Rotary Axial Spindles | 67 |
| 2.4.4 Magnetic Guide for Photolithography. | 68 |
| 2.4.5 Machine Tool with Active Magnetic Guides | 69 |
| 2.4.6 Magnetic levitation | 69 |
| 2.4.7 Dynamic characteristics of a direct-drive air-bearing slide system with squeeze film damping: | 70 |
| 2.4.8 Porous Ceramic Water Hydrostatic Bearings for Improved for Accuracy Performance | 70 |
| 2.4.9 Hybrid Bearings | 71 |
| 2.4.10 New Slide with Friction Drive | 71 |
| 2.4.11 A Twist-Roller Friction Drive for Nanometre Positioning - Simplified Design Using Ball Bearings. | 72 |
| 2.4.12 Ultra precision Feed System Based on Walking Drive: | 72 |
| 2.4.13 Electrohydraulic actuator | 73 |
| 2.4.14 Voice coil motor infer meter and ball screw sub nanometre drive | 73 |
| 2.4.15 Voice coil /dc motor hybrid | 74 |
| 2.4.16 Adaptive preloading of rack and pinion drive systems. | 74 |
| 2.4.17 Main Points from Drive centre gravity | 74 |
| 2.4.18 Energy optimized jerk-decoupling technology for translator feed axes | 75 |
| 2.4.19 Magnetically Levitated six degree of freedom rotary table | 75 |
| 2.4.20 Control of a dual stage magneto strictive actuator and linear motor ed drive system | 76 |
| 2.4.21 Linear motor and ball screw hybrid feed drive | 76 |
| 2.5 CONCLUSIONS FROM LITERATURE REVIEW (<i>Gap Knowledge</i>). | 77 |
| 2.5.1 Magnetic Bearings vs Air Bearings. | 77 |

| | |
|-------------------------------------------------------------------------------|-------------------------------------|
| CHAPTER 3: METHODOLOGY..... | 79 |
| 3.1 METHOD UNDERTAKEN..... | 79 |
| 3.2. PROJECT MANAGEMENT..... | 81 |
| CHAPTER 4: THEORY AND PRELIMINARY STUDY..... | 82 |
| 4.1. THEORY AND PRELIMINARY ANALYSIS..... | 82 |
| 4.2. CONCEPT GENERATION AND DESIGN EVALUATION..... | 83 |
| 4.2.1 Concept generation Methodology: | 83 |
| 4.2.2 Concepts generated. | 85 |
| 4.2.3 Concept Evaluation | 88 |
| CHAPTER 5: DESIGN AND COMPUTATIONAL VALIDATION..... | 91 |
| 5.1 MECHANICAL DESIGN OF HYBRID BEARING/GUIDE..... | 91 |
| 5.1.1 Hybrid Bearing Design Bill of materials: | 92 |
| 5.1.2 Detailed Design and Specifications | 94 |
| 5.1.3 Mechanical design of the Hybrid Bearing Prototype | 127 |
| CHAPTER 6: DISCUSSION..... | 151 |
| 6.1 ACHIEVEMENTS..... | 151 |
| 6.1.1 Objectives Met and Delivered Solution. | 151 |
| 6.2 FUTURE DIRECTION..... | 155 |
| 6.2.1 Experimental Vibrational analysis of the Prototype Design: | 155 |
| 6.2.2 Errors due to roller bearings in measurement. | 155 |
| 6.2.3 Active vibration Suppression | 155 |
| 6.2.4 ERF fluids. | 155 |
| 6.2.5 Reduce the bearing size: | 156 |
| 6.2.6 Anti-debris guide: | 156 |
| 6.2.7 Novel feed drive elements: | 156 |
| 6.2.8 Control Design: | 156 |
| 6.2.9 Thermal Insulation Design | 156 |
| 6.2.10 DFMA Considerations | 156 |
| CHAPTER 7: REFERENCES AND BIBLOGRAPHY..... | 157 |
| CHAPTER 7: APPENDECIES..... | 167 |
| APPENDEX A..... | 167 |
| RACK-AND-PINION VERSUS BALL SCREWS | 167 |
| PROCEDURE TO SET UP AIR BEARINGS | 168 |
| Piezo Actuator Design Calculations: | 168 |
| CHAPTER A: THEORY AND PRELIMINARY STUDY..... | Error! Bookmark not defined. |

A.1 BACKGROUND THEORY 173

A.1.1 Modal Analysis: 173

A.1.2 Digital Signal Processing Theory: 177

A.2 SIMULATED MODAL ANALYSIS OF THE BRIDGEPORT BALL SCREW FEED DRIVE SYSTEM DESIGN. . 188

A.2.1 Rig design Schematic 188

A.2.2 Importance of Computational Analysis and Introduction to Finite Element Analysis: 188

A.2.3 Materials Assigned: 190

A.2.4 Mesh quality and Convergence: 190

A.2.5 Mechanical Contacts: 192

A.2.6 Boundary Conditions: 193

A.3 EXPERIMENTAL MODAL ANALYSIS OF THE SCREW DRIVE. 198

7.1 APPENDIX B 209

LIST OF FIGURES

| | |
|---------------------------------------------------------------------------------------------------------------------------------------------------------------------------------------------------------------------------|----|
| <u>Figure 1: Schematic of a Coordinate measuring Machine (High accuracy CMM - High accuracy 3D CMM - 3D COORDINATE MEASURING MACHINE CMM SOFTWARE XI'AN HIGH-TECH AEH INDUSTRIAL METROLOGY CO., LTD. (2018)).</u> | 15 |
| <u>Figure 2: Shows Different configurations of friction guides (Altintas, Y., Verl, A., Brecher, C., Uriarte, L., & Pritschow, G. (2011). Machine tool feed drives).</u> | 16 |
| <u>Figure 3: Friction Guide Friction guides made easy with Accuride's engineering excellence - Automation. (2018).</u> | 16 |
| <u>Figure 4 : Shows Recirculating Roller bearing (Linear ball bearing and guideway assemblies. (2018)).</u> | 17 |
| <u>Figure 5: Shows Schematic of Roller bearing (Sun, Wei & Kong, Xiangxi & Wang, Bo & Li, Xingzhan. (2014). Statics modelling and analysis of linear rolling guideway considering rolling balls contact).</u> | 17 |
| <u>Figure 6 : Shows the Spring Diaphragm Clamp Mechanism (PL55-2-6B - PL - LOCKED PL - Clamping Elements - Safety Products - Products - ACE Controls Inc. (2018)).</u> | 18 |
| <u>Figure 7: Shows the spring diaphragm clamp system using Air as a clamping force. Altintas, Y., Verl, A., Brecher, C., Uriarte, L., & Pritschow, G. (2011). Machine tool feed drives.</u> | 18 |
| <u>Figure 8: Shows Hydrostatic Linear guide way schematic (left) and basic dimensions (right) (Hydrostatic linear guiding for standard design spaces. (2018)).</u> | 19 |
| <u>Figure 9: Shows Different types of non-recirculating linear guide bearing arrangements (Collins, D. (2018). What are recirculating linear bearings?).</u> | 20 |
| <u>Figure 10 : Shows the arrangement and components of Air bearings (Air Bearings Application. (2018)).</u> | 21 |
| <u>Figure 11 : Shows a planar motor levitated by Tekniker (Altintas, Yusuf & Verl, Alexander & Brecher, C & Uriarte, L & Pritschow, Guenter. (2011). Machine tool feed drives.</u> | 21 |
| <u>Figure 12 shows ball bearing drive assembly(Layosa, C., & Layosa, C. (2018). Belt Drive vs. Ball Screw Actuators MISUMI USA).</u> | 22 |
| <u>Figure 13: Shows a Ball Screw Drive Bearing for SFU12 Ball Screws - LMN4207 0 at Phidgets. (2018).</u> | 22 |
| <u>Figure 14 Shows the switch pinion system (Linear ball bearing and guideway assemblies. (2018)).</u> | 23 |
| <u>Figure 15 Shows a Rack and Pinion Drive, Drive System solutions for rack and pinion applications - Drive Lines. (2018).</u> | 23 |
| <u>Figure 16: Prismatic adjustable friction bearing Components</u> | 26 |
| <u>Figure 17: Shows Friction reduction with oscillation parameters.</u> | 27 |
| <u>Figure 18 : Shows Linearization and Friction reduction</u> | 27 |
| <u>Figure 19: With the help of passive and active bearings Comparison of the positioning error on 10 um steps has been depicted.</u> | 27 |
| <u>Figure 20: Assembly of Rotary flexural bearing</u> | 28 |
| <u>Figure 21 Outer and inner cage nested design</u> | 28 |
| <u>Figure 22 Machining Centre Structure.</u> | 30 |
| <u>Figure 23 Gantry x Slide honeycomb structure.</u> | 30 |
| <u>Figure 24 Standard ball bearing guide (c=4kN/um ,D=0.01) and Magnetic guide (m=400kg, λ=-400s) Compliance frequency response</u> | 31 |
| <u>Figure 25: Guide deflection with exemplary steel milling and control force on an active magnetic guide.</u> | 32 |
| <u>Figure 26 Shows the Arrangement of the Gantry Design.</u> | 33 |
| <u>Figure 27 Sectional view a and b prototype of superconducting EMS feed drive System.</u> | 33 |
| <u>Figure 28 Results achieved from the experiment</u> | 34 |
| <u>Figure 29 Air bearing Slide consisting of direct drive motor and squeeze film dampers</u> | 34 |
| <u>Figure 30 Slide Vibration Principle Modes</u> | 34 |

Figure 31 Response to offset vertical force..... 35

Figure 32 Vertical force response of air slide..... 35

Figure 33 Offset Vertical force on slide of carriage 35

Figure 34 Response of Horizontal force given by Air Slide..... 36

Figure 35 Vertical force on leading edge of carriage response of Air slide36

Figure 36 Response to offset horizontal force given by the slide 36

Figure 37 With the inclusion of pore smearing a SEM Analysis of diamond turned porous graphite is shown. 37

Figure 38 :Shows Uniform pressure distribution due to porous media, Non-Contact Hydrostatic Fluid Bearings - ULS Innovation. (2020). 37

Figure 39 Viscous permeability with powder size..... 38

Figure 40 A Hybrid Bearing supported by hydrodynamic bearing at high speeds (b) and at low speeds supported by rolling bearing (a)..... 39

Figure 41 Start up and Shut down process cage speed comparison..... 40

Figure 43 Magnetic Ring Coordinates 41

Figure 44 Prototype set up..... 41

Figure 45 Hybrid Bearing Design Schematic..... 42

Figure 46 Double roller type (21) force absorption 43

Figure 47: 2:1 Rule..... 43

Figure 48 Hydrostatic bearing Preloading..... 44

Figure 49 Hydrostatic bearing schematic 45

Figure 50 Friction drive mounting..... 45

Figure 51 Slide bearing and drive stiffness comparison..... 46

Figure 52 Hydraulic bearing Characteristics with varying preloads 46

Figure 53 Vibrational Analysis of the drive..... 46

Figure 54 Twist Roller Friction drive mechanism 47

Figure 55 Twist roller friction drive nanometre precision system 47

Figure 57 Open loop Constant angular velocity feed motion 48

Figure 58 Positioning stepwise result With 5nm step..... 48

Figure 59 Straight motion and feed motion errors after utilising the feedback control for error compensation left and Command vs measured position Comparison right..... 48

Figure 60 Developed Position feedback control system Diagram..... 49

Figure 61 Contouring control result 49

Figure 62 errors and positions plotted against time 50

Figure 63 Point to Point Positioning Control Result..... 50

Figure 64 Measured positions and Command 50

Figure 65 Set up of the test 51

Figure 66 Proposed table system structural concept..... 51

Figure 67 Developed Table system specifications..... 51

Figure 68 Table System Appearance 52

Figure 69 Tracking error at feedrate of 100nm/s..... 52

Figure 70 Shows long range (150mm) tracking error..... 52

Figure 71 Stepwise response of sub nanometre..... 52

Figure 72 Shows a feed drive with mechanically coupled ball screws (Hsieh, M. , Yao, W. and Hsu, C. (2012), Modelling and control of a feed drive with multiple mechanically coupled ball screws) 53

Figure 73 Shows and roller pinion (left) and its performance chart (right) (Nexen Product Navigation. (2018)) 53

Figure 74 Motion Contour Simulated in Evaluation 1 54

Figure 75 Motion contour Simulated Evaluation 2 54

Figure 76 Evaluation 1 Experimental results 55

Figure 77 Evaluation 2 Experimental results 55

Figure 78 Jerk decoupling principle 56

Figure 79 Decoupling unit comprising of rubber elements 56

Figure 80 Stiffness Vs Frequency 57

Figure 81 Axis noise vs step 57

Figure 82 Shows the Schematic of the Hybrid actuator drive 58

Figure 83 shows the proposed model of hybrid feed drive (Chinedum Okwudire, Jason Rodgers, (2013) Design and control of a novel hybrid feed drive for high performance and energy efficient machining 60

Figure 84 Proposed feed drive prototype used for experiments Chinedum Okwudire, Jason Rodgers, (2013) Design and control of a novel hybrid feed drive for high performance and energy efficient machining) 60

Figure 85 Shows feed drive test bench with travel range 700 mm , ball screw diameter 40 mm and load mass 1200 kg. (A.Verl, S. Frey, (2012) Improvement of feed drive dynamics by means of semi-active damping) 61

Figure 86 Shows frequency response between table and motor velocity 62

Figure 87 Shows the Command Tracking frequency response 62

Figure 88 Shows the Nyquist plot of the open loop position controller 62

Figure 89 Shows position command step and tracking error for a disturbance step of 2000 N 63

Figure 90 Shows High speed tracking test with and without semi active damping 63

Figure 91 Shows all four configurations tested (Advances in Mechanical Design. (2018).) 64

Figure 92 Dual stage feed drive assembly single axis. (A.T. Elfizy, G.M. Bone, M.A. Elbestawi,(2005) Design and control of a dual-stage feed drive) 65

Figure 93 two axis dual stage feed drive design. (A.T. Elfizy, G.M. Bone, M.A. Elbestawi,(2005) Design and control of a dual-stage feed drive) 65

Figure 94 Flexure base of Single Axis PA (A.T. Elfizy, G.M. Bone, M.A. Elbestawi,(2005) Design and control of a dual-stage feed drive) 65

Figure 95 Shows the dual stage feed drive configuration with sensor assembly (left) and Milling machine configuration (right) (Hendra Syahputra, Hyeon Yang, Byeong Chung, Tae Ko. Dual-Stage Feed Drive for Precision Positioning on Milling Machine. Svetan Ratchev). 66

Figure 96 Classical Design Methodology diagram The Engineering Design Process. (2020) 79

Figure 97 : Shows Work breakdown structure of the project. 81

Figure 98: Concept Design by Component breakdown 83

Figure 99 Decomposition of Functions 84

Figure 100 Concept 1 Unibody Bearing Design 85

Figure 101 Concept 4 (Table Separation) 86

Figure 102 Concept 5 Graphene based Sliding bearing 86

Figure 103 (ER-Hybrid-twist roller/capstan/ Rp Drive and aerostatic drive): 87

Figure 104 (Anti-Vibration pads Sandwiched): 88

Figure 105 Shows Color code mapping of the Hybrid Bearing 91

Figure 106 Shows machining time vs "x" force component **Error! Bookmark not defined.**

Figure 107 Shows Machining force Components Vs time 96

Figure 108 maximum Cutting force for a steel Chromium 210 Cr12 Steel 96

Figure 109 Cutting force vs Cutting speed for Chromium 96

Figure 110 Graphs showing Cutting force parameters 97

Figure 111 Comparison of Temperature rise between experiments and simulations (left) , Temperature rise comparison in terms of convective heat coefficient (right)98

Figure 112 Bearing loading vs Lift graph 100

Figure 113 O type Linear roller bearings Vs X type linear roller bearing configuration..... 101

Figure 114 INA- Medias Bearing Modules..... 101

Figure 115 Deflection of Linear guide with no preload , light preload and medium preload..... 103

Figure 116 Stiffness of the linear recirculating bearing 103

Figure 117 Shows the original bearing used 103

Figure 118 Shows the Hybrid bearing Sides A and B..... 104

Figure 119 Equilibrium equations for Machining forces in Z Direction..... 106

Figure 120 Equilibrium equations for Machining forces in X Direction 107

Figure 121 Hybrid Piezo Actuator drive color mapping 109

Figure 122 Lead Nut bearing bronze used 110

Figure 123 manganese bronze properties 111

Figure 124 bearing bronze properties..... 111

Figure 125 Shows the corresponding gauge design value 115

Figure 126 Shows the Design table obtained for the hollow tube..... 115

Figure 127 Shows the Design table obtained for the hollow tube (upper part) 116

Figure 128 Shows the final design of actuator housing 117

Figure 129 Shows 4 ×M6 18-8 stainless steel thread locking socket head Screw..... 117

Figure 130 Shows the Hybrid bearing final housing design 118

Figure 131 Vertical boundary conditions 120

Figure 132 Horizontal boundary condition 121

Figure 133 Number of nodes and elements during the convergence 121

Figure 134 Fea results of Deflection in Y 122

Figure 135 Fea results of deflection in x..... 122

Figure 136 Fea Results of deflection in x full load condition (right) (top surface), half load condition left (left surface), 123

Figure 137 Fea Results of deflection in Y full load condition (right) (top surface), half load condition left (left surface), 123

Figure 138 Final design of Novel Hybrid guideway 124

Figure 139 Linear bearing for Bearing modules 125

Figure 140 Shows the blanking plate 126

Figure 141 Original Hybrid Bearing Design..... 127

Figure 142 Prototype Hybrid bearing Design 128

Figure 143 Shows the schematic of the hybrid bearing prototype 129

Figure 144 Shows the picture of (40 ×80) Air bearing and its Load vs Lift graph..... 131

Figure 145 Shows the detailed specifications of the (40 ×80) Air bearing..... 131

Figure 146 Shows the Polished Stainless steel Guide way Cad Model and original part 132

Figure 147 Shows the location of Surface roughness measurement micro areas for top surface 133

Figure 148 Shows the location of Surface roughness measurement micro areas for Lateral surface 1.... 134

Figure 149 Shows the location of Surface roughness measurement micro areas for Lateral surface 2.... 134

Figure 151 Shows all the aerial parameters taken on alicona 135

Figure 150 Shows all the parameters taken from Alicona 135

Figure 152 the surface texture of the micro area 136

Figure 153 Local top surface flatness (right) Full top surface flatness (left) 137

Figure 154 local central flatness and full Surface flatness of Right Surface..... 137

Figure 155 local central flatness and full Surface flatness of Left Surface 138

Figure 156 S Shaped Clamps (left) and M12 x 80) Bolt (Right)..... 139

Figure 157 Free Body Diagram 140

Figure 158 Meshed S bracket with given nodes and Elements..... 141

Figure 159 Boundary Conditions of S clamp 141

Figure 160 Fea Deflection results of the S Bracket..... 142

Figure 161 Aluminium Air Bearing housing 143

Figure 162 Block of Aluminium 6082T6 square bar (203.2 x 203.2 x 270)..... 143

Figure 163 Shows the Meshed Air bearing housing with the nodal and element values 144

Figure 164 Shows Vertical boundary Conditions..... 144

Figure 165 Horizontal boundary conditions of Air bearing housing 145

Figure 166 Fixed Constrains of Air Bearing Housing 145

Figure 167 For y Direction load , top face (left) left face (right) 146

Figure 168 For x Direction load , top face (left) left face (right)..... 146

Figure 169 Bearing Air supply data taken from new way air bearing design guide..... 147

Figure 170 Polyurethane tube Amazon (2020) 147

Figure 171 3 port 1/4 Bsp Manifold with 4 Outputs 3 x 6mm and 1 x 8mm (Right), Straight Pneumatic Push to Quick Connect Fittings M5 Male x 6mm Union (left)..... 147

Figure 172 Air Bearing Housing to Linear recirculating bearing Adaptor Cad (left) , Manufactured Part (right)..... 148

Figure 173 SMDE-45-S by INA Linear bearing guide..... 149

Figure 174 Table 10 Data of Load Capacity of SMDE-45-S by INA Linear bearing 150

Figure 175 Table 10 Data of SMDE-45-S by INA Guide 150

Figure 176 Table 10 Data of SMDE-45-S by INA Linear bearing..... 150

LIST OF TABLES

Table 1 Concept evaluation Matrix 89

Table 2 Shows Hybrid bearing components 91

Table 3 Shows the estimated Total Mass and hence the weight of the Test feed drive rig 94

Table 4 Shows Bearing details 102

Table 5 Shows the specifications required for the fine actuator 112

Table 6 Desired characteristics of three chosen actuators..... 113

Table 7 Shows the Values of corresponding Roughness values in micro areas..... 133

Table 8 Shows the Values of corresponding Roughness values in micro areas for Lateral Surface 134

Table 9 Shows the Values of corresponding Roughness values in micro areas for Lateral Surface 134

Table 10 Characteristics of SMDE-45-S by INA Linear bearing guide 149

CHAPTER 1: INTRODUCTION AND BACKGROUND

This section involves project background in general and the History of Precision manufacturing systems followed by an overview of existing solutions of feed drive systems.

1.1 INTRODUCTION

In order to improve production efficiency, there is a high demand for in-process measurement and flexible manufacturing systems. Complex machining tasks are performed on CNC machine tools their design has an additional axis and can also perform on machine dimensional measurement with the help of retrofit probing systems. However, high power requirements of machining operations are the prime attributes that their feed drive system must possess this gives rise to high levels of vibration consequently causing high dynamic errors. Due to this reason when compared with Coordinate measurement machines they are less accurate in measurement operations. In order to solve this problem, there is a need for a novel feed drive system that can help in the reduction of vibration during measurement, this can lead to more accurate machining operations as well as efficient use of scanning probes.

In this thesis, various solutions of high dynamically stiff novel feed drive solutions capable of Nano positioning have been studied in detail. Since the goal of the project is based on feed drive systems two major areas were explored including, Bearings Design and Drive Train Design. Other miscellaneous options were also studied which fall in either of the groups or is just a combination of them. Two parameters are at the core of the research problem, 1) High Stiffness capability of Machining operations and 2.) Precision measurement. Studies reveal that many possible solutions exist but many of them are not economically viable while others provide Nano positioning but are incapable of having high stiffness required on the machining centre. Also, Integration of Air bearings in Medium to large-sized machine tool CNC is missing. This results in a gap knowledge, in terms of Bearings Design which was studied thoroughly to result in a novel hybrid feed drive.

The study was focused more on the bearing design as it offered many promising solutions. It is deduced in the later section that the magnetic bearings and air bearing provide an alternative solution. The hybrid bearing concept has been developed in this paper with its detailed design specified, All the relevant Engineering design calculations have been carried out to produce an initial detailed design of the Hybrid bearing. This is followed by testing the main features of the hybrid bearing by manufacturing a prototype that can validate the main features of the Hybrid bearing design. Experimental Test on the already existing feed drive has also been carried out to Validate its digital twin's Finite element analysis. This will help in Analysing the effect of new hybrid bearing computationally in detail which will be done in future. This leads to the future Direction section where all the gaps that need to be filled to carry out the next phases of the design are validated. .

1.2 BACKGROUND

1.2.1 History of CNC

The history of NC machines dates back to the 1940s with more advancements in the 1950s. John parsons after world war II was involved in research to improve aircraft by designing stiffened skins. Due to this at MIT various Air force research projects were carried out starting in 1949. An experimental milling machine was designed in the early stages of the research, the team also included Prof J.F Reintjes.

A system was developed by Parsons corporation located in traverse City Michigan for helicopter blade templates. The aerofoil coordinate calculation was discovered by John Parsons who was the founder of the company using an IBM 602A multiplier, these data points were then fed into Swiss jig borer. Since it manufactured goods it was considered the first-ever numerical controlled machine. Helicopter templates were produced with the help of pre-programmed information which the system read. This was done by feeding punched cards into the system.

With the advancements in Numeric control technology during the 1960s, 1970's the CNC machine familiar with the modern CNC was gradually coming into existence.

Furthermore, due to advancements in digital technology and efficient automated processes in industries further led to its development. Nowadays, CNC can be even homemade with the help of advanced computing that is very common in the 21st century.

Although there has been a tremendous amount of advancement in CNC machines since its early conception to a modern-day CNC three components are still at the core. These include a drive motion system, Command Function and a feedback system. (CNC.com. (2018)).

The need for precise measurement requirements has been vital in today's era of modern manufacturing where parts and assemblies are more refined and complex than ever. Due to this reason, CMM plays a very important role in delivering a measurement solution. They enable measurement on the shop floor without the need of taking away the parts to a dimensional lab this saves time drastically. Since they are portable they are space savers, this helps in saving floor space and using it more effectively. Heavy parts do not need to be moved to large distances and this is where CMM plays another important role in saving costs and time in moving such parts.

The role of precision measurements extends from formula 1 to pharmaceutical to aerospace. Extremely high level of accuracy is required in designing parts and components for the aerospace industry, it becomes vital to eliminate any production errors and lack of attention to detail. Due to their high costs for failing to meet the standards which authorise the functionality, safety and reliability and their critical application nature it becomes necessary to manufacture and release the parts to the highest level of accuracy. (Accuracy in aerospace – Aerospace Manufacturing Magazine. (2018)).

One major example is the automotive industry, the life of cars increased tremendously, in early times it was considered an accomplishment to have a car lasting for 100,000 miles, nowadays cars can easily last for 200,000 and sometimes even 300,000 miles with a potential of being used further with ease. Such achievements can be related to the perfect fit of components in the assembly which are given the highest level of attention to detail. One of the key reasons behind this is metrology technology. (What is Metrology & Why is it Important in Manufacturing? (2018)).

The evolution of CMM was quick with the help of various CMM manufacturers in the USA, European countries and also Japan which entered in the area in the mid-1960s with the introduction of touch trigger probe by Renishaw in early 1970's the use of coordinate measuring machines grew rapidly. A stepping stone for CMM's was a challenge to solve a specific inspection requirement for Olympus engines with the help of Touch-Trigger Probe invented by Sir David McMurty. These Olympus engines were used in the supersonic Concorde Aircraft. The success leads to the revolution in CMM allowing accurate and automatic measurement of finished assemblies and machined components.

Further, development was pushed forward by Renishaw again through the introduction of a motorised probe head in the early 1980s this led to the birth of modern CMM. The core technology has been static during the past three decades of Renishaw innovation which is remarkable. A more accurate motion path both along a defined vector, its capability to perform circular motion path analysis with the capability of operating under high accelerations and speeds are one of the key functions that the CNC controller has enabled for the CMM structure.

The technology is also improving in terms of CMM structure, conventional granite and steel are being replaced with high technology allow materials providing a lighter and stiffer structure with the improvement in thermal exposure and hence less deformation. Measuring scales located in sub-straits mounted to CMM structure come integrated with allowing structures since these structures are independent of the structure movements the accuracy is considerably increased. The advancement in computing has also allowed in the development in the geometric compensation errors further increasing the accuracy of CMM over "mechanical accuracy only structure". COORD3 developed the Z ram of Coordinate measuring machine by introducing silicon carbide which is lighter and stiffer replacing granite.

The CMM design around 20 years old utilising granite is still being manufactured by traditional CMM companies. Although the new modern CMM renders granite obsolete their investment in internal house granite production is causing a resistance for change.

Due to low cost, abundant supply and minimum effort for the production of granite the investments are minimized due to fast marketing time.

However, due to economic pressures, the majority of these suppliers have now been consumed leaving a high number of obsolete machines behind. In the near future, the consolidation of new world CMM in China and India is inevitable.

There are three orthogonal axes, X, Y and Z in a typical CMM working a three-dimensional coordinate system. The position of each axis is indicated with the scale system that each axis possesses. CMM reads touch probe input as assigned by the computer program or the operator. Determination of size and position under micrometre precision is then carried out with the help of X, Y, Z coordinates. (The History of the Coordinate Measuring Machine. (2018)). Since the cutting and

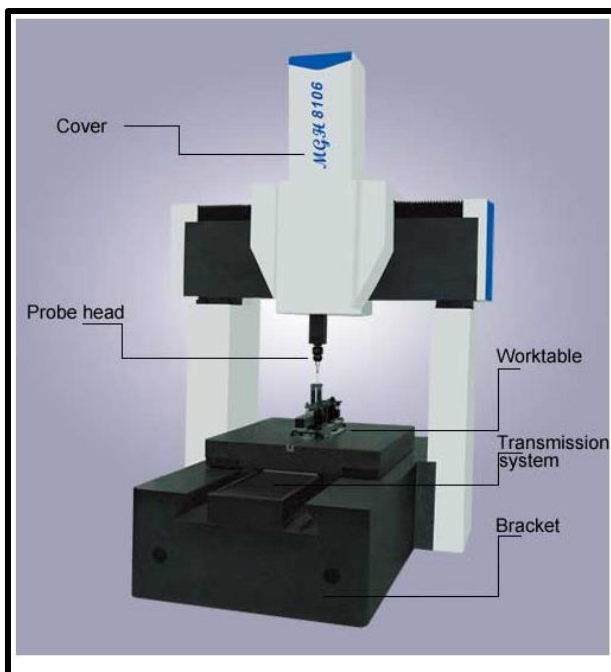


Figure 1: Schematic of a Coordinate measuring Machine (High accuracy CMM - High accuracy 3D CMM - 3D COORDINATE MEASURING MACHINE|CMM SOFTWARE|XI'AN HIGH-TECH AEH INDUSTRIAL METROLOGY CO., LTD. (2018).)

other machining forces are absent in a CMM, for smooth functioning CMM uses Air bearings which operates with the help of thin gap of Air between the guide and the bearing itself. This offers smooth motion without any stick-slip phenomenon and excessive vibrations due to stiff components. See Figure 1

1.2.2 Existing Technology

A number of design concepts have fully matured and Commercially applied in Coordinate machines as discussed in the earlier section, they can be divided into two groups, Linear Guide types and different Mechanical Drive configurations.

1.2.2.1 LINEAR GUIDES:

They primarily consist of a Linear Bearing and a guideway and can be further divided as follows;

Friction Guides:

These types of guides have a high load capacity of up to 140 MPa. They provide high strength against impact loads and allow good damping. These guides are used in applications where speeds under 0.5m/s are required. On contact surfaces, uniform marks are left by scraping which enables the least adhesion between the bed and the slide. To reduce friction these guides can be coated with thick polymers within a few mm of thickness. Friction guides come with various configurations.

The primary materials used for the sliding are Casting, bronze, special polymers, and steel. During operation sometimes, static friction becomes more than dynamic friction causing a stick-slip phenomenon which needs to be controlled for smooth operation and control. Turcite SKC or Moglice are few polymers which favour lubrication with the help of additives. These significantly reduce the stick-slip phenomenon. (Altintas, Yusuf & Verl, Alexander & Brecher, C & Uriarte, L & Pritschow, Guenter. (2011)). See figure 2 and figure 3.

Rolling Guides:

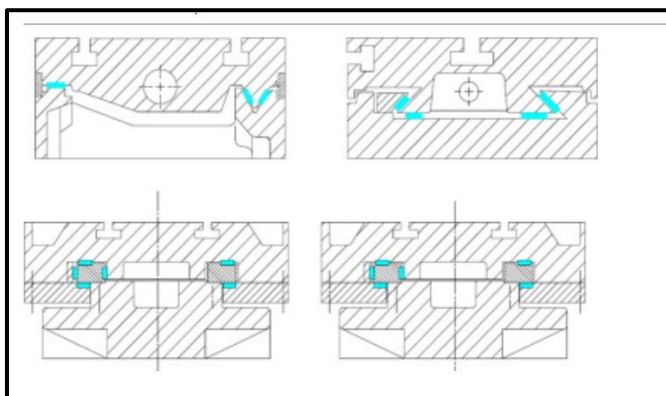


Figure 3: Shows Different configurations of friction guides (Altintas, Y., Verl, A., Brecher, C., Uriarte, L., & Pritschow, G. (2011). Machine tool feed drives)



Figure 2: Friction Guide Friction guides made easy with Accuride's engineering excellence - Automation. (2018).

Modern-day machine tool applications use stationary and recirculating roller-based guides frequently. Applications where the stroke is short usually use stationary roller-based guides. Rollers, needles and steel balls are used as rolling elements. Attached to stationary and moving parts are two cages where these rollers are preloaded. They have low structural damping but offer high stiffness and load capacities with low friction characteristics. Different manufacturers produce recirculating roller guides based on load capacity and size (Altintas, Yusuf & Verl, Alexander & Brecher, C & Uriarte, L & Pritschow, Guenter (2011)). See figure 5 and Figure 4 below.

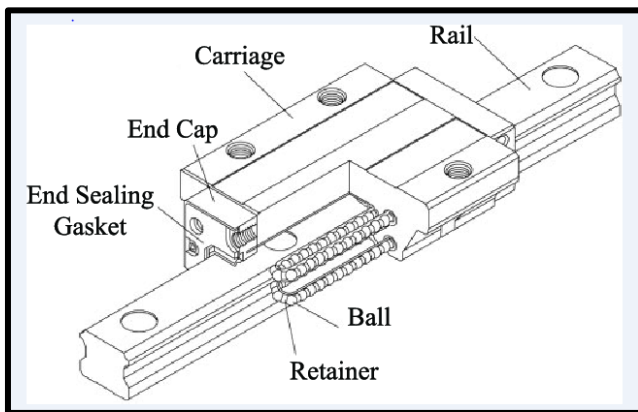


Figure 5: Shows Schematic of Roller bearing (Sun, Wei & Kong, Xiangxi & Wang, Bo & Li, Xingzhan. (2014). Statics modelling and analysis of linear rolling guideway considering rolling balls contact)

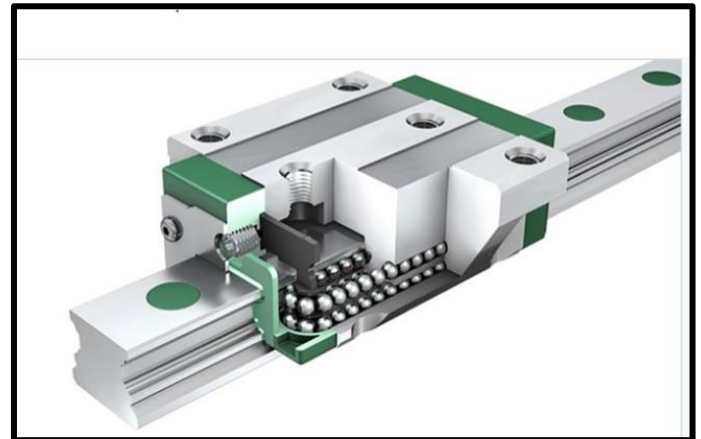


Figure 4 : Shows Recirculating Roller bearing (Linear ball bearing and guideway assemblies. (2018))

Clamping systems:

Through Safety clamps the clamping action is released with the help of compressed air which fills the chamber between two spring diaphragms. In this way, an original relaxed position is achieved by the clamping body as the diaphragms deflect outwards this allows the brake blocks to lift off the rail. The diaphragms move back when not inflated thus clamping the carriage 5-6 bar of pressure is used during this operation. Air can be used to activate the clamping action, the compressed air fills chamber under the spring diaphragm this pushes the spring sheet upwards and stretches it, the fulcrum is provided by the horizontal strut consequently brake is applied through the attachment of blocks against the linear rail. Under no inflation bent position is retrieved by the diaphragm with the upper body clamp coming back to its original position enabling the clamp to lift, this process requires around 4-6 bar of pressure. (Altintas, Yusuf & Verl, Alexander & Brecher, C & Uriarte, L & Pritschow, Guenter. (2011)). See figure 6 and 7 below.

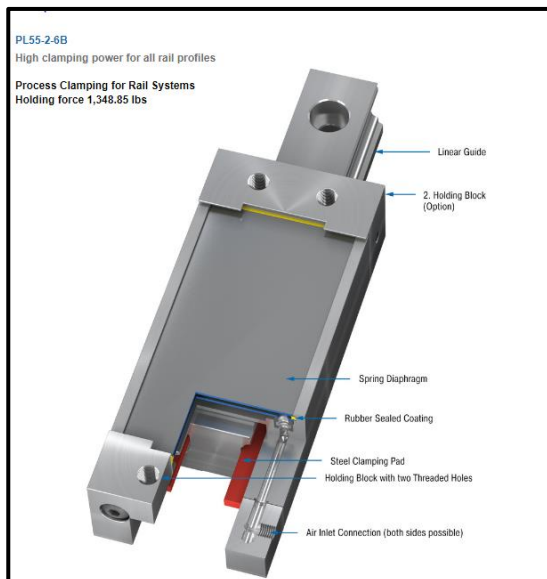


Figure 6 : Shows the Spring Diaphragm Clamp Mechanism (PL55-2-6B - PL - LOCKED PL - Clamping Elements - Safety Products - Products - ACE Controls Inc. (2018))

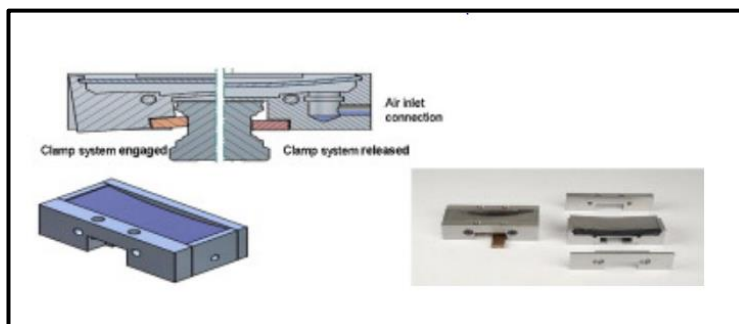


Figure 7: Shows the spring diaphragm clamp system using Air as a clamping force. Altintas, Y., Verl, A., Brecher, C., Uriarte, L., & Pritschow, G. (2011). Machine tool feed drives

Hydrostatic Guides:

Hydrostatic guides don't have any stick-slip phenomenon this is primarily due to the small pockets or cells pressurised with thin oil which separate the components of sliding surfaces. With the loss of pressure in the oil it is released to surrounding Land this creates an oil gap which is a distance between the land the other sliding mate, oil gap "h" is about 10 -40 micrometres. Resistance R_c against the flow of the fluid Q , from oil cell to outside is generated by the oil gap. Cell pressure P_c is defined as the difference in pressure between the atmospheric pressure and the cavity. Compared to roller-based guides hydrostatic guides offer higher damping perpendicular to the cell achieved through the friction of the oil lamina by sliding. (Altintas, Yusuf & Verl, Alexander & Brecher, C & Uriarte, L & Pritschow, Guenter. (2011)). See figure 8 Below.

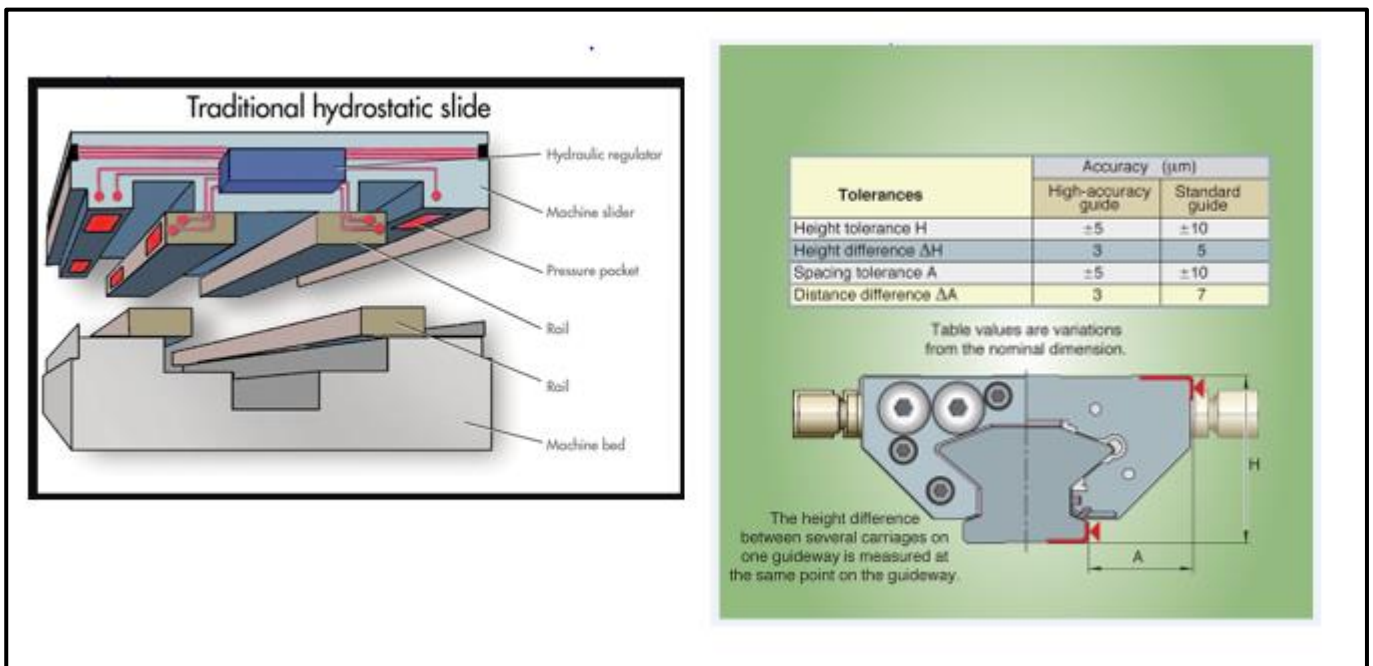


Figure 8: Shows Hydrostatic Linear guide way schematic (left) and basic dimensions (right) (Hydrostatic linear guiding for standard design spaces. (2018)).

Non- recirculating guides:

Linear carriages with ultra-low precision requirements use cylindrical non-recirculating bearings. The minimum degrees of freedom required to drive the configuration which should be kinematic. Constant preload method dominates the constant displacement method in cases of high precision this can be achieved in horizontal guides through the weight of the system. And through mass counterbalancing or locking the system through springs in vertical guides. This suppresses the imperfection in cylinders' elements. (Altintas, Yusuf & Verl, Alexander & Brecher, C & Uriarte, L & Pritschow, Guenter. (2011)). *See figure 9 below.*

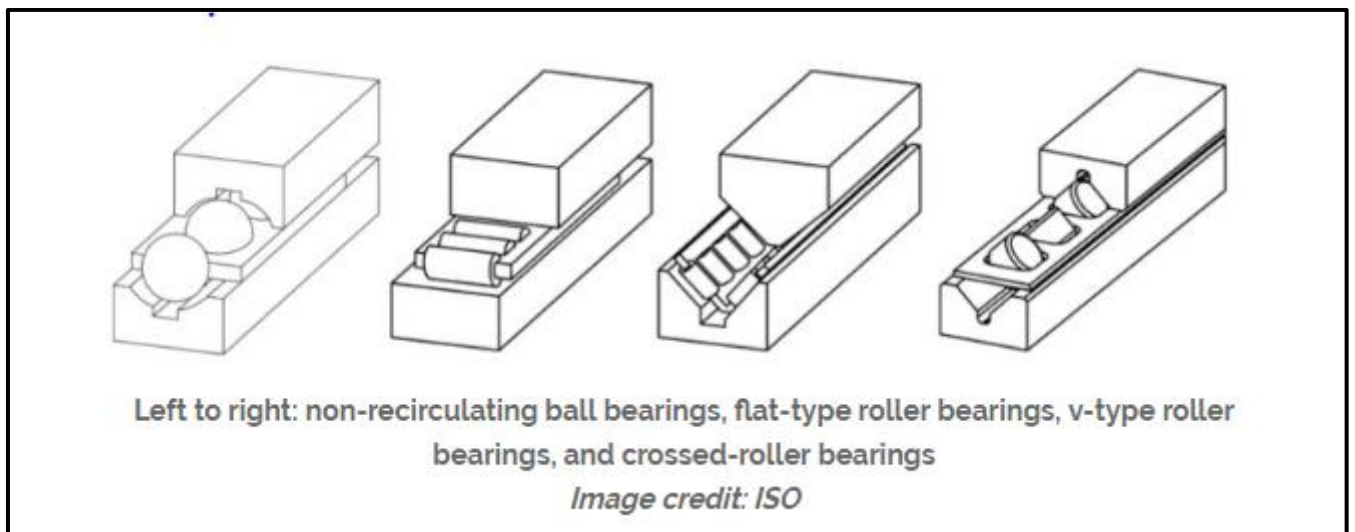


Figure 9: Shows Different types of non-recirculating linear guide bearing arrangements (Collins, D. (2018). What are recirculating linear bearings?)

Aerostatic Guides:

A thin layer of air supports the load of the system when these guides are used. high assembly and manufacturing tolerances are required due to low compressibility and viscosity of air, even at higher speeds, the frictional losses are very less due to low viscosity of air. The temperature variation of Air viscosity is larger than Oil based hydrostatic guides due to this they can perform well in a wide range of temperature settings. However, due to the low damping and high compressibility issues, hydrostatic guides outperform aerostatic guides in terms of dimensioning during design. The smooth working of these types of guides may be hindered by the phenomenon of air hammering causing self-excitation. Due to a less stiff structure, they are not commonly used in machining systems. The gap has to be very small 5-10 micrometres due to this the surfaces under sliding operation need to be very smooth and precise. The damping is improved with the help of optional damping elements with an example being Electro-rheological fluid

dampers. Vibration reduction can be done by incorporation more cells each having their restrictor or the use of highly porous materials which provides the same operation. See figure 10 below.

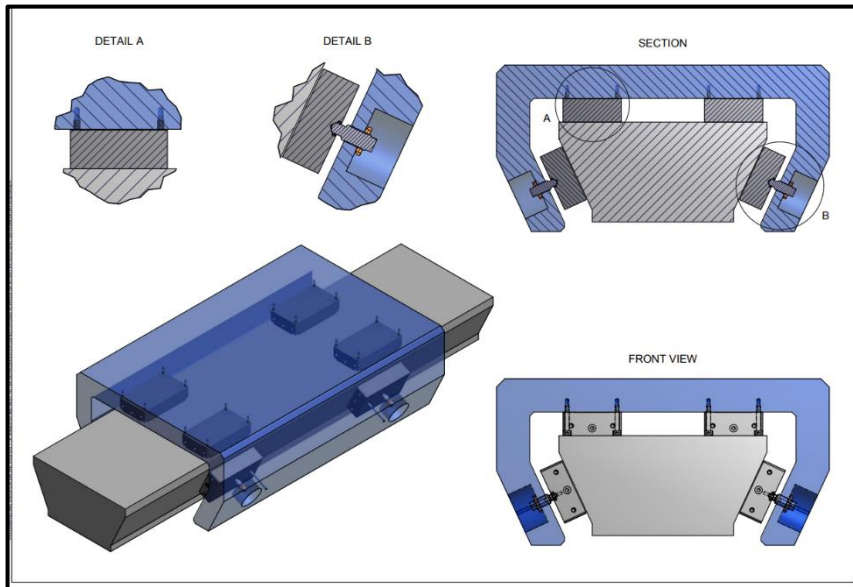


Figure 10 : Shows the arrangement and components of Air bearings (Air Bearings Application. (2018)).

Magnetic Levitation:

This method proved zero friction with wear free conditions, due to less damping and a need for a highly sophisticated control system for more linear axis operations this is not widely used. (Altintas, Yusuf & Verl, Alexander & Brecher, C & Uriarte, L & Pritschow, Guenter. (2011)). See figure 11 below.



Figure 11 : Shows a planar motor levitated by Tekniker (Altintas, Yusuf & Verl, Alexander & Brecher, C & Uriarte, L & Pritschow, Guenter. (2011). Machine tool feed drives

1.2.2.2 Mechanical Drives:

According to ((Altintas, Yusuf & Verl, Alexander & Brecher, C & Uriarte, L & Pritschow, Guenter. (2011)) machine tool feed drives that are commonly used include Ball screws and Rack and pinion system. However, there are many other configurations as well but due to their good overall performance they are preferred over other configurations.

Ball Screw Feed Drive System:

Machine tools feed drives nowadays are highly populated with the use of ball screws this is due to their low wear, low heating characteristics with a tendency to avoid the stick-slip effect. Their efficiency ranges from 95% to 98%. Ball screws have two major components, A nut with recirculating balls connected to the table and the screw itself. It is supported at two ends with the help of thrust bearings which restrict motion along the longitudinal direction. The ball screw is driven by a motor on one end, the motor can be of various types depending on the application. The motor is either connected directly or indirectly through a gear/belt mechanism for reduction. To avoid backlash the nut is usually preloaded with oversized balls or leads. irregularity in grinding the pitch at uniform intervals results in positional errors. Machine tools with long travel strokes can use ball screws with 12 m of length. The range of pitch can be from 5 to 40 mm while as screw diameter from 16 to 160 mm depending on the application. By applying 2g acceleration travel ball screws can result in up to 100m/min of travel speed. Friction, wear, deflection reduction has been achieved through a coating of ball screws which had proved to be very advantageous in terms of accuracy and speed. Two types of ball recirculation mechanism exist. One with internal recirculation of balls within the nut and the other being external recirculation design principle which uses external tube or channel allowing for more tangential entry which helps in a smooth flow and achieving higher speeds. Since the tube is external it is exposed to damage, if this happens a slight bent can choke the balls causing significant damage to the drive. The internal design principle works on balls passing through channels located near each thread end since they don't have a good alignment entry they often cause noise and rolling. (Altintas, Yusuf & Verl, Alexander & Brecher, C & Uriarte, L & Pritschow, Guenter. (2011)). See figure 12 and 13 below.

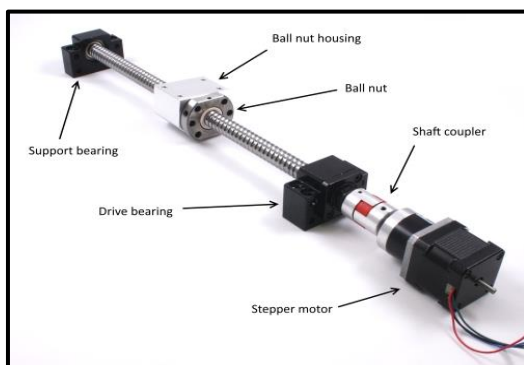


Figure 13: Shows a Ball Screw Drive Bearing for SFU12 Ball Screws - LMN4207_0 at Phidgets. (2018).



Figure 12 shows ball bearing drive assembly (Layosa, C., & Layosa, C. (2018). Belt Drive vs. Ball Screw Actuators | MISUMI USA)

Rack and Pinion Drives:

Machines with long travel distances (approx. above 4 feet) use rack and pinion mechanisms. This drive is not limited by length, by joining small racks a long feed travel can be achieved. The length of travel distance has no effect on the total stiffness of rack and pinion. The contact stiffness and the torsional stiffness of pinion shaft and gear are mainly responsible for total stiffness of the system. There should be no backlash between the pinion teeth and the rack it should be free of clearance. This is achieved through 2 key methods. One method utilises 2 pinions on each side of the rack these two pinions are connected with two different motors, one of the motors drives the pinion through high torque in the desired direction and the other motor applies less torque in opposite direction resulting in tensions which consequently gets rid of clearance.

Other method helps in achieving backlash in both ways. This done with the help of pinion separation, the pinions are helical in nature. The gear error compensation is done with the help of axial movement of the lower gear through spring force on a spline shaft shoulder enabling bearing of pinions with opposite rack flank. (Altintas, Yusuf & Verl, Alexander & Brecher, C & Uriarte, L & Pritschow, Guenter. (2011)). See figure 14 and 15 below.

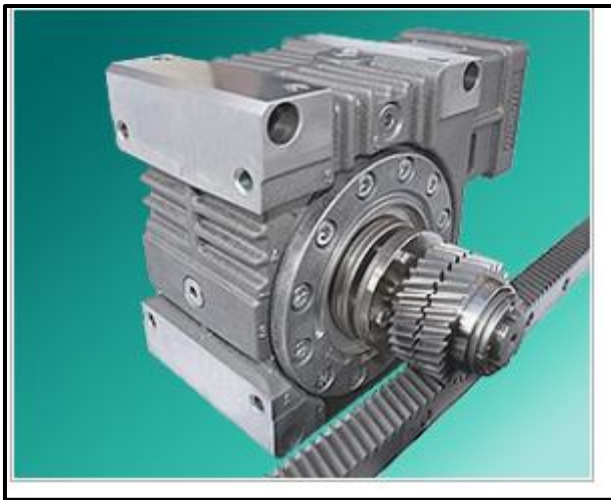


Figure 14 Shows the switch pinion system (Linear ball bearing and guideway assemblies. (2018))

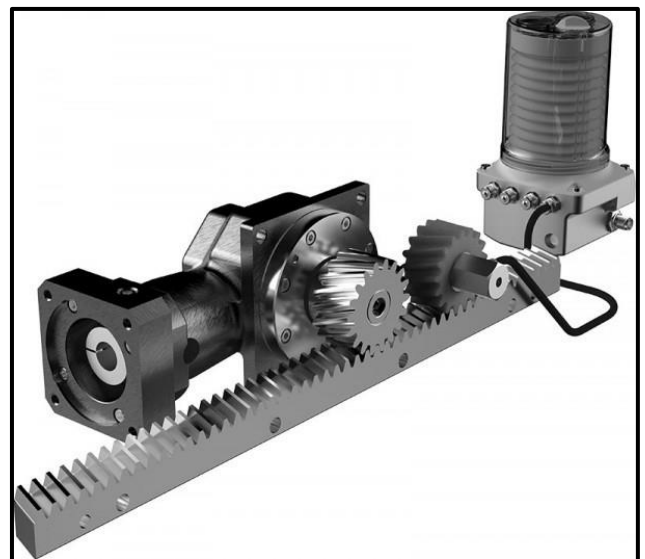


Figure 15 Shows a Rack and Pinion Drive, Drive System solutions for rack and pinion applications - Drive Lines. (2018).

1.3 PROJECT AIM/SCOPE:

Increasing demand for highly efficient production systems have been one of the primary subjects in the 21st century, this has led to the development of complex and flexible manufacturing systems and in-process measurement tools. Compared to CMM machines, CNC machines require high power leading to high levels of Vibration hence high dynamic errors rendering them incompatible with in-process measurements and micromachining.

In order to solve this problem, this project aims to look into the design of a novel feed drive system that can help in the reduction of vibration during in-process measurement on a CNC, this can lead to more accurate machining operations as well as efficient use of scanning probes.

1.4 OBJECTIVES:

1. To carry out the breadth and depth of the Literature review of already existing and developing new technologies relevant to feed drive systems. Various Scientific publications will be studied and critically reviewed.
2. To identify the knowledge gaps, and present a variety of solutions through concept generation hand in hand with the knowledge of existing technological advancements.
3. To perform benchmark testing by collecting the relevant data through Experimental Modal Analysis using Data Physics acquisition unit and Signal mobiliser carried out on the Conventional Test Feed drive system to obtain the system response.
4. To Validate the Finite Element Method carried out on the entire Conventional Feed drive rig, thorough evaluation with the benchmark test, this method will then be implemented on a newly developed technology to computationally check for Vibrations and accuracy of the system.
5. To undertake and carry out the Design and Analysis of the Novel Feed Drive solution with the ultra-low vibration with the help of general design and analysis methodology.
6. To Build a simple prototype for the validation of the major parameters of the new Design.
7. To critically evaluate the performance of the new design.
8. To Recommend improvements that are vital for further development.

1.5 STRUCTURE OF THE THESIS

The Thesis is divided into six Chapters following in the Chronological order as follows.

Chapter 1, Introduction and Background: This section involves the general project background and the History of Precision manufacturing systems followed by an overview of existing solutions of feed drive systems.

Chapter 2, Literature and Critical Review: This Section covers all the relevant research that has been carried out in developing new technologies relevant to feed drive systems. Various Scientific publications have been studied and critically reviewed. Besides Scientific literature it also involves some known technologies that may lead to a solution. This section was primarily divided in Bearing Design and Drive System Design and various other combinations; hence due to the nature of the project this section covers a broad spectrum of research and concludes a knowledge gap.

Chapter 3, Methodology: The Aim of the paper is to undertake and carry out the Design and Analysis of the Novel Feed Drive solution with the ultra-low vibration, therefore, it becomes logical to use the general design and analysis methodology which is detailed in this section.

Chapter 4, Theory and Preliminary Study: The theory behind Vibrations and Data acquisition have been clearly demonstrated, and the data preliminary to the design has been collected and analysed. Concept generation is also included here. An experiment and computational Analysis of conventional test rig were carried out to collect the data for a reference as well as to Validate the finite element method that will later be employed to the Novel feed drive System.

Chapter 5, Design and Computational Validation:

This Section covers 2 major Topics, First the full Mechanical design of the chosen concept i: e the hybrid bearing and Secondly, the Mechanical design of its simplified version to test some major parameters. It also includes relevant calculations undertaken during the design and verification of the computational Methods including Finite Element analysis

Chapter 6, Discussion: Critical evaluation of the performance of the design and its limitations has been discussed and the achievements in relation to the pre-set Aims and Objectives have been clearly defined.

Chapter 7, Future Direction: Future recommendations regarding the project have been given this section

CHAPTER 2: LITERATURE/CRITICAL REVIEW

This Section covers all the relevant research that has been carried out in developing new technologies relevant to feed drive systems. Various Scientific publications have been studied and critically reviewed. Besides Scientific literature, it also involves some known technologies that may lead to a solution. The Research was primarily divided in Bearing Design and Drive System Design and various other combinations; hence this section covers a broad spectrum of research and concludes a knowledge gap.

2.1 BEARING DESIGN:

Research related to Feed Drive Novel Bearing Design has been carried out in this section.

2.1.1: Friction reduction Based Bearing

In his paper ultrasonic frequencies are used to reduce friction and hence stiction resulting in a loss of vibrational amplitudes and hence good positioning accuracy. To achieve such ultrasonic vibrations piezo stacks are used. This is done by incorporating a piezo actuator that slides the bearing surface at these frequencies. (Engel, T; Lechler, A; Verl. (2016)).

The design of the bearing consists of an inertial mass and bolt going through inertial masses, the resonators, the mounting plate and a guiding rail. See figure 16 below.

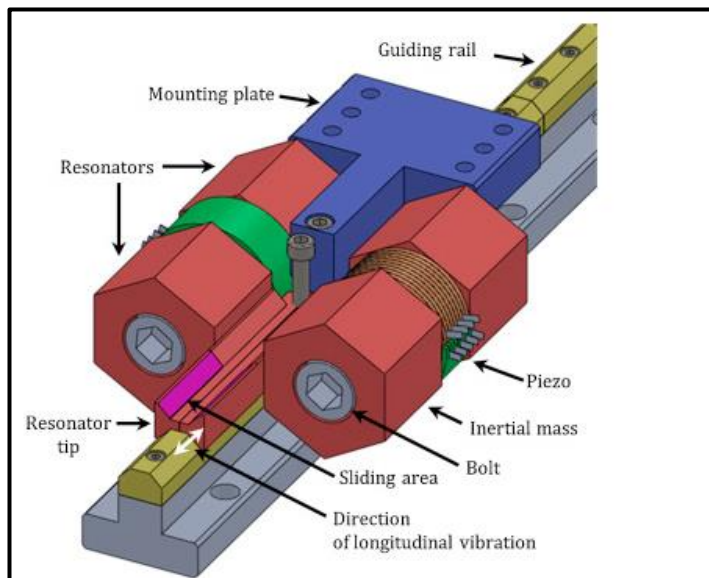


Figure 16: Prismatic adjustable friction bearing Components

With the reduction factor of 0.3 at a feed velocity of 100 mm/s following oscillation parameters can be achieved.

| Friction reduction example and oscillation parameters | | | |
|--------------------------------------------------------------------------------------------------------|-------------------|--------------------|-------------------|
| 70% reduction $\rightarrow \gamma = 0.3 \rightarrow v_f/v_s = 0.45 \rightarrow v_s = 220 \text{ mm/s}$ | | | |
| f_s | 300 Hz | 3 kHz | 30 kHz |
| x_s | 116 μm | 11.6 μm | 1.2 μm |

Figure 17: Shows Friction reduction with oscillation parameters

Increasing the voltage increases the frequency and hence reduces the Friction coefficient which is measured with the help of a force sensor measuring this at different velocities. The reduction in height (93%) from $\mu = 0.21$ to 0.015 in case of feed velocity at 0.5mm/s and lower as we go higher for instance 73% at 80 mm/s reduced from $\mu = 0.3$ to 0.08. The friction can be now controlled following the requirements. See figure 17 above and 19 below.

The position error results show that the with passive bearing setup the remaining errors range from 3.5 to 5 μm with the highest values (peaks) of -8.2 μm and 5.4 μm Contrarily The peak in active friction reduction is reduced to 2 μm with other values being -0.59 μm .

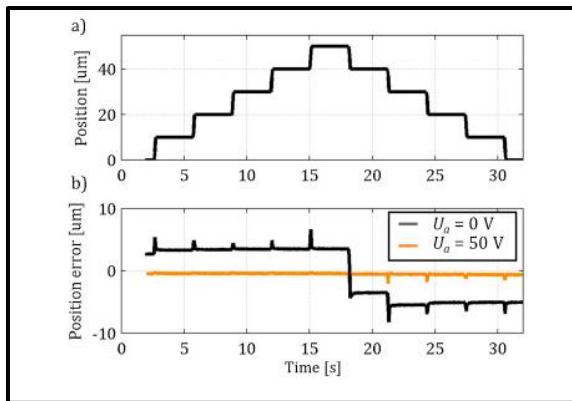


Figure 18 Shows Linearization and Friction reduction

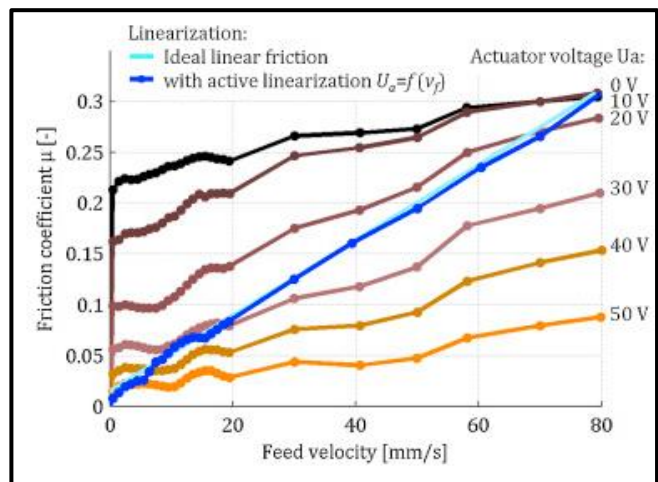


Figure 19: With the help of passive and active bearings Comparison of the positioning error on 10 μm steps has been depicted

2.1.2: Flexural Design

The paper describes a novel flexural bearing design that can provide rotational oscillations of 360 degrees with high repeatability. Straight flexures with inner and outer cores are used in combination, these straight flexures allow motion in circumferential direction whilst keeping other directions restrained. (Luo, H.P; Zhang, B; Zhou, Z.X. (2008)).

The problem with using only one flexural element is that it can deform axially causing an error while as using two cores the axial error can be cancelled. Also due to asymmetric nature, the thermal expansion is even in all directions causing no errors. See figure 20, and 21 Below.

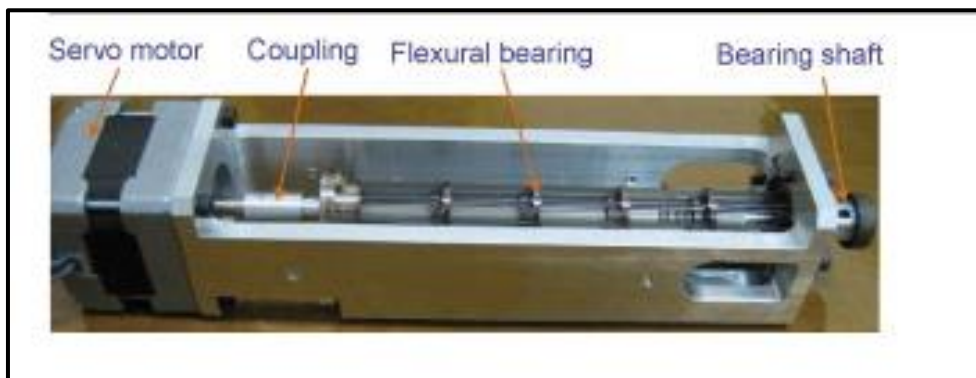


Figure 20: Assembly of Rotary flexural bearing

The application is usually in precision equipment especially micro machines or microdevices with nanometre accuracy level. It has no friction, no lubrication and hence it is lightweight and has high accuracy. The bearing was manufactured for a micromachinery that can manufacture products to nanometre level, for example, μ -ECM μ -EDM [3], μ -ECM [4], ultrasonic micromachining, laser micromachining and CMM'S this is due to the fact that current technology like LIGA and MEMS widely manufacture 2d or 2.5 d micro-manufacturing applications as they can't do 3d efficiently. It has a nested design that reduces axial errors.

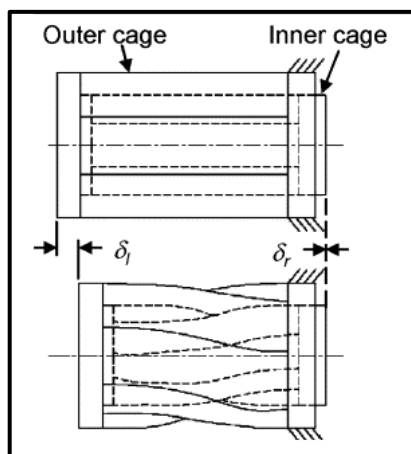


Figure 21 Outer and inner cage nested design

2.1.3: Magnetic Guide for Photolithography

Without rigidly containing the DOF of a system a magnetic bearing can apply torques and forces to a system. Only sensors limit the resolution of magnetic bearings as they themselves are very precise, accurate and fast. In the paper, magnetic bearings are chosen over a dual-stage control system where the fine stage is controlled by the voice coil or PZT'S in photolithography. The compound flexures are connected to the platen and the whole system has poor dynamics. The fine stage provides 100 um of travel and six degrees of freedom control while a coarse stage provides 200 mm travel.

The flexures and mechanical actuators are eliminated because the magnetic bearings themselves control the six degrees of freedoms with accuracy and rapidness.

The five degrees of motion are controlled with the help of variable reluctance actuators (two transitional and three rotational) with the help of magnetic bearings and the long travel direction is controlled by a Lorentz linear motor with the 50 mm travel. A 13 kg platen has been used here. the bearing centre contains 5 capacitive probes with nanometre resolution.

The laboratory experiments were carried out to test the acceptance and performance requirements of the linear a magnetic bearing.

The linear bearing experiment shows that noise has a 3nm peak to peak maximum value dominates at 430 Hz, the commanded lateral step was 10nm. It was observed that the noise was coming from the floor where the air conditioning system is located underneath the previous floor. This confirms the acceptance of linear bearing in photolithography.

2.1.4: Machine Tool with Active Magnetic Guides

The main importance of this paper is that the application in real machining CNC centre where high loads are present is shown.

In this paper, the application of active magnetic guides on actual machining centre has been designed and tested undercutting conditions with the further improvement of dynamic stiffness for the whole range of frequency.

The axis X and Y are driven with the help of linear motors; these axes are located under the workpiece. The active magnetic guide providing guidance has been incorporated in the z-axis which is located under the tool. The machine has a workspace of 500 ×500×300 mm³. In order to provide higher acceleration forces, the slides x and z are driven by two parallel drives. Conventional ball type guides are used to guide X and Y axes. The maximum feed acceleration that the drives were selected for was 5g in all three axes. *See Figure 22 Below.*

The drives were selected for a maximum feed acceleration of 5 g in all three axes. The cutting power at maximum speed of 60,000 rpm of the HSC work spindle is 15Kw.

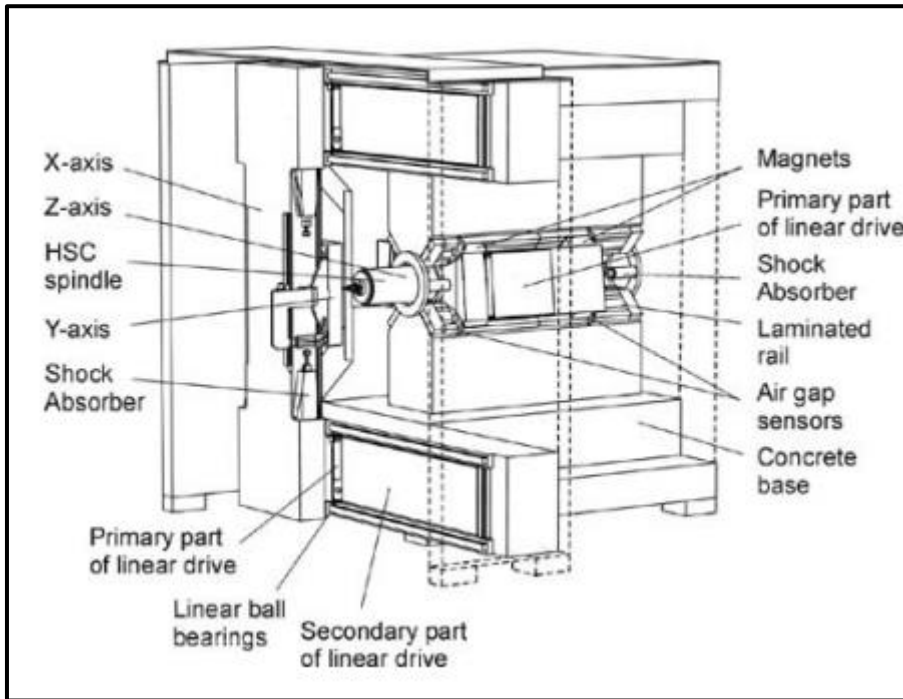


Figure 22 Machining Centre Structure

The machine frame needs to have a high damping ratio in order to absorb the machine dynamics (Vibrations). This is done by using Hydropol @ This is a composite filled with Cement concrete encased in the steel-reinforced sheet metal cover. See Figure 23 Below.

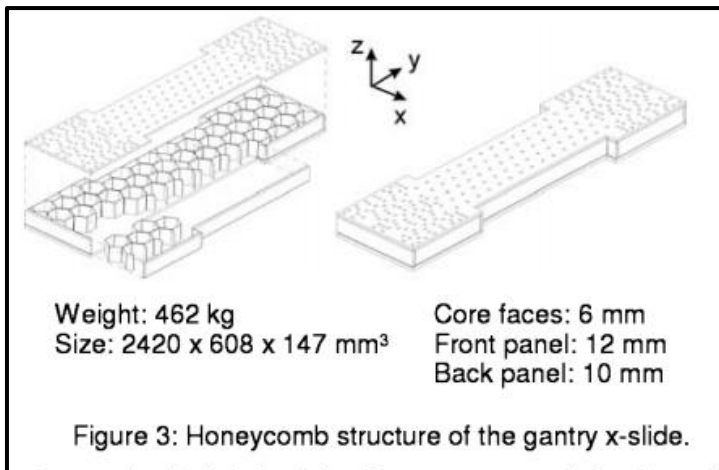


Figure 23 Gantry x Slide honeycomb structure

The active magnetic guide has been used in the Z-axis due to the space requirements.

The dynamic stiffness of the magnetic guides over a frequency range is low except for the low-frequency range while as the ball bearing has the low dynamic stiffness in the high-frequency range. Also from the locus plots (See Figure 24 below), it can be seen that for magnetic guides most of the real part of compliance frequency is positive this means higher stability there is energy dissipation from the structure compared to ball guides. The maximum chip thickness is limited by chatter sensitivity which is a function of the maximum negative real part of the compliance frequency. This is higher in ball guides than in magnetic guides. In order to tackle this high damping is required which unfortunately in ball guide is less $D=0.01$. Also, the maximum real part of the compliance frequency is negligible as magnetic guides can be damped to a very high value. Also, there is low dynamic stiffness at low frequencies of magnetic guides but since the machine spindle is designed for higher frequencies this can be avoided.

Infinite stiffness can be incorporated by using integral control in magnetic guides.

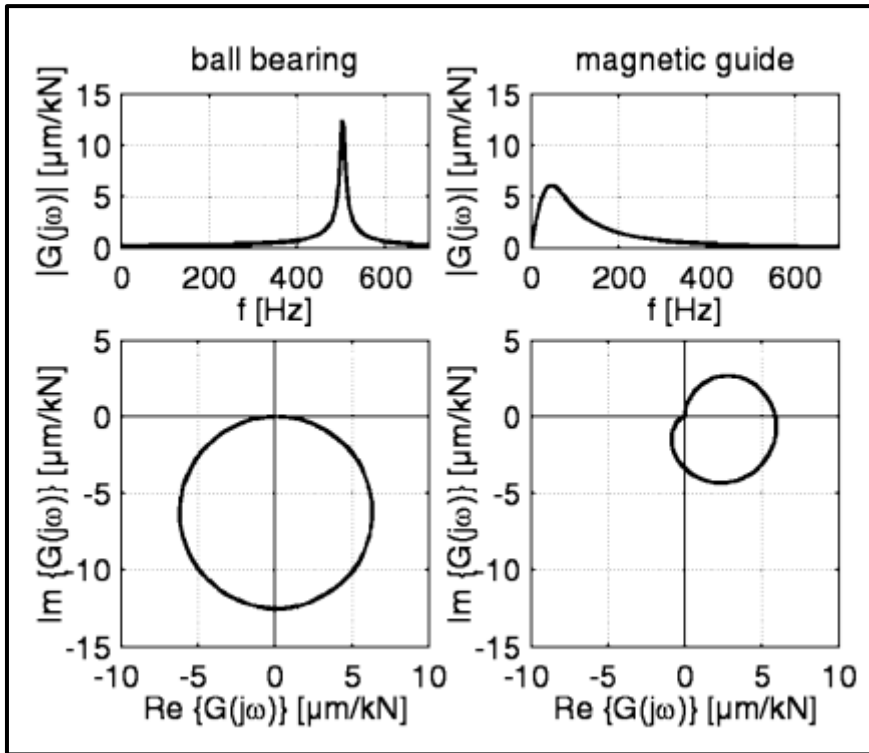


Figure 24 Standard ball bearing guide ($c=4\text{kN}/\mu\text{m}$, $D=0.01$) and Magnetic guide ($m=400\text{kg}$, $\lambda=400\text{s}$) Compliance frequency response

The maximum dynamic compliance of the ball guides is different than the magnetic guides under linear behaviour as in case of magnetic guides mass comes into play which means higher mass is always good for maximum dynamic compliance however magnetic guides are limited in this case.

The practical tests included experiment which presented the scenario in the worst-case setting under milling operation. The frequency was set low, the smaller prototype guide with less mass (65kg) than original was used for steel milling. The maximum force applied was 1.6Kn. The deflections show that even at low frequency where maximum compliance occurs they have a very low value. Furthermore, the original system is 7 times heavier than the prototype and hence influencing its dynamic stability further. The cutting frequencies will be higher than the low frequency used here. *See Figure 25 Below. (Denkena, B; Kallage, F; Ruskowski, M.(2004)),*

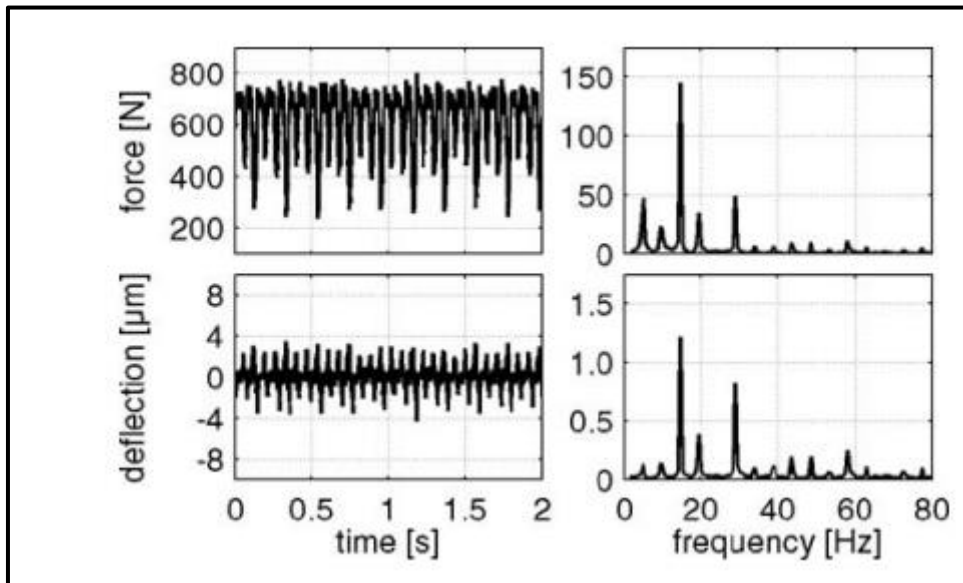


Figure 25: Guide deflection with exemplary steel milling and control force on an active magnetic guide

2.1.5: Magnetic levitation

The air gaps between the moving parts and the mechanical guide rails are limited by the gas film and oil film. Due to limited gap height resulting as a result of the limitation of oil film or gas film between the mechanical guide rails and the moving part aerostatic and hydrostatic guideways does not result in the elimination of the effect on moving parts by the mechanical guide ways.

This demands an efficient system that can have a large gap with better controllability.

In gantry type mechanism the deformation of the cross beam (6m) can affect the precision of guide rails. This also demands isolation of the moving part.

The z-axis Suspension is achieved with the help of Superconducting EMS which lifts the cross beam moving part. Due to cutting forces, the loads are exerted on the y-axis demanding for suspension in this direction as well, this can be achieved by normal conducting EMS scheme this can be generated with the help of linear motors normal force. The translation motion in the x-direction is achieved with the help of linear motors thrust force. See Figure 27 ,Figure 26 Below.

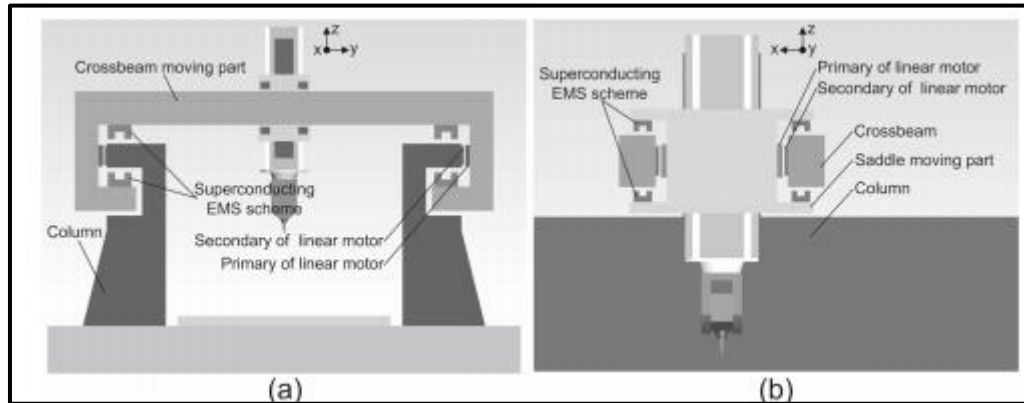


Figure 27 Shows the Arrangement of the Gantry Design

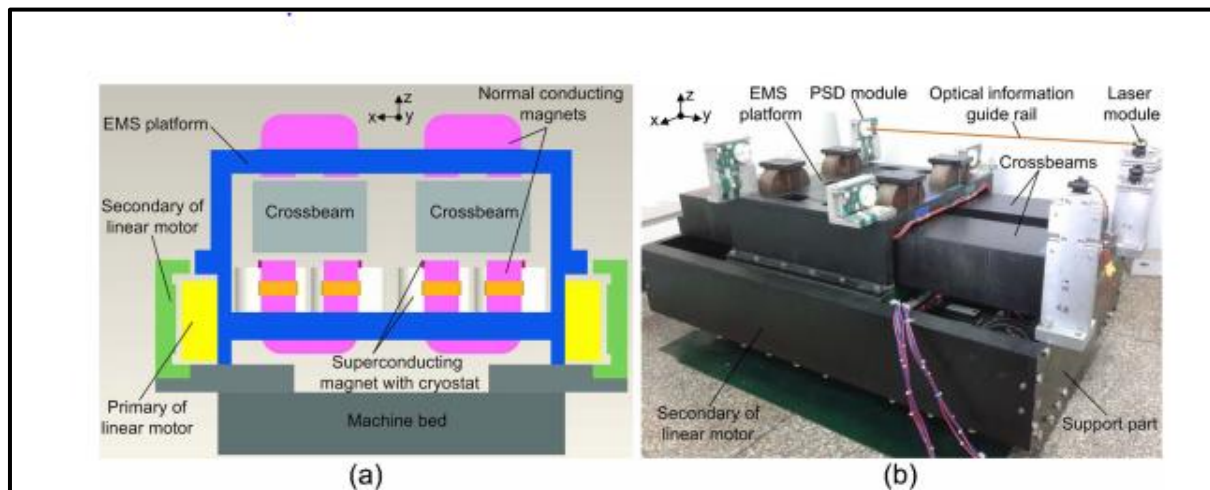


Figure 26 Sectional view a and b prototype of superconducting EMS feed drive System

A suspension accuracy of $5\mu\text{m}$ can be achieved, the super conduction coils need cryogenic conditions to keep the temperature under control, this is done by using cryostats, for heavy machine tools such cooling power is acceptable.

The experimental results showed that there is a reduction of power consumption of the coil is about 96.1% electromagnetic power consumption amounts to about 72.2 %.

For further reduction in power consumption superconducting drive circuit line resistances should be reduced,

The system was also tested under varying suspension height reduced from 300 um to 200um, due to decreasing of suspension height the air gap increases.

The average regulation current of the normal-conducting magnets kept being small, and the electromagnet power consumption can be greatly reduced by the proposed scheme under the varying working conditions.

At 200 μm the power consumption is similar as seen from the table the coil power 96.6% reduction and power consumption of to 72.5 % reduction. See Figure 28.

The normal conducting current and superconducting current is coordinated successfully under dynamic conditions. (Jiang, Wenxue; Zhou, Kai; Lv, Jiangwei; (2014))

| EMS scheme | 300 μm | | | 200 μm | | | Unit |
|-----------------------------------------|-------------------|-------------------|-----------------|-------------------|-------------------|-----------------|------|
| | P_{coil} | P_{line} | P_{em} | P_{coil} | P_{line} | P_{em} | |
| Proposed superconducting EMS scheme | 10.9 | 84.4 | 95.3 | 10.5 | 102.5 | 113.0 | W |
| Comparable normal-conducting EMS scheme | 255.6 | 84.4 | 340.0 | 308.2 | 102.5 | 410.7 | W |
| Reduction of power consumption (%) | 95.7 | 0 | 72.0 | 96.6 | 0 | 72.5 | |

Figure 28 Results achieved from the experiment

Again, the size of electromagnets to levitate an operational stacked system in CNC possess a problem in magnetic bearings and their relative cost.

2.1.6: Dynamic characteristics of a direct-drive air-bearing slide system with squeeze film damping:

The dynamic stiffness of the air bearing slide depends on the availability of the damping in them which is quite low. In order to increase the dynamic stiffness, the damping must be increased this can be done with the help of integral oil-lubricated squeeze film dampers. No sealing arrangements are required as magnetic oil is used in the dampers. The resulting position accuracy and motion errors are less and the slide has little size variance.

The air bearing damping is a function of bearing area and operating gap, increasing the area of bearing and reducing the operating gap increases damping.

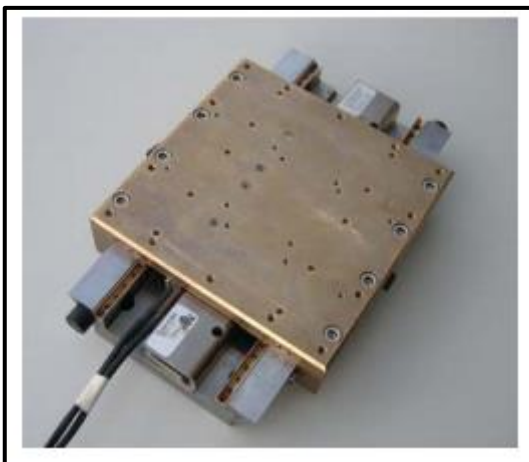


Figure 29 Air bearing Slide consisting of direct drive motor and squeeze film dampers

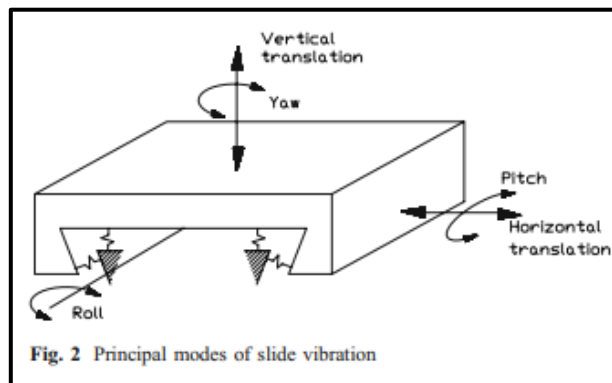


Fig. 2 Principal modes of slide vibration

Figure 30 Slide Vibration Principle Modes

The results can be summarised as follows,

Three conditions were taken one with no damping oil, one with squeeze damping with oil viscosity of 5000 cp and the other with oil viscosity of 1000 Cp.

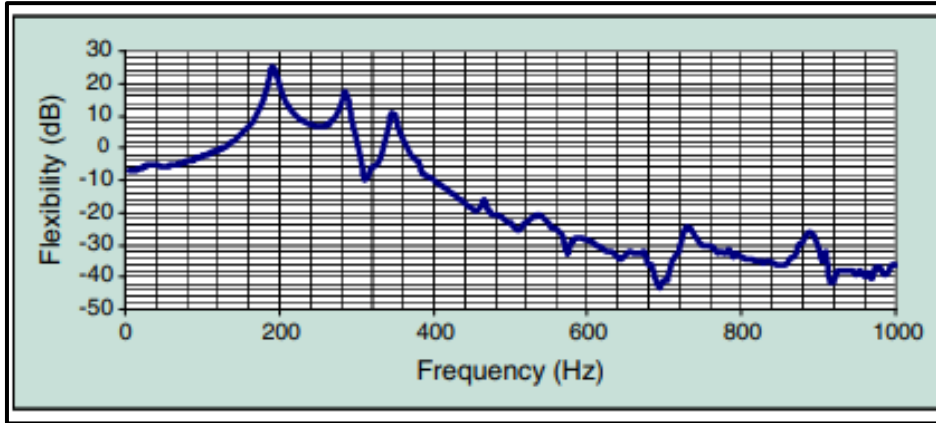


Figure 31 Response to offset vertical force

The dynamic flexibility in the vertical direction by 1000 cp viscous oil was reduced from $0.72 \mu\text{m/N}$ to $0.14 \mu\text{m/N}$ and to 0.061 by 5000 Cp of viscous oil (see Figure 32), To excite the roll mode and the vertical mode of the slide a force was applied at the carriages side edge, this also resulted in the pitch mode. This caused the dynamic flexibility under 1000 cp viscous oil to reduce from 1.5 to $0.48 \mu\text{m/N}$ and under 5000 cp viscous oil to reduce to $0.28 \mu\text{m/N}$ (see Figure 33), Vertical and pitch modes were excited by applying a vertical force at the leading edge in between the bearings midway, the result was also the excitation of roll mode. The corresponding reduction of Dynamic flexibility was almost from 1.54 to $0.36 \mu\text{m/N}$ for all cases approximately (See Figure 35). The roll mode of vibration was excited when the yaw plus horizontal translation and horizontal translation was excited the dynamic flexibility reduced significantly but has a lesser difference between the flexibility at different oil viscosities.

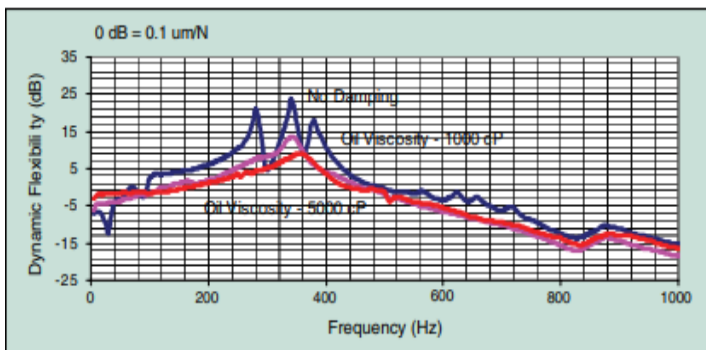


Figure 33 Offset Vertical force on slide of carriage

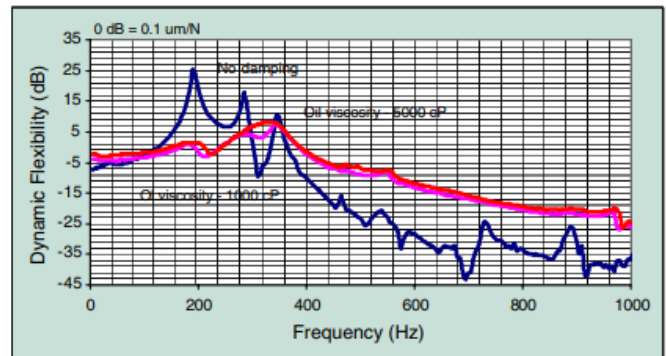


Figure 32 Vertical force response of air slide

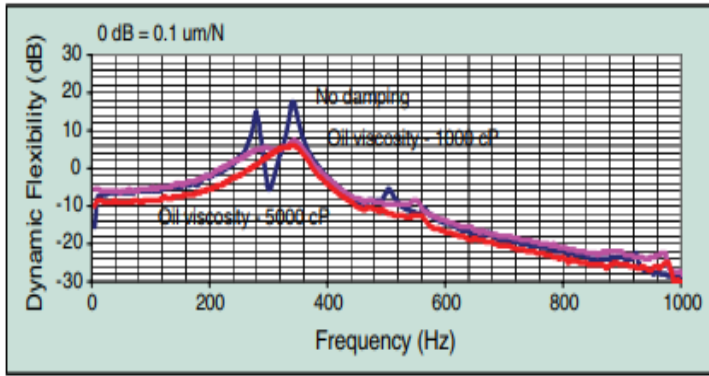


Figure 34 Response of Horizontal force given by Air Slide

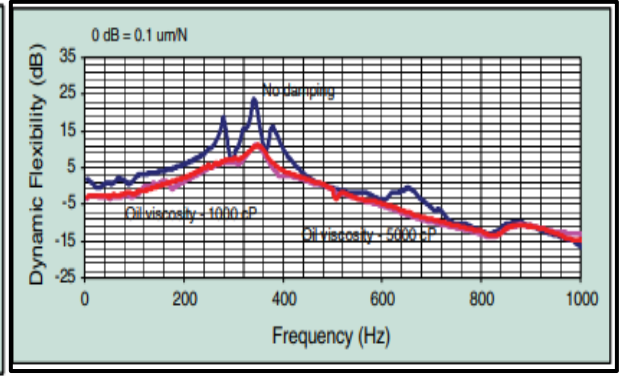


Figure 35 Vertical force on leading edge of carriage response of Air slide

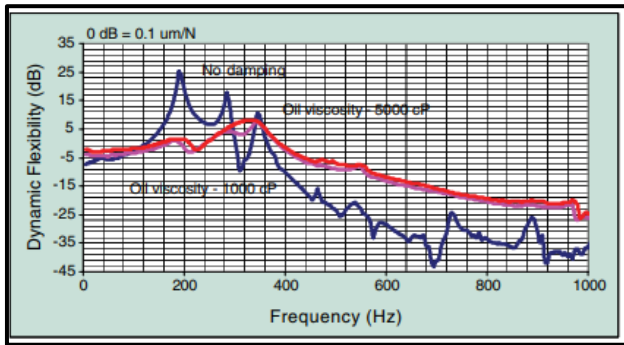


Figure 36 Response to offset horizontal force given by the slide

The dynamic flexibility reduced from 0.74 to 0.19 N/ μ m See Figure 35, it reduced from 1.83 to 0.24 μ m/N. See Figure 37 above.

Also, Dynamic performance under machining condition was investigated using a face turning with the motion of the slide being in parallel to the disc face. This results in the forces due to cutting acting horizontally dominant (normal forces) and shear forces or vertical forces perpendicular to the translational direction. The results show that the surface finish without damping accounts for 0.51 μ m Ra gets reduced to 0.01 μ m Ra under the damped system.

The measurement was carried out with the help of the impulse response of the slide. This was done with the help of readings taken at five different positions corresponding to the effect on five rigid body modes of vibration. Dynamic flexibility as a function of frequency was automatically formed by FFT.

2.1.7: Porous Ceramic Water Hydrostatic Bearings for Improved for Accuracy Performance

Aerostatic bearings are very good at thermal stability compared to hydrostatic bearings which have a bad reputation for thermal drift, but because of the stiffness required for various machining processes, hydrostatic bearings are much stiffer than aerostatic bearings.

The porosity in the porous material in hydrostatic bearings increases the load capacity of the bearings as many feed restrictors can be integrated in the porous material spreading the pressure with optimal distribution around the surface (See Figure 38). This requires careful control of porosity. Studies show that porous metal bearings block the pores when they get smeared due to local plastic deformation, this reduced their life and workability (Kumar). The machining process of these porous materials is also responsible for the smearing of pores. (Kwan). This demands the following design.

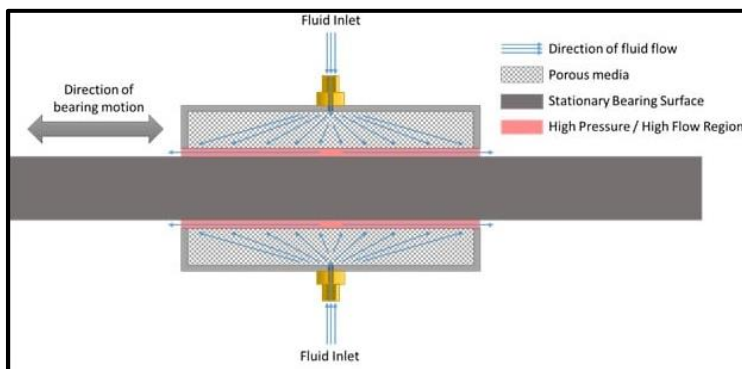


Figure 38 :Shows Uniform pressure distribution due to porous media, Non-Contact Hydrostatic Fluid Bearings - ULS Innovation. (2020).

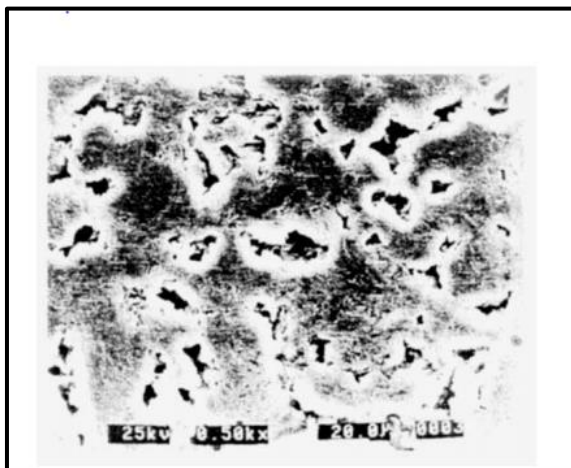


Figure 37: With the inclusion of pore smearing a SEM Analysis of diamond turned porous graphite is shown.

Ceramic advantages:

Problems of thermal drift don't exist as a low coefficient of linear expansion is present, over a wide range of temperature ranges the dimensional stability is maintained along with stiffness. Wear is comparatively less; corrosion is nearly negligible in most ceramics when immersed in water.

Water advantages:

Friction power and heat generation reduction due to low viscosity, clean environment than oils, the wide range of temperature controllability due to higher specific heat than oil.

Porous Bearing advantages:

Load capacity and stiffness are increased with the number of pores with the help of uniform pressure distribution, the hydrostatic bearing pocket is eliminated and the utilisation of the lubricant film hydrodynamic pressure is more efficient, before the onset of turbulence the higher speeds are more possible with the elimination of the hydrostatic bearing pocket, damping is considerably increased with the bearing gap being adjacent to the permeable surface and the due to the squeeze film effect.

To manufacture these types of bearings new machining methods must be established and many problems must be overcome. This guarantees the structural control for bearing performance. The processing aims discussed in this paper are:

Influence on mechanical properties of the porous ceramic structure and the fluid flow driven by processing parameters, Control of processing parameters demand an establishment of a mathematical model for their precision which has been carried out in this paper, pore size distribution and the porosity level has been correlated with the fluid flow properties.

Flat discs and Journals were used as test specimens made out of alumina powders of size range 5 μm to 400 μm , the fluid in the former was air and later was water for which a separate rig was designed. (Corbett, J; Almond, R.J; Stephenson, D.J;(1998)). (Porosity and the mechanical properties of aluminium welds. (2020)),

| <u>Powder size</u> | <u>Viscous permeability</u> |
|--------------------|-----------------------------|
| 23 μm | 0.625 μm^2 |
| 13 μm | 0.111 μm^2 |
| 7 μm | 0.071 μm^2 |

Figure 39 Viscous permeability with powder size

2.1.8: Cage Speed of Hydrodynamic Rolling Hybrid Bearings

Due to absence of sufficient film pressure the sliding surfaces of bearing system are unavoidable during start-up and shut down processes this causes extreme wear in the hydrodynamic bearings this consequently leads to changes in the thermos-hydrodynamic performance and Dynamic and static characteristics of the regime, gaseous cavitation's and its stability.

In order to avoid these conditions, a new hybrid bearing has been proposed in the paper. The rolling element bearing with some clearance and hydrodynamic bearings combined together in parallel forms the new hybrid bearing

The bearing operates under two operational modes.

The shafts are supported by the roller element bearing when the oil film pressure in the hydrodynamic bearing is not sufficiently high to levitate the rotating shaft. This takes care of sliding of the shaft with the hydrodynamic surface.

At high speeds, the rotor starts to levitate under the action of oil film until it floats in the clearing of rolling bearing. This disconnects the roller bearing from the rotor. A clearance is kept between the inner ring and the roller elements with the help of magnets attached to the outer ring that keep the rollers attached to the outer ring this ensures no contact with the roller elements at low load high-speed conditions. *See Figure 40 below.*

Due to large clearance less, preload is there in the roller bearings and this can cause low stiffness at high speeds and more dynamic flexibility to avoid this bearing is designed so that the roller only supports the shaft at very low speeds.

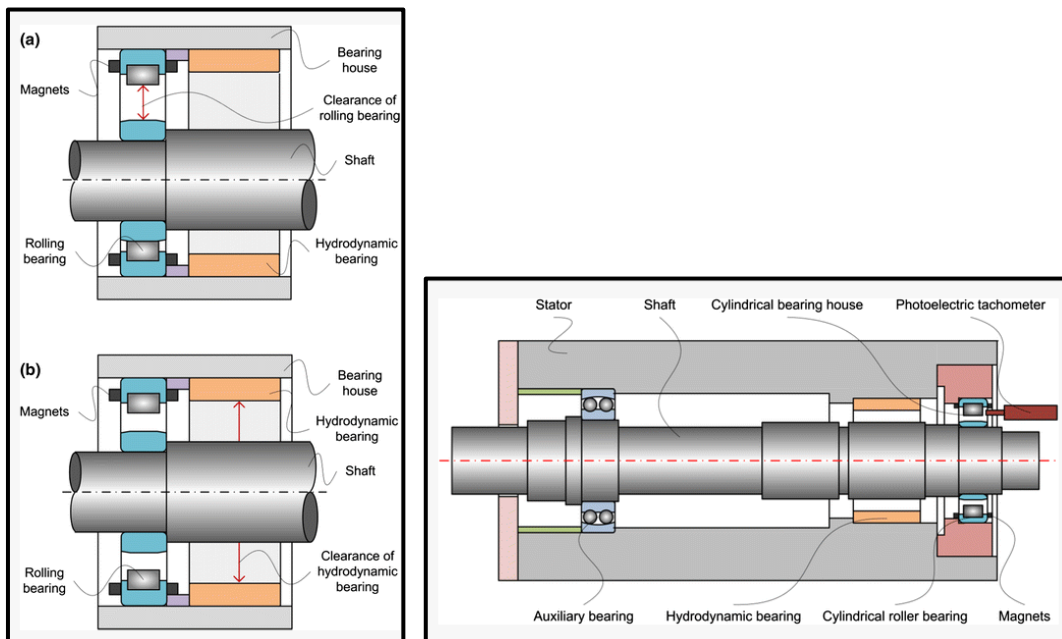


Figure 40 A Hybrid Bearing supported by hydrodynamic bearing at high speeds (b) and at low speeds supported by rolling bearing (a)

Comparing the start-up and shut down processes leads to the graph as shown in *Figure 41* where the speed increases from 0 to 1500 rpm and decreases from 1500 to 0. It can be noted the cage does not start to rotate until the speed reduction of 900 rpm, it suddenly starts to rotate at 214 rpm, therefore, the start speed in the slow down process is lesser 25 % than end speed of the start-up process.

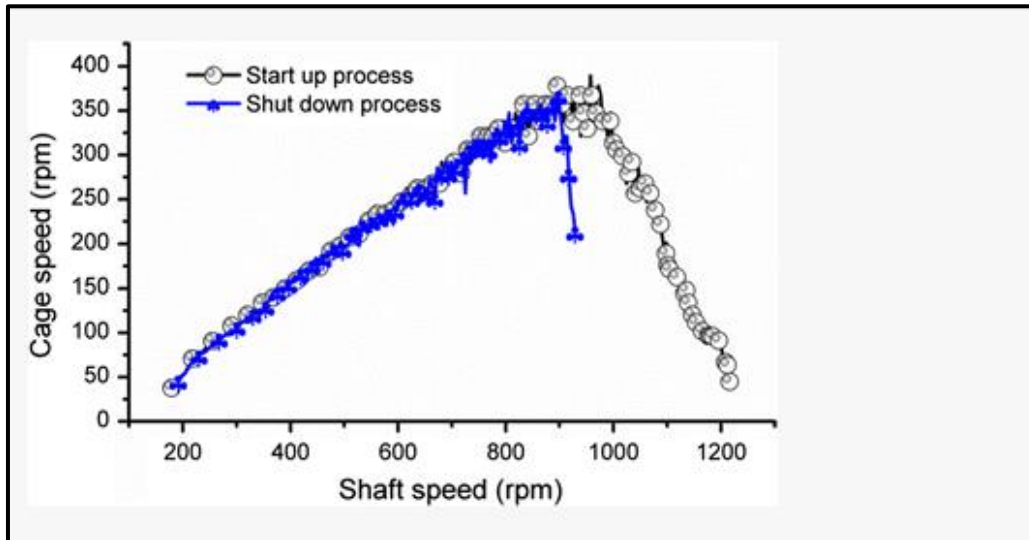


Figure 41 Start up and Shut down process cage speed comparison

Severe wear in the hydrodynamic bearing during starts and stops is avoided in this structure because the rolling bearing prevents direct contact between the rotor and the hydrodynamic bearing. (Lu, Dun; Zhao, Wanhua; Lu, Bingheng;(2013)).

2.1.9: Investigations on a permanent magnetic–hydrodynamic hybrid journal bearing:

Another similar hybrid bearing has been developed. Instead of roller elements, this design uses permanent magnets in combination with the hydrodynamic bearing. The design uses a permanent magnet instead of electromagnets because of the addition of power amplifiers, controllers and sensors in electromagnets which increases the cost.

A pair of permanent magnet rings and a regular journal bearing bush together form the hybrid bearing. The radial repulsive force between the inner and outer rings is formed by the axial magnetisation of the rings. The rings and the bush are axially separated. The outer magnetic ring is adjusted relative to the inner magnetic ring to generate the force. Increasing the Eccentricity decreases the magnetic force. Thus, it levitates the rotor and avoids any sliding with the bush during start-up and slow down at low speeds when a hydrodynamic film is not formed. Magnetic film force equations have been developed in the paper and

classical hydrodynamic calculations are used for another bearing. see *Figure 43 below*.

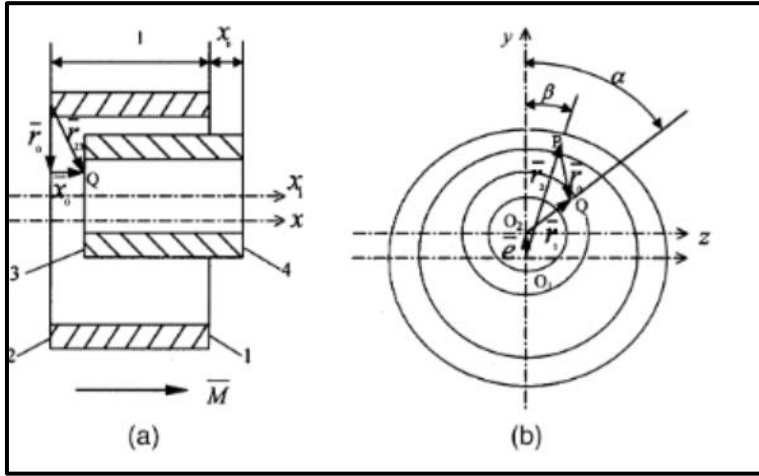


Figure 42 Magnetic Ring Coordinates

It can be concluded that at a developed high speed the force can be represented as the combination of the hydrodynamic and the magnetic force. when the shaft slows down. The experiment adds two vertical loads one (W_a) at which the magnetic eccentricity is created by the inner ring due to shifting down and the other (W_b) at which the bearings on fully supported by a hydrodynamic bearing. Sensors are used to measure the eccentricity of the magnets and of the shafts and bushing centres etc. See *Figure 44 below*

Due to restrictions of the gap between the bush and the inner ring the eccentricity is limited hence the magnetic force is limited, due to higher stiffness of hydrodynamic bearing (low dynamic flexibility) than the magnetic film the magnetic force uncouples (or has no effect on the hydrodynamic film and the shaft rotates on hydrodynamic film. (*Tan, Qingchang; Li, Wei; Liu, Bo (2002)*)).

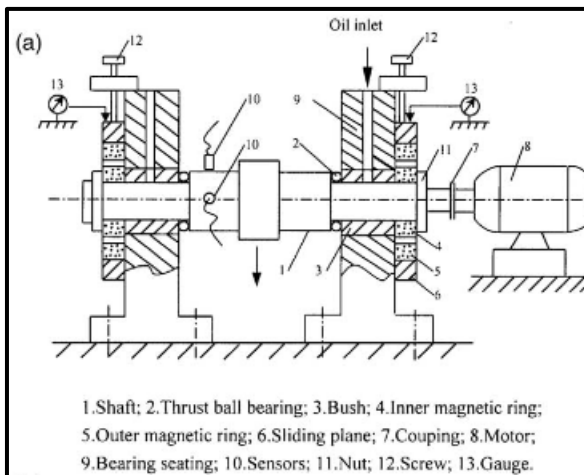


Figure 43 Prototype set up

2.1.10: Hybrid bearings for turbopumps

Us patent by inventors v have also solved the problem of start-up and or shut down issues of hydrodynamic bearings with the help of optimised hybrid bearing design. Due to lack of high-pressure during start-up and shutdowns not enough lubrication is present to produce a hydrodynamic film in the bearing. These bearings have the application in the turbopumps which mix, pressurise and direct the fuel and oxidiser used for rocket engine power combustion. The first design as shown in (See Figure 45) utilised two bearings duplex bearings having their outer rings locked to the rotating annular collar or sleeve. The inner races are

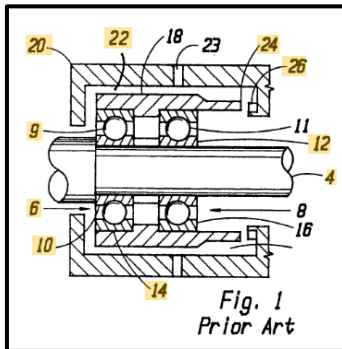


Figure 44 Hybrid Bearing Design Schematic

locked to the shaft or the journal, outside the collar there is a gap between the bearing housing and the collar itself this is used as the gap for hydrodynamic film and the flow for the hydrostatic fluid. Liquid enters through 23 and flows. The collar has a thrust plate attached to it with its other mate being attached to the housing itself to avoid any thrust forces to the ring collar due to the pump.

This design has disadvantages: As the pump speed increases the hydrostatic bearing stiffness increases causing the collar lag behind the journal speed and due to this speed difference wear in the roller bearings can occur. Another disadvantage is that the wear in duplex bearings is not even. To avoid this the new design has been proposed, this design mounts the roller bearing and locks it stationary housing. The new design includes a bearing housing on which the roller bearings is mounted. the housing contains the journal and between the journal and the housing is the gap for the fluid to flow. A transient support ring is used to switch the modes from roller bearing to hydrodynamic support. The key has teeth that latch or lock into the grooves in the roller ball bearing. as the speed of the journal increases the centrifugal force pushes the teeth out and the system latches making the journal float on hydrodynamic film. As the speed lowers the centrifugal force becomes less and the keys are locked making the journal rest on the ball bearing. The Transient ring centre is keyed to the journal centre so that there is minimum eccentricity. The support retainer is also attached to the shaft adjacent to the transient ring. At higher Rpm's instabilities can occur which causes the system to vibrate in order to avoid this the load is shared by the ball bearing too for compensation with the help of this retainer that force the fingers into the groove. (John F. JustakGregg R. Owens, US5348401A).

2.1.11: WJRM hybrid linear bearing

To reduce the impact of heavy loads and the drive force required by the system Hybrid linear bearings comprising of rollers and plain plastic bearing surface which is tribologically optimised has been designed. Plain bearings protect against the friction or any lateral loads while as the rollers reduce the drive forces. The bearings are very useful in manual handling applications where the absorption of abuse forces is necessary.

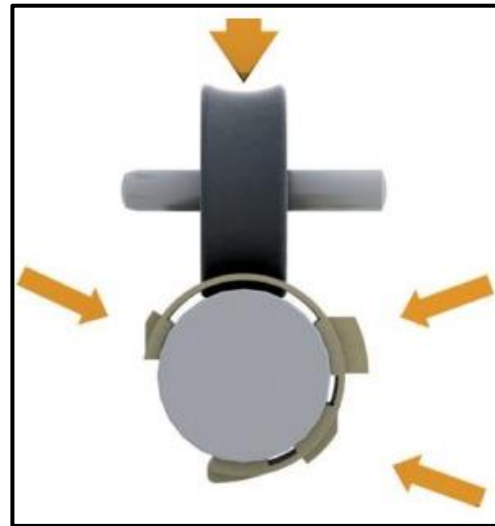
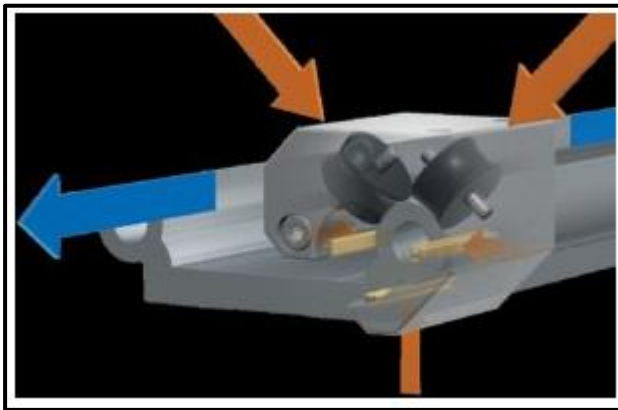


Figure 45 Double roller type (21) force absorption

The bearings are very efficient for example 25 pounds of drive force (at static coefficient of friction 0.2-0.25) is required in manual sliding application of moving a door of 100 pounds with the help of sliding bearing but the hybrid bearing reduces it to 5 pounds. Also, they don't require any external lubrication and are a good alternative to cam rollers or linear ball bearings. (See Figure 46)

Two configurations are present a hybrid bearing with one roller, a bearing housing and plain bearing liner and a hybrid bearing with two rollers comprising of two rollers set at an angle usually 70 to 80 degrees used in heavy loading applications. Here the 2:1 (chatter or binding happens if the applied force location is greater than twice the bearing length) this rule can be increased to 5:1 rule. (The 2:1 Rule and How to Define Fixed and Floating Bearings. (2020)), (Santora, M. (2020)).

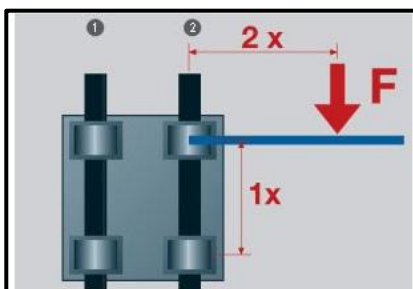


Figure 46: 2:1 Rule

2.2 DRIVE TRAIN DESIGN:

This section covers the areas of research concerning the drive train component of the feed drive system various new concepts have been researched thoroughly studied in-depth and critically appraised.

2.2.1: New Slide with Friction Drive

The position precision of 16 nm has been achieved with the help of the new linear slide design. The system works within 220 mm range and incorporates a high axial stiffness. A friction drive is used in the system to cause the translation motion this is used as an actuator. Thermal expansion can cause various issues in the geometry of the structure and hence the precision of the slide to avoid this a Zerodur Material is used in the guideways and hydrostatic bearings have a controlled temperature environment. The optical quality of flatness equal to $\lambda/2$ is posed by the guideways. Due to the 15 times better, internal damping ratio than steel and a very low thermal expansion coefficient of ($7.5 \mu\text{m}/^\circ\text{C}$) the base used is made of granite.

Three hydrostatic bearings are used which helps the steel carriage to float over them. This ensures smooth translation motion with a less stick-slip phenomenon. The yaw is minimised with the help of lateral bearings which also ensures maximum straightness in the lateral direction. The chosen load and supply pressure require the related film thickness and the stiffness which is defined by the fixed element in each bearing. The pistons in the preload bearing part apply the adjustable pressure and hence the adjustable preload. Also, the natural frequency of the piston bearing preload pad is higher $\omega_{np}/\omega_{nm} \approx 10$ about 10 times the main pad due to its lower mass compared to the main pad bearing the slide too. This ensures that the effect of the natural frequency of the preload pad has less effect on the overall resultant natural frequency and also the precision movement. The stability of the bearing is also kept in higher-order due to the presence of bearing surface, fluid viscosity alveolar pressure and capillary length which increase it and the presence of capillary gap and diameter which decrease it. See Figure 48 and Figure 49 below.

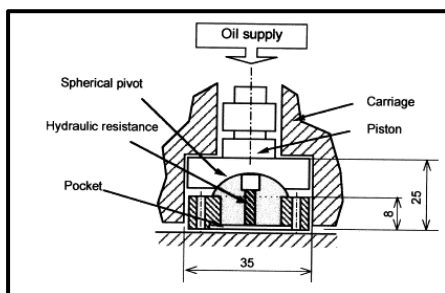


Figure 47 Hydrostatic bearing Preloading

The parasitic movements can be reduced by using flexural Components which provides dynamic decoupling of the actuator and the slide. High frequencies of above 1 kHz can be related to the carriage vibration.

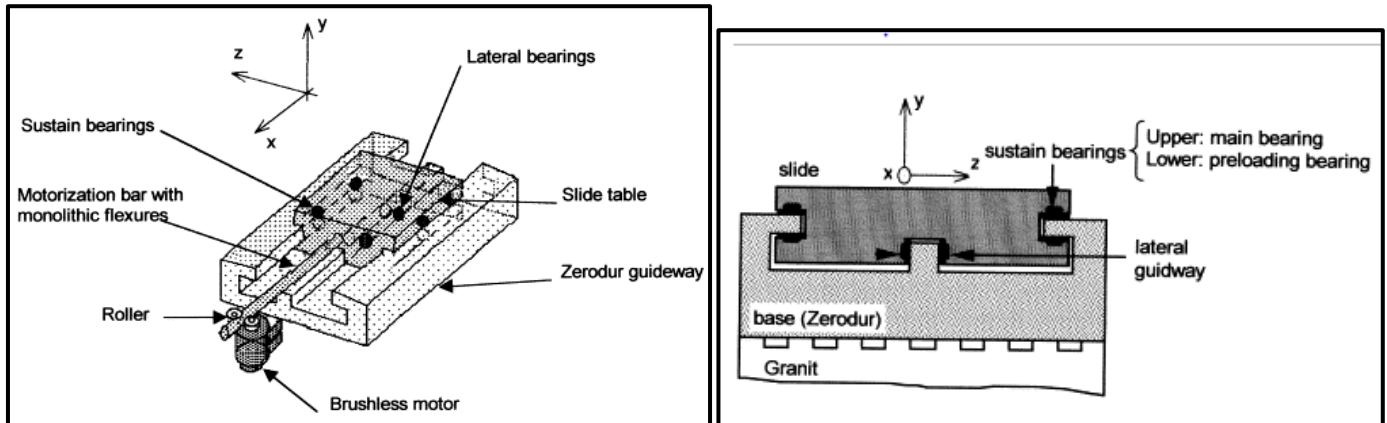


Figure 48 Hydrostatic bearing schematic

Natural frequencies of the whole system show a preponderance of vibration modes of the friction drive; the carriage vibrates at high frequencies (>1 kHz).

A monolithic flexure was used between the slide and the traction bar while as coupled reinforced flexures were used between the friction drive and the base thereby reducing the forced geometric congruence. See Figure 50 Below.

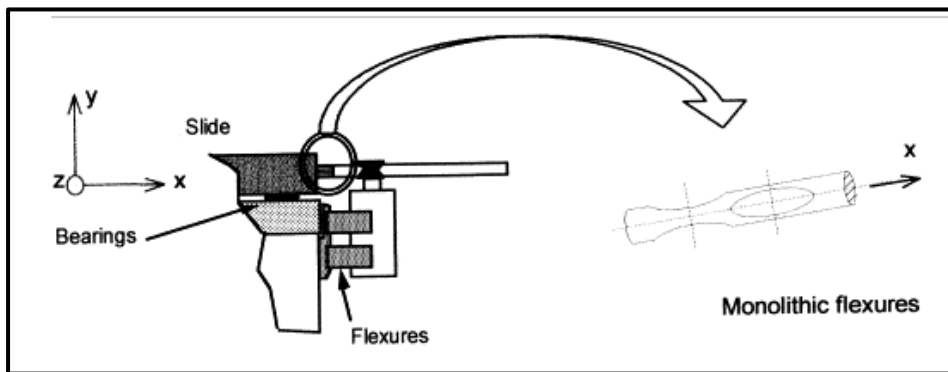


Figure 49 Friction drive mounting

Dynamic Stiffness of the table should be higher than the Dynamic stiffness of the friction drive this consequently reduces the effect of friction drive parasitic torques on the table.

The experiment shows that this has been achieved.

| Input pressure (bar) | Pre-load (bar) | Stiffness (N/ μm) | Film thickness (μm) | Dissipated power (W) |
|----------------------|----------------|-------------------------------|----------------------------------|----------------------|
| 100 | 80 | 240 | 11.7 | 1.8 |
| | 90 | 258 | 10.8 | 1.6 |
| | 95 | 265 | 10.4 | 1.5 |
| | 100 | 277 | 9.9 | 1.4 |

Figure 51 Hydraulic bearing Characteristics with varying preloads

| Modes of vibration | Drive dynamic stiffness (N/ μm) | Carriage stiffness (N/ μm) |
|-------------------------|---------------------------------------------|----------------------------------------|
| Mode 1 Flexion around Y | 25.3 | 44.5 |
| Mode 2 Pitch | 46.5 | 67.3 |
| Mode 3 Roll | 246.7 | |

Figure 50 Slide bearing and drive stiffness comparison

The vibration in the carriage happens at high frequencies at around 1 kHz and the Vibrations of the friction drive happen around when the pitch is at 227.6 Hz a, the roll is at 673.4 Hz and yaw is at 49.8 Hz. The experimental natural frequencies also agree well with the simulation data. The experiment was carried with the help of hammer tests using piezoelectric force transducers and B and K accelerometers. See Figure 53 Below.

The Dynamic analysis of the combination of friction drive and the carriage has also been carried out and the vibration from friction drive laterally is about 122 Hz and the pitch are about 249 Hz. This proves that the carriage has a high level of damping and suppresses these vibrations and is not excited until a natural frequency above 1000 Hz is transferred to it. See Figure 53 below.

In the simulation, the carriage was analysed with the help of meshing it to 3d elements with bearings acting as spring elements. Similarly, the whole friction drive was modelled as 3d elements and meshed with the contact between the rollers and the bar being represented as spring elements. (Mekid, Samir, 2000)

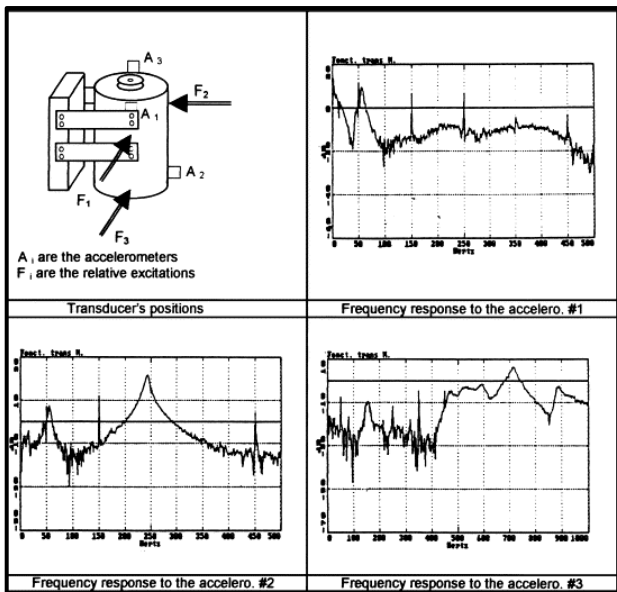


Figure 52 Vibrational Analysis of the drive

2.2.2: A Twist-Roller Friction Drive for Nanometre Positioning - Simplified Design Using Ball Bearings

Some sub nanometre positioning systems employ, the capstan friction drive, hydrostatic lead screws and ball screws.

A new driving mechanism called the twist roller friction drive has been redesigned and experimented in this paper. The new designed drive reduces the use of hydrostatic bearings in the drive to the simple roller bearing design. Since there is a friction between the rollers and the drive shaft a hydrostatic bearing was employed that also used the hydrostatic guideway in the system, but this design is complicated and requires difficult machining process for the rollers. Also, the oil used in the whole positioning system makes the environment less clean and prone to contamination. (Mizumoto, H; Arii, S; Yoshimoto, A; (1996)). See Figure 54 and Figure 55 below.

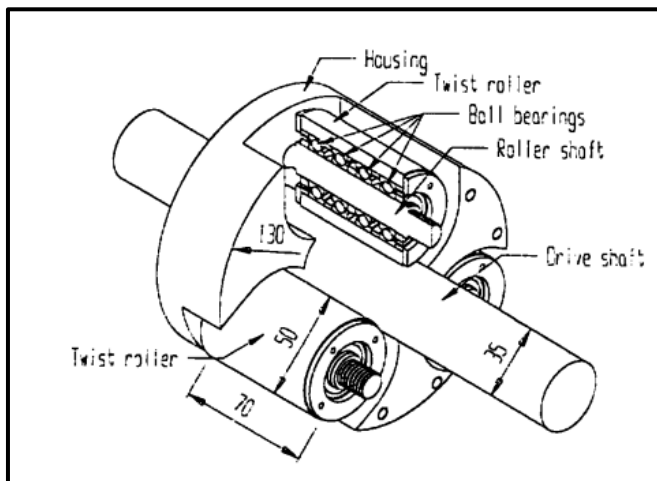


Figure 54 Twist Roller Friction drive mechanism

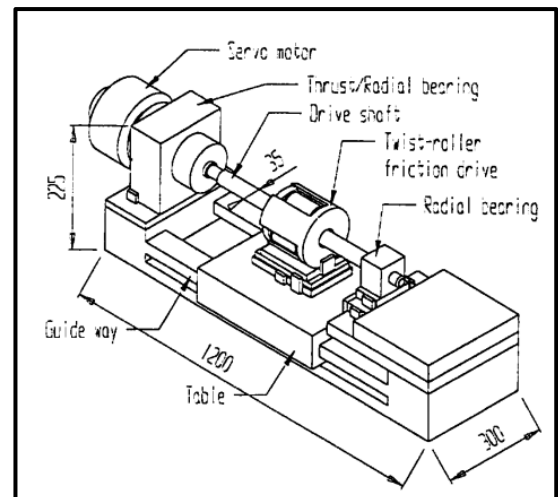


Figure 53 Twist roller friction drive nanometre precision

2.2.3: Ultra precision Feed System Based on Walking Drive:

2D Dimensional Design:

In this paper, the stroke of a piezo-electric actuator has been increased directly through the development of a mechanism based on alternative clamping or walking. Utilising the deformations in the piezo electric actuators a new feed system that has a long stroke and can feed with smooth and continuous action with high rigidity has been developed. Similar to the walking motion of animals each clamp set (a pair of clamps) uses 4 piezoelectric actuators 2 for clamping and decamping action and 2 for feed action. The motion of the table is controlled using the laser feedback.

As shown in the *Figure 57 and Figure 58*, the moving part is fed smoothly and continuously even in the open loop mode. The static stiffness of the feed device in the feed direction measured is about 400 N/ c1 m, which is extremely high as compared with the conventional feed devices.

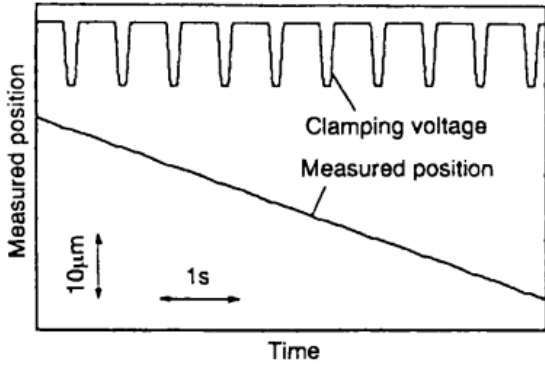


Figure 57 Open loop Constant angular velocity feed motion

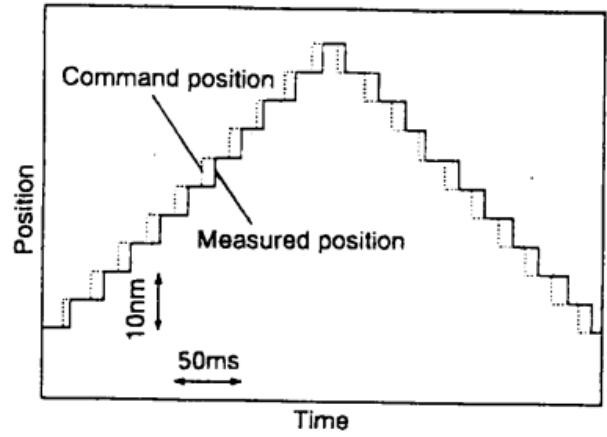


Figure 58 Positioning stepwise result with 5nm step

Fig shows that the in the clamping direction the errors have been reduced to 0.02 μm and to 0.05 sec in the yawing direction with the help of additional position control. Also, a slight deformation in the clamping voltage can be depicted as compared to the clamping voltage graph without control this is simply because additional control voltage is added to clamping voltage,

Also, there is an extremely high static stiffness of 400N/ μm in the feed direction. The motion resolution was tested at 5nm increasing and decreasing steps. See *Figure 59 below*, this is also the corresponding resolution for the laser interferometer. Increasing the resolution of laser interferometer can yield even better results.

The feed motion produced by each PZT is 1.5 μm . (*Moriwaki, Toshimichi; Shamoto, Eiji, (1996)*).

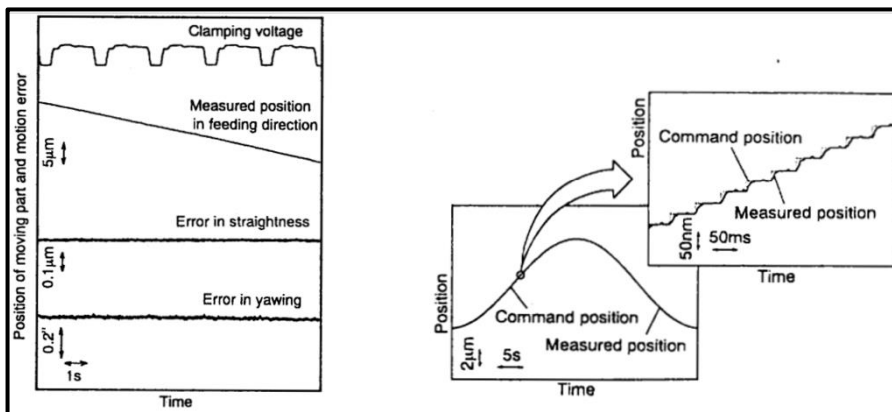


Figure 59 Straight motion and feed motion errors after utilising the feedback control for error compensation left and Command vs measured position Comparison right.

3-Dimensional Design

In this paper, the application of the walking drive concept on the 2 axis X, Y and One rotational axis has been developed, designed and experimented. The system consists of a table with three drive block pairs each block has three piezoelectric actuators that deform in X, Y and Z directions respectively. When the conventional mechanism is applied to multi-axis motion control, one table driven in each axis is stacked upon another table. Thus, it is difficult to realize a simple and rigid feed system. The piezoelectric actuators attached to the table through contact block in each drive unit and hence there is no need for the guide system as the contact blocks both drive and support the table this gets rid of the stick-slip phenomenon that's common in other feed drives. The stroke each PZT is 8.4 $\mu\text{m}/85\text{V}$ and the table has the stroke of 100 mm, 40 mm and 20 degrees in the X, Y and rotational direction around the z-axis. When two pair of blocks support the table the vertical stiffness of the table is 134N/ μm and 98 N/ μm in the feed direction. and when one block supports the table the feed stiffness is around 53 μm and vertical stiffness is around 100 μm , with the weight of 13 kg the load capacity of the table is 33N.

The results from contouring control show that the control is very well followed by the drive with the errors of less than 10 nm. With vertical errors of 0.4 μm , See Figure 61, Figure 62. The point to point motion with 1mm stepwise positioning commands also confirm that steady state errors are less than 10 nm and there are no overshoots. See Figure 63

Also due to no stickup conditions as the errors are less and the system is rigid as the whole planar motion involves only drive for continuity. (Shamoto, Eiji; Moriwaki, Toshimichi, (1997)).

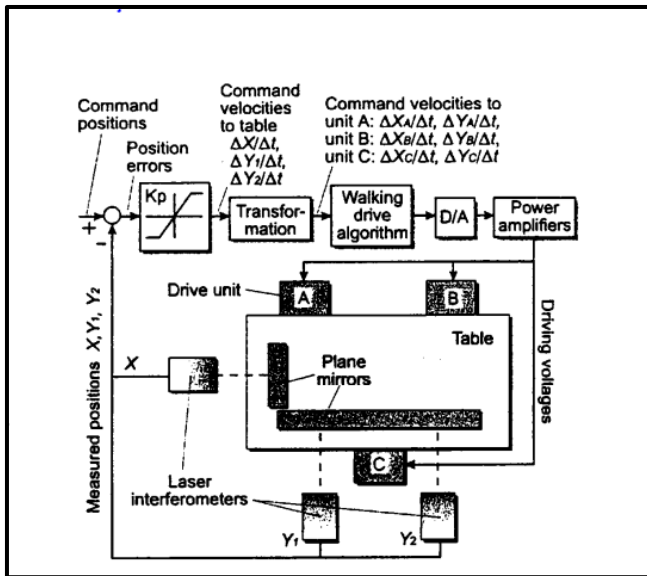


Figure 60 Developed Position feedback control system Diagram

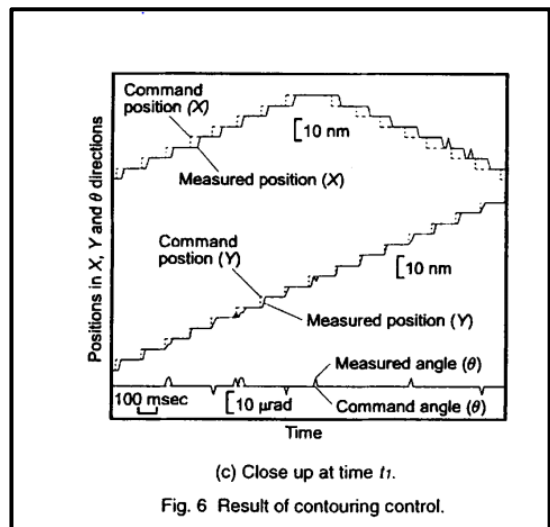


Figure 61 Contouring control result

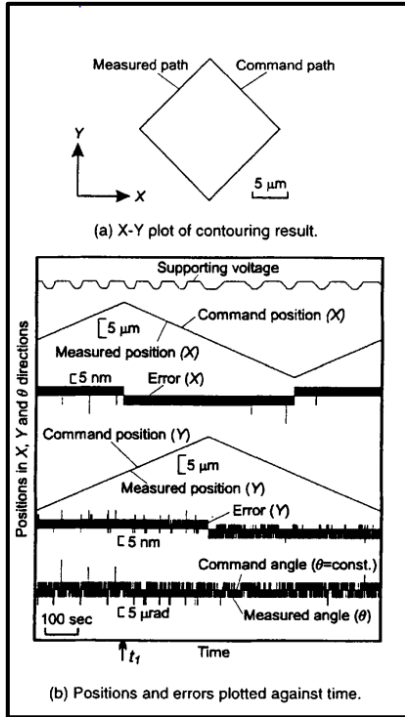


Figure 62 errors and positions plotted against time

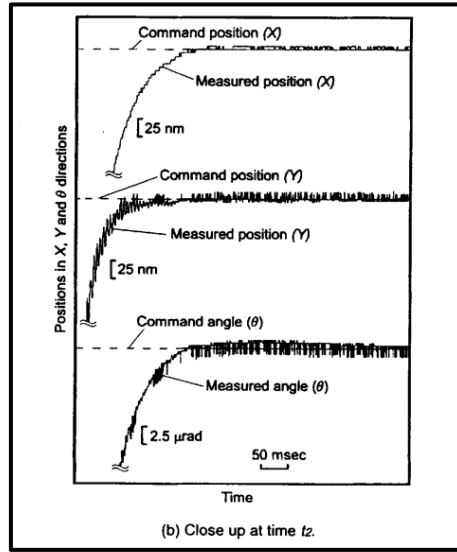


Figure 63 Point to point positioning Control result

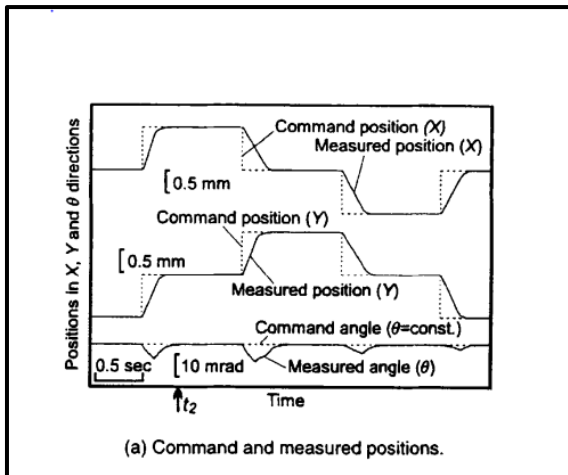


Figure 64 Measured positions and Command

2.2.4: Electrohydraulic actuator

In this Paper an Electrohydraulic actuator is used as an active damping device with the velocity loop feedback. The Chatter is reduced by reducing the dynamic flexibility of the machine by 80% and hence stability. The damper was put on the workbench that had a workpiece on it *See Figure 65 below*. The dynamics were in relation to the tool and the workbench. as the tool cuts the work piece in steps it can be observed chatter vibrations were reduced. It uses servo valves which controls the oil flowrate. See (Brecher, C; Schulz, A;(2005)) *for results*. It may limit the size of work piece to be used. (Brecher, C; Schulz, A;(2005)).

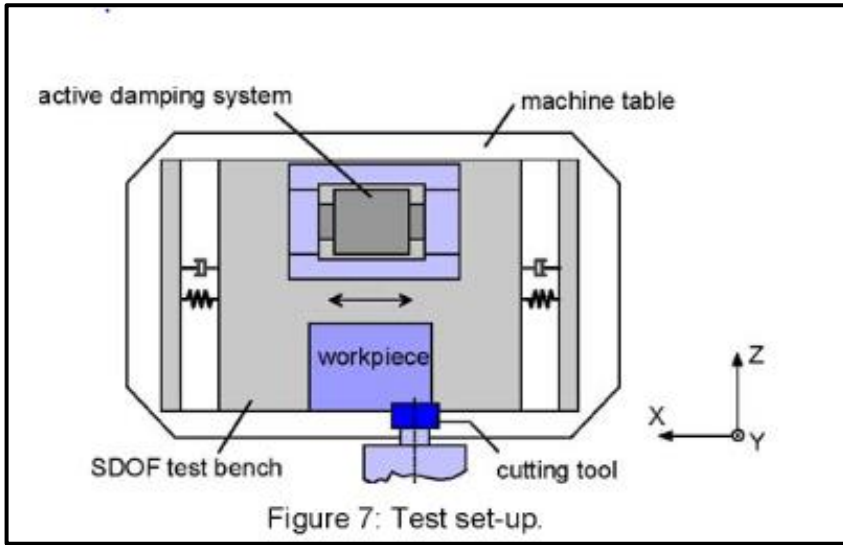


Figure 65 Set up of the test

2.2.5: Voice coil motor infer meter and ball screw sub nanometre drive

A sub Nano-metre (0.3nm) feed drive is designed and implemented in this paper , The laser interferon meter (homodyne interferometer) feedback system in combination with hybrid actuator system comprising of Voice coil motor and a ball screw are responsible for long stroke (150mm) sub Nano-positioning

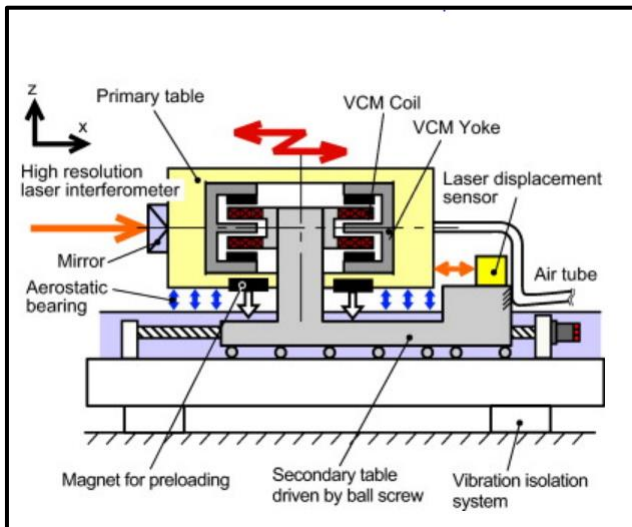


Figure 66 Proposed table system structural concept

| | |
|-------------------|-----------------------|
| Full stroke | 300 mm |
| Stroke of VCM | ±2.5 mm |
| Mass of table | 7.8 kg |
| Max. velocity | 220 mm/s |
| Max. acceleration | 5.35 m/s ² |
| Sensor resolution | 9.7 μm |
| Control frequency | 33 kHz |
| Stiffness | |
| Vertical | 326 N/μm |
| Horizontal | 326 N/μm |
| Straightness | |
| Vertical | 0.10 μm/100 mm |
| Horizontal | 0.18 μm/100 mm |

Figure 67 Developed Table system specifications

conditions. The primary table is isolated from the aerostatic guideways and is preloaded with the help of permanent magnets. The bearing used is aerostatic bearing for smooth motion. See Figure 66 and Figure 67. Above.

A relative constant displacement between the primary table and secondary table is maintained and the laser interferometer enables sub nanometre positioning. Since ambient temperature and external vibrations cause disturbances to the infer meter measurement the drive was isolated from the floor with the help of vibration isolation system and the temperature was controlled between $22 \pm 0.2 \text{ }^\circ\text{C}$. See Figure 68.

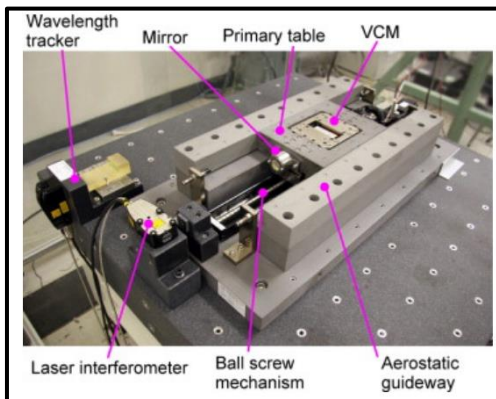


Figure 68 Table System Appearance

The Results in Figure 71 show 0.5 nm and 0.3 nm responses. At a feed rate of 100 nm/s and acceleration of 200 nm/s^2 a tracking error of less than $\pm 2 \text{ nm}$ is achieved See Figure 69 . At a federate of 100 mm/s and acceleration of 500 mm/s^2 the Figure 70 shows the command, tracking error and relative displacement between primary and secondary table. Between both the tables the maximum relative displacement of 1.5 mm can be observed with tracking errors of negligible margin.

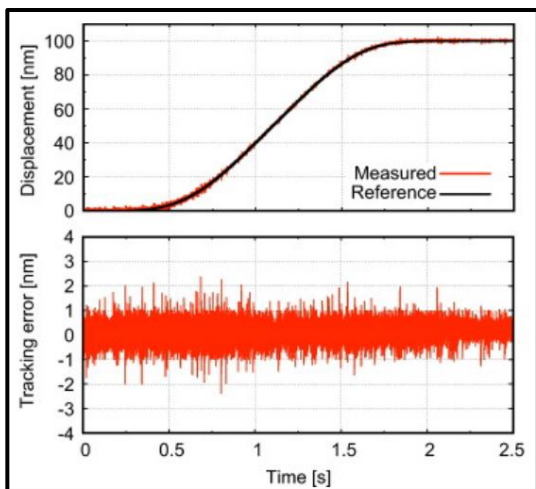


Figure 69 Tracking error at feed rate of 100 nm/s

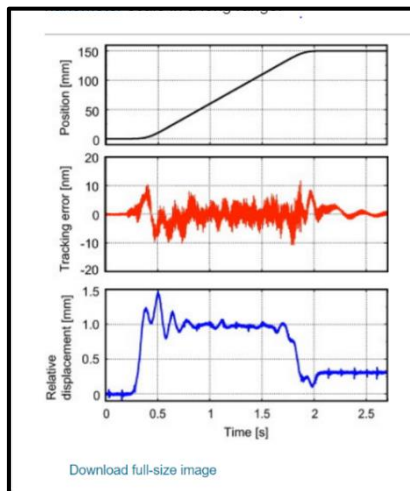


Figure 70 Shows long range (150 mm) tracking error

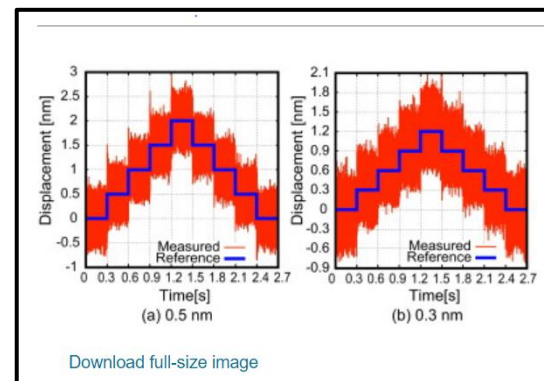


Figure 71 Stepwise response of sub nanometre

2.2.6: Using 3 Ball Screws for high Thrust with a Coupling.

Control and modelling of a single axis feed drive driven by a joint mechanism of three ball screw/motor units have been carried out in this paper. A mechanical coupling joins screw/motor system together for high power output. A system identification technique has been developed in this paper to derive a mathematical model for this coupled system. To further improve the performance of the system with mechanical coupling the master-slave control is adopted and designed. To design the synchronous compensators a genetic algorithm was used. The results show that there is a reduction of 50% in the synchronous error. Steady-state and tracking errors are also satisfactory. See Figure 72 ,(Hsieh, M., Yao, W. and Hsu, C. (2012),

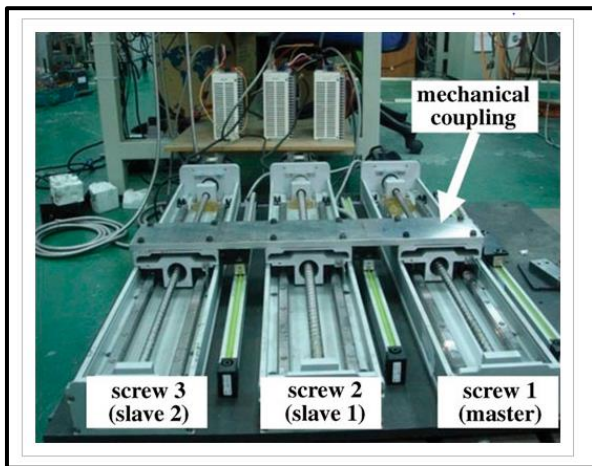


Figure 72 Shows a feed drive with mechanically coupled ball screws (Hsieh, M. , Yao, W. and Hsu, C. (2012), Modelling and control of a feed drive with multiple mechanically coupled ball screws)

2.2.7: Concept design with rack and roller pinion:

One of the novel methods could include designing a system with a drive system consisting of Rack and roller pinion drive by Nexen. Nexen claims that their less patented RPS has zero backlash for any required length with unmatched accuracy. The system doesn't need any

lubrication is 99 per cent efficient and emits extremely less noise. It has a proven record with a speed capability of 36 fps and accuracy to within ±0.00118 inch. This can be incorporated into the design or with the hybrid design with a disengagement mechanism for a linear motor switch. See Figure 73. (Nexen Product Navigation. (2020)).

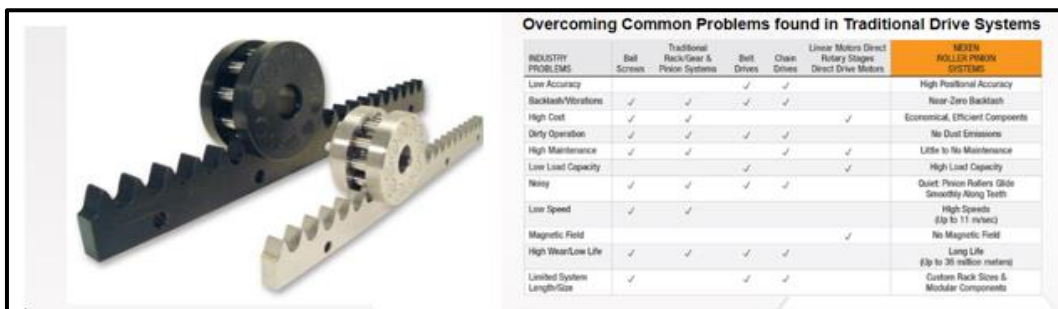


Figure 73 Shows and roller pinion (left) and its performance chart (right) (Nexen Product Navigation. (2018))

2.3 MISCELLANEOUS TECHNOLOGY AND HYBRID FEED DRIVES

2.3.1: Main Points from Drive centre gravity

This paper develops a system that uses twin screws to eliminate the yaw moments of y saddle that are responsible for Vibrations at high acceleration. Because the drive systems are not exactly near the centre of gravity of the system they can induce moments and these moments cause vibrations.

Vibration magnitude reduction with twin drive is reduced to 73 % using single axis simulation with twin control and to 82% in a dynamic state where both axes move. this was compared with the system driven with a single ball screw with the same machine.

They were based on simulation in CAE based on friction, elastic etc models.

The experimental data doesn't agree with simulation all times but at corners, it can be seen that twin-screw dominates. This is due to the non-linearity of the real machine and other noise. See Figure 74 Figure 75. Figure 76 and Figure 77 below.

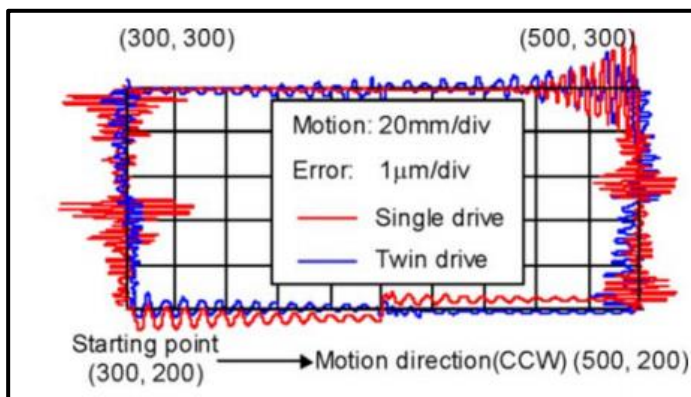


Figure 74 Motion Contour Simulated in Evaluation 1

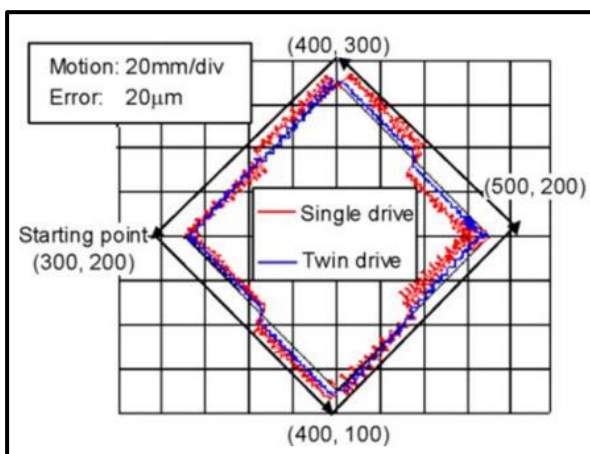


Figure 75 Motion contour Simulated Evaluation 2

Speeds at short and long corners are 22348mm/min and 15610mm/min. respectively. (Hiramoto, K; Hansel, A; Ding, S;(2005)).

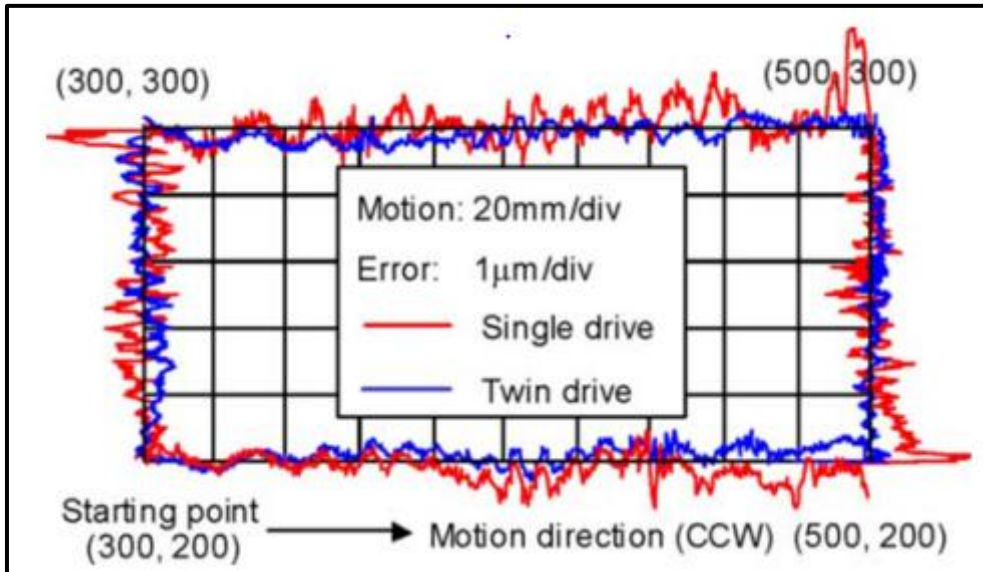


Figure 76 Evaluation 1 Experimental results

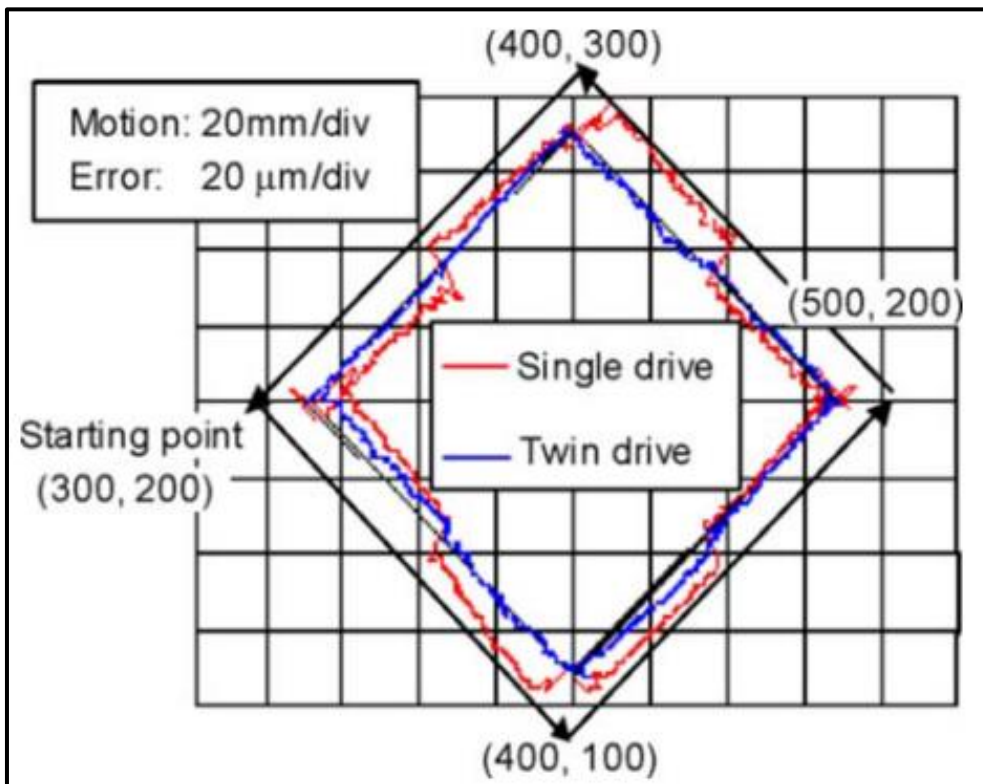


Figure 77 Evaluation 2 Experimental results

Twin screw may reduce moments, but if the motors are not synchronised crawling can occur, also it increases the mass and cost of the system to a significant level.

2.3.2: Energy optimized jerk-decoupling technology for translator feed axes

Jerk decoupling mechanism is very advantageous when it comes to vibration suppression in feed drive systems. This technology has proven records. In case of linear motors, the secondary part of the motor is mounted to the frame while as the primary part which is the moving part translates. Due to jerk, the force is transferred to the secondary part which is responsible to create equal and opposite force such impulses are then transferred to the mounting frame hence generating vibrations and limiting the dynamics of the system. See Figure 78

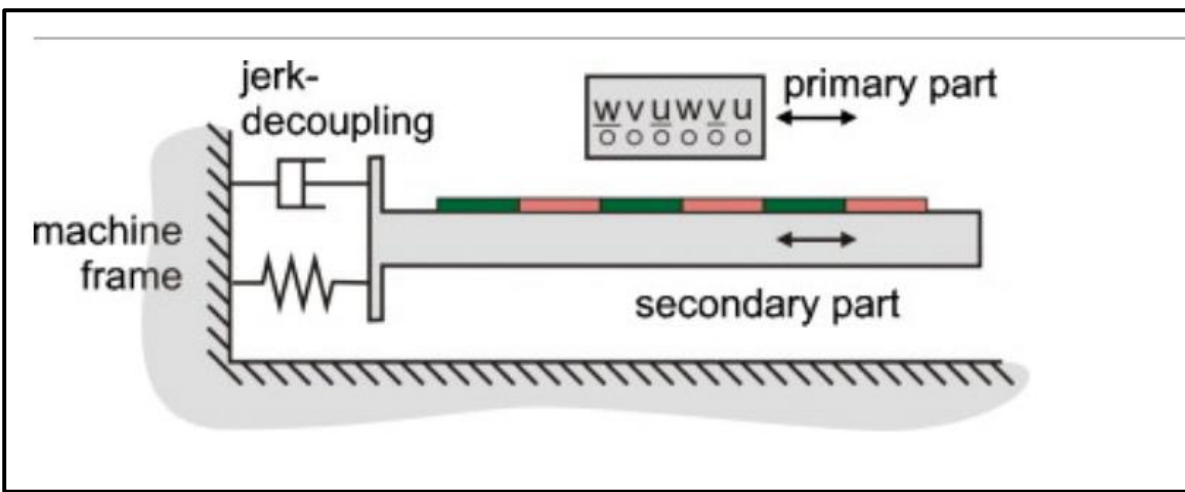


Figure 78 Jerk decoupling principle

Jerk decoupling mechanism works by isolating the secondary part from the mounting frame with the help of a passive spring-damper system which suppresses any impulses that can cause vibration.

Another paper by *Drossel, Welf-Guntram; Junker, Tom; Schmidt, Stefan; (2016)* uses Rubbers elements to damp the vibration which is an alternative. See Figure 79 below.

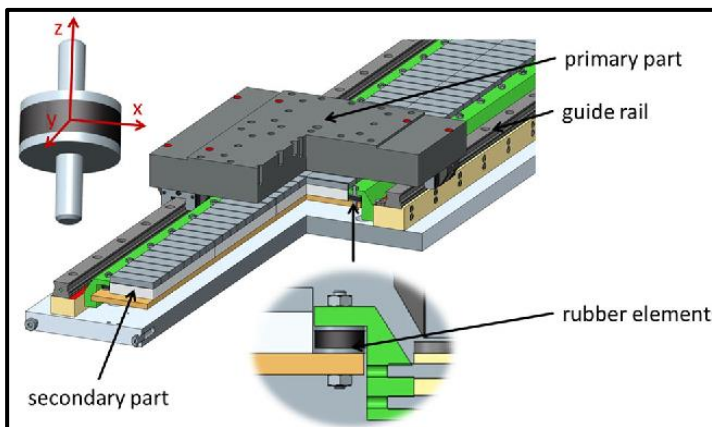


Figure 79 Decoupling unit comprising of rubber elements

2.3.3: Magnetically Levitated six degree of freedom rotary table

The concept of magnetic levitation is used in this paper to develop a micromachining centre, this concept was chosen because under varying loads air bearings don't provide the required stiffness whereas the roller bearings produce error due to error in their roller balls. In order to get a friction less drive with no roller bearings, no stacked stages that further create errors and a high stiff system magnetic levitation (with the table being a circular disc) was used.

Minimum dynamic stiffness of $0.34 \text{ N}/\mu\text{m}$ is achieved *See Figure 80*. The system consists of a mover and a stator.

Due to the nature of the 2D motion of this system the stiff constraints in both the directions are missing this can be a problem during machining operations. The system developed cannot be used in macro machining operations due to limited stiffness (Minimum dynamic stiffness of $0.34 \text{ N}/\mu\text{m}$) offered by printed electronics. Also due to high loads during machining a shock landing can occur which has a potential to damage the system. *See Figure 81* which shows the response of axial noise to step.

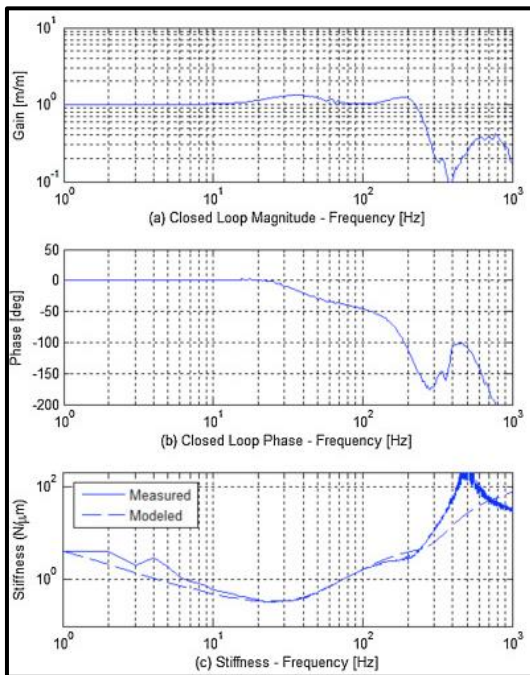


Figure 80 Stiffness Vs Frequency

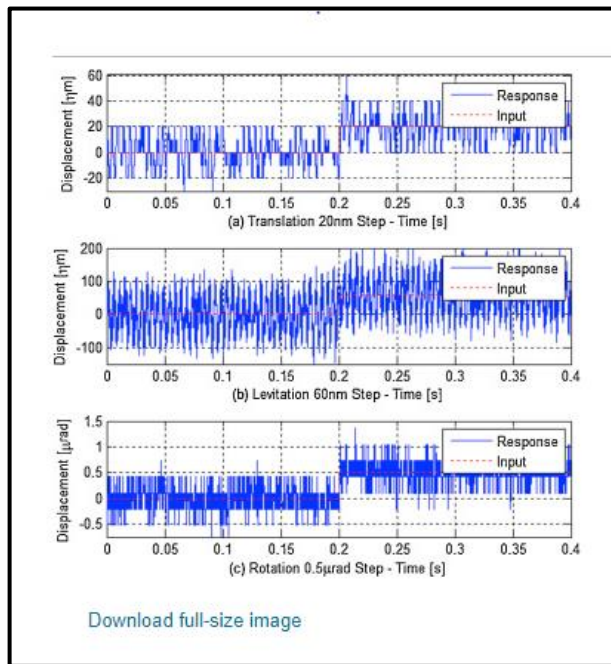


Figure 81 Axis noise vs step

The permanent magnet generates the magnetic field in the mover and the moving charge generates the current in the stator, the interaction between them gives rise to Lorentz force which has a direction orthogonal to the magnetic field and the current is responsible for actuation. (Lu, Xiaodong; Dyck, Mark; Altintas, Yusuf, (2015))

Application is only for micro milling due to limited dynamic stiffness and this method is very costly due to high level electronics.

2.3.4: Control of a dual stage magneto strictive actuator and linear motor ed drive system

Solid-state actuators are now part of the field of modern machining

The one-stage hybrid solution has been proposed in this paper comprising of a linear motor attached to the magneto strictive actuator and work table in series. The linear motor is responsible for the course stage and the magneto strictive for the fine stage which is connected to the table on the right side and the linear motor on the left side. The magneto is however carried by the course actuator resulting in high mass, this is advantageous as for high-frequency it acts as the low pass filter. The course stage carries the work piece and the table in the space of accurate reference positions. Very accurate small motions and high stiffness with short stroke is given by the fine actuator as high stiffness corresponds to high frequency deliverance due to this fact the system is designed so that it carries low mass for higher acceleration. To ward off the disability to detect high frequency cutting force disturbance of the course actuator the fine actuator corrects the tracking error and hence the required dynamic stiffness of the system is completed. *See Figure 82 below.*

The fine actuator corrects for the tracking error made by the coarse actuator due to its inability to respond to high frequency cutting force disturbances and to make up for its lack of dynamic stiffness. (Tong, D; Tong, D; Veldhuis, S C;(2007)).

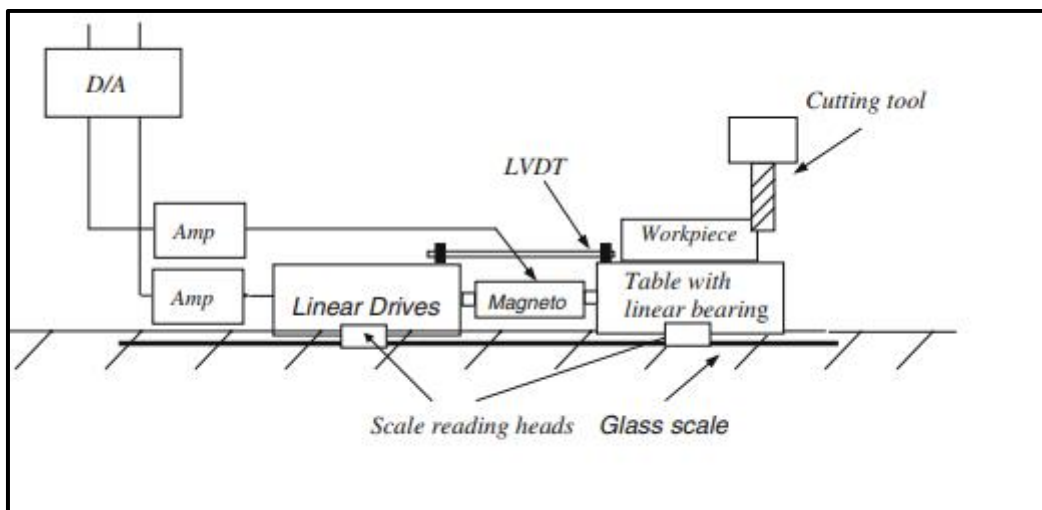


Figure 82 Shows the Schematic of the Hybrid actuator drive

Although good stiffness is achieved by the system along the axial direction, it lacks the reduction of Vibration in the other direction in case the tool cuts at an angle.

2.3.5: Linear motor and ball screw hybrid feed drive system

Rapid traverse and Cutting are two major types of modes in the machining process, rapid traverse requires zero feed-force positioning moves and high speeds while as a medium to high feed forces and low feed rates are present in cutting.

This type of hybrid design solves the following Problems:

Using Linear motors in rapid traverse enables the table to move with high speed and acceleration and due to less mechanical components, there is less vibration and residual vibration, the consumption of energy is also low. The linear motor is placed at the centre of gravity of the table (resulting force vector).

The lead screws are used during cutting operation as they enable high dynamic stiffness through large moving mass/inertia.

Screw drives during cutting produce dynamic and quasi-static errors and the yaw vibrations of the table during operation to solve this problem linear motor drive can also be used as a compensating tool.

The main goal of this research paper was also to design an engagement and disengagement mechanism to ensure a rapid switch between the linear drive and Screw drive. Linear motor (Kollmorgen IL18-100A3) has been employed into the design, the Motor has an air core instead of an iron core the major reason behind this is the linear motor is not used for heavy cutting processes for which iron core is the better choice. Iron core motors provide less accurate motion than air core because of large attractive friction forces and force ripples present in iron core motors. This significantly increases precision. A brushless rotary motor (Kollmorgen AKM-33H) drives the Screw drive. The process of engagement and disengagement of the screw drive with the table is achieved by a Roh'lix® nut, In Roh'lix® nut rolling-element ball bearings forming an imaginary screw track converts rotary motion to linear motion along a smooth shaft. The maximum slippage thrust force that the nut can provide is 444 N. The nut comprises of two parts which are spring loaded, they can be disengaged or engaged at any time along the shaft.

To separate the two halves a toggle mechanism has been designed. This incorporates fast-acting pneumatic pistons (SMC MDUB32-8DZ). Since this is a toggle mechanism there is no energy required to keep the nut halves separated. During re-engagement there are impact forces which are reduced by using shock absorbers. The attachment of the nut to the table is achieved through linear bushings

Two optical linear encoders (LE1 and LE2) with an optical resolution of 0.2 μm are used to measure the position of the table. Furthermore 250 brad resolution motor

-mounted optical rotary encoder is used to measure shafts angular position. See *Figure 83 and Figure 84*.

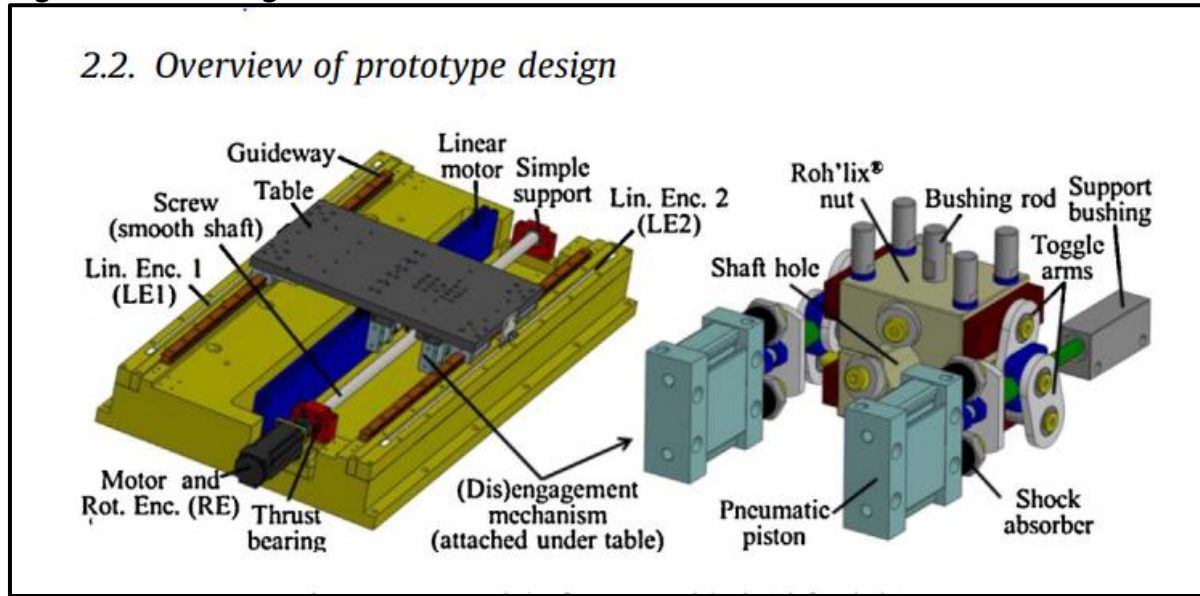


Figure 83 shows the proposed model of hybrid feed drive (Chinedum Okwudire, Jason Rodgers, (2013) Design and control of a novel hybrid feed drive for high performance and energy efficient machining

There may be a mechanical distortion in the coupled drive if the same reference position commands were fed, for this reason a master- slave setup provides the solution; this setup compares the feedback and torque values to each drive. (Chinedum Okwudire, Jason Rodgers, (2013) Design and control of a novel hybrid feed drive for high performance and energy efficient machining). See *Figure 83* above and *Figure 84* below.

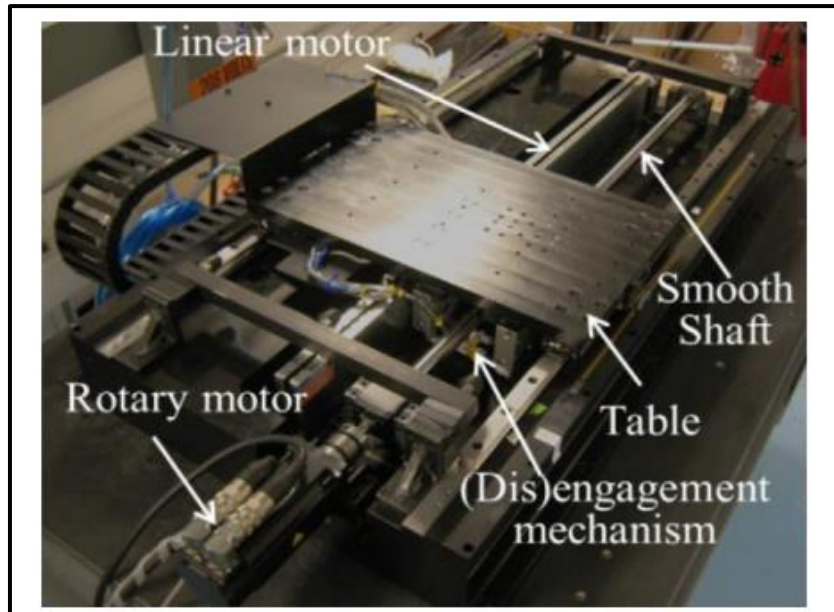


Figure 84 Proposed feed drive prototype used for experiments Chinedum Okwudire, Jason Rodgers, (2013) Design and control of a novel hybrid feed drive for high performance and energy efficient machining)

2.3.6: Incorporating active damping control technique:

This paper uses the semi-active damping control to reduce the ball screw feed drive oscillations thereby enhancing the dynamical performance. This is done with the help of a friction-based actuator.

In most cases, an axial deformation of the ball screw shaft and the nearby components is the major cause behind the first eigenfrequency of a ball screw feed drive. During transient processes requirement of high damping is only for a specific mode of operation. In this paper, Axial vibration mode suppression of the feed drive has been achieved selectively. A properly integrated additional actuator is used to apply the concept in accordance with the given requirements. An economical, selective and highly damping system can be acquired.

Active damping of the axial vibration mode of the ball screw feed drive is achieved through the application of a force on the table. For the purpose of integration, force was transmitted using the feed drive system linear guides of the drive system. Damping in this semi-active system is acquired through the capability of the dissipating energy of the adaptable frictional damper.

The system comprises of a linear encoder for table position feedback, pre-loaded ball screw and a servomotor controlled through current. *See Figure 85 below.*

the average nominal force is of minor importance considering the low duty cycles of the actuator

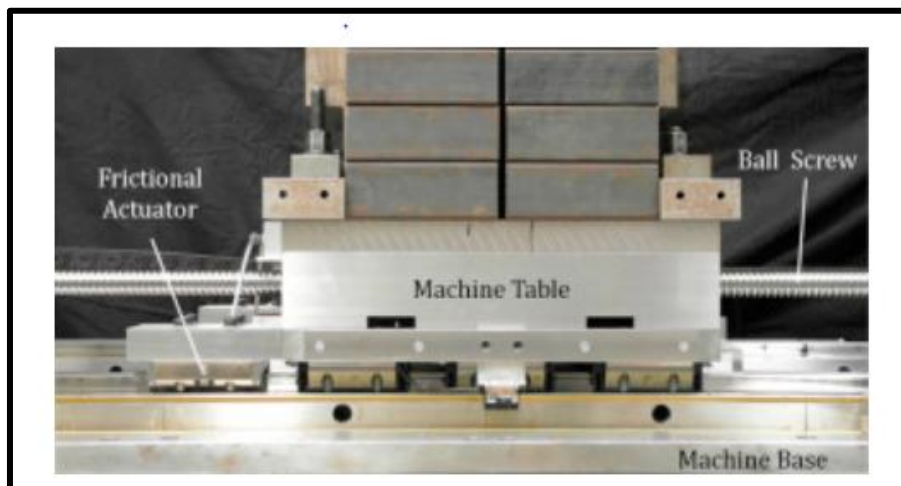


Figure 85 Shows feed drive test bench with travel range 700 mm , ball screw diameter 40 mm and load mass 1200 kg. (A.Verl, S. Frey, (2012) Improvement of feed drive dynamics by means of semi-active damping)

Experimental results show that with the gradual increase in the value of damping parameter “Kd” until the best damping effect was attained at $k_d = 380\text{Ns/mm}$. The amplitude has been reduced to 18 Db with the phase increase at 90-degree cut-off frequency being 10 Hz approximately. Increasing the k_d further had no

significant improvements because the electro-hydraulic actuator has limited dynamics. See *Figure 86, Figure 87 and Figure 88* below.

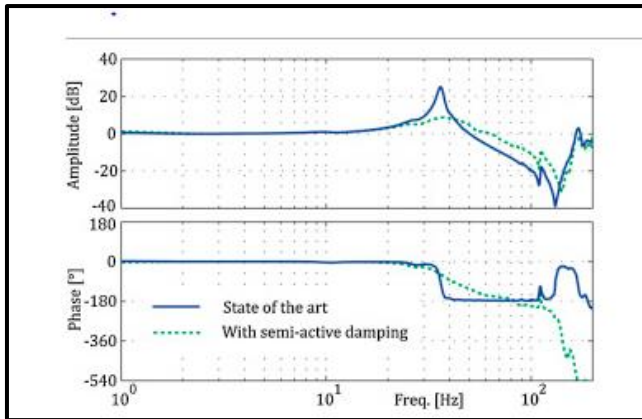


Figure 86 Shows frequency response between table and motor velocity

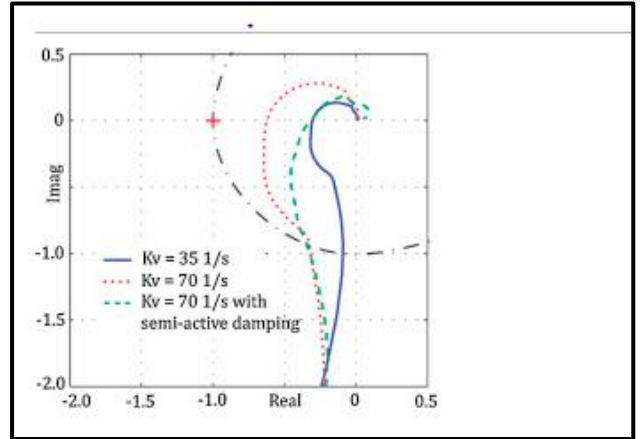


Figure 88 Shows the Nyquist plot of the open loop position controller

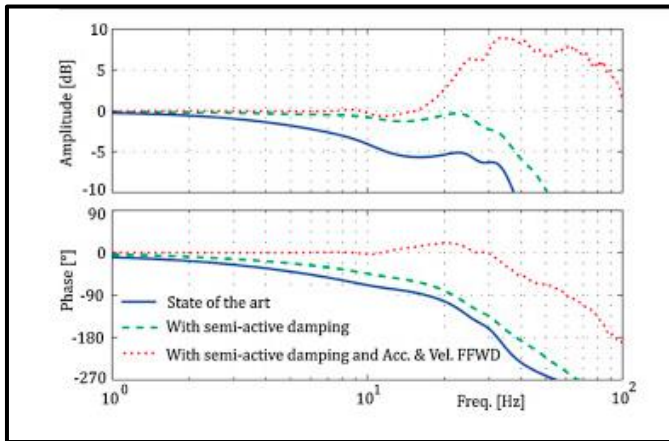


Figure 87 Shows the Command Tracking frequency response

Figure 88 shows Nyquist plot implicating that the velocity gain factor of $K_v = 701/s$ related to the first reached amplitude margin. An amplitude margin of 10 Db has been defined for robust control yet dynamically efficient behaviour. This derives the 100% increase in bandwidth in contrast to feed drive lacking semi-active damping. As seen from the *Figure 89* below, the amplitude is stable with semi active damping and holds to a value of 200 μm . *Figure 90* Shows the applied damping force and tracking test in alongside the acceleration and velocity for 500mm trajectory. The system response has also been improved and command tracking performance has also been enhanced. (A. Verl, S. Frey, (2012) Improvement of feed drive dynamics by means of semi-active damping).

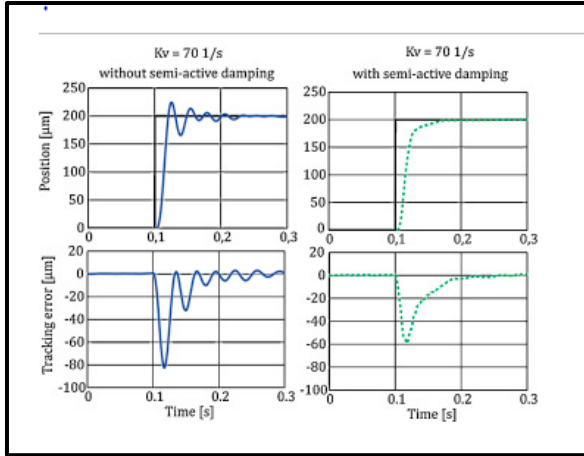


Figure 89 Shows position command step and tracking error for a disturbance step of 2000 N

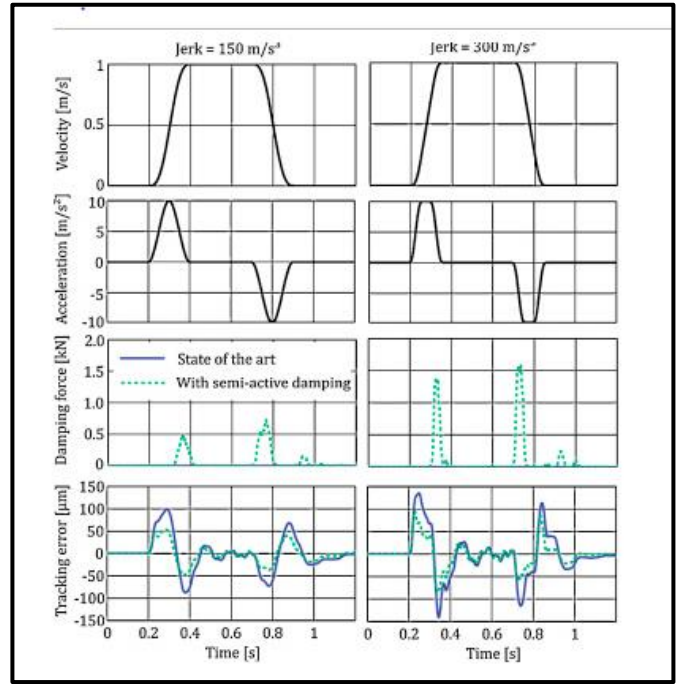


Figure 90 Shows High speed tracking test with and without semi active damping

2.3.7: Structure optimisation of longitudinal feed system design of CNC spinning machine.

This paper proposes the structural optimization of the CNC spinning machine, to achieve high accuracy and stability through increasing anti-vibration characteristics and reducing static deformation. The structurally weak link as analysed through Ansys in the spinning machine is longitudinal feed system. Based on this, four structural models were established and analysed. Single factor analysis is incorporated and used to contrastively analyse the static and dynamic characteristics. The results prove that double screw three guide design is the most efficient design it is shown that the value maximum deformation is reduced by 81.4, 80.3 and 46.8 percent respectively. In addition, maximum equivalent stress is reduced by 56.2, 53.5 and 21.8 percent respectively. There is an improvement in the natural frequency of the first six orders in different degrees validated through modal analysis. This proves the superiority of the structural design of the double screw three guide system having anti vibration capabilities and least static deformation. Also, the vibration of the carriage structure is responsible for low order modes as shown by modal vibration mode, this leads to the idea of optimisation of the carriage for improving the dynamic performance.

The optimisation design for carriage is carried out to make the system more efficient through topology optimisation. (Advances in Mechanical Design. (2018)). See Figure 91.

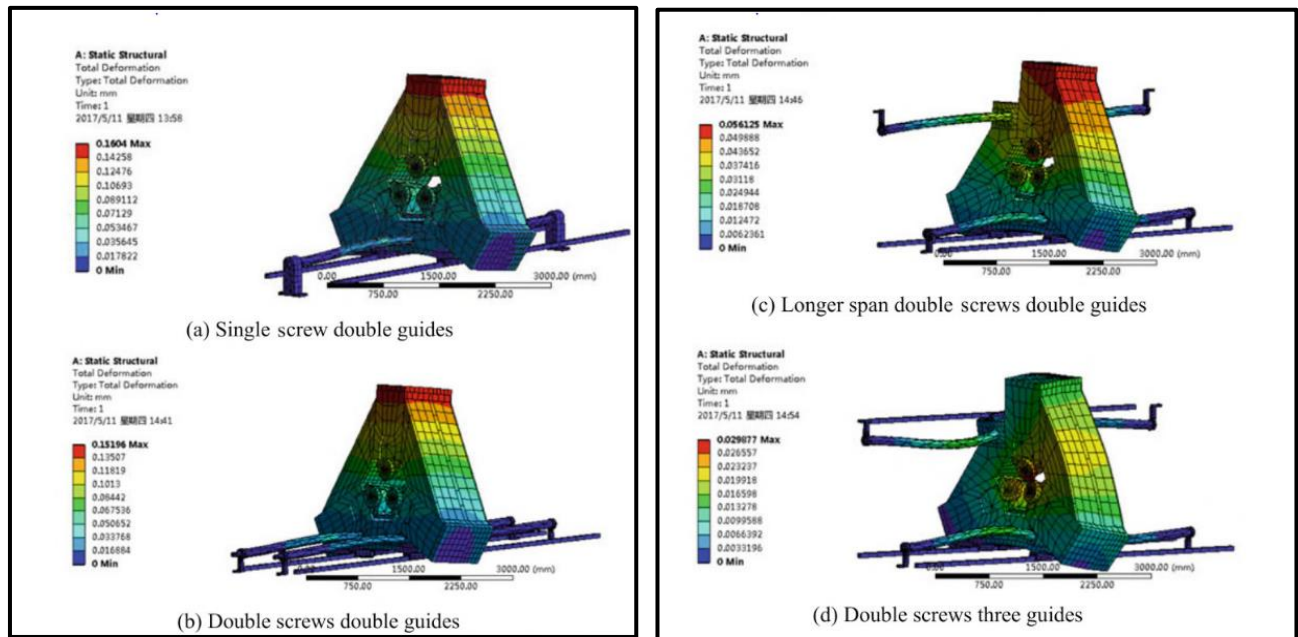


Figure 91 Shows all four configurations tested (Advances in Mechanical Design. (2018).)

2.3.8: Dual stage feed drive using piezo electric actuators:

This paper demonstrates the design of an in series dual stage drive for larger stroke coarse action and high-resolution fine drive stages in order to meet the high precision accuracy of the precision machine. The applications of this drive system can be found in fast tool servos for online suppression chatter and to create asymmetric surfaces, it is also used in micro and macro robots for high precision assembly. The application of the design is for machine tools, two designs are carried out in the paper including single axis and two axis DFSD'S. The DFSD consists of piezoelectric actuators for high precision high resolution stages and Linear motors for coarse stages. The design for a milling machine and meets its static and dynamic requirements through frictionless precision motion using flexures. Both stages are integrated together through a model-based control algorithm in a complementary fashion. Compared to a similarly controlled linear motor drive the tracking error by single axis DFSD is reduced by 75%. This paper also concludes that the between the machine base and coarse stage the dynamic couplings were unlikely to induce any tracking error or affect machined surface finish. See Figure 92, Figure 93 and Figure 94 below.

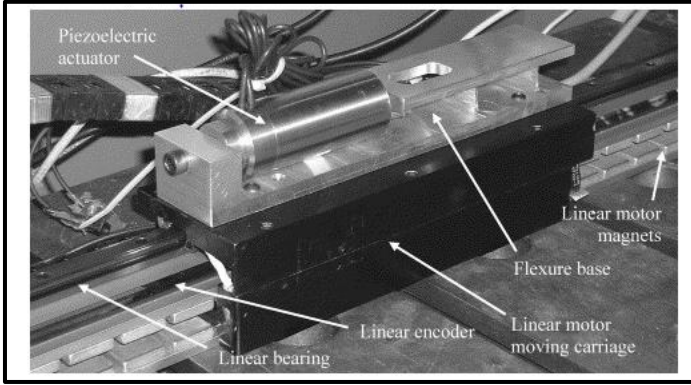


Figure 92 Dual stage feed drive assembly single axis. (A.T. Elfizy, G.M. Bone, M.A. Elbestawi,(2005) Design and control of a dual-stage feed drive)

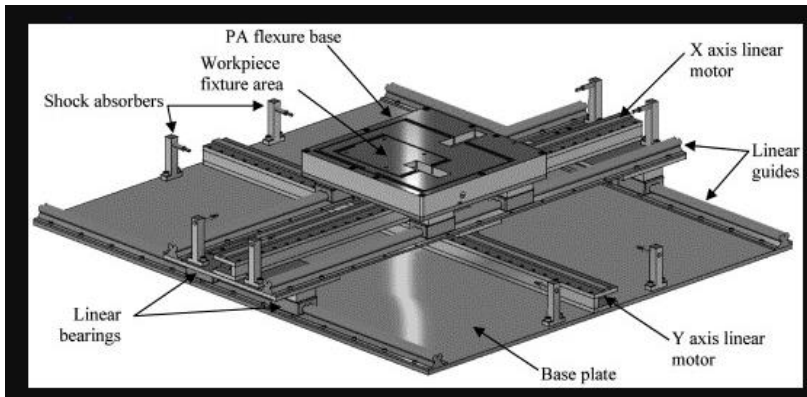


Figure 93 two axis dual stage feed drive design. (A.T. Elfizy, G.M. Bone, M.A. Elbestawi,(2005) Design and control of a dual-stage feed drive)

Furthermore, to perform milling operation a sinusoidal profile cutting was carried out by a 2 axis DFSD reducing the maximum tracking error by 83% with an average reduction of 63%. In addition, the maximum tracking error in the sharp cutting corner is reduced by 38% with an average magnitude reduction of 39 %. (A.T. Elfizy, G.M. Bone, M.A. Elbestawi, (2005) Design and control of a dual-stage feed drive).

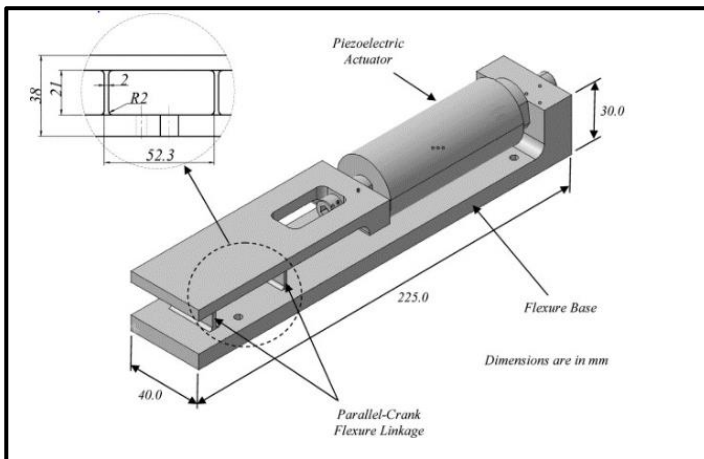


Figure 94 Flexure base of Single Axis PA (A.T. Elfizy, G.M. Bone, M.A. Elbestawi,(2005) Design and control of a dual-stage feed drive)

Long stroke mechanism:

This paper also deals with the Dual stage feed drive mechanism, combining the coarse stage long range linear mechanism with the piezoelectric actuators. In this paper the piezo electric actuator travel is suggested to increase from 15 micro meters to 0.05-0.5 mm or more using flexure hinge mechanical displacement amplifier which helps in magnifying the travel output of the actuators. The applied linear mechanism has the travel ranges of 116.26 for x axis and 106.81 for y axis. 8 mm ball screw lead and stepping motors with 50000 pulse/rev were used for coarse stages. The control strategy used was of a dynamic compensation type feeding the error from linear stages to piezoelectric actuators as input signals. The paper suggests that with the help of a dual stage drive positioning error in 1 mm stroke of 30 micro meters can be reduced to 2 micro meters

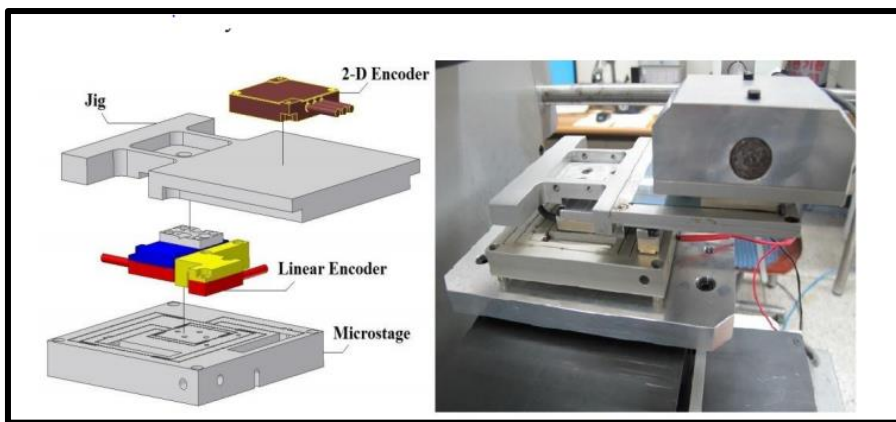


Figure 95 Shows the dual stage feed drive configuration with sensor assembly (left) and Milling machine configuration (right) (Hendra Syahputra, Hyeon Yang, Byeong Chung, Tae Ko. Dual-Stage Feed Drive for Precision Positioning on Milling Machine. Svetan Ratchev).

The linear trajectory motion test shows that y axis results in the large errors than x axis due to the positioning of x axis drive on y axis. The maximum positioning error in y axis using the dual stage feed drive was decreased from 37.58 μm to 10.7 μm and the average overall error from 19.60 μm to 0.93 μm respectively. For x axis the maximum positioning error decreased from 22.51 μm to 8.67 μm with the average overall fall from 12.07 μm to 1.04 μm . To the check the x, y planar collaboration a circular motion test was carried out. The test showed that the maximum circular motion error reduced from 40.73 μm to 5.11 μm with an average drop from 19.72 μm to 0.995 μm . Similarly, for axis the maximum circular error decreases from 59.06 μm to 6.76 μm with an average decrease from 27.81 μm to 0.93 μm . (Hendra Syahputra, Hyeon Yang, Byeong Chung, Tae Ko. Dual-Stage Feed Drive for Precision Positioning on Milling Machine. Svetan Ratchev). See Figure 95 above.

This concludes the precision accuracy efficiency of the dual stage feed drive over single stage drive.

2. 4 CRITICAL APPRAISALS

All the papers that are crucial to the research have been critically analysed in this section.

2.4.1 Friction reduction Based Bearing

In his paper ultrasonic frequencies are used to reduce friction and hence stiction resulting in a loss of vibrational amplitudes and hence good positioning accuracy. To achieve such ultrasonic vibrations piezo stacks are used. This is done by incorporating a piezo actuator that slides the bearing surface at these frequencies. (Engel, T; Lechler, A; Verl. (2016)).

Although the paper clearly depicts the reduction in positioning errors and power consumption of motor, one of the major weaknesses that arise in this design is the mechanical wear caused due to micro vibrations in the sliding elements, the paper has not discussed the type of materials used in order to tackle this problem.

The author offers no explanation of how can this design be applied in cases of higher masses involving the mass of the work piece and the table itself. Achieving micro vibrations at higher masses demands large resonators. The author has not reported the mass of the table under which the experiment was done.

2.4.2 Flexural Design

The paper describes a novel flexural bearing design that can provide rotational oscillations of 360 degrees with high repeatability. Straight flexures with inner and outer cores are used in combination, these straight flexures allow motion in circumferential direction whilst keeping other directions restrained. (Luo, H.P; Zhang, B; Zhou, Z.X. (2008)).

Despite of covering the basic general design requirements of the bearing one criticism of much of the literature is that the characterization of fatigue life, tilt, axial and radial error motion accuracy is not covered quantitatively. Material yielding is also a concern when designing flexural systems. Also, to apply such a concept to CNC that demands high inertial force effects is hard, due to limited yielding properties its motion transmission is limited to few millimetres.

2.4.3 Rotary Axial Spindles

One possible solution for replacing aerostatic journal and thrust bearing is active magnetic bearings they offer frictionless motion, high resolution with high stiffness. This paper discusses the transmission system for precision machine tool spindles. Magnetic bearings also have very high operating speeds.

This paper presents a prototype where a radial position is controlled with the help of externally pressurised aerostatic bearing while as the thrust resistance forces

are controlled by large stroke magnetic thrust bearing/actuator. (Lu, X.-D; Paone, M.P; Usman, I. (2009)).

Although the paper clearly shows the application of magnetic bearings with actuation of mm travel no attempt was made to show how can the system be applied to large travel situations. (Lu, X.-D; Paone, M.P; Usman, I. (2009)).

The paper is limited to controlling only the spindle axis while rest of the axis are still exposed to problems. The axial stroke of the spindle actuator is also limited in both the promised large-scale design having 1.5 mm stroke and the current design with 1mm and thus the conventional feed drive will still be used for large strokes. the dynamic stiffness in radial direction is still weak due to air bearings is also limited.

2.4.4 Magnetic Guide for Photolithography.

Without rigidly containing the DOF of a system a magnetic bearing can apply torques and forces to a system. Only sensors limit the resolution of magnetic bearings as they themselves are very precise, accurate and fast. In the paper magnetic bearings are chosen over a dual stage control system where fine stage is controlled by the voice coil or PZT'S in photolithography. The compound flexures are connected to the platen and the whole system has poor dynamics. Fine stage provides 100 um of travel and six degrees of freedom control while as coarse stage provides 200 mm travel. (M.E.Williams;D.L.Trumper;R.Hocken (1993)).

This paper mainly focuses on photolithography, the mass is limited to 15 kg with a light base table used, in reality applying such a concept to CNC would demand huge magnetic actuators and permanent magnets for the lift this is one of the major drawbacks of magnetic bearings. The lift achieved by the magnet at 6 mm air gap is 170 N which is not even close to the CNC application as they mostly use roller bearings with a load carrying capacity of over 10000 N.

2.4.5 Machine Tool with Active Magnetic Guides

The main importance of this paper is that the application in real machining CNC centre where high loads are present is shown.

In this paper the application of active magnetic guides on actual machining centre has been designed and tested under cutting conditions with the further improvements in dynamic stiffness for the whole range of frequency. (*Denkena, B; Kallage, F; Ruskowski, M.(2004)*),

The paper doesn't clearly show the application and performance of such guides at a higher frequency range, also the experiment does not contain the experimental results of a full-scale machining centre running at higher frequencies. Again, magnetic guides are only used for the milling centre and not the entire feed drive. Controlling the axial direction is not clear in the paper. It seems there is no direct compensation along the axis axial force.

2.4.6 Magnetic levitation

The air gaps between the moving parts and the mechanical guide rails are limited by the gas film and oil film. Due to limited gap-height arising as a result of limitation of oil film or gas film between the mechanical guide rails and the moving part aerostatic and hydrostatic guideways, the elimination of the effect on moving parts by the mechanical guide ways does not result. (*Jiang, Wenxue; Zhou, Kai; Lv, Jiangwei; (2014)*)

This demands for an efficient system that can have a large gap with better controllability.

In gantry type mechanism the deformation of the cross beam (6m) can affect the precision of guide rails. This also demands isolation of the moving part.

Again, the size of electromagnets to levitate an operational stacked system in CNC possesses a problem in magnetic bearings and their relative cost.

2.4.7 Dynamic characteristics of a direct-drive air-bearing slide system with squeeze film damping:

The dynamic stiffness of the air bearing slide depends on the availability of the damping in them which is quite low. In order to increase the dynamic stiffness, the damping must be increased this can be done with the help of integral oil lubricated squeeze film dampers. No sealing arrangements are required as magnetic oil is used in the dampers. The resulting position accuracy and motion errors are less and the slide has little size variance. (*Wardle, Frank P; Bond, C; Wilson, C (2010)*).

This paper provides a great insight into the application of magnetic fluid to increase the damping of air bearing but the author offers no explanation of how this concept can be applied to large scale CNC's. Also, as the author has stated the major disadvantage of this type of system is the heat generation due to viscous friction. In order to avoid foreign particles during machining operation condition a better sealing system is required despite the authors claim of a simple sealing system.

2.4.8 Porous Ceramic Water Hydrostatic Bearings for Improved for Accuracy Performance

Aerostatic bearings are very good at thermal stability compared to hydrostatic bearings which have a bad reputation for thermal drift, but because of the stiffness required for various machining processes hydrostatic bearings are much stiffer than aerostatic bearings. (*Corbett, J; Almond, R.J; Stephenson, D.J;(1998)*). (Porosity and the mechanical properties of aluminium welds. (2020)).

A bearing that can avoid critical thermal conditions whilst maintaining the static and dynamic stiffness has been designed. Fatigue life and loss of traverse tensile strength are one of the major disadvantages of porosity and hence would be taken into consideration. Furthermore, the report does not show any comparison between the old and new design and how the dynamic and static stiffness of the machining quantitatively got effected.

2.4.9 Hybrid Bearings

Due to absence of sufficient film pressure the sliding surfaces of bearing system are unavoidable during start up and shut down processes this causes extreme wear in the hydrodynamic bearings this consequently leads to changes in the thermo-hydrodynamic performance and Dynamic and static characteristics of the regime, gaseous cavitation's and its stability.

In order to avoid these conditions a new hybrid bearing has been proposed in the paper. The rolling element bearing with some clearance and hydrodynamic bearings combined together in parallel forms the new hybrid bearing. Another similar hybrid bearing has been developed. Instead of roller elements this design uses permanent magnets in combination with the hydrodynamic bearing.

US patent by inventors John F. Justak and Gregg R Owens has also solved the problem of start-up and or shut down issues of hydrodynamic bearings with the help of an optimised hybrid bearing design.

Although Hybrid bearings of various configurations have been designed they mostly are rotary in nature, research in linear hybrid bearings is less. In terms of linear bearings using hydrodynamic film possess many problems including the cost of sealing the system. The magnetic forces produced by bearing in paper is comparatively low than what's required in machining centres hence large magnetic forces demand increase in size of geometry of the bearing which is a major problem as it also increases cost and compactness

2.4.10 New Slide with Friction Drive

The position precision of 16 nm has been achieved with the help of the new linear slide design. The system works within 220 mm range and incorporates a high axial stiffness. A friction drive is used in the system to cause the translation motion hence does the job of an actuator. Thermal expansion can cause various issues in the geometry of the structure and hence the precision of the slide in order to avoid this a Zerodur Material is used in the guideways and hydrostatic bearings have a controlled temperature environment. Optical quality of flatness equal to $\lambda/2$ is posed by the guideways. Due to the 15 times better, internal damping ratio than steel and the a very low thermal expansion coefficient of ($7.5 \mu\text{m}/^\circ\text{C}$) the base used is made of granite. (Mekid, Samir, 2000)

The short stroke is again the major gap in this paper, the stroke here is 220 mm. Also, the drive is prone to axial elastic displacement due to the nature of contact mechanics which is rolling friction. The drive also limits the thrust force required to maintain the static friction hence their application to large CNC'S can be of crucial concern. The author has used the zerodur guideway which can be very expensive to manufacture for commercial CNC'S that are usually longer in size. The use of hydrostatic bearings demands complex sealing arrangement which has not been covered by the author.

2.4.11 A Twist-Roller Friction Drive for Nanometre Positioning - Simplified Design Using Ball Bearings.

Some sub nanometre positioning systems employ, the capstan friction drive, hydrostatic lead screws and ball screws.

A new driving mechanism called the twist roller friction drive has been redesigned and experimented in this paper. The new designed drive reduces the use of hydrostatic bearings in the drive to the simple roller bearing design. Since there is a friction between the rollers and the drive shaft a hydrostatic bearing was employed that also used the hydrostatic guideway in the system, but this design is complicated and requires difficult machining process for the rollers. Also, the oil used in the whole positioning system makes the environment less clean and prone to contamination. (*Mizumoto, H; Arie, S; Yoshimoto, A; (1996)*).

Despite having a large stroke/resolution value compared to other frictional drives a serious weakness of such drives are the limitations of thrust force. Author has not shown any comparison of dynamic and static stiffness with respect to other drives such as ball screws. The positioning resolution achieved through this design is 0.5 nm but due to replacing hydrostatic bearings with ball bearings stick slip phenomenon can occur and other influences including imperfections of balls are introduced. Such issues are not quantified and explicitly shown in the paper.

2.4.12 Ultra precision Feed System Based on Walking Drive:

In this paper the stroke of a piezoelectric actuator has been increased directly through the development of a mechanism based on alternative clamping or walking. Utilising the deformations in the piezo electric actuators a new feed system that has a long stroke and can feed with smooth and continuous action with high rigidity has been developed. Similar to the walking motion of animals each clamp set (a pair of clamps) uses 4 piezoelectric actuators 2 for clamping and decamping action and 2 for feed action. The motion of the table is controlled using the laser feedback.

In this paper the application of the walking drive concept on the 2 axis X, Y and One rotational axis has been developed, designed and experimented. The system consists of a table with three drive block pairs each block has three piezoelectric actuators that deform in X, Y and Z directions respectively.

The first paper, clearly depicts the axial stiffness to be 400N/um There is no mention of vertical stiffness. Also, the stroke of the part is limited to 105mm. (*Moriwaki, Toshimichi; Shamoto, Eiji, (1996)*).

The second paper has the limited weight of 13 kg with the load capacity of the table is 33N and limited stroke of 100 mm ,40 mm in X and Y directions

respectively. parallel beam elastic deformations. (*Shamoto, Eiji; Moriwaki, Toshimichi, (1997)*).

In the present case, the weight is about 73 kg, and the load capacity measured is 33 N.

Axial stiffness of 100N/um 2 pairs of contact blocks When two pair of blocks support the table the vertical stiffness of the table is 134N/um and 98 N/um in feed direction.

The author has not explained the mechanism by which the blocks are connected to the table, even if there is such a mechanism it would be weak so in other directions the system is not constrained well.

The travel speed of such systems is not shown it seems the system would be slow due to the walking mechanism alternate clamping action.

2.4.13 Electrohydraulic actuator

In this Paper an Electrohydraulic actuator is used as an active damping device with the velocity loop feedback. The Chatter is reduced by reducing the dynamic flexibility of the machine by 80% and hence stability. The damper was put on the work bench that had a work piece on it *See Error! Reference source not found..* The dynamics were in relation to the tool and the workbench. as the tool cuts the work piece in steps it can be observed chatter vibrations were reduced. It uses servo valves which controls the oil flowrate

It may limit the size of work piece to be used. (*Brecher, C; Schulz, A;(2005)*).

2.4.14 Voice coil motor infer meter and ball screw sub nanometre drive

A sub nanometre (0.3nm) feed drive is designed and implemented in this paper , The laser infer meter (homodyne interferometer) feedback system in combination with hybrid actuator system comprising of Voice coil motor and a ball screw are responsible for long stroke (150mm) sub Nano positioning conditions. The primary table is isolated from the aerostatic guideways and is preloaded with the help of permanent magnets. The bearing used is aerostatic bearing for smooth motion.

The guide uses aerostatic table as its main bearing surface, this poses limitations in the machining environment where high stiffness values are required with good damping properties which are not viable options in air bearings. Furthermore, the use of magnetic bearing surface for preloading is directly applying a normal force to the secondary table which may cause ball screw axial deflection which is the major cause of Eigen frequency the thrust force of voice coil motors is limited and can pose a problem in case of large work pieces. Complex large work pieces with irregular shapes can cause roll and pitch moments.

2.4.15 Voice coil /dc motor hybrid

The table uses aerostatic guideways which has porous bearings for smooth motion. A non-contact feature of the table is achieved as the table is driven by contact less system involving air bearings and voice coil motor. The pros of voice coil motor are its non-contact feed drive capability, no magnetic attraction, easy control, quick response and no force ripple as present in linear synchronous motors. (*Shinno, H; Hashizume, H. (2001)*).

The intermediate drive used in the design is the pulley/rope system, the tension in the lead wire will not able to bear the high loads and machining conditions due to limitation in the tension and the nature of friction drives. Due to the structure of the design the main load is carried by the air bearing guide which again is the problem due to low damping of air bearing and restriction at high loads due to machining. The voice coil may need a cooling system to operate in a continuously running machine like CNC.

2.4.16 Adaptive preloading of rack and pinion drive systems.

Rack and pinion are better in terms of performance and cost for large travel distances compared to BSD and LDD for large machines. Since there is an increase in moment of inertia of the spindle reducing drive dynamics because for large travel distances spindle diameter needs to be increased for high stiffness to avoid whipping etc in BSD. In contrast, LDD can also be used but due to their high energy consumption and increase in the number of secondary parts the cost gets high in relation to Rack and pinion. (*Verl, A; Engelberth (2018)*).

As stated by the author the system still needs more validation in terms of path accuracy during dynamics of the machine on the positioning behaviour using adaptive preloading. Although the system is efficient in terms of energy consumption the paper does not add up the energy of the control systems involved which might reduce the "reduction in energy attained".

2.4.17 Main Points from Drive centre gravity

This paper has been written by (*Hiramoto, K; Hansel, A; Ding, S;(2005)*). In this paper, twin screw may reduce moments, but if the motors are not synchronised crawling can occur, also it increases the mass and cost of the system to a significant level.

This paper develops a system that uses twin screws to eliminate the yaw moments of y saddle that are responsible for Vibrations at high acceleration. Because the drive systems are not exactly near the centre of gravity of the system they can induce moments and these moments cause vibrations.

2.4.18 Energy optimized jerk-decoupling technology for translator feed axes

Jerk decoupling mechanism is very advantageous when it comes to vibration suppression in feed drive systems. This technology has proven records. In case of linear motors, the secondary part of the motor is mounted to the frame while as the primary part which is the moving part translates. Due to jerk the force is transferred to the secondary part which is responsible to create equal and opposite force such impulses are then transferred to the mounting frame hence generating vibrations and limiting the dynamics of the system. . (*Denkena, B; Hesse, P; Gümmer, O, (2009)*).

The load on the primary part guide increases due to this design as it incorporates the internal guides which carry the secondary part. It is unknown if the jerk decoupling provides any nanometre resolution which is very crucial for new precision systems. The vibrations transmitted by other major vibration source components like bearings cannot be suppressed with this design. As the author has stated both the slides used in conventional jerk decoupling systems has to be of high stiffness due to linear motor normal forces, the high stiffness is provided by linear roller bearings which cause additional vibrations in of itself.

2.4.19 Magnetically Levitated six degree of freedom rotary table

The concept of magnetic levitation is used in this paper to develop a micromachining centre, this concept was chosen because under varying loads air bearings don't provide the required stiffness whereas the roller bearings produce error due to error in their roller balls. In order to get a friction less drive with no roller bearings, no stacked stages that further create errors and a high stiff system magnetic levitation with the table being a circular disc was used. (*Lu, Xiaodong; Dyck, Mark; Altintas, Yusuf, (2015)*).

Only for micro milling due to limited dynamic stiffness and this method is very costly due to high level electronics.

2.4.20 Control of a dual stage magneto strictive actuator and linear motor ed drive system

Solid-state actuators are now part of the field of modern machining

The one stage hybrid solution has been proposed in this paper comprising of a linear motor attached to the magneto strictive actuator and work table in series. The linear motor is responsible for the course stage and the magneto strictive for the fine stage which is connected to the table on the right side and the linear motor on the left side. The magneto is however carried by the course actuator resulting in high mass, this is advantageous as for high frequency it acts as the low pass filter. The course stage carries the work piece and the table in the space of accurate reference positions. Very accurate small motions and high stiffness with short stroke is given by the fine actuator as high stiffness corresponds to high frequency deliverance due to this fact the system is designed so that it carries low mass for higher acceleration. (*Tong, D; Tong, D; Veldhuis, S C;(2007)*).

Although good stiffness is achieved by the systems along the axial direction, it lacks the reduction of Vibration in the other direction if the tool cuts at an angle.

2.4.21 Linear motor and ball screw hybrid feed drive

Rapid traverse and Cutting are two major types of modes in machining process, rapid traverse requires zero feed-force positioning moves and high speeds while as medium to high feed forces and low feed rates are present in cutting. there may be a mechanical distortion in the coupled drive if the same reference positions commands were fed for this reason a master- slave setup provides the solution; this setup compares the feedback and torque values to each drive. (*Chinedum Okwudire, Jason Rodgers, (2013) Design and control of a novel hybrid feed drive for high performance and energy efficient machining*).

2.5 CONCLUSIONS FROM LITERATURE REVIEW (*Gap Knowledge*).

Followings points can be noted down:

- Integration of Air bearings in Macro Machining centre is missing.
- No Hybrid Linear Bearing Combination of Air-roller or Magnetic-roller solution exists until now.
- Magnetic levitation can be further researched.
- Design of Roller pinion racking System in combination with linear motor or Piezo electric actuators is not present.
- Use of integrated Servo- ball screw mechanisms can be a solution.
- A completely sealed hydrostatic bearings can also provide a potential concept which has not been covered.

As proven above magnetic or air bearings in combination with a roller bearing can provide a potential solution to the problem. The other literature gaps can be fulfilled by the choice of drives used. At first one needs to determine what combination of hybrid bearing is valid with the roller bearing design, magnetic or air bearing? This requires further proof of choosing one combination. The comparison is shown as follows:

2.5.1 Magnetic Bearings vs Air Bearings.

The following points can be made as a comparison of Magnetic and Air bearings.

- The driving forces have oscillations which need to be controlled, in case of magnetic bearings very little (if any) damping is present. Due to the Compressibility effects of air, it provides damping which can be enhanced by squeeze film effect, the air bearing damping is a function of bearing area and operating gap, the damping in air bearing is 15 times higher than damping roller bearings. (*Wardle, Frank P; Bond, C; Wilson, C (2010)*).
- In magnetic bearings heat generated by windage losses and electrical winding losses requires cooling adding to the complexity while as in air bearings run purely on air which has negligible heat generation effects and hence require no cooling.
- In Magnetic bearings in case of power or control failure a backup bearing is required for shut down and start-up which adds to the complexity. This back up bearing can be a large clearance roller bearing which during sudden power shut down can have shock loads due to impact resulting in premature failure.

- Load capacity of magnetic bearings are limited due to their large requirement of envelop size to relatively small load capacity. Air bearing pads are simple and require lesser area for the same load capacity and due to their porous and light weight material they have very less weight.
- The magnetic force can also attract iron/steel chips and other types of metallic debris in the machining process. On the other hand, Air doesn't attract any type of metallic debris in fact it can wash it away if present hence make it more suitable for Machining environment.
- The associated hardware for magnetic bearing is also sophisticated and expensive. (*Magnetic bearings – Mc Nally Institute. (2020)*). (*Disadvantages of Magnetic Bearings. Wikimechanical.blogspot (2020)*).
- Due to all the aforementioned conditions the bearing weight and cost increases considerable in magnetic bearings, also Air bearings have no electronics present therefore they are safer and their maintenance costs are less.

Due to the reasons mentioned above Air bearings provide a more viable and economical solution for the new hybrid bearing design and therefore will be used in the novel Concept generation process.

CHAPTER 3: METHODOLOGY

3.1 METHOD UNDERTAKEN

The Aim of the paper is to undertake and carry out the Design and Analysis of the Novel Feed Drive solution with the ultra-low vibration therefore it becomes logical to use the general design and analysis methodology.

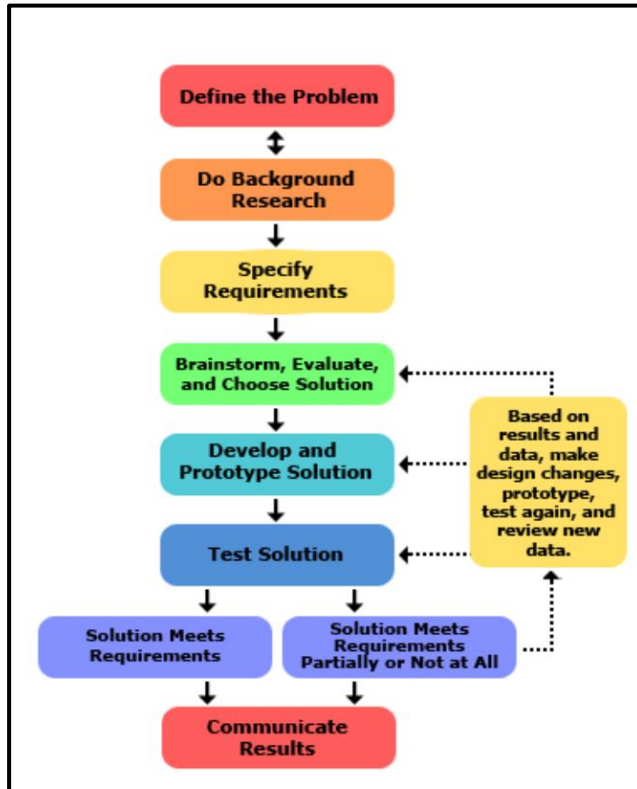


Figure 96 Classical Design Methodology diagram The Engineering Design Process. (2020)

The General Methodology carried out in the project is as follows;

1. **Define the Problem:** Definition of the problem and its scope has already been dealt with in the section of Introduction, through Problem statement and its Objectives.
2. **Do Background Research:**
 - Literature and critical review were carried out to study various research papers, patents and publications of novel machine tool feed drive design.
 - Critical review was carried out which would identify the gaps related to the current problem.

- Various feed drive systems and motion control theory was studied in detail to gain basic engineering design and analysis skills suited for the project development.

3. **Specify Requirements/Preliminary Information:**

- Specification requirements relevant to the project will be laid out including the factors such as maximum damping, dynamic stiffness and hence the resolution as these are the major parameters to be taken into consideration.
- Experimental Modal Analysis using Data Physics acquisition unit and Signal mobiliser will be carried out on the Test Feed drive system to obtain the system response.
- Once the validity of the Finite Element Analysis carried out on the entire Feed drive rig is evaluated with the experiment, this method can now be implemented to analyse the effect of newly designed components on the same or similar rig by replacing the similar components of the test rig computationally to check for Vibrations and accuracy of the system

4. **Brainstorm, evaluate and choose the solution:** Brainstorming and evaluation of Concept generation will be undertaken based on the knowledge gained through background research. A matrix of concept design will be developed.

5. **Develop and Prototype/Test Solution:**

- Design of the new Hybrid bearing Concept is chosen and its Preliminary Analysis and development will be implemented.
- In order to Verify and Validate the Design various types of Analysis will be carried out during the design phase. Computational analysis including Finite element analysis and Vibrational Analysis using various software packages i: e Ansys, Solid works and MATLAB.
- A prototype will be designed and tested with the help of experimental modal analysis to obtain the desired parameters for the validation of the novel Hybrid bearing concept.

6. **Communicate Results:** Finally, Report writing will be undertaken that will document all the background relevant to the research, the gaps in the research and the need to develop new machine tool system. it will also document all the calculations and the experimental data compared with other papers to prove the validation of the solution.

3.2. PROJECT MANAGEMENT

A transient and unique plan comprising of SMART objectives is often referred to as Project. Due to the limited time scale and the existence of final deliverables the project management is different than just “ management’ ’The one of the most important work-packages in the project management is the project plan which is essential in defining and meeting the goals and objectives with greater efficiency and coherence. (Apm.org.uk. (2018)).

A work breaks down structure (WBS) was first laid down to define the work packages in a hierarchical manner. This includes Project planning involving problem definition and background, definition of work packages, basic risk assessment and project scheduling. In order to attain the skills and data required for the research progression the next work package is Preliminary study comprising of Control Theory and Mechanical Vibrations Theory, Theory of Feed drives, Dimensional Measurement error parameters, Experimental Validation to quantify errors. Literature Review-Possible Solution is the following work package, this will help in collecting already existing solutions and their loop holes and hence providing a proof for novelty of a concluded solution, this work package includes, Comparison of Different existing solutions, Concept generation and Justification of current selection. Once the data is gathered and a possible solution is found the design and Analysis phase begins, Kinematic design is carried out prior to the frame design as it defines the structural integration with CNC and other frame-based components. This followed by Analysis where Finite element analysis and vibrational analysis will be carried out to justify the efficiency and performance of the design any changes that might arise from this work packages will then be amended in the adjacent work package called final design which will conclude our design and analysis phase. The Comparative analysis of several components is carried out in parallel with the original design to arrive at the results with the help of computer aided simulation old existing designs will be compared with the new design. The project will end with Report writing documenting all the proof of concept and evidence of research progressively developing into a thesis. *See Figure 97 below.*

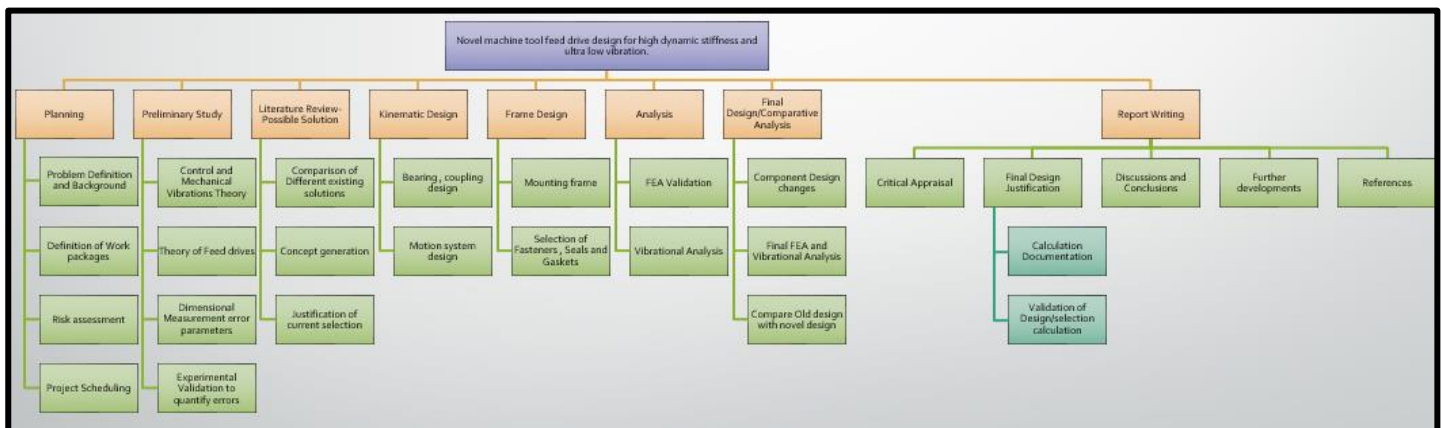


Figure 97: Shows Work breakdown structure of the project.

CHAPTER 4: THEORY AND PRELIMINARY STUDY

4.1. THEORY AND PRELIMINARY ANALYSIS.

4.1.1 Introduction:

In this Section, the theory behind Vibrations and Data acquisition has been clearly demonstrated, and the data preliminary to the design has been collected and analysed. Concept generation is also included here. This is Vital for the entire project into order to understand the behaviour of conventional rig to obtain benchmark tests of which theory is an integral part.

An experiment and computational Analysis of conventional test rig was carried out to collect the data for a reference as well as to Validate the finite element method that will later be employed to the Novel feed drive System.

Please Refer to appendix A Chapter A where Theory, Simulation and Experiments and their results are discussed in more detail.

4.1.2 Conclusion:

A well-defined Finite Element Model was Simulated with boundary conditions that are very close to actual boundary conditions of the rig. The mode shapes are satisfactory but the frequency at which they occur may not be accurate as compared with the experimental modal Analysis. The Comparison was done by inspecting and guessing the evident dominant displacement directions (mode shapes) in FEA for each mode to be analysed while as in experimental modal analysis case it was carried out with the help of manual graphical analysis. Such an approach can lead to many errors and therefore demands a Spatial Modal Analysis where the Mode shapes and their natural frequency data can be experimentally visualised and compared with the Finite element model to attain better results. Such a model has been prepared for the novel rig design.

4.2. CONCEPT GENERATION AND DESIGN EVALUATION

Based on the literature review and the related gap knowledge more areas primarily focusing on optimising the Bearing design and accordingly making relevant changes in the entire feed drive were brain stormed resulting in novel concepts, some of these concepts were then rated based on the following criterion. (See) Basic design parameters including Design Simplicity, Adjustability Low Cost Maintenance Durability Performance (Medium Loads) Performance (High Loads).

4.2.1 Concept generation Methodology:

Describe with flow charts how the method was undertaken by describing the nature of the problem and dividing it into functions and then sub functions. Morphological analysis?

As described earlier the design of a novel feed drive can be divided into two sections namely Bearings Design and Drive Design. Further development in one or both of these branches can enhance results of metrology and Machining. I only one of them is changed for example bearing, then the changes arising from this design need to be reflected in entire conventional feed drive system and vice versa. Bearings and Drive Design is then further sub divided into its constituent components.

For Bearings section it can either be the Bearing System in itself or the just the Guideway. The bearings, guides and Drive train design Sections are further divided into its Sub-Sections as seen from *Figure 98 below*.

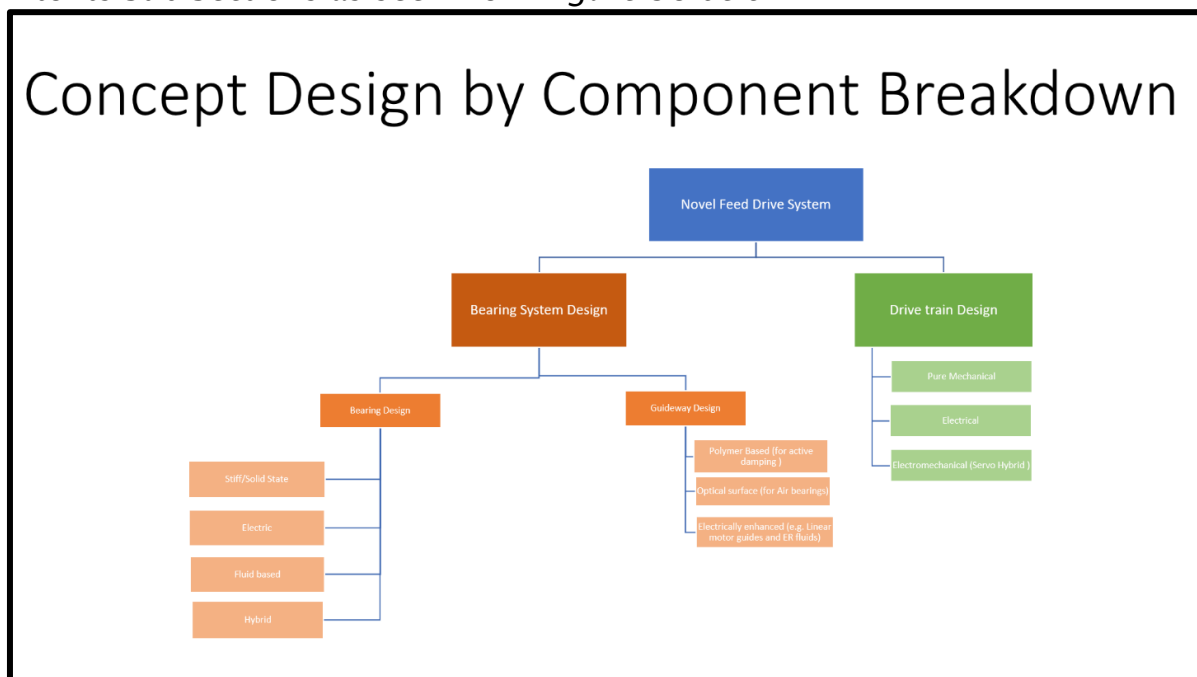


Figure 98: Concept Design by Component breakdown

The Main Function was divided into sub functions and then sub functions into sub- sub functions, the nature and physics of sub-functions was clearly understood. The solutions to solve such a problem related to sub-functions was analysed and solutions presented through concepts generation.

Three main Sub-Functions that must be achieved are: Vibration reduction, Stiffness, Rapid response. Vibrations can be further divided into sub sections such as frictionless, more Damping properties, less geometric discrepancies in contact mechanics etc. Stiffness can be subdivided into, Material properties, System rigidity and rapid response into design of a contact that can achieve frictionless high velocities.

The process leads to Sub-Assembly to Component to feature breakdown See *Figure 99 below*.

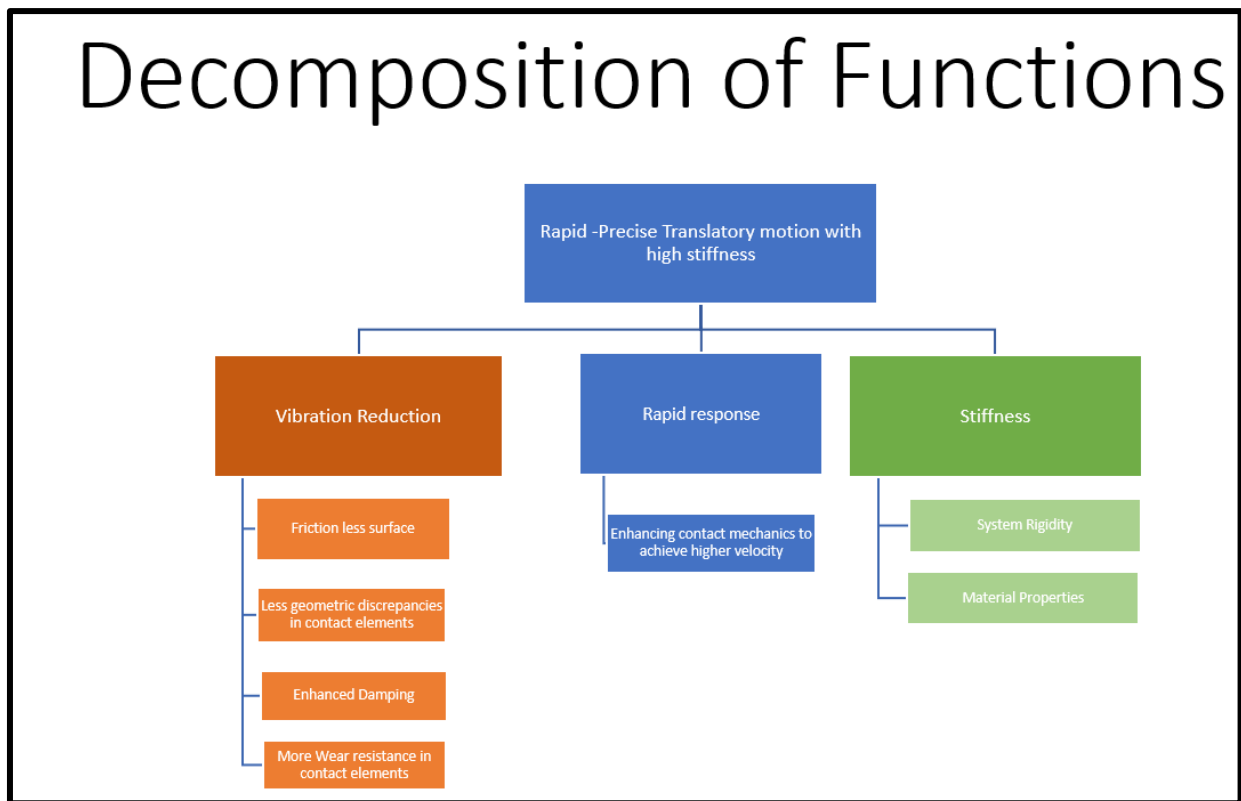


Figure 99 Decomposition of Functions

-

4.2.2 Concepts generated.

Various Concepts were generated based on the previous knowledge and brain storming sessions. These Concepts are divided into Bearing Design, Drive Design or the combination of both (a full-on system) similar to the division in literature Review. 20 concepts were generated out of which only 4 were chosen for further evaluation based on various factors including cost, performance and ease of manufacture. These 4 concepts are as follows.

4.2.2.1 Hybrid Bearing:

In order to achieve both the Precise CMM operations as well as the stiff machining operations, this concept consists of a mechanism that uses Air bearings in CMM Mode, and in machining mode adds the roller bearing modules to the already existing Air bearing mode. The system by nature needs a hybrid bearing guide as seen below. This way both CMM and Machining operations can be performed by just a simple switch from Air Bearings to a combination of Air bearings and roller bearing modules. In the Machining stage the air bearing pads and further help to dampen the effect of vibrations coming from the roller bearings. *See Figure 100.*

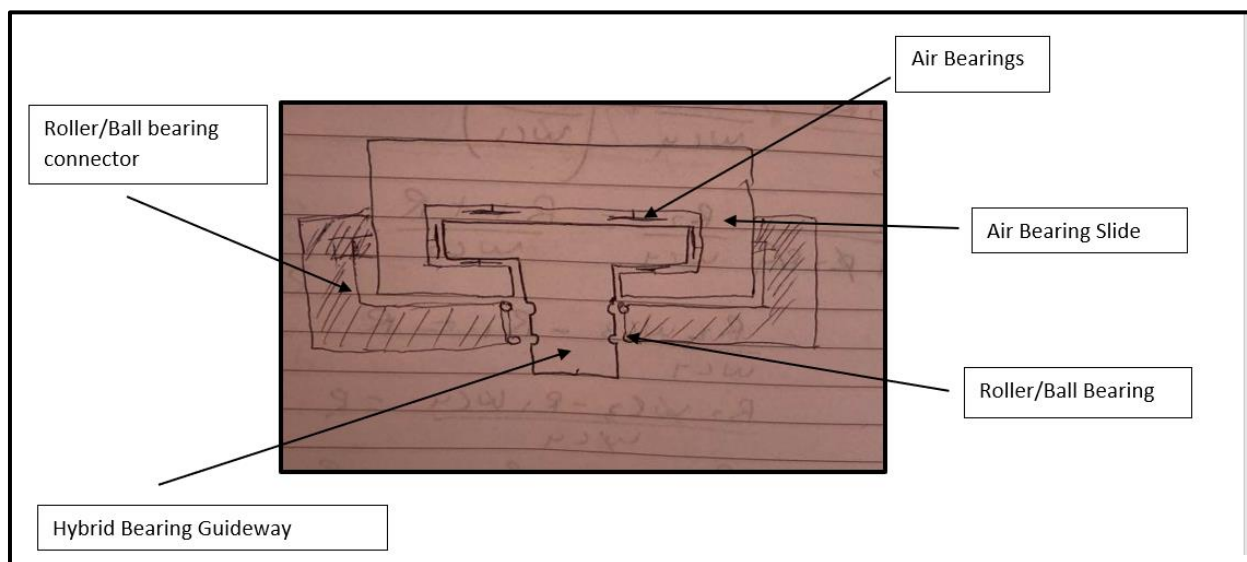


Figure 100 Concept 1 Unibody Bearing Design

4.2.2.2 Table Separation:

This concept is similar to the hybrid bearing concept it also allows the capability to transform a standalone Air bearing mode used in CMM to a hybrid CMM and Roller Bearing mode combination for Measurement as well as Machining operations. The key difference here is the switch method, here the table (work table) that rests on the Air bearings which are arranged in series in the middle can be engaged or disengaged with the roller bearing sides with the help of some coupling-decoupling mechanism. See Figure 101.

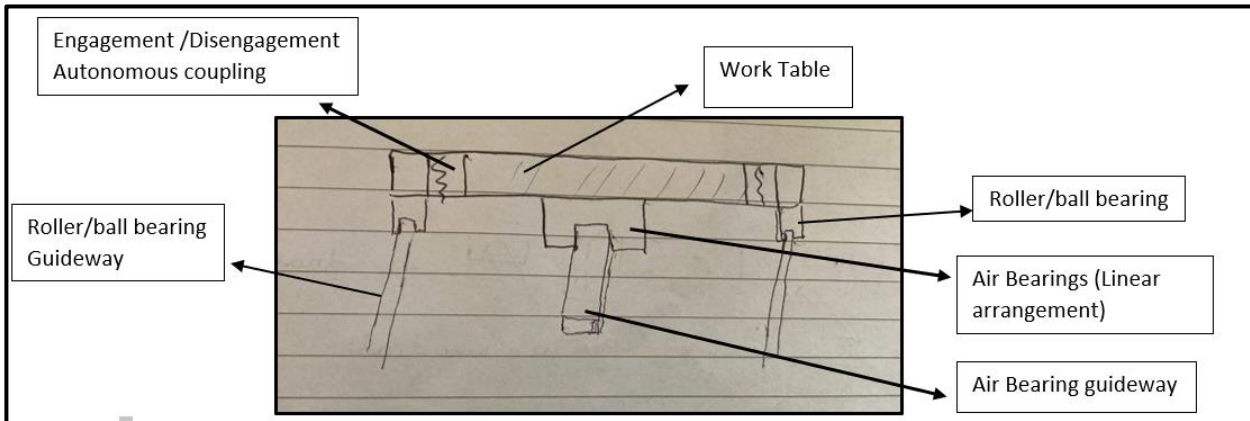


Figure 101 Concept 4 (Table Separation)

4.2.2.3 Graphene Based Super Lubricant Sliding bearing:

This is a very simple concept that uses thin 2D layers of graphene coated on some already existing friction bearing material (Steel coated with thick Turcite SKC or Moglice) housed in a rectangular block through which the 2D graphene coated guideway passes. The Layers provide a smooth friction less motion with less irregularities between the surface to surface contact. This concept can also get rid of stick slip phenomenon and can be used easily in the CMM mode. In the Machining mode however more, information is desired as to where it can sustain the heavy loads and the shop operation environmental conditions such as temperature, Chemical Resistance etc See Figure 102.

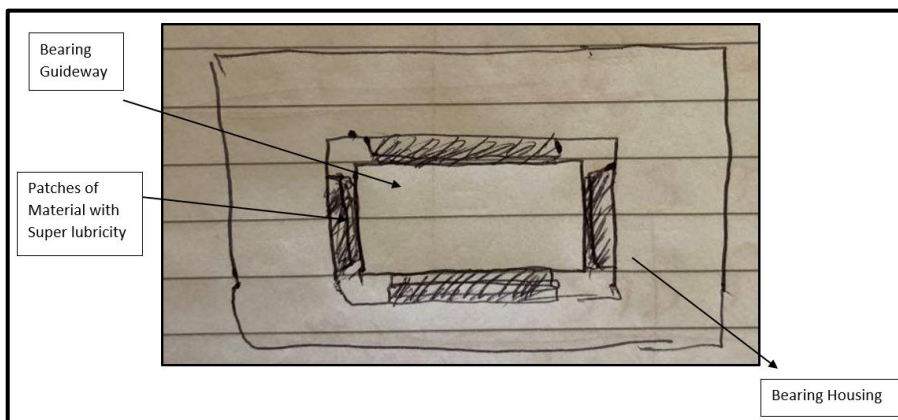


Figure 102 Concept 5 Graphene based Sliding bearing

4.2.2.4 (ER-Hybrid-twist roller/capstan/ Rp Drive and aerostatic drive):

.This concept is unique in a sense that it uses two drives an aerostatic drive (Primary) and a stiff Conventional Drive such as Capstan, hybrid twist roller or the Novel roller pinion drive (whichever is used)., a stiff Linear roller/ball Bearing, and a reservoir containing Electrorheological Fluid. The damping of any Vibrations is attained by the Er Fluid in conjunction with the damping capabilities of the Aerostatic drive itself. ER fluid not only absorbs the vibrations of the roller bearings but also of the secondary drive such as stiff Capstan, hybrid twist roller or the Novel roller pinion drive (whichever is used). The system is driven by Aerostatic Drive alone in CMM mode and both Aerostatic Drive and a secondary drive in the machining mode in both the cases ER Fluid will be active *See Figure 103.*

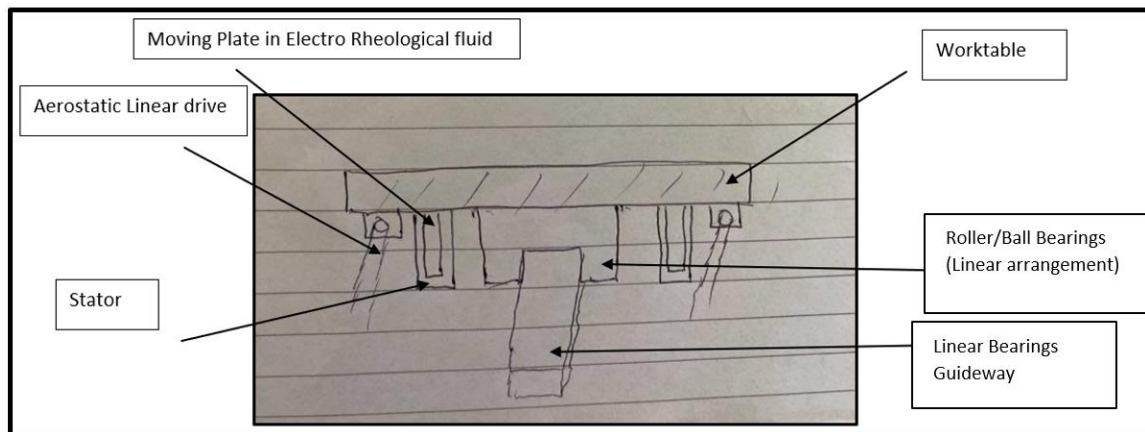


Figure 103 (ER-Hybrid-twist roller/capstan/ Rp Drive and aerostatic drive):

4.2.2.5 (Anti-Vibration pads Sandwiched):

Lastly, another method to provide smooth linear motion with ultra-low vibration was generated. This Concept used highly sensitive vibration mounts made of a special material sandwiched in between the aerostatic drive and the Work Table on the top side and the base and aerostatic drive on the bottom (same is the case on the other side of the table). In the middle however, the Linear Bearings have the Anti Vibrations pads sandwiched in between work table and the bearing at the top and at the bottom between the air bearing guide and the base. This way the all the dominant vertical vibrations can be compensated. Also, due to the shear force damping of the pads , horizontal damping may also be possible. The system is driven by aerostatic drives and uses linear roller/ball bearings in the middle See *Figure 104*.

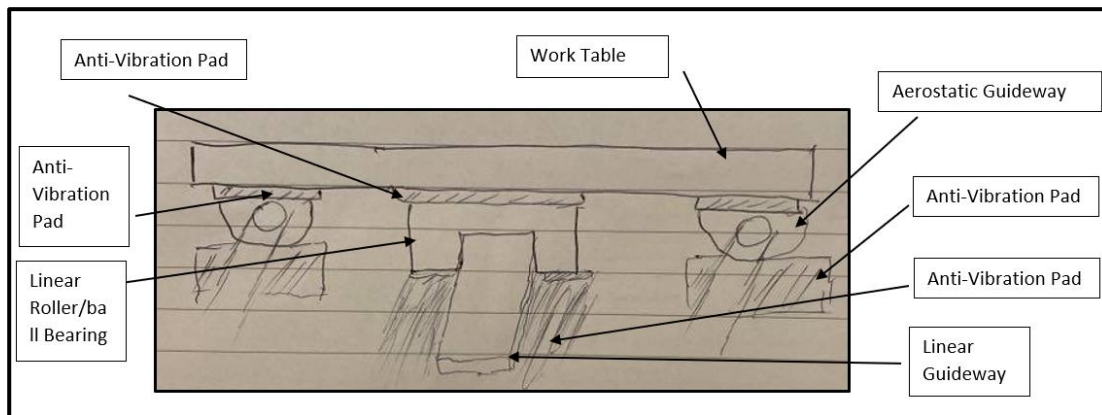


Figure 104 (Anti-Vibration pads Sandwiched):

4.2.3 Concept Evaluation

Out of all the concepts generated above only 5 of them were taken into consideration based on the various design and performance criterion. The concepts chosen were (Unibody Bearing), (Anti-Vibration pads Sandwiched),(ER-Hybrid-twist roller/capstan/aerostatic drive,(Table Separation),Super lubricant Sliding Bearing.

The evaluation was done based on 6 parameters namely, Adjustability, low cost, low maintenance, Durability, performance at Medium and Loads respectively.

Based on this criterion each concept was rated out of 5 and then the concept with the highest total was chosen. The rating is highest for the Unibody Hybrid Bearing due to following reasons: See *Table 1 below*.

| Concept | Concept 1 (Unibody Bearing) | Concept 2 (Anti-Vibration pads Sandwiched) | Concept 3 (ER-Hybrid-twist roller/capstan/aerostatic drive) | Concept 4 (Table Separation) | Concept 5 Super lubricant Sliding Bearing |
|-------------------------------|-----------------------------------|-----------------------------------------------------|-------------------------------------------------------------------|------------------------------------|-------------------------------------------------------|
| Design Simplicity | 4 | 4 | 2 | 3 | 5 |
| Adjustability | 3 | 5 | 5 | 2 | 5 |
| Low Cost | 3 | 3 | 1 | 3 | 2 |
| Low Maintenance | 3 | 3 | 2 | 3 | 2 |
| Durability | 3 | 3 | 2 | 3 | 3 |
| Performance (Medium Loads) | 5 | 2 | 4 | 3 | 4 |
| Performance (High Loads) | 5 | 3 | 3 | 5 | 3 |
| Total | 26 | 23 | 19 | 22 | 24 |

Table 1 Concept evaluation Matrix

4.2.3.1 Design Simplicity

Out of All the chosen concepts Unibody Hybrid Bearing was chosen, the bearing although has the design simplicity rating next to super lubricant-based bearing, it is similar in comparison with Anti-Vibration pads Sandwiched. Unibody Hybrid bearing uses a conventional stiff ball screw drive rather than complicated less stiff aerostatic drives with ER Fluid reservoirs as is the case with Concept 3. Furthermore, it's like a simple module similar to Super – Lubricant bearing and hence dominates over Table separation method as well due to lack of complex coupling on design simplicity criterion.

4.2.3.2 Performance

Although it's hard to judge about the performance at this stage, but it's evident that due to switching of Air bearing stage to linear roller/ball bearing stage both the processes of Precise measurement and Machining stiffness can be easily attained and each mode has a proven record of their capability in the metrology and Machining environment as compared to other drive options. In contrast, In the Table Separation concept switching is difficult to achieve at any given time compared to Hybrid bearings and in others such a switching is missing.

The Super lubricant Sliding Bearing needs to be tested from scratch as its not used in linear friction drives yet, ER-Hybrid-twist roller/capstan/aerostatic drive due to

its complex nature also needs to be tested from scratch. The Anti vibration pads in concept 2 need to be very advanced to sense the vibrations at micro-level and dampen their effect this also has not been widely proven yet.

Thus, the performance at both high and low loads is easily achieved by Hybrid Bearing.

4.2.3.3 Durability/Low Maintenance

The lesser the parts, the lesser the spread out, the more the flexibility and hence lesser the durability. ER-Hybrid-twist roller/capstan/aerostatic drive by its very nature is less durable due to many components. In Contrast, all the other concepts have a same rating as their construction had a level of complexity on a similar scale for example the effect on durability due to continuous friction and chemical attack on the super-lubricant bearing despite its compact nature is same as the aging effects of Anti -Vibrations mounts and table separation coupling. The more durable concept will always save the maintenance time and additional costs therefore the low maintenance section was filled based on low cost and durability ratings.

4.2.3.4 Low Cost

(ER-Hybrid-twist roller/capstan/aerostatic drive) will of course be very expensive due to a variety of components used, the super lubricant used can also be very expensive because besides its lubricant nature it requires other additional properties for example 2D Graphene that can resist shock loads, offer High performance under high machining loads and are chemically resistant. The Table Separation, Anti -Vibration pads, and Unibody Hybrid bearing concepts may all fall within the same price range therefore they have the same low-cost rating.

4.2.3.5 Adjustability

There is no need of adjustability in Super lubricant Sliding Bearing, (ER-Hybrid-twist roller/capstan/aerostatic drive) and (Anti-Vibration pads Sandwiched therefore they are at the top in this rating. In Comparison, however both Table separation and Unibody Hybrid bearing concept requires switching which is in turn easier in the Unibody Hybrid bearing concept as the switch is possible at any given time (in-situ) while as in the Table Separation concept one has to arrive at a coupling position.

Based on the evacuation carried out in the section above it can be concluded that the Concept 1 (Unibody Bearing) will be chosen for further development.

CHAPTER 5: DESIGN AND COMPUTATIONAL VALIDATION

This Section covers the Mechanical design of the chosen concept i: e the hybrid bearing. It also includes relevant calculations undertaken during the design and verification of the computational Methods including Finite Element analysis.

5.1 MECHANICAL DESIGN OF HYBRID BEARING/GUIDE.

In this section full detailed design and the related specification will be discussed in depth followed by justification of each component design.

| Main housing | Flat Ball end mounting screw. | Piezo electric actuator | Plan linear friction bearings |
|----------------------|-------------------------------|-------------------------------------------|-------------------------------|
| Main Air Bearings | Lead Nut | Linear recirculating ball bearing modules | Novel Hybrid Guideway |
| Preload Air bearings | M8 × 16 Threaded rod | Actuator housing | Blanking Plate |
| Ball Mounting Screws | lead screw | M6 bolts | |

Table 2 Shows Hybrid bearing components

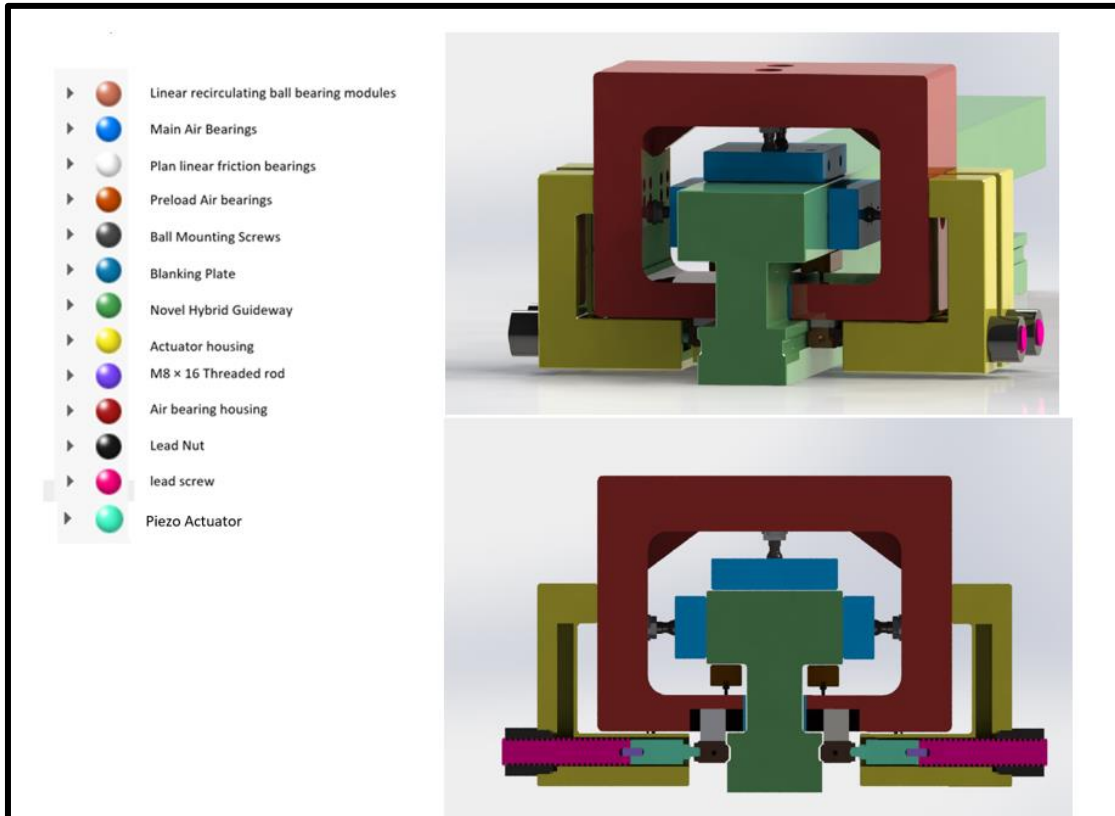


Figure 105 Shows Colour code mapping of the Hybrid Bearing

5.1.1 Hybrid Bearing Design Bill of materials:

The hybrid bearing system is made up of following components:

5.1.1.1 Main housing:

The main housing contains an envelope for Air bearings. Four (50 ×100) Flat rectangular air bearing pads two on the top and one on each side of guide and two (25 ×50) Flat rectangular air bearings for preloading. The main (50 ×100) Air bearings are attached to the housing via 13 mm Diameter /M10 ×0.75 ×54 mm lg ball mounting screws while as two preload bearings are connected with the help of 6mm Diameter /M5 ×0.8 × 27.5 mm lg flat ball end mounting screw. *See Figure 105 .*

5.1.1.2 Actuator housing:

The actuator housing contains the lead screw and its corresponding nut with one end of lead screw passing through Lead Nut, BN Style, 18 mm nominal Diameter screw and 8 mm lead Right handed Screw with a design load above 1000 lbf made of SAE 660 Bronze, while the other end is attached to the piezo electric actuator for active damping through an 18-8 Stainless steel M8 × 16 Threaded rod. *See Figure 105 .*

The actuator housing is attached to the Main housing with the help of 4×M6 bolts. There are 4 actuator housings in total containing 4 corresponding hybrid actuators. *See Figure 105 for detail. See Figure 105 .*

5.1.1.3 Linear recirculating ball bearing modules:

linear recirculating ball bearing modules are connected to 2 Hybrid actuators on both sides of the hybrid bearing with the help of 4 × M8 threaded head of piezo. *See Figure 105 .*

5.1.1.4 Novel Hybrid Guideway:

In order to allow a transit from Air bearing stage to a Hybrid bearing stage a novel guideway is designed. The upper surface of the guideway provides a floating surface for six Air bearings, while as the lower half accommodates the linear ball recirculating bearing modules in its grooves one on each side. *See Figure 105 .*

5.1.1.5 Plain Bearings:

The linear bearing is bolted to the Plan linear bearing for translational joint requirement during connection and disconnection of modules. *See Figure 105 .*

Refer to section for in depth details of each component

5.1.1.6 Solution Statement:

The Hybrid Bearings enable the Machining centre to do smooth rapid operations up to 30-50 m/s without any noise and accurate scanning probe operations which are comparable to modern offline CMM machine. This is mainly due to the fact that use of air bearings compared to linear roller bearings solve the following issues of linear recirculating bearings:

- The flatness issues in the guide cause truck of the linear bearing to move as well as damage the rail while as in air bearings the irregularities are averaged in the rail to prevent damage. There is no contact as well.
- Unwanted motion due to difference in size of balls in all directions that cause unwanted vibrations.
- Velocity ripple due to changing velocity direction in between truck and rail, also causing vibrations.
- Lubrication, causing out grassing.
- Stick slip phenomenon causing overshooting especially light loads for short distances
- Due to preload wear degrades the rail and truck. causing friction changes, the wear is a function of load, acceleration, velocity and distance.

5.1.1.7 Working principle (Solution):

Machining mode:

The Linear Bearings Modules and the Air bearings operate together to perform machining operations; this combination takes the advantage of High stiffness of Linear recirculating bearings (The Bearings allows for a stiff operation at high machining forces) whilst using damping from air bearings (with the help of squeeze film damping effect) to enhance the machining performance in order to achieve precise and accurately machined parts.

CMM (Coordinate measuring machine) Mode:

There is no need of Linear recirculating roller bearings in measurement mode as it doesn't demand a highly stiff structure (no machining forces are present), In addition to that linear roller bearings are major source of errors in precision measurement therefore the linear bearing modules are disconnected from the guide. This is done by releasing the force in the piezo electric actuators and then using the lead screw to detach and move the linear bearing modules away from the guideway grooves (see fig). In this way the machine runs on Air bearings stage only, enabling rapid, frictionless and vibration free motion ideal for measurements up to a nanometre accuracy level. (See Details)

5.1.2 Detailed Design and Specifications

5.1.2.1 Justification of external forces and thermal effects:

In order to start the designing process, the evaluation of external forces becomes an essential requirement. The 2 major types of external forces that the bearings withhold are Static Forces due to the weight of the Assembly carried by the bearing and the machining forces which are dynamic in nature as their amplitude varies with spatial coordinates at constant machining parameters.

The machining forces which are dynamic were taken to be of a constant magnitude for ease in design purposes. This magnitude was chosen in a way that it should cause a very high load and moment reaction of bearings. This selection of magnitude is not easy as it varies with machining parameters (Feed rate, depth of cut, Spindle speed etc.), the tool geometry and material, the size of the machine tool centre and the material of the work piece and several other parameters. This demands an investigation to validate the required maximum dynamic forces.

A medium sized machine is widely used; therefore, they were taken as the basis for enquiring high amplitude machining forces with the hardest manufactural material being titanium.

Determination of Static Forces:

A Conventional 2 axis drive system like comparable to Hurco VMX 3001 consists of a saddle, 8 linear recirculating bearings, a table, 2 Ball screws, A motor and 2 Nuts. The other parts were ignored as they have lesser weight compared to these major components. The highest work piece that a bed usually takes is 100 kg.

The *table 3 below* shows the values for each component obtained from Hurco VMX 3001 machining centre CAD data as well as the similar drive system of a Bridgeport VMC 1000 Vertical milling machine.

| Component | Units | Total Mass (Kg) | Weight (N) |
|------------------------------|-------|-----------------|------------------|
| Machine Table | 1 | 1×264.18 | 2591 |
| Saddle | 1 | 1×262.51 | 2575 |
| Linear Recirculating bearing | 8 | 8×0.26=2.08 | 20.40 |
| Ball screw Nut | 2 | 2× 16.3 | 320 |
| Ball Screw | 2 | 2 × 11.6 | 227 |
| Motor | 1 | 1× 21 | 206 |
| Work piece (Max) | 1 | 1×100 | 980 |
| Total Weight: | | | 1733+5186=7000 N |

Table 3 Shows the estimated Total Mass and hence the weight of the Test feed drive rig

This gave a total force of 7000 Newton. This force is divided among 4 linear bearings at the embedded drive axis that carries the stacked axis.

This relates to the weight of 1800 N on each bearing, thus the determined Static force on each bearing drives the selection of the Air bearing pads.

2000 max (200 kg work piece), 1733 max (100 kg). See table 3 above.

Determination of Machining Forces:

Hybrid bearings are exposed to high loads during machining and these loads change. The design is driven by the maximum machining force that bearings have to withstand therefore, in order to determine this, first a machining experiment was carried out on Cincinnati arrow which has the same volume as the Hurco VMX 3001. A dynamometer kristler was connected during machining a gild copper rectangular bar. The data was generated with the help of dyno ware.

Machining Experiment:

At a feed rate of 716 mm/min, with the spindle speed of 4775 Rev/sec and a depth cut of 5 mm on a copper-based alloy (gild copper).

The results show that the X direction easily reaches 500 N of force value, The Graph is windowed representation of the original data for approx. 0.134 secs. (See Figure 106 and 107 below.)

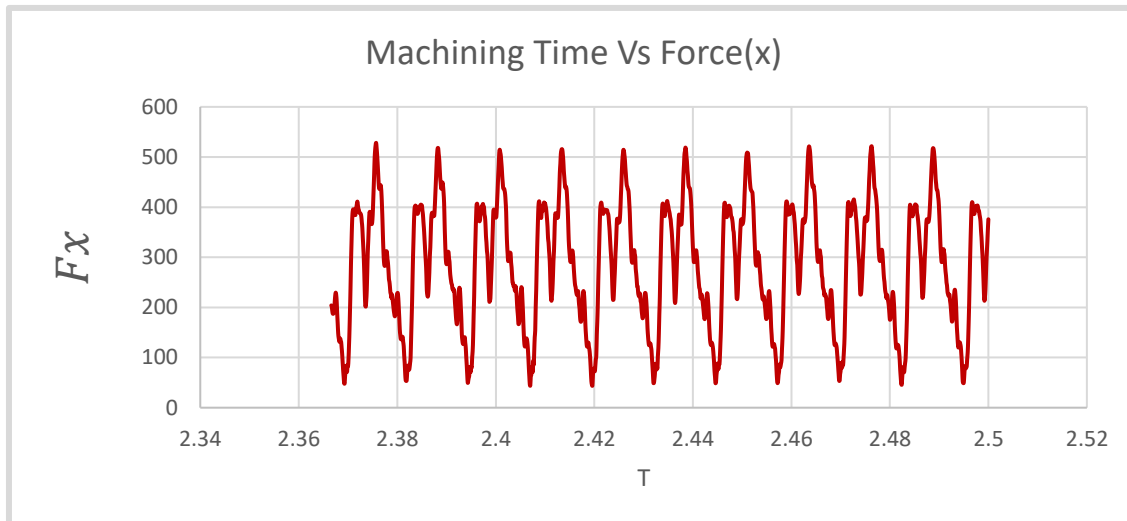


Figure 106 Shows machining time vs "x" force component

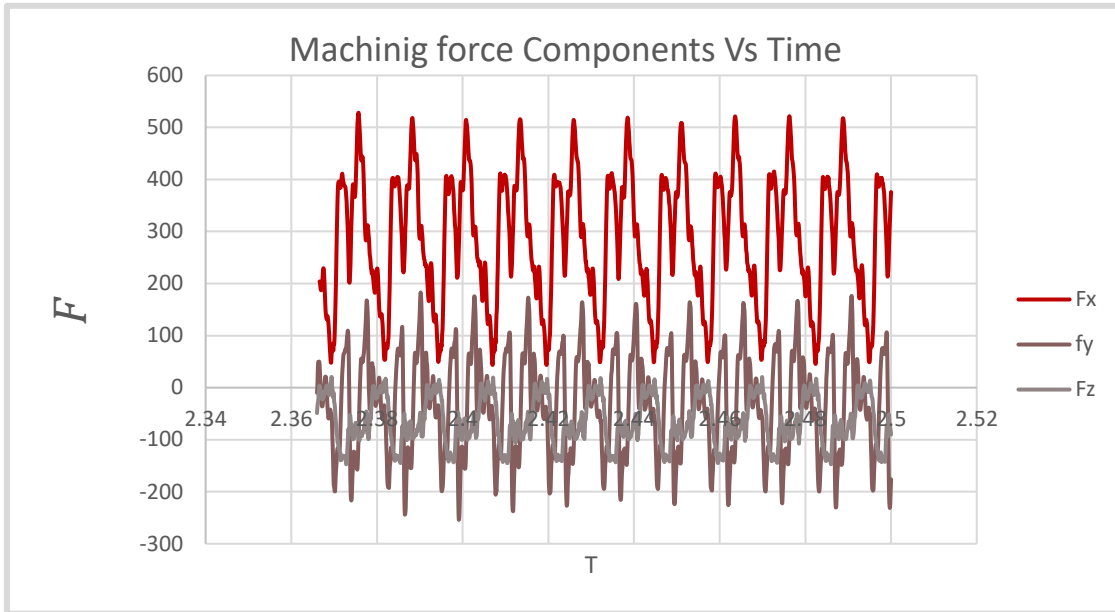


Figure 107 Shows Machinig force Components Vs time

Data from Papers:

Higher young’s modulus 210 GPA than. of copper, and Lower cutting speeds with the same depth of cut at 5 mm may be a reason of why 5000 N is achieved instead of 500N. Other variation May be the chip load, Feed rate etc. Also, in the cutting force experiment of Inconel 718 nickel the highest cutting force of 500 N at 1.2 mm depth cut, Feed rate of 32mm/min and cutting speed of app 10 m/min by (Alauddin, M; Mazid, M.A; El Baradi, M.A;(1998)). Since the cutting force increases linearly with the cut depth (Conversation, C., Conversation, C., & profile, V. (2020). See Figure 110 , the depth of 5 mm demands a force of 4 times higher than the force at 1.2mm. This also points out that the forces in the machine tool can easily reach the order of 10^3 . Also, from the paper (Altin, A. (January 01, 2014).) can be seen that the chromium steel with a depth cut of 1 mm, cutting speed of 70 m/min, feed rate 0.30 mm/rev under certain machining parameters is 800 N. Increasing the depth of cut to 5mm increases the cutting force from 800 N to 4000 N See

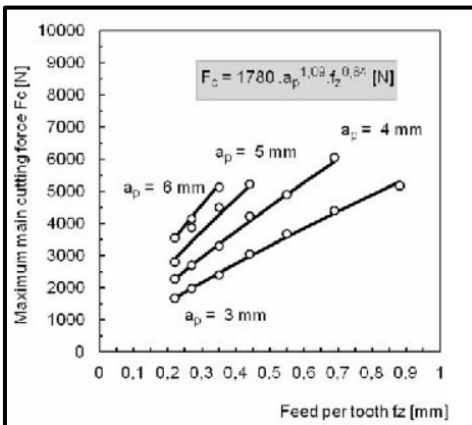


Figure 108 maximum Cutting force for a steel Chromium 210 Cr12 Steel

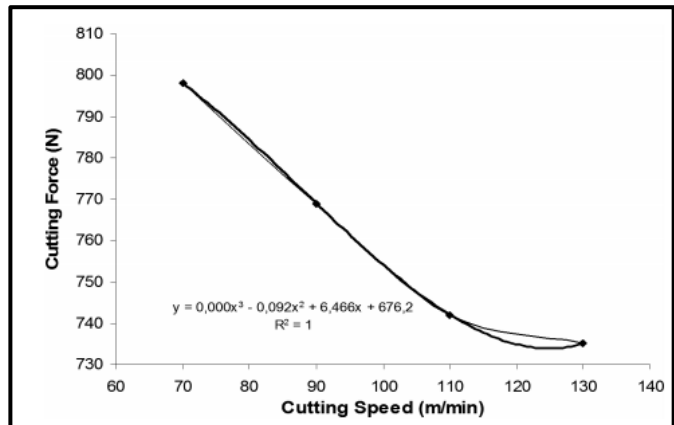


Figure 109 Cutting force vs Cutting speed for Chromium

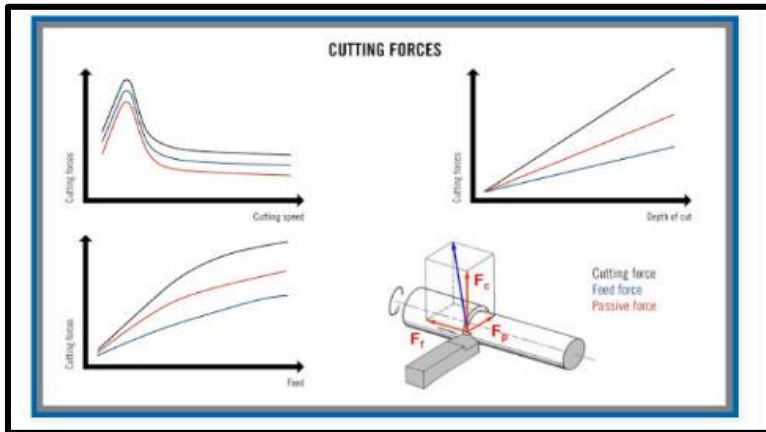


Figure 110 Graphs showing Cutting force parameters

Figure 109 . As seen from Figure 108 the maximum Cutting force for a c45 workpiece cutting can easily go above 5000 N. (Bono, J; Markova, I; Vrabel, M;(2012)).

From the experiment and the literature review it can be noted that when a cutter cuts in certain direction where the bearings have to bear certain number of loads (both the Air bearing and linear recirculating bearing must withstand at least 6000 N of force in total).

6000N when divided by 4 gives a value of 1500 N. This is the amount of machining force each linear bearing module must handle.

Determination of Thermal effects:

In terms of thermal effects, the critical thermal loads in a CNC range between 800 to 900 degree Celsius (Managing thermal loads in milling processes | Secotools.com. (2020)), but these temperatures are only confined to machine tool cutting area and not the feed drive system where the new hybrid bearing is located, Due to intermittent nature of the milling cutter during the cutting operation the temperature alternates, In the CNC the only elements that absorb this metal cutting heat energy is the workpiece itself absorbing 10% of heat generated, 10 percent goes into the tool and the remaining 80 percent is carried by the chips. Therefore, for a primary case only components closest in the vicinity of air bearing will be considered and they are the components of the feed drive.

In the feed Drive however the temperature in the ball screw can rise from 25 up to 50 degree Celsius (Li, Y., Su, D., Cai, X., Wu, W., Zhang, J., & Zhao, W. (2020)).

Also, Jang, S., Jang, S., Khim, G., Khim, G., Park, C., & Park, C. (2017), shows that a linear recirculating bearing maximum temperature rise due to friction is nearly about 5 degree Celsius from ambient temperature of 20.5 degree Celsius. See Figure 111 below.

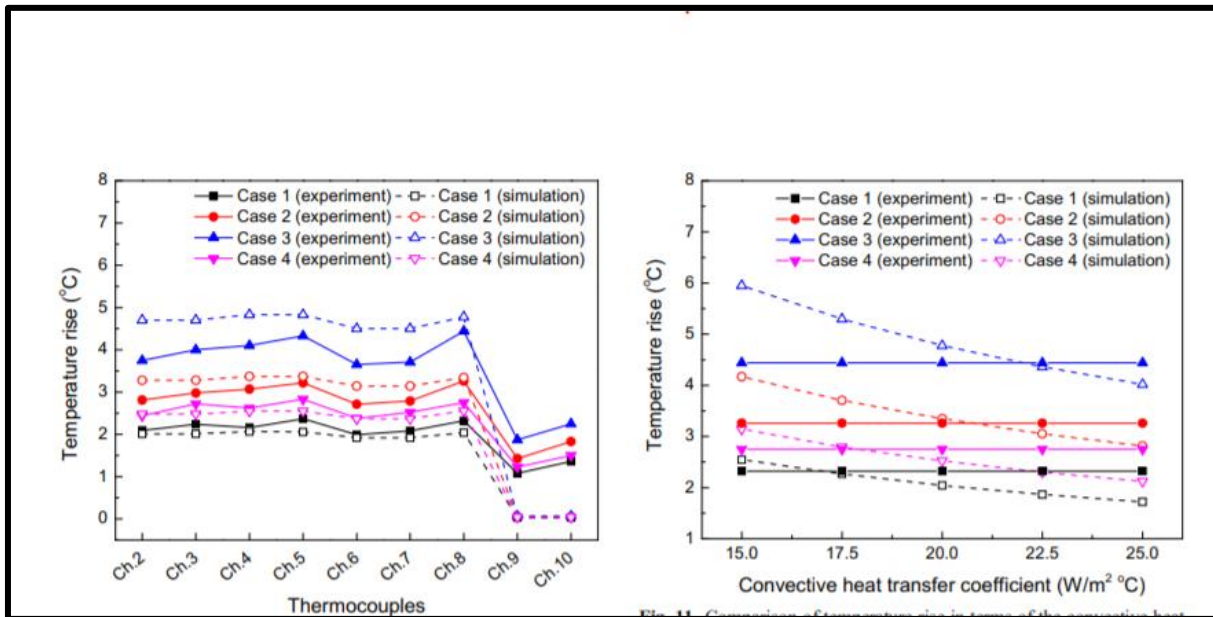


Figure 111 Comparison of Temperature rise between experiments and simulations (left), Temperature rise comparison in terms of convective heat coefficient (right)

Hua, W., Zhou, W., Liu, B., Yu, S., & Wong, C. H. (2009)), shows the flying height tends to decrease by 2nm in hot and humid environment, although this seems to be the case for sub nanometre levels of flying heights it may well be considered for micrometres levels for safety. Currently the Air bearing operates near room temperatures with very low tolerance of +/-30-degree F. Any temperature above this can cause pressure loss as temperature lowers the density and hence pressure. This loss can then lower the bearing height. Thermal Insulation maybe

an important consideration, this can be achieved by using thermal cladding on main frame of the bearing and between the roller bearing and frame contact to avoid any further heat transfer to the air bearings. The flying height tends to decrease by 2nm in hot and humid environment. (Hua, W., Zhou, W., Liu, B., Yu, S., & Wong, C. H. (2009))

The temperatures in the CMM mode however reduce due to less loads on the screw and no load on roller bearing modules.

Although the air bearing guide recommends use of material such as chromed steel, granite, stainless steel, hard-coated aluminium and ceramics, glass, more research needs to be conducted on guide systems thermal expansion. The thermal expansion may result in protrusions which can alter the flying gap of air bearing resulting in failure.

5.1.2.2 Justification of Air bearings.

The static forces as determined from previous sections are 1800N and dynamic forces 1500N respectively.

The static forces due to the weight of the structure and the forces due to machining operation obtained were used for the selection of Air bearing pads for the Hybrid Bearing.

There are already various established air bearing companies available in the market including OAV Air bearings, PI (Physik Instrumente) and New way air bearings etc. New Way air bearings were selected they are one of the leading air bearing design and manufacturing companies with a good engineering support. Flat rectangular air bearings were chosen due to their simplicity.

The Static force due to the weight of the machine assuming the system is mostly horizontal almost lies entirely in the z direction and hence the pressure due to air film in the z direction has to be comparatively higher than the air pressure in lateral directions i.e +y and -y. The force in z direction is the static force due to weight of feed drive and its relative components which amounts to 1800 N and the machining force (approximate Maximum) of 1500 N resulting in a total force of 2300 N.

In reality the bearing should have forces much higher than 2300 N, safety factors of above 2 or so, but in case of air bearings the safety factor is quite low due to the air gap being the function of operating air pressure, more air pressure means more force on the bearing this demands lesser gap. The larger the gap the lesser the stiffness of the bearing. In order to maintain an optimal gap of 3 to 5 microns, pressure should not exceed a certain value. Also, air flow is a cube function of the

gap, the lesser the gap the lesser the airflow resulting in low airflow supply which reduces costs.

Due to this condition the air bearings that can sustain a load > 2300 N is required but the load should not be too high.

Also, according to the handbook (Air bearing application and design guide by new way air bearings) Bearing with lower pressure, large surface provides higher damping and stiffness and reduced flow requirements and higher safety factor than bearings sized at marginal capability with high pressure.

A flat rectangular bearing with an ideal load of 1112 N at 414 Kpa (60 psi) is selected This load can be easily increased up to app 1500 N floating at 3 microns at 414 Kpa (60 psi) and up to 2000N floating at 3 microns at 552 Kpa (80 PSI), including 2 such bearings in vertical direction can easily achieve a total load configuration of 2300 N at approximately 4.5 microns, at low pressure which is 414 Kpa (60 psi) which is ideal for damping during cutting as well. If a work piece of 100 kg is used the air (200kg work piece give) bearings will still provide at 552 Kpa (80 psi). See Figure 112 below.

The lateral air bearings restrict the lateral movement of the feed drive and withstand small contact forces transferred by the scanning probe in CMM mode.

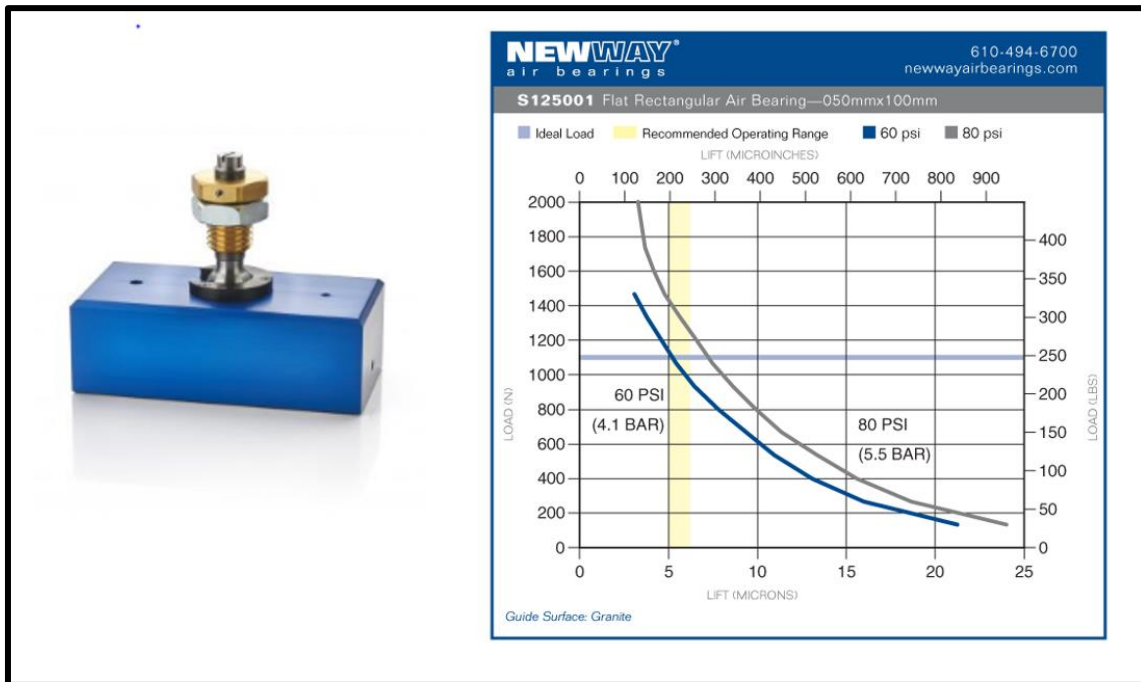


Figure 112 Bearing loading vs Lift graph

In machining mode, the Air film in the lateral sides withstand a tiny portion of static forces due to the X components of weight of some elements (in addition to lateral machining forces) whilst sharing this with the linear recirculating bearings. This however is a very tiny portion the major design goal of the air bearing in lateral direction in machining mode is to provide enough damping to absorb the

machining vibrations. A small bearing may have been used as the machining forces are now supported by the Linear roller element bearing modules, but in order to increase damping using larger surface area and operating the bearing at low pressure gives high damping. In order to achieve only one bearing is used on each side of the guide. The Total Load 2300 N is now shared by the linear ball bearing modules as well as the Air bearings.

5.1.2.3 Justification of Roller element bearings.

The overall performance of the metal cutting is significantly determined by the linear bearings, it has a direct effect on the profits, better quality parts and hence customer satisfaction. In addition to bearing tolerances and travel smoothness the resistance to deflection is one of the primary design goals of linear bearings this drives the tool point accuracy at high cutting loads and accelerations.

As seen from *Figure 113* the one major advantage of O pattern over X pattern is the ability to handle moments, due to the narrow size of the geometry formed by X pattern the distance of couple arm is less meaning the forces on the balls are high while as in O type the distance of couple arm is more hence the forces required to stay in equilibrium by balls is lesser comparatively. O style bearings can help in reducing the maintenance and the addition of rigidity elsewhere in the machine extending the overall life of the machine. Due to these advantages of O type configuration was chosen.

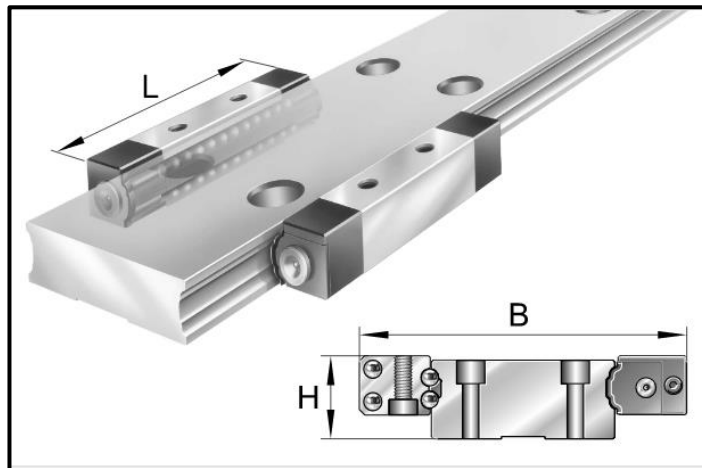
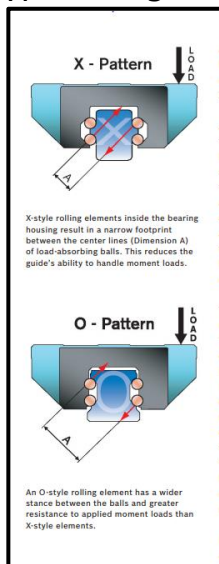


Figure 114 (INA- Medias Bearing Modules)

Figure 113, O type Linear roller bearings Vs X type linear roller bearing configuration

| Bearing Name | Basic Static Load rating (N) | Basic Dynamic Load rating (N) | Length (Containing linear recirculating balls) | Height | Width | Mass | Stiffness |
|---------------------|------------------------------|-------------------------------|-------------------------------------------------|--------|--------|--------|-----------|
| INA-KUVS17-B | 46500 N | 26000 N | 96 mm | 18mm | 116 mm | 0.2 kg | 600N/um |
| Bridge Port Bearing | 167000-222000 N | 101000-123000 N | 137 mm | 45 mm | 120mm | 3.5 kg | 1560 /um |

Table 4 Shows Bearing details

In one module $F_{tz} = \frac{3500 N}{2} = 1750 N$

The bearing module should possess static load $> \sqrt{N_z \cos^2 \alpha + N_z \sin^2 \alpha} = \sqrt{\left(\frac{3500}{2}\right)^2 + \left(\frac{3500}{2}\right)^2} = 2475 N$

This gives the normal reaction force of $N_z = 2475 N$

It can be seen that the static loading rating safety factor is $S_f = \frac{\text{Basic Static Load rating}}{\text{design load}} = \frac{46500}{2475} = 19 .$

The length and the width are nearly comparable, the height is not a factor as the linear bearing module doesn't have a structure to it and it depends on the air bearing housing thickness. The load rating Values are however higher in the bridge port linear bearing nearly twice the stiffness of the 2 linear bearing modules combined (as this will be equivalent to the linear bearing) .

This might seem over engineered but such a high safety factor is desired when the system parameters and behaviour is not entirely predictable e.g. the effect of moments about all three axes (pitch, roll and yaw moments), and other shock loads that often occur during machining operations, they also effect the dynamic loading. Due to shock loads an unpredicted condition appears this forces the need to implicate the static load safety factor = basic static load/maximum combined static load. Maximum combined static load contains shock loads plus other static loads and ranges from 2 to 6.

Safety factor of around -4 to 6 static.

Although, the Static stiffness of linear recirculating bearings was missing it was confirmed from few sources that the stiffness varies from 400 N/um to 600N/um approximately. This value is a function of preload as can be seen from the (See Figure 115) below. (Tong, Van-Canh; Khim, Gyungho; Hong, Seong-Wook;(2019). Assuming a medium to light preload situation, a stiffness value of 600 N/um can be assumed (Collins, D. (2020) (See Figure 116)

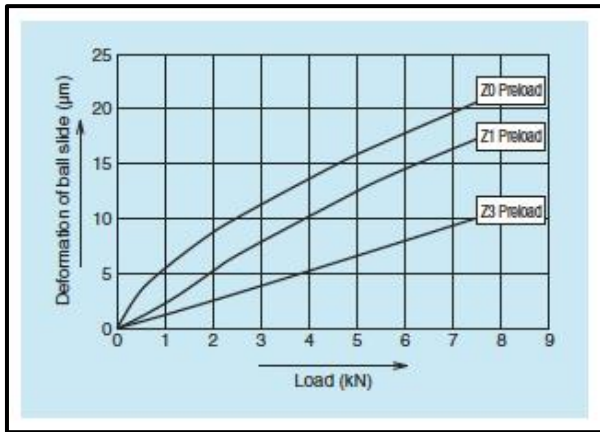


Figure 115 Deflection of Linear guide with no preload, light preload and medium preload

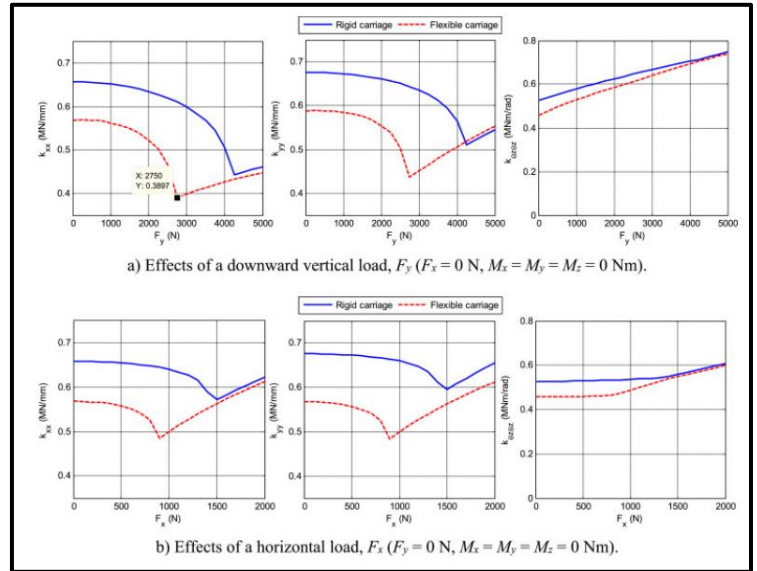


Figure 116 Stiffness of the linear recirculating bearing

The length of the guide that determines the no of rolling elements in the linear guide is similar (99 mm) in the paper from where the stiffness was assumed of the bearing and the INA-KUVS17-B that has (96 mm). (Tong, Van-Canh; Khim, Gyungho; Hong, Seong-Wook;(2019).

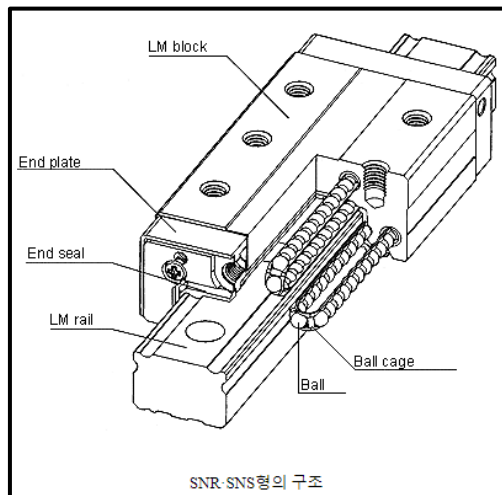
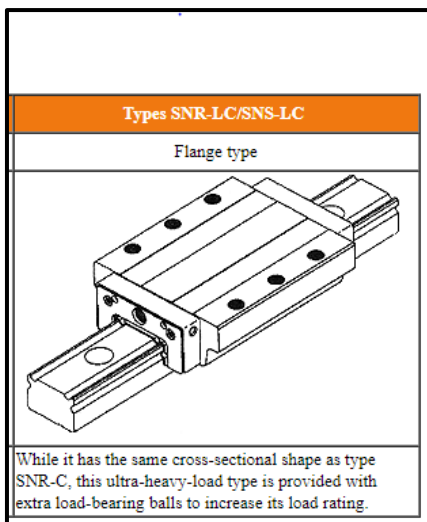


Figure 117 Shows the original bearing used

5.1.2.4 Justification of actuator Design.

Derivation of Clamping Force:

The Linear bearing modules need to be clamped to the Novel Hybrid guideway in order to carry the X Component of the static forces due to the weight of the 2-axis feed drive. Therefore, the actuator must provide a force that can withstand the X component of static forces as well as machining forces. Using 2d equilibrium equations one can derive these forces as follows: (Refer to Figure 118, Figure 119 and Figure 120 below).

$$\sum F_z = A_l + N_{za} + N_{zb} - F_{tz} = 0$$

A_l = Total Air bearing load by $2 \times (50 \times 100)$ air bearing pads in +ve z direction

N_{za} = Total Normal force on side A in +ve z direction

N_{zb} = Total Normal force at side B in +ve z direction

F_{tz} = Total Force in -ve z direction

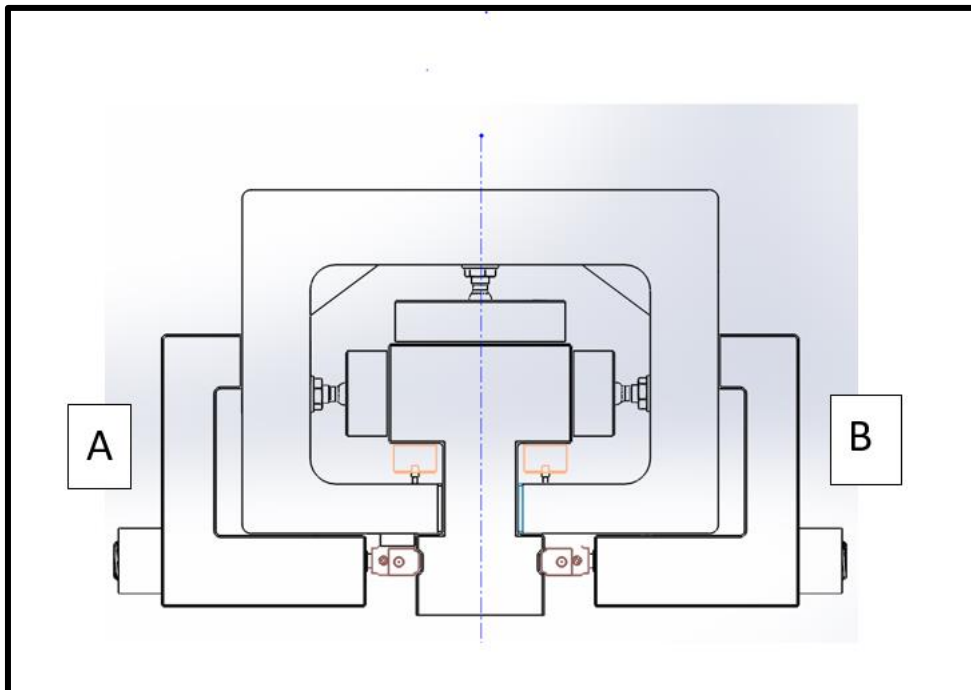


Figure 118 Shows the Hybrid bearing Sides A and B

The Bearing External forces are symmetric about the Z axis therefore the normal forces provided by Linear recirculating bearing support are equal i.e $N_{za} = N_{zB}$

When the forces in x direction dominate, the following equilibrium equation can be used as an initial guess.

$$F_{tx} = \text{Total Force in } -ve \text{ x direction}$$

$$N_{xa} = \text{Normal force provided by the bearing in } +ve \text{ x direction}$$

$$\frac{A_l}{2} = \text{Total air bearing load in } +ve \text{ x direction, including preload}$$

$$\sum F_x = \frac{A_l}{2} + N_{xa} - F_{tx} = 0$$

The Equations can be manipulated to get the best anti-vibration characteristics from the Hybrid bearing, specifically by enhancing the damping of air bearing without causing negative effect in linear recirculating bearings.

The general 2d Equilibrium equation for a Z load and 4 row linear recirculating bearing is with a certain contact angle (α) is given as:

$$\sum F_Z = A_l + N_1 \cos\alpha + N_2 \cos\alpha - N_3 \cos\alpha - N_4 \cos\alpha - F_{tz} = 0$$

the equation...will be manipulated to match maximum force condition for Both X and Y applied directions

Operation under Maximum Force Conditions:

Using Symmetry and equilibrium on side A only, using the equation *See Figure 119*.

Machining in Z:

$$\sum F_Z = \frac{A_l}{2} + N_{w1} \cos\alpha + N_{mz1} \cos\alpha - N_{w3} \cos\alpha - N_{mz3} \cos\alpha - \frac{F_{tz}}{2} = 0$$

$$N_{mz1} = \text{Machinig force}$$

Assuming the force is only carried by lower rail in z direction, and upper rolling elements barely contact due to large forces in z direction along the centre line of novel hybrid guide.

$$-N_{w3} \cos\alpha - N_{mz3} \cos\alpha = 0$$

The equation can be rewritten as:

$$\sum F_Z = \frac{A_l}{2} + N_{mz1} \cos\alpha + N_{w1} \cos\alpha - \frac{F_{tz}}{2} = 0$$

$$N_z = \frac{(F_{tz}/2 - A_l/2)}{\cos\alpha}$$

$$N_z = (N_{mz1} + N_{w1})$$

$(N_{mz1} + N_{w1})\cos\alpha =$ Force required by in z direction during Z machining forces

$(N_{mz1} + N_{w1})\sin\alpha =$ Force required by Piezo actuators during Z machining forces

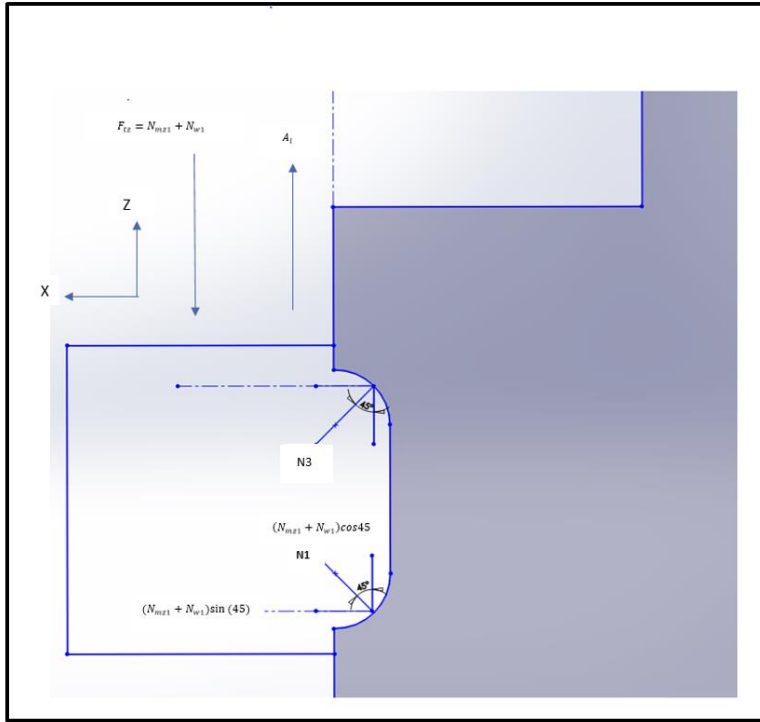


Figure 119 Equilibrium equations for Machining forces in Z Direction

In X direction or Lateral direction both the rows are affected, See Figure 120

$$\sum F_x = \frac{A_l}{2} + N_{w1}\sin\alpha + N_{w3}\sin\alpha + N_{mx1} + N_{mx3} - F_{tx} = 0$$

Since the static load is assumed to be high enough so that the upper left row (the section under analysis) normal reaction is nearly zero as discussed in the previous case. In addition to this the bearing load $\frac{A_l}{2}$ by the air bearing on this section (Left side) of Hybrid Novel guideway is cancelled by the air bearing load on the opposite side and hence has no effect on the max clamping force. Therefore,

$$N_{w3}\sin\alpha = 0$$

$$\frac{A_l}{2} = 0$$

$$\sum F_x = N_{mx1} \sin \alpha + N_{mx3} \sin \alpha + N_{w1} \sin \alpha - F_{tx} = 0$$

$$\sum F_x = N_{mx} \sin \alpha + N_{w1} \sin \alpha - F_{tx} = 0$$

$$N_{mx} \sin \alpha = N_{mx1} \sin \alpha + N_{mx3} \sin \alpha$$

= total Normal reaction against machining force alone by the whole linear recirc module

$$N_x = \frac{(F_{tx})}{\sin \alpha}$$

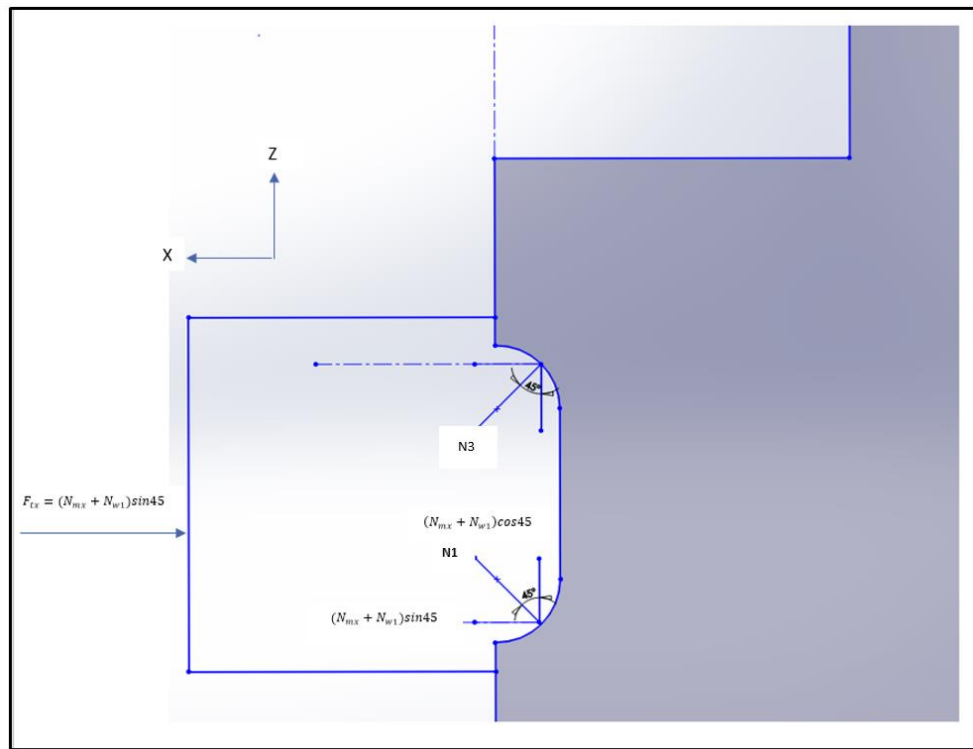


Figure 120 Equilibrium equations for Machining forces in X Direction

Total normal reaction , $(N_{mx} + N_{w1}) \sin \alpha = N_x =$

Force required by peizo actuators during x machining process

Determination of Forces in X and Z directions:

Using equations derived above during machining in z direction, the maximum force is achieved when A_l is assumed to be zero. Therefore, using

$$N_z = \frac{(F_{tz}/2 - A_l/2)}{\cos\alpha}$$

$$N_z = \frac{(3500 - 0)}{\cos 45} = 4950 \text{ N}$$

During machining in z direction, the maximum force is achieved when A_l is assumed to be zero. Therefore, using

$$N_x = \frac{(F_{tx})}{\sin\alpha}$$

$$N_x = \frac{(3500)}{\sin 45} = 4950 \text{ N}$$

This confirms that the force required for Piezo in X direction should be greater than 4950 N.

By keeping the Gap constant and adjusting the pressure In CMM mode at 6 microns the pressure can be varied from 80 psi to achieve 2400 N to 60 psi to achieve 1800N.

Why change the force in machining mode? In order to increase preload, one may change the pressure to get an optimal pressure distribution that fits well with the damping criterion.

(Study of the effect of Force distribution from air to roller at constant gap on damping)

Same is the case with lateral forces, the gap, pressure and the load distribution in fixed in a way so as to achieve maximum damping performance.

This justifies initial design phase of the Air bearing Selection which might change in future.

Working Principle:

The active vibration suppression actuator is connected to the linear bearing module with the help of M6 bolts on one end and to the coarse actuator (a lead screw drive shaft) to the other end with the help of a threaded rod M8 × 16 Threaded rod.

The main purpose of the coarse actuator is to enable long distance translation motions along x direction required in the process of connecting and disconnecting the linear bearing module. A translation of 8 mm is required in order to fully disconnect the bearing module from its mating groove in the guideway. Such a travel is not achievable with the help of active vibration suppression actuator such as a piezo actuator at the amount of axial stiffness required by the fine actuator due to its limited travel range. The piezo actuator acts as a secondary drive that is responsible for providing the clamping force of Bearing module as well as to resist the machining force reaction transferred by the guide to the bearing module. The piezo acts as a spring- damper system to absorb any vibrations coming axially from the bearing module and the table (x direction). *See 121 below.*

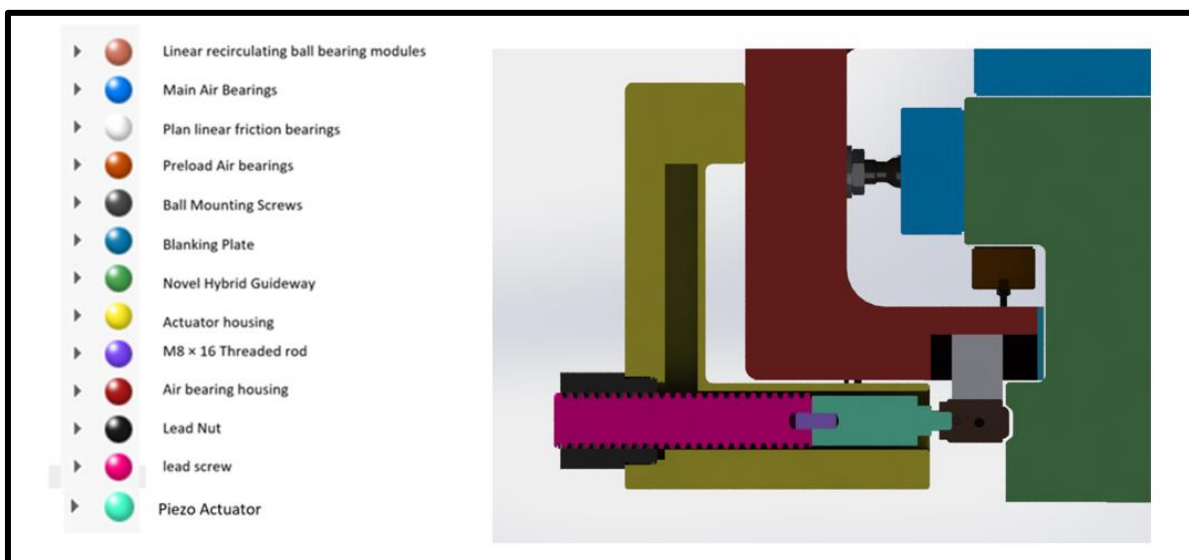


Figure 121 Hybrid Piezo Actuator drive colour mapping

5.1.2.5 Actuator design:

The actuator design is an important factor in determining the effectiveness of the concept. This is due to the fact that the design allows for relative movement of the Linear ball bearing module and the table. This can be achieved in both X and Z directions meaning there is now an active vibration suppression connection with some stiffness and Damping between the linear bearing module and the table. This concept has a potential to help in reducing the Vibrations coming from the truck of the linear recirculating bearing and the table due to machining forces in both X and Z directions.

In order to prove its effectiveness only the X direction is considered.

Coarse Actuator Design:

The Coarse Actuator is Simply a lead screw mounted in the actuator housing assembly, this was chosen based on two parameters axial stiffness to withstand forces coming from the piezo and to compensate for the limited travel of the piezo in order to disconnect the bearing modules from the drive.

The Coarse actuator consists of a precision ACME Externally Threaded Nut, Right hand, 673 Bronze, 7/8”-6 Thread size (Refer to Appendix B Figure 2 B) and a Right hand, 7/8”-6 Thread size 1018 Carbon Steel precision ACME Lead Screw. (Refer to Appendix B Figure 1B). (McMaster-Carr. (2020)).

Load capacity of the Nut has to be similar to the one given on the website () as the geometry and the Material Tensile strength and young’s modulus for 660 bearing bronze is 240 Mpa and 99.97 Gpa respectively (Optimized, T. (2020), (LTD, M. (2020) (See Figure 122 and Figure 124) ,while as for 673 manganese bronze its 517 Mpa and 110.32 Gpa respectively (mat web(2019), See Figure 123,therefore the modulus is more in the lead screw material selected, it can therefore be assumed that the Load capacity achieved will be around 8451 N. (McMaster-Carr. (2020)).

The Tensile strength of lead screw on the other hand is 441.3 Mpa

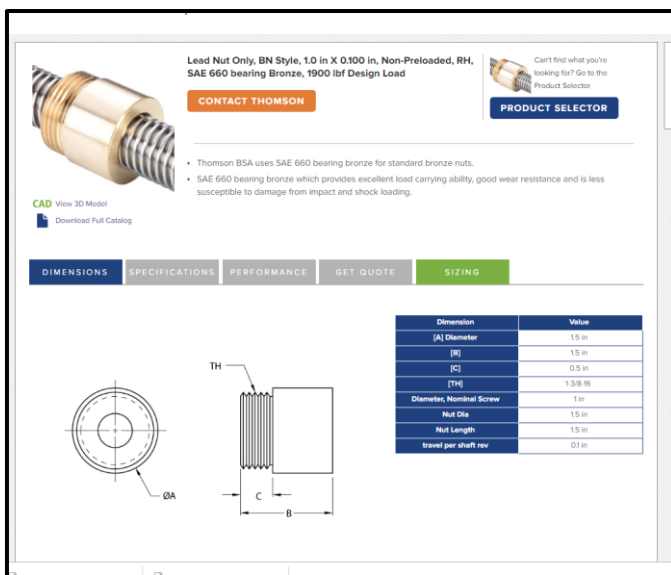


Figure 122 Lead Nut bearing bronze used

| Physical Properties | Metric | English | Comments |
|-------------------------------|--------------------------------------|----------------------------------------|------------|
| Specific Gravity | 8.35 g/cc | 8.35 g/cc | |
| Density | 8.30 g/cc | 0.300 lb/in ³ | |
| Mechanical Properties | Metric | English | Comments |
| Hardness, Brinell | 153 | 153 | 3000 kg |
| Tensile Strength, Ultimate | 517 MPa | 75000 psi | |
| Tensile Strength, Yield | 379 MPa | 55000 psi | |
| Elongation at Break | 15 % | 15 % | |
| Modulus of Elasticity | 110 GPa | 16000 ksi | |
| Modulus of Rigidity | 41.0 GPa | 5950 ksi | |
| Poissons Ratio | 0.34 | 0.34 | Calculated |
| Thermal Properties | Metric | English | Comments |
| CTE, linear | 18.9 µm/m-°C @Temperature 20.0 °C | 10.5 µin/in-°F @Temperature 68.0 °F | |
| Specific Heat Capacity | 0.380 J/g-°C | 0.0908 BTU/lb-°F | |
| Thermal Conductivity | 83.0 W/m-K | 576 BTU-in/hr-ft ² -°F | |
| Component Elements Properties | Metric | English | Comments |
| Copper, Cu | 60 % | 60 % | |
| Lead, Pb | 2.2 % | 2.2 % | |
| Manganese, Mn | 2.5 % | 2.5 % | |
| Silicon, Si | 1.0 % | 1.0 % | |
| Zinc, Zn | 34 % | 34 % | |

Some of the values displayed above may have been converted from their original units and/or rounded in order to display the information in a consistent format. Users requiring more precise data for scientific or engineering calculations can click on the property value to see the original value as well as raw conversions to equivalent units. We advise that you only use the original value or one of its raw conversions in your calculations to minimize rounding error. We also ask that you refer to MatWeb's [terms of use](#) regarding this information. [Click here](#) to view all the property values for this dataset as they were originally entered into MatWeb.

Figure 123 manganese bronze properties

| | Cu | Pb | Sn | Ni | Zn | P |
|-----|------|-----|-----|------|-----|-------|
| Min | 81.0 | 6.0 | 6.3 | | 2.0 | |
| Max | 85.0 | 6.0 | 7.5 | 1.00 | 4.0 | trace |

Mechanical Properties of SAE 660

| Manufacturing Process | Tensile Strength MPa | Yield Strength 0.2% MPa | Elongation % | Hardness range HB |
|-----------------------|----------------------|-------------------------|--------------|-------------------|
| Continuous Cast | 240 | 140 | 10 | 95 |
| Centrifugal Cast | 205 | 95 | 15 | 95 |

Physical Properties of SAE 660

| Thermal Conductivity BTU/(sq ft-hr-°C) | Specific Heat BTU/lb-°F @ 20°C | Thermal Expansion Per °C from 20°C to 200°C | Density lb/cu in @ 20°C | Electrical Conductivity* (Annealed) % IACS @ 20°C | Modulus of Elasticity KSI |
|----------------------------------------|--------------------------------|---------------------------------------------|-------------------------|---------------------------------------------------|---------------------------|
| 33.6 | .09 | 000010 | 322 | 12 | 14,500 |

Figure 124 bearing bronze properties

The Active Vibration actuator is connected to the lead screw with the help of a M8 × 16 Threaded rod. The details are as shown in Appendix B (Figure 3B) (McMaster-Carr. (2020)).

Fine Actuator Design:

Various actuators were explored, piezo offers the best vibration suppression a control over a Su Nanometer accuracy.

A Piezo actuator company called PI (Physik instruments) was consulted and the following conclusions were made.

Specifications of the actuator:

The required clamping force as calculated from the section, was 3500 N at maximum machining force (1500N) and Static load at max work piece weight 200kg (2000 N).

The Dimensions of the Actuator are limited by desired overall bearing size which needs to be as close as possible to a conventional linear bearing. The stiffness of the actuator in the axial direction must be comparable to the stiffness of the linear recirculating bearing which is usually above and around 600 N/ um *See Table 5 below.*

The Actuator calculations needs the control frequency value; this has three alternatives depending on the frequency of interest to control.

- Supress Vibrations coming from Bearing Module only.
- Supress Vibrations from the machining forces only.
- Supress them both simultaneously.

This demands the quantification of frequency values, the vibration frequency range coming from bearing module and the vibration frequency range coming from the machining forces. The vibration frequency range coming from bearing module has a range of 1500 -5000 Hz (*OHTA, HIROYUKI; HAYASHI, EIJI(2000)*). the vibration frequency range coming from the machining forces are 500-700 Hz. (*Hesselbach, J; Hoffmeister, H.-W; Schuller, B.-C;(2010)*).

The mass is also an important factor in determining the effectiveness of the Piezo actuator design therefore, the mass of feed drive sub assembly is equivalent to a Static force on each bearing modules due to maximum workpiece weight and sub assemble plus the max machining force with work piece this results in $((2000 N + 3500 N)/4 \times 9.81) = 90kg$ as deduced in the earlier section and the mass of the bearing module (0.2kg) is taken into consideration.

| Dimensions range l×b×h (mm) | Stiffness (N/um) | Accuracy (nm) | Blocking force (Min) N | Linear bearing module controllable Frequency range (Hz) | Table controllable Frequency Range (Hz) | Mass of sub ASSY- Module (Kg) | Mass of Bearing Module (Kg) |
|-----------------------------|------------------|---------------|------------------------|---------------------------------------------------------|-----------------------------------------|-------------------------------|-----------------------------|
| (50-90) ×(20-30) × (15-20) | 600 | Sub-Nanometer | 3300 | 1500 -5000 | 500-700 | 90 | 0.2 |

Table 5 Shows the specifications required for the fine actuator

Piezo Actuator Design Calculations:

Piezo actuators were initially considered , please refer to APPENDIX A for detailed Calculations.

Three Actuators based on their desired characteristics were chosen and the following calculations were obtained using previous equations; See Table 6 below.

| Vibration control of Bearing module | $\Delta L(\mu m)$ | f_0 (Khz) | Dimensions (l×w×h) (cm) | Stiffness (N/um) | Controllable freq range open loop (khz) | Controllable freq range closed loop (Khz) | Power density $\frac{w}{(cm^3)}$ (1500Hz) | Power density $\frac{w}{(cm^3)}$ (1500Hz) |
|----------------------------------------------------|-------------------|-------------|-------------------------|------------------|-----------------------------------------|-------------------------------------------|----------------------------------------------|----------------------------------------------|
| P-016.10 | 15 | 59 | 1.7 × 1.6 × 1.6 | 320 | 0-4.7 (0-4.3) | 0-0.683 (0-0.626) | 0.97 | 9.355 |
| P-016.20 | 30 | 36 | 2.9 × 1.6 × 1.6 | 190 | 0-3.7 (0-4.37) | 0-0.534 (0-0.626) | 1 | 9.66 |
| P-016.80 | 120 | 11 | 10.1 × 1.6 × 1.6 | 54 | 0-1.9 (0-3) | 0.276 (0-0.435) | 0.29 | 2.84 |
| Vibration Control of Machine table Assembly | | | | | | | Power density $\frac{w}{(cm^3)}$ (200 Hz) Sg | Power density $\frac{w}{(cm^3)}$ (200 Hz) Lg |
| P-016.10 | 15 | 59 | 1.8 × 1.6 × 1.6 | 320 | 0-0.220 (0-0.201) | 0-0.031 (0-0.029) | 0.129 | 1.247 |
| P-016.20 | 30 | 36 | 2.9 × 1.6 × 1.6 | 190 | 0-0.175 (0-0.209) | 0-0.025 (0-0.030) | 0.13 | 1.288 |
| P-016.80 | 120 | 11 | 10.1 × 1.6 × 1.6 | 54 | 0-0.1 (0-0.222) | 0-0.014 (0-0.032) | 0.04 hdf | 0.379 hdf |

Table 6 Desired characteristics of three chosen actuators

Conclusions:

In an Ideal case or a desired case:

In order to reduce the operating frequency, reduce the force needed for clamping. to get a good heat generation below 0.1 W/Cm³, The frequency

Vibration control of Bearing module

In case of damping the large mass system i: e the machine table, the force required to block is Clamping force plus the force due to moving mass. This will consequently lead to high voltage requirement and hence generate more heat. It can be seen from the table that all the best actuator selections fail as they give a very small range of frequency values of 200 Hz which won't be able to damp the vibrations from the machine table or the bearing module as the target vibration frequencies are high. Also, the heat generation in all the cases except P-016.80 has a higher value more than 0.1 which is the maximum an actuator can bear. Although P-016.80 generates less heat it has a dynamic force greater than the max blocking force of the actuator also the stiffness 54 N/um is undesirable. Therefore, all these actuators can't be used in this case.

Vibration control of Machine Table Assembly:

In case of damping the vibration coming from the bearing modules which are of a magnitude of 1500 -5000 Hz According to (OHTA, HIROYUKI; HAYASHI, EIJI(2000)). Open loop control can easily achieve that but the heat generated is again above 0.1 at 1500 Hz of control frequency. this needs additional cooling systems which add up to the complexity and the costs. The P-016.80 gives a comparatively lesser value than other actuators in terms of power density, but at the cost of low stiffness value which is 54N/um.

The cost of Piezo is way too high starts from 7000 pounds without the controller, the controller adds up more.

High voltages and high frequencies are not good for heat. Unfortunately, high voltage generated is due to high forces and high displacements which can't be reduced.

This concludes looking further into other alternative forms of actuators that can be captured within the same dimensions of the overall bearing envelop.

5.1.2.6 Justification of Actuator housing.

The actuator housing encases the Hybrid drive consisting of a (Piezo actuator, The lead screw, a lead screw Nut and a threaded rod). The actuator housing mounts the Hybrid drive to the main bearing housing. Following design consideration were made during its design process.

The geometry of the housing was limited by the overall size of the hybrid bearing, after a rough estimation of the size was formulated the initiation of the structure design was executed with the help of a Tube Design calculator as it closely resembles a tube.

The stress bearing sections are the bottom horizontal section and the upper horizontal section as this has to withstand the forces coming from the actuator clamping and the machining. The tube of bottom horizontal section was designed first for reference. By inputting twice, the maximum Load (3300N) applied by the clamping and machining action of the hybrid drive giving resulting in a value of 6600 N (1483 Lbs). 120mm (4.72441 Inch) is the length of the initially assigned to the column that fits well with the overall hybrid bearing dimensions. The calculator gives a list of choices out of which the obtained maximum beam load is 63685 N (14317 Lbs) with the square dimensions of 38.1 mm (1 ½ inch) and at the gauge of 11 which corresponds to the wall thickness of the square tubing to

a value of 5.334 mm (0.12 inch) as shown in Figure 125 and Figure 126 (Atc mechanical (2020)).

| | | |
|----|---------------------|-------|
| 15 | 0.066 through 0.074 | 0.072 |
| 14 | 0.075 through 0.085 | 0.083 |
| 13 | 0.087 through 0.097 | 0.095 |
| 12 | 0.101 through 0.111 | 0.109 |
| 11 | 0.112 through 0.122 | 0.12 |
| 10 | 0.126 through 0.136 | 0.134 |
| 9 | 0.140 through 0.150 | 0.148 |
| 8 | 0.157 through 0.167 | 0.165 |
| 7 | 0.175 through 0.185 | 0.18 |

Figure 125 Shows the corresponding gauge design value

Specify Size and Load Requirements

Length/Height: 4.72441 in ft. Load: 1483 lbs

Based on the length and load criteria that you specified, these are the available options of Allied Tube & Conduit's galvanized steel tubing products.

| LENGTH/HEIGHT | LOAD | TUBE BASE | TUBE ALLOWED | DESIRED OUTPUT |
|---------------|-----------|---------------------------------------|-----------------------------------------------------------------|------------------------------------------------------------------|
| 4.72441 in | 1483 Lbs. | Select Tube based on Simple Beam LOAD | Use Any Size (all round, squares, rectangles, flat-sided ovals) | Size Summary / Every Gauge / O.D. Size fraction (if appropriate) |

Results

ALLIED MECHANICAL TUBING THAT MEETS OR EXCEEDS THE MAXIMUM ALLOWABLE LOAD FOR A SIMPLE BEAM LOAD, WHERE THE LENGTH IS 4.72441 IN AND THE LOAD IS 1483 LBS

| Shape | Size | Gauge | Max. Beam Load | Max. Beam Load w/Defl. Limit |
|---------------|--------------|----------------------|----------------|------------------------------|
| Square | 1-1/2 | 0.072 (15 ga) | 9,470 | 9,470 |
| Square | 1-1/2 | 0.083 (14 ga) | 10,677 | 10,677 |
| Square | 1-1/2 | 0.095 (13 ga) | 11,929 | 11,929 |
| Square | 1-1/2 | 0.109 (12 ga) | 13,303 | 13,303 |
| Square | 1-1/2 | 0.120 (11 ga) | 14,317 | 14,317 |
| Square | 1-3/4 | 0.072 (15 ga) | 13,166 | 13,166 |
| Square | 1-3/4 | 0.083 (14 ga) | 14,890 | 14,890 |

Figure 126 Shows the Design table obtained for the hollow tube

Similarly, to the upper part the length of 47.244 mm (1.86 inch) was the input with the same load requirements giving a value of max load to be 161764 N (36,366 lbs) which is a way high above the applied load of 6596 N.

Based on this the Actuator housing was designed by adding material to the reference geometry obtained from calculations wherever necessary to accommodate the assembly parts whilst maintaining the obtained 63685N (14317 lbs) and 161764 N (36366 lbs) of the bottom horizontal and upper horizontal section respectively. See Figure 127.

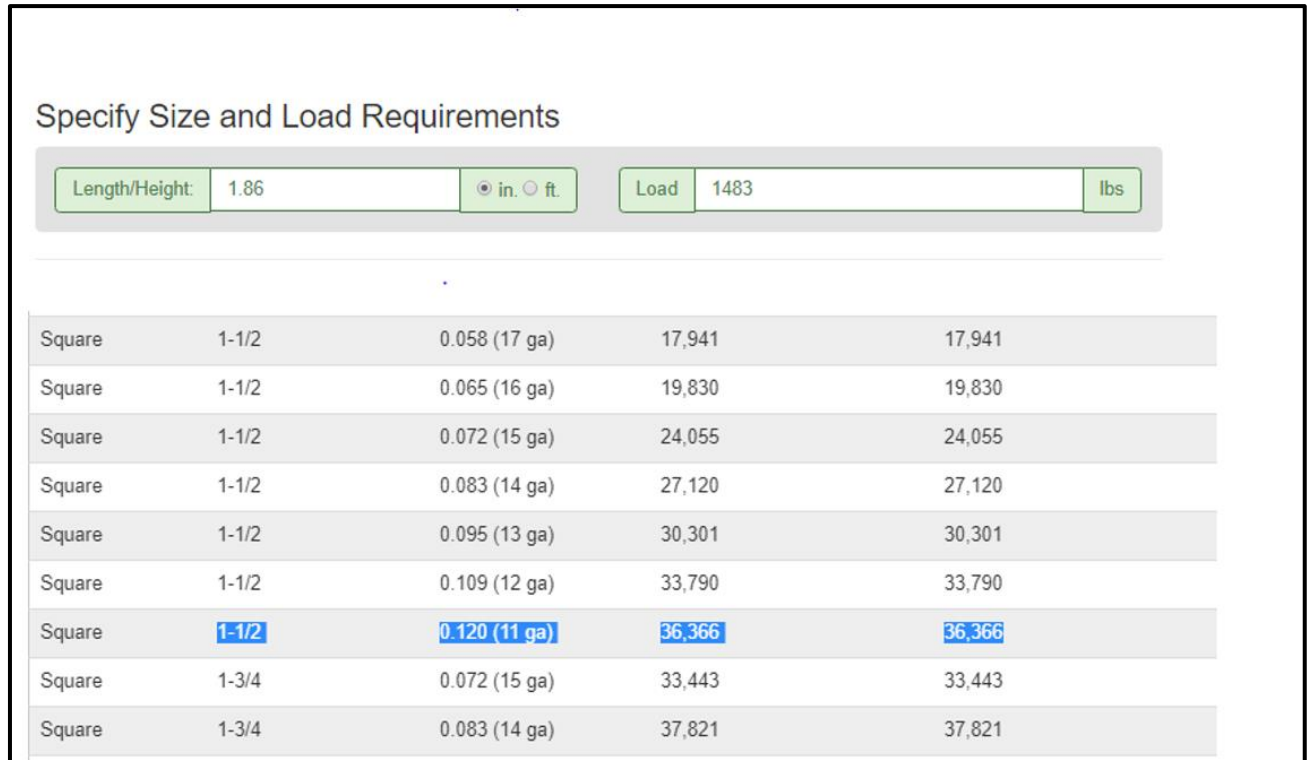


Figure 127 Shows the Design table obtained for the hollow tube (upper part)

The Figure 128 below shows the base actuator housing designed according to the calculation, and picture shows the changes made to the housing effected by hybrid bearing and the air bearing housing. The material used for calculation was Allied galvanized steel.

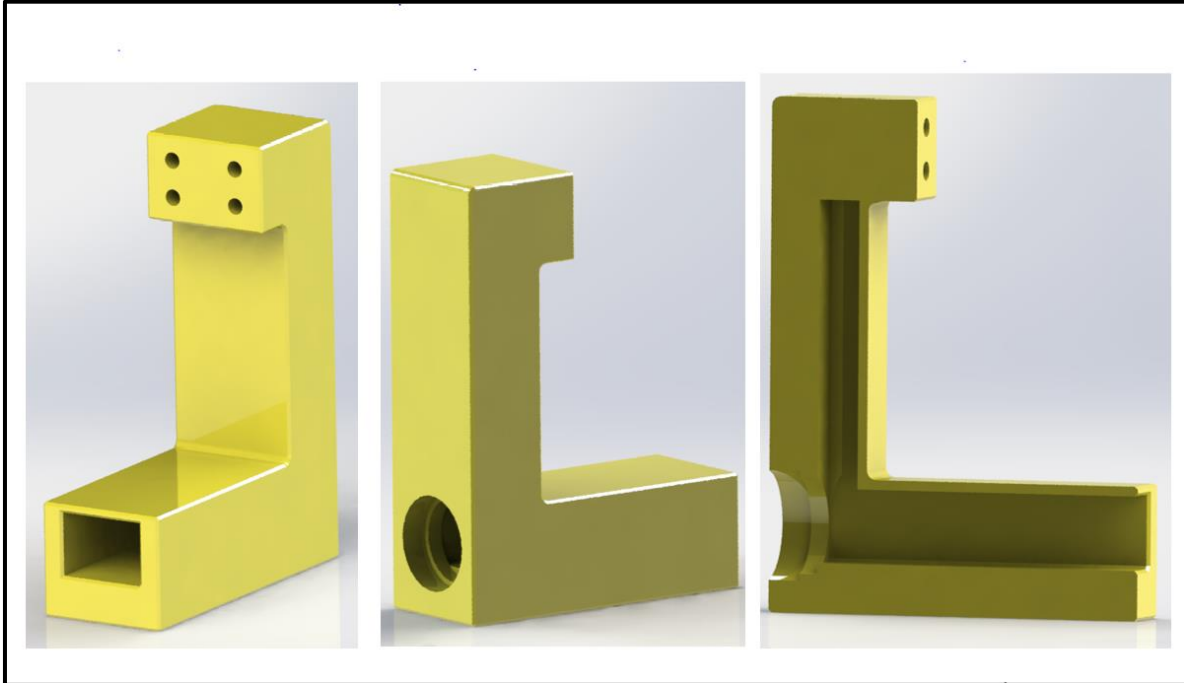


Figure 128 Shows the final design of actuator housing

4 ×M6 18-8 stainless steel thread locking socket head screws were used for each actuator housing at the top horizontal section in order to connect it to the air bearing housing. (See Figure 129 below). The tensile strength 482 Mpa (70000 psi) of screws is large enough to bear the actuator clamping and machining forces. (McMaster-Carr,(2020)). (Refer to Appendix B Figure 4B)

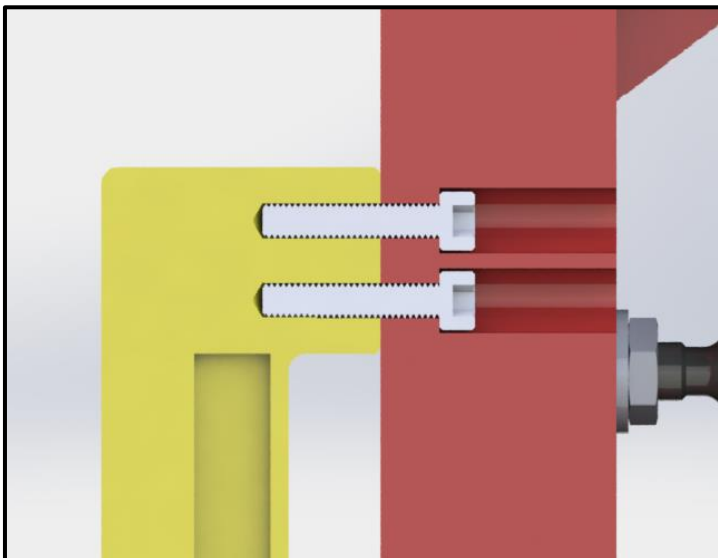


Figure 129 Shows 4 ×M6 18-8 stainless steel thread locking socket head Screw

5.1.2.7 Justification of air bearing housing.

The main housing contains an envelope for Air bearings as discussed in the section earlier. Four (50 ×100) Flat rectangular air bearing pads two on the top and one on each side of guide and two (25 ×50) Flat rectangular air bearings for preloading are incorporated. The main (50 ×100) Air bearings are attached to the housing via 13 mm Diameter /M10 ×0.75 ×54 mm lg ball mounting screws while as two preload bearings are connected with the help of 6mm Diameter /M5 ×0.8 × 27.5 mm lg flat ball end mounting screw.

The pocket shown in the figure reflects the guideway for the linear plain bearing. The rib is present for extra rigidity in the rib plane. The 8 clearance holes reflect the 8 ×M6 18-8 stainless steel thread locking socket head screws that connect the actuator housing to the air bearing housing. See Figure 130 below.

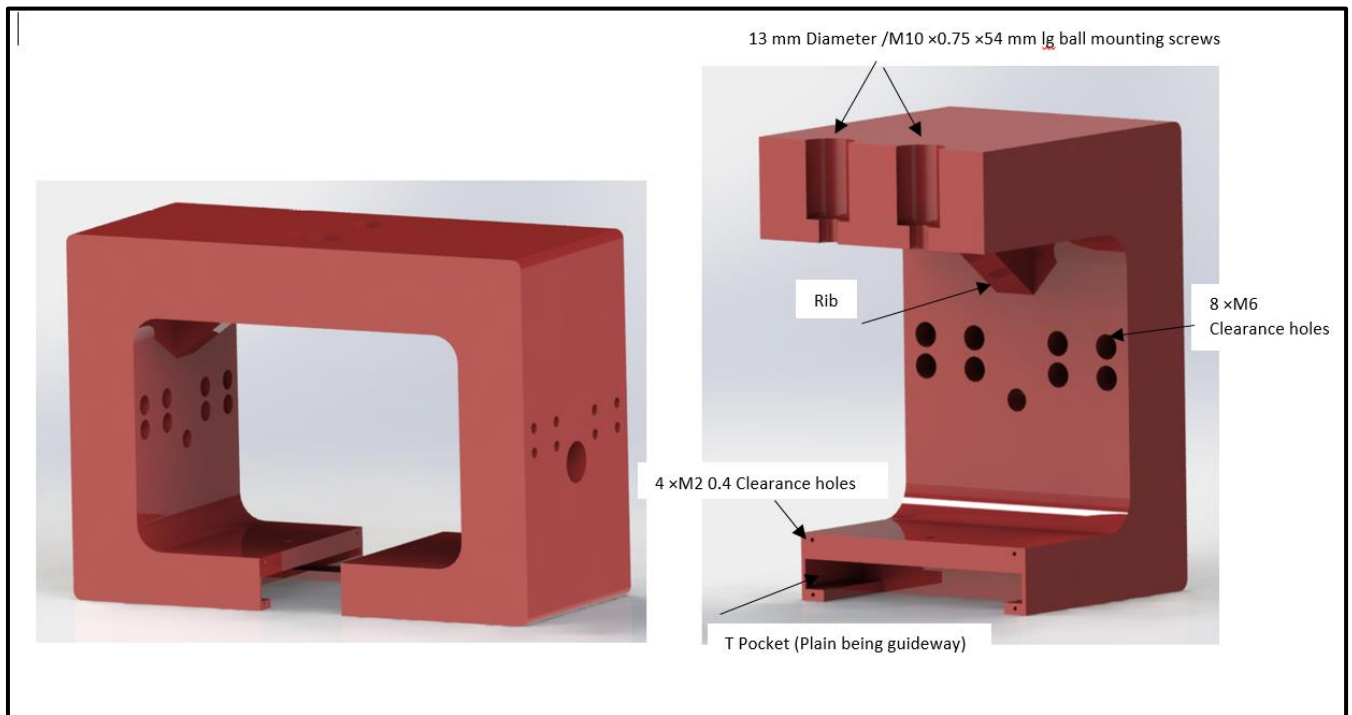


Figure 130 Shows the Hybrid bearing final housing design

5.1.2.8 DFMA Considerations (Design for manufacture and Assembly):

The Rib in the middle of the main frame is difficult and time consuming to manufacture through milling, therefore instead of having the rib in the middle the rib would extend end to end have the same width as that of the frame and not This will then be a one-step milling process provided the tool is deep enough to cut through the depth.

According to New Way air bearing catalogue the parallelism between the air bearing surface and the guideway is important, for example for a 75 mm air bearing a few microns of out of parallelism can cause issues with the performance of the bearing. This means the bearing will need to be held in place with sufficient rigidity and tight parallelism tolerances this is expensive and can be eliminated by introducing a Spherical Socket and ball stud which makes it self-aligning once the air pressure is supplied. Also, the thread on the stud will allow for change in air gap very easily making the Assembly process easier. Due to the nature of self-adjustment of the ball joint tight tolerances on the drilled holes is not required therefore all holes as per GD and T will have a nominal tolerance range of cylindricity near about 0.08 mm.

Main shape of the guideway will be manufactured with the help of cold extrusion and later on the surface will be polished with the help of Computer controlled optical surfacing machine CCOS. Manufactured part will need to qualify the flatness and surface roughness requirements as mentioned in section 4.1.3.2, it will be also advantageous although costly to polish the grooves that provide a race for roller bearings. This will considerably reduce the vibrations coming from the Roller bearing module.

The tolerances for the guide had already been given in section 4.1.3.2, having surface roughness below 16 RMS, 0.0005 MM Flatness optically polished stainless steel or Aluminium 2024-T351.

The Actuator Housings will be manufactured with the help of milling process, a metal block will cut into the general shape, the circular and the rectangular cross section for actuator will be milled as well. In the previous design due to negligence of manufacturing considerations the vertical hollow volume will inside the housing will not be present.

Although the prime manufacturing considerations have been considered and discussed a detailed DFMA (Design for manufacture and Assembly) on a commercial scale cannot be analysed as the concept is in its very early stages. Also, the entire assembly consists of only three parts that need manufacturing i.e the main housing, the actuator housing and the Hybrid guideway. The Design is still in its pre-mature Stage, for example a lot of work needs to be done in terms of deciding whether the actuator housing will be used in the final design or should there be any type of shock absorber to be incorporated to further dampen the vibration in the vertical direction. At this stage damping in the horizontal direction was taken into consideration.

5.1.2.9 Computational Analysis:

The housing behaves more like a pressure vessel; the housing walls are under a distributed force that is applied to them by the air bearings transferred evenly through the spacers. The walls specially the area near the air bearing vicinity is sensitive to outward deflection. Some microns of deflection outwards can cause the bearing gap to increase and hence loss of pressure which consequently effects the performance. Therefore, the deflection in this area must be controlled within few microns that are within the capacity of the ball retainer to be corrected in case of any deflection. Finite element analysis was carried out in order to prove check for deflection at the air bearing spacer vicinity.

Two materials were tested in FEA Structural Steel and Aluminium alloy in order to check for deflection.

Boundary Conditions:

The load at the top was applied as if the machine tool is applying a maximum machining force plus the static load of the assembly parts constituting 3500 N. Each bearing through the holes provides a nominal load of 1200 N opposite to the external load. See Figure 131 below.

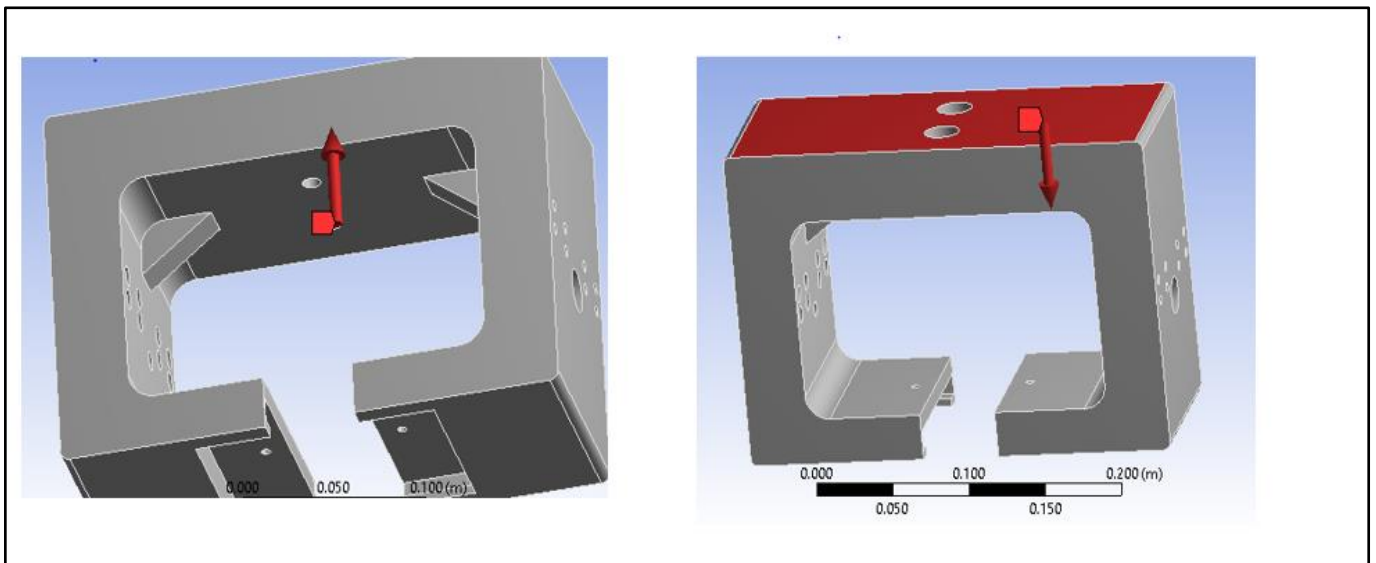


Figure 131 Vertical boundary conditions

On The left face, the 8 holes stretch the housing outwards due to the reaction from the hybrid actuator max force of 3500 N and he ball end threaded hole on this face transfers a force of 1200 N outwards due to air bearing. See Figure 132 below.

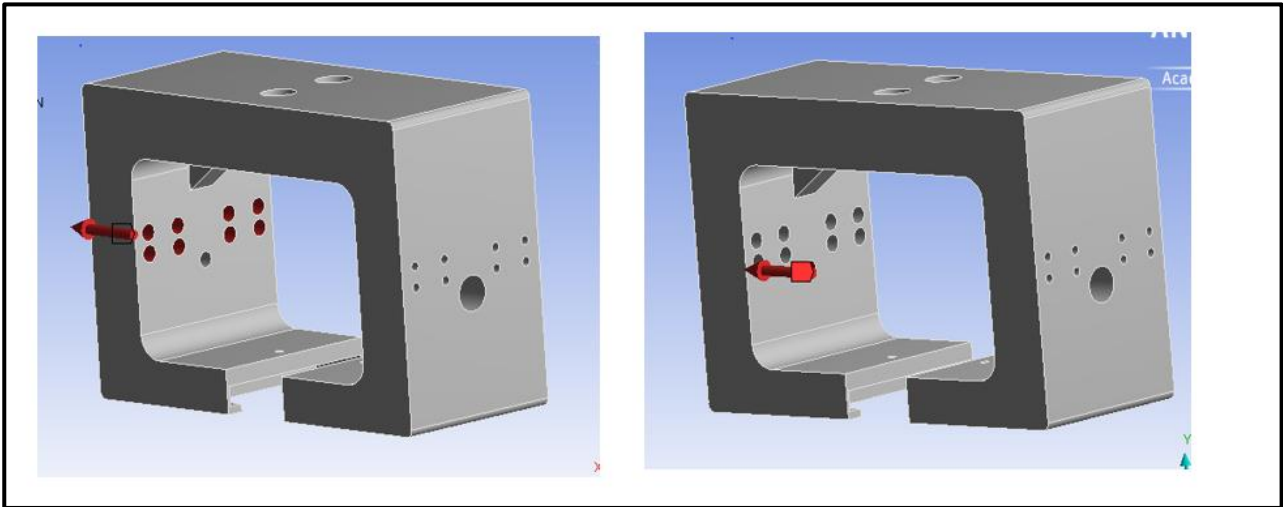


Figure 132 Horizontal boundary condition

The Right face and the bottom face were constrained and fixed in 6 DOFS in order to attain the relative effects of load on other faces.

The number of nodes and elements were set to a value of 1477711 and 1056550 respectively at which mesh convergence can be approximated as the values do not change significantly by refining. See Figure 133 below.

| Statistics | |
|-----------------------------------|---------|
| <input type="checkbox"/> Nodes | 1477711 |
| <input type="checkbox"/> Elements | 1056550 |

Figure 133 Number of nodes and elements during the convergence

Case 1 Aluminium Housing:

The deflection near the bearing area in Y direction varies within a range of 3.1686×10^{-6} to 1.931×10^{-6} for Full Load Condition, and from 3.149×10^{-6} to 2.229×10^{-6} for half load Condition. See Figure 134.

The deflection near the bearing area in x direction varies within the range of 1.9593×10^{-6} to 1.2107×10^{-6} and from 1.86×10^{-6} to 1.191×10^{-6} for half load Condition. See Figure 135.

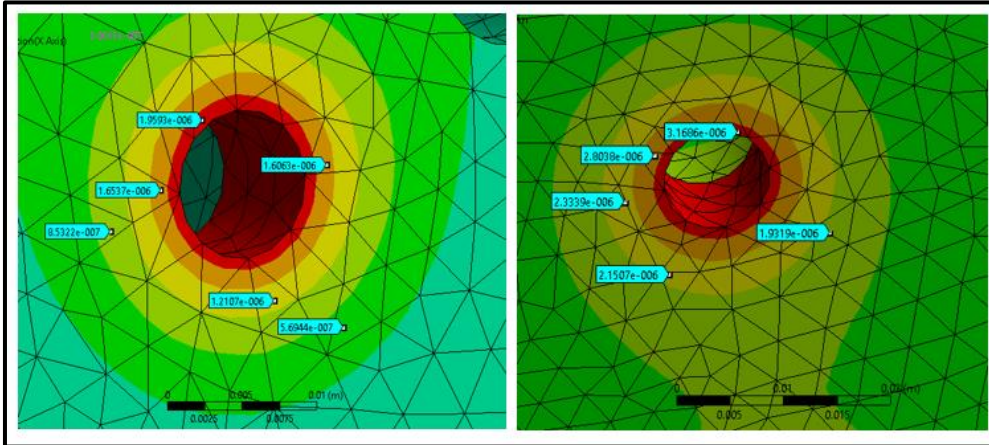


Figure 134 FEA results of Deflection in Y

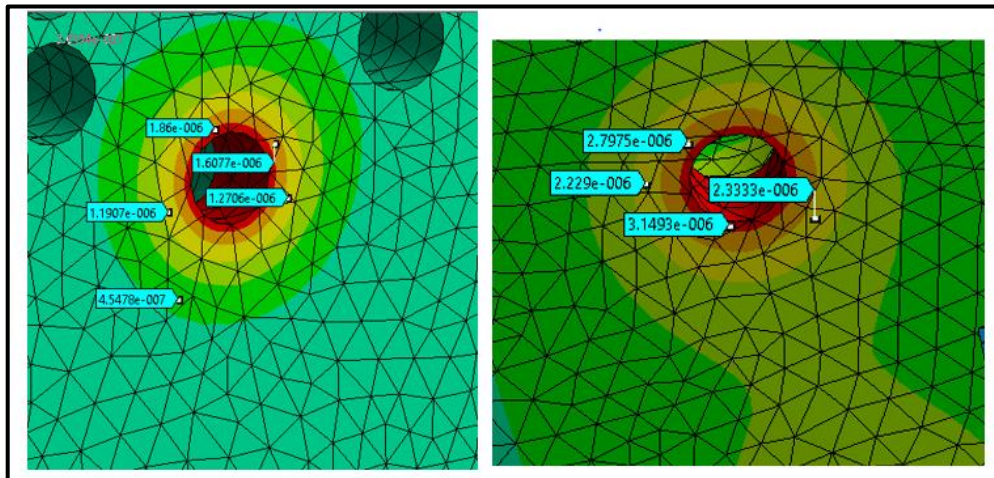


Figure 135 FEA results of deflection in x

Case 2 Stainless Steel Housing:

The deflection near the bearing area in Y direction varies within a range of $1.1046 \text{ e-}006$ to $9.326 \text{ e-}007$ for Full Load Condition, and from $1.0944 \text{ e-}006$ to $8.3525 \text{ e-}007$ for half load Condition. See Figure 136 and Figure 137.

The deflection near the bearing area in x direction varies within the range of $6.808 \text{ e-}007$ to $4.2275 \text{ e-}007$ and from $6.8227 \text{ e-}007$ to $4.635 \text{ e-}007$ for half load Condition. See Figure 136 and Figure 137.

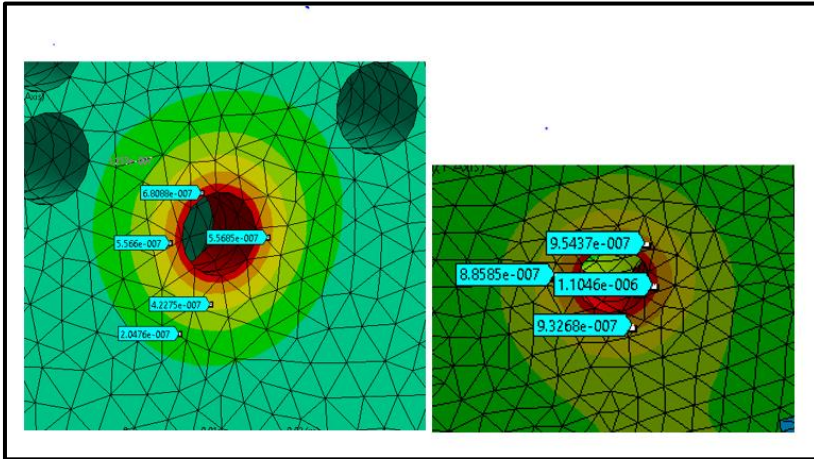


Figure 56 FEA Results of deflection in Y full load condition (right) (top surface), half load condition left (left surface),

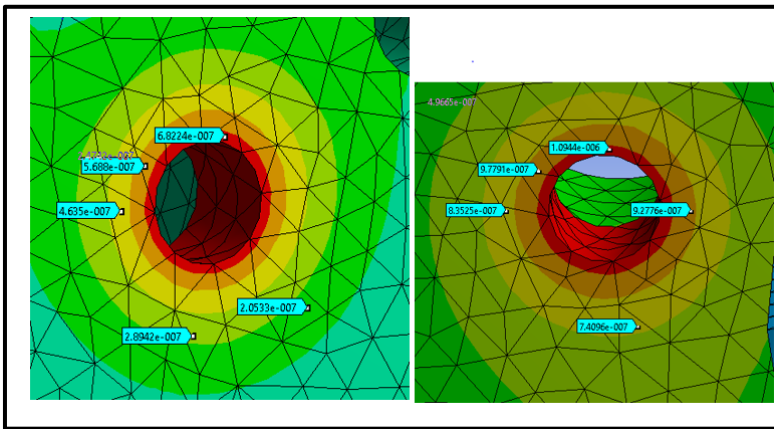


Figure 136 FEA Results of deflection in x full load condition (right) (top surface), half load condition left (left surface),

Although the maximum deflection is $3.1686 \text{ e-}006$ exactly near the circumference of the hole, on average 2 microns of max deflection can be assumed as in reality the spacer plate will distribute the load along its span and will help in reducing deflection. and this seems very controllable, further optimisation of the structure can reduce this value down. This proves that Structural Steel main bearing housing is better in terms of deflection stability but its weight is about 17 kg higher than the aluminium bearing as confirmed in solid works through mass properties feature.

In order to reduce weight, the housing structure will be made from 6061-T6 Al and the rail 2024-T351 Al as used in New way air bearing Slides.

5.1.2.10 Justification of the Guideway

The Guide rail is hybrid in construction, the top portion consists of 4 surfaces having surface roughness below 16 RMS, 0.0005 MM Flatness optically polished stainless steel or Aluminium 2024-T351 acceptable for all Flat rectangular air bearing pads.

The bottom half portion contains the grooves for the attachment of the linear bearing module. The rail will be manufactured from Aluminium 2024-T351 or a stainless-steel grade with optically polished air bearing surfaces as used by new way air bearing guides in practical applications. Steel will be good for linear bearing module as well as it will provide a highly stiff surface for the Hertzian contact.

Note: The guideway can't be connected directly to the machine bed as it would require holes to be drilled from the top which is not acceptable for the air bearing surfaces and therefore a separate adaptor needs to be design that can attach the bottom end to the machine table. *See Figure 138.*

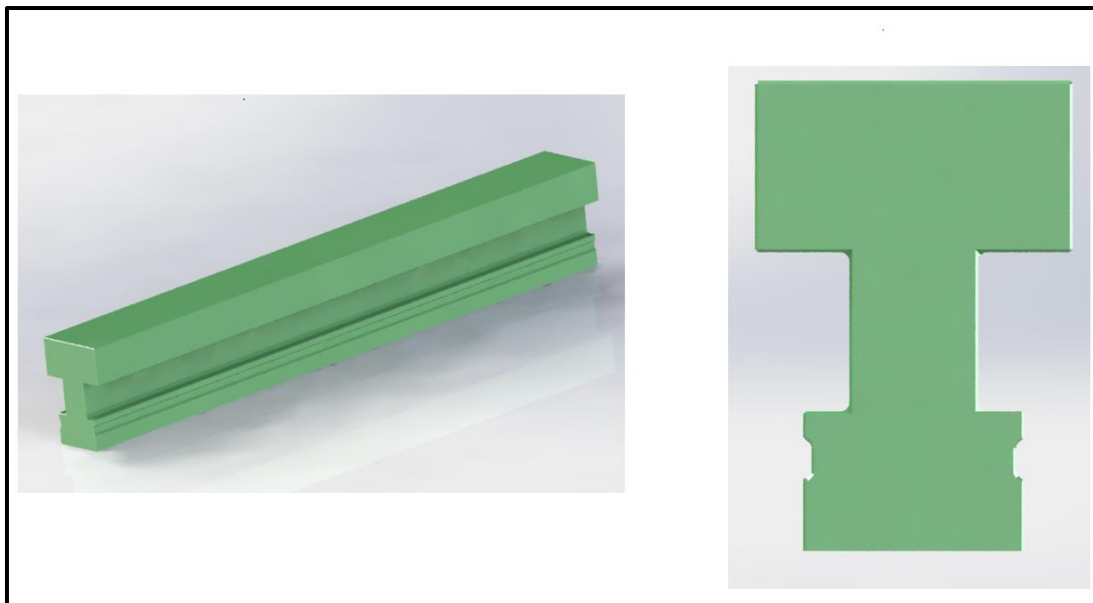


Figure 138 Final design of Novel Hybrid guideway

5.1.2.11 Justification of the linear actuator slide

As Mentioned in section earlier the primary materials used for the sliding are Casting, bronze, special polymers, and steel. Sometimes static friction becomes more than dynamic friction during operation causing a stick slip phenomenon which causes instability for smooth operation and control. Turcite SKC or Moglice are few polymers which favour lubrication with the help of additives. These significantly reduce stick slip phenomenon. (Altintas, Yusuf & Verl, Alexander & Brecher, C & Uriarte, L & Pritschow, Guenter. (2011)).

The bearing would be primarily made of steel and coated with the thick layer of Turcite SKC or Moglice to reduce wear and to enable smooth operation. Other variables including the surface roughness and flatness this is the critical part as it can cause unwanted bending moments other than axial moments, this can be problematic for actuators for example in piezo electric actuator the stiffness is affected if it's not axial aligned as they have less stiffness to bending. *See Figure 139 below.*

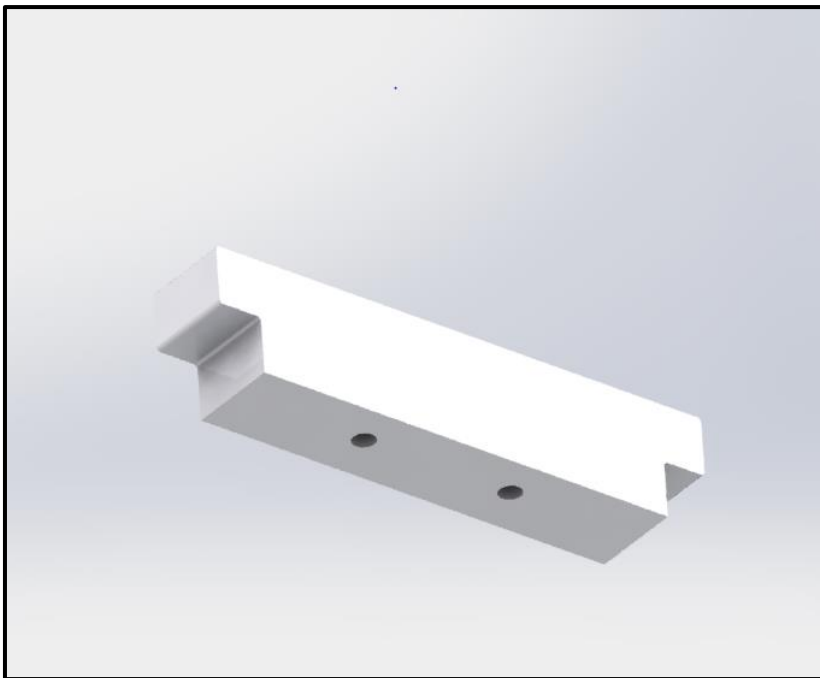


Figure 139 Linear bearing for Bearing modules

5.1.2.12 Justification of the Blanking Plate

The Sliding pocket in the air bearing housing also needs to be closed with the help of proper encasing so as to avoid any foreign material to enter and cover the sliding surface this can be done by using a blanking plate. A blanking plate of 2.5 mm thick steel sheet was used; the blanking plate is attached to the Air bearing housing with the help of 4 × M2 0.4 316 Stainless Steel Hex Drive Head Screws. One Blanking plates were used on each side of the housing. See *Figure 140 and (Refer to Appendix B Figure 5B)*. (McMaster-Carr (2020)).

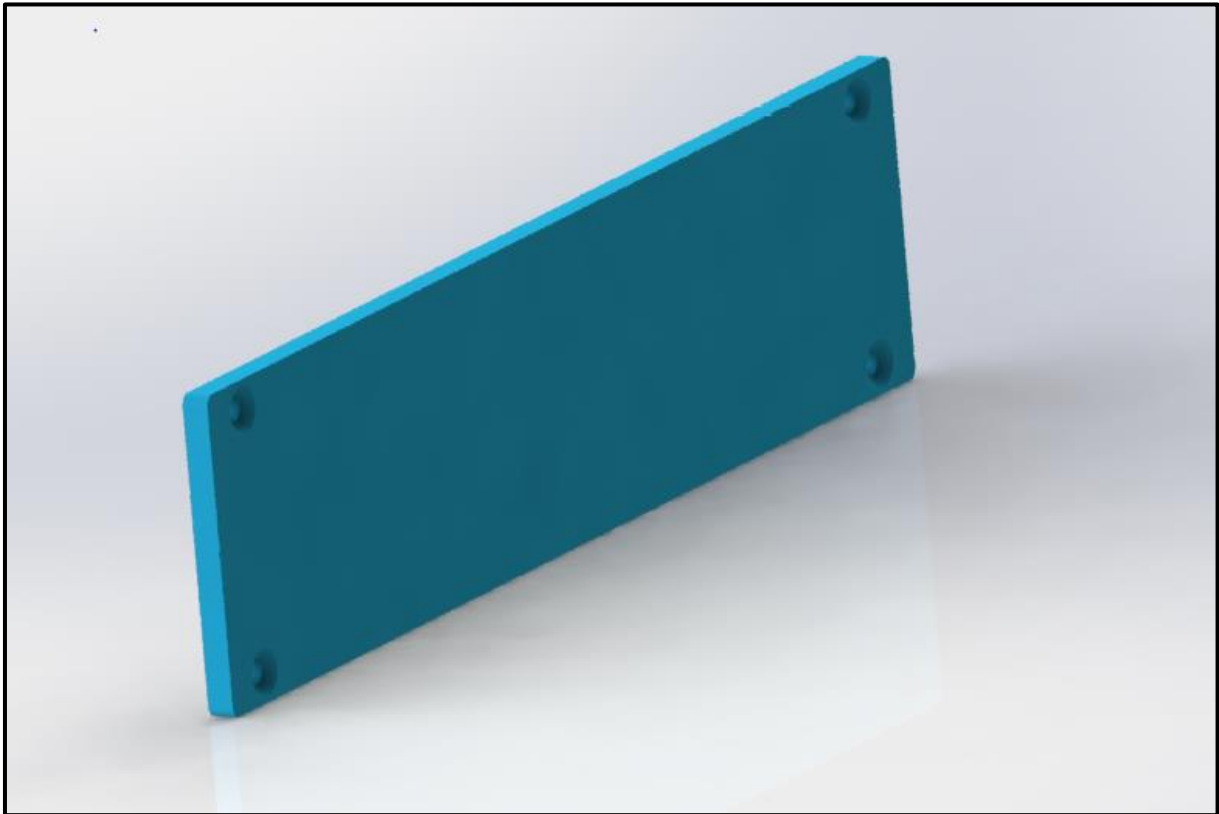


Figure 140 Shows the blanking plate

5.1.3 Mechanical design of the Hybrid Bearing Prototype

5.1.3.1 Statement of Purpose.

During the machining operation, the active air bearing film generated by air bearings was assumed to be advantageous due to its damping effects being almost 15 times higher than the stiff linear recirculating bearings. This damping can have considerable effect on the Vibrations coming from the truck of linear recirculating bearing and the machining vibrations from the table which in turn effects the accuracy and precision of the machined parts.

In order to quantify the effect of Hybrid Bearing stage on the machining performance a separate rig was designed, commissioned and manufactured at the University of Huddersfield manufacturing facility. *Figure 141* shows actual design. It can be easily noticed that the new prototype rig (*See Figure 142*) does not have the same design as originally proposed in the earlier section, it does not have the roller bearing modules and their active switching mechanism, Also, the air bearings are of different sizes and configuration, this difference is purely due to the scope of the intention of the tests, cost and time involved in making such a product at an initial stage. The Experiment using this prototype is purely designed to validate the damping effect of the air bearings on the roller bearing vibrations and their ability to work in integration, Such an Experiment is critical to design as switching from Air bearing to Roller/ball bearing is not a something that needs to be proven, Also the drive running on CMM mode entirely on-air bearings is not critical as this has already been proven on current CMM'S, therefore the intention of the entire prototype is to quantify the effect of hybrid bearing Stage on machining performance and hence why it has been designed to meet the low-cost and ease of manufacturability thereby deviating from the original design.

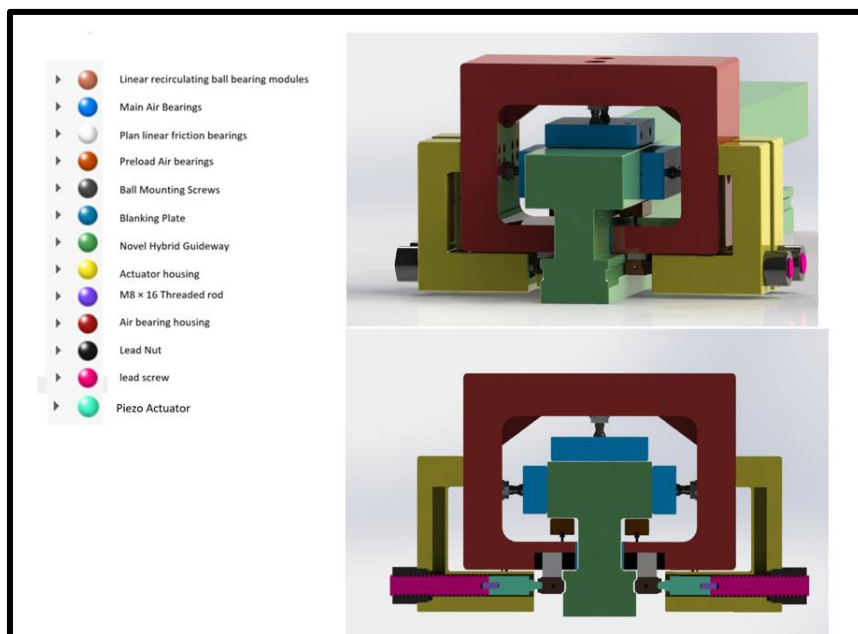


Figure 141 Original Hybrid Bearing Design

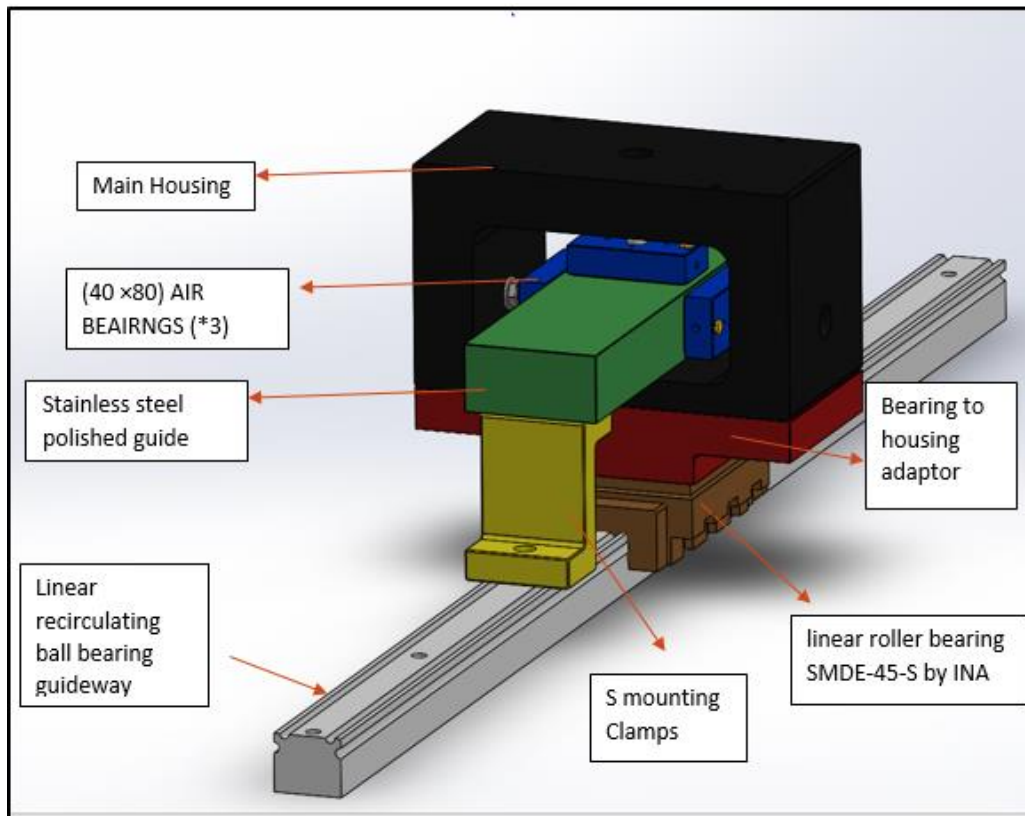


Figure 142 Prototype Hybrid bearing Design

This rig therefore replicates the original prototype hybrid bearing stage with the only difference being the lack of active vibration control hybrid actuator that has the additional effect of damping on the vibrations. Again, this is something that will be proven in future prototypes once the purpose of this test is met.

In order to determine the effectiveness of the Air bearings a highly accurate probe used on CNC versus the use of same probe on linear circulating bearings This Rig will be used for determination of the effects of scanning probe errors present in the CNC machining Centre, one of the sources of these errors are linear recirculating bearings therefore this prototype will allow to use a monorail with only linear bearing stage to quantify the effect of Vibration coming from the Linear roller bearing truck on the scanning probe parameters on Zeiss CMM with the advanced probe similar to CNC probe.

This will prove the requirement of the Air bearings during measurement operation rather than the conventional high accuracy probes operating on CNC feed drive that have Linear recirculating bearings. In short, this prototype can solve two Objectives stated as follows.

- Quantify the effect of hybrid bearing Stage on machining performance.
- Quantify the effect of using an Air bearing stage on CMM in terms of measurement accuracy compared to measuring with the same probe on conventional feed drive on CNC.

Brief Description and Bill of Materials

The Prototype Hybrid bearing is made up of following components *See Figure below:*

1. Main housing
2. Air Bearings
3. 13 mm Diameter /M10 ×0.75 ×54 mm lg Ball Mounting Screws
4. M8 × 16 Threaded rod
5. Linear recirculating ball bearing guideway
6. S Clamps
7. Bearing to housing adaptor

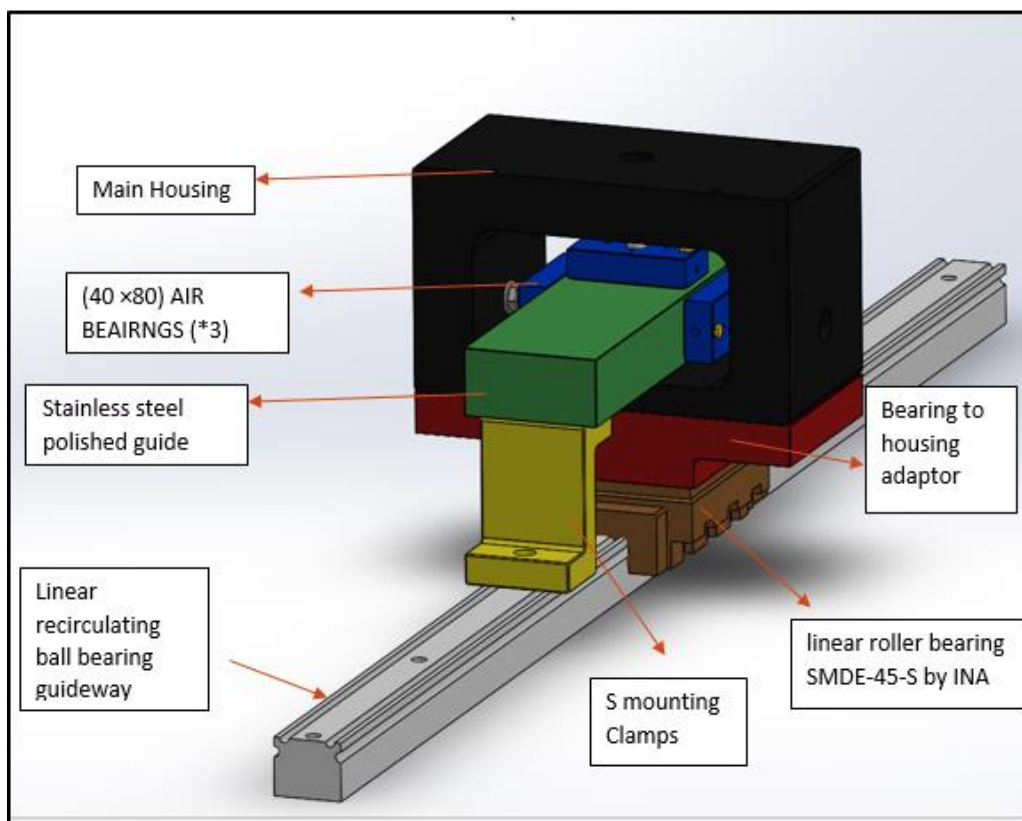


Figure 143 Shows the schematic of the hybrid bearing prototype

The Prototype design consist of the MTT linear guideway using linear roller bearing SMDE-45-S by INA. An Air bearing housing that envelops three (40 ×80) Flat rectangular air bearing pads one on the top, one on the left and one on the right side of the Air bearing inner housing walls. The air bearings are connected to the housing via 13 mm Diameter /M10 ×0.75 ×54 mm lg ball mounting screws which help to adjust the air bearing gap.

The stainless-steel polished surface provides the surface parameters close to 16 RMS roughness and the desired 50% of the nominal flying height Flatness required

by the air bearings to accept it as a guideway. The polished guideway is clamped to the linear recirculating bearing guide way with the help of S shaped brackets through the 2 × M12 bolts and the lower surface of the polished guideway being glued to the S shaped brackets using a layer of epoxy.

The Air bearing housing is attached to the linear recirculating guideway with the help of an Adaptor that is connected to the housing via 4 × (M10 ×40 hex head screws and to the linear recirculating guideway with the help of 6 × (M10 ×45 cap head screws.

In order to generate a ball socket joint between the air bearing pad and the housing, the ball screw is constrained axially and attached to the air bearings with help of 3d printed C shaped 13 mm ball retaining clips using 3 ×M3 screws for each retainer.

For air Supply, 8 mm Polyurethanes Tube, connected to the 3 port 1/4 Bsp Manifold with 4 Outputs 3 × 6mm and 1 × 8mm. The 8mm tube is connected at one end and the 3 × 6mm tubes on the other end. The 3 × 6mm Polyurethanes tubes are then connected to each of the air bearings separately through Straight Pneumatic Push to Quick Connect Fittings M5 Male × 6mm Union.

Prototype Operation:

The 3 air bearings create an air film which create a high pressure within the 5-micrometre gap allowing for the reduction of load in the balls of the linear recirculating bearing and hence entering into the active mode for vibration control as it causes effects into force flow of the system. This provide the same situation of hybrid stage as proposed in the concept hybrid bearing. The air film now influences the vibrations in the linear recirculating bearing truck, in this way the damping and other modal parameters can be obtained to quantify the dynamics of the hybrid stage.

The system can be turned back to the linear reticulating bearing stage by just cutting off the air supply in air bearings.

Also, the compliance present between the balls, the guideway and the truck are utilised in the experiment

5.1.3.2 Detailed Design and Specifications

Justification of Air bearings:

The bearing used for the experiment were three (40 ×80) Flat rectangular air bearing pads. The characteristics of the bearings are given in the picture below. The ideal load of the bearing is of major importance as the bearing choices below or above a certain load capacity can cause problems. A load above a certain load capacity would give an extra stiff over engineered requirement that would not be suitable to check the effect of damping as the forces applied would be relatively very small. In the case where the load is far below the required or desired load capacity the bearings have low stiffness and ideal load requirements would fail if the extreme operational conditions were applied given the configuration of the prototype system. A Bearing that can provide max load of 600 N or higher is required as the shaker force (200N), Shaker weight (100N) the air bearing housing mass (80 N) directly impact the load capacity of the bearing. Also, according to the handbook Bearing with lower pressure, large surface provides higher damping and stiffness and reduced flow requirements and higher safety factor than bearings sized at marginal capability with high pressure therefore, the bearings with a slightly higher Load capacity running at low pressure 414 Kpa (60 psi) would be ideal. This selection also reduced the costs considerably. The Schematic of (40 ×80) Flat rectangular air bearing with via 13 mm Diameter /M10 ×0.75 ×54 mm lg ball mounting screw and 13mm 3D printed ball retainer is shown as seen in See Figure 144 and Figure 145.

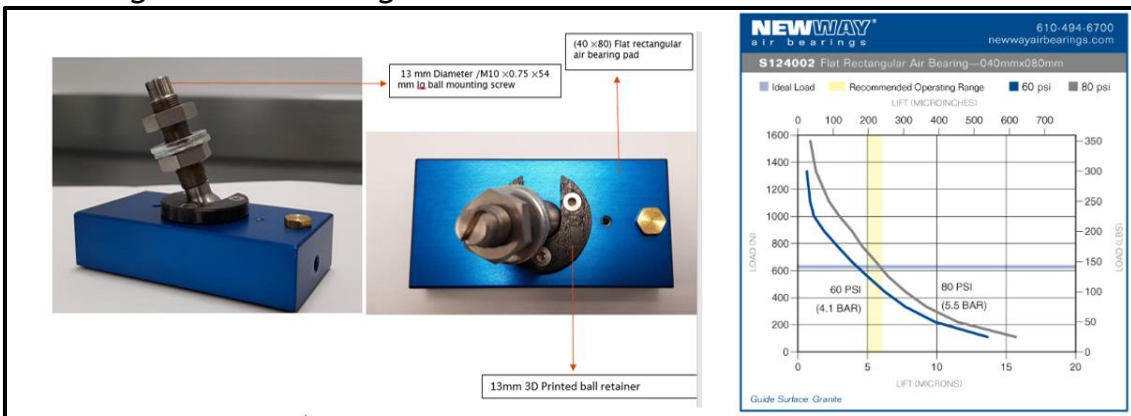


Figure 144 Shows the picture of (40 ×80) Air bearing and its Load vs Lift graph

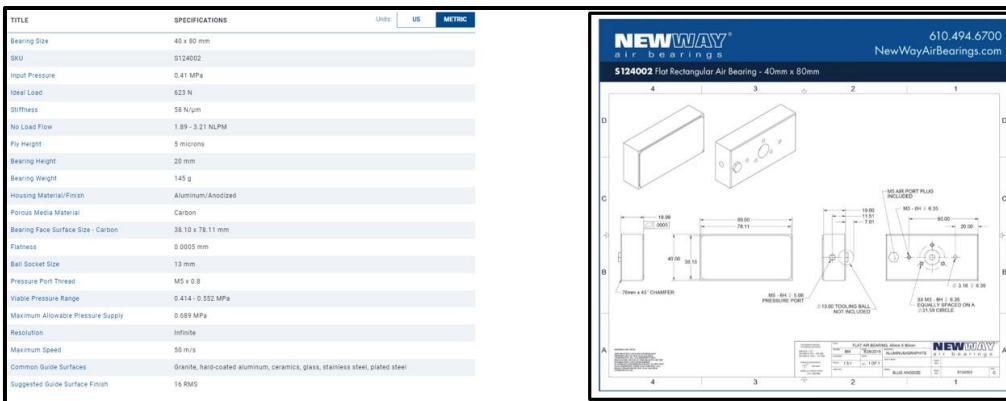


Figure 145 Shows the detailed specifications of the (40 ×80) Air bearing

Justification of Air bearing Guideway.

As discussed in section the stainless-steel optical guide can only be used as the air bearing surface if it has the surface roughness below 0.41(μm) RMS and the flatness of 50% of its nominal flying height which is 5 μm . See Figure 146

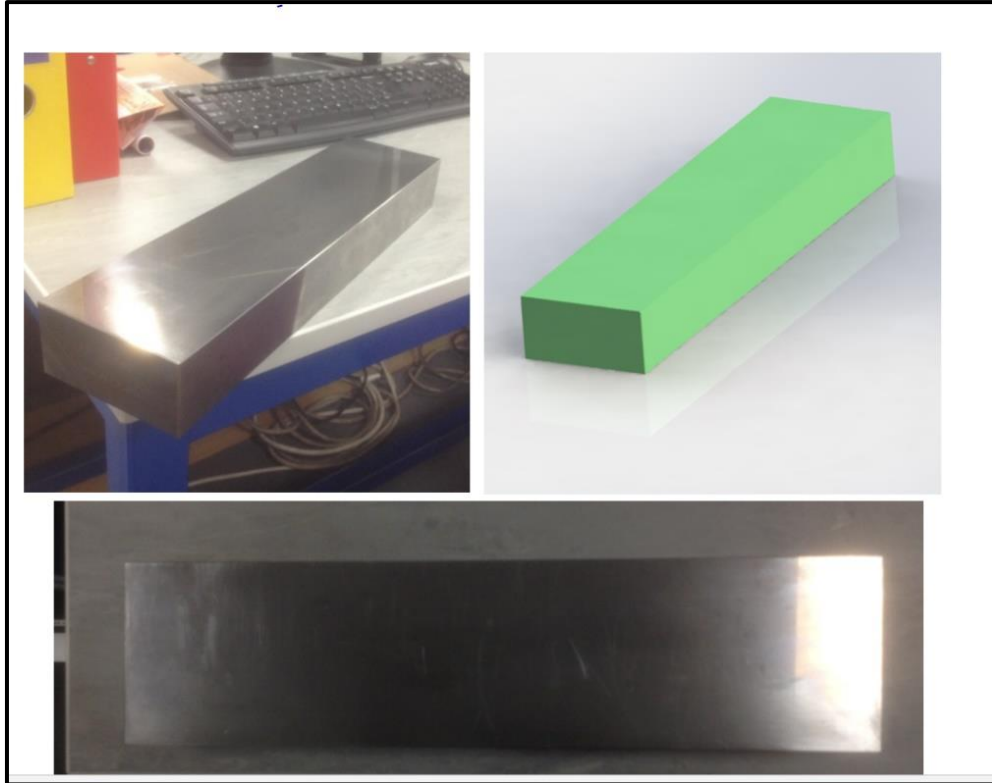


Figure 146 Shows the Polished Stainless-steel Guide way Cad Model and original part

Discussion for Surface Roughness

16 rms or better finish is required for the air bearing Guideway, if the gap is to be considered low the rough surface can damage the pad due to touch down. Also, the valleys of the surface may take the place of gap. In order to avoid this, the experimental validation needs to be carried out to prove if the Surface roughness of the Optical stainless-steel guideway meets the desired requirements for the Air bearing pad to float without any touch down or disruption.

The surface rough Experiment was carried out on Alcona Infinite Focus G4, With the help of Alcona LU Plan ELWD 20X/0.40 Lens. Two parameters were measured, Rq or Rms (Root mean square roughness of profile) and an aerial parameter Sa (Root mean square height of the selected area). These parameters were then matched with the required RMS.

Top Surface measurement: 9 micro-areas were chosen to obtain the surface roughness values, with the length of the micro area being 3.8466 mm and width being 545.0477 μm with a small height of 5.2784 μm . This was used for all 9 measurement see table for all RMS and SA values both in micro meters (μm) and nm respectively. See Table 7 and Figure 147 below.

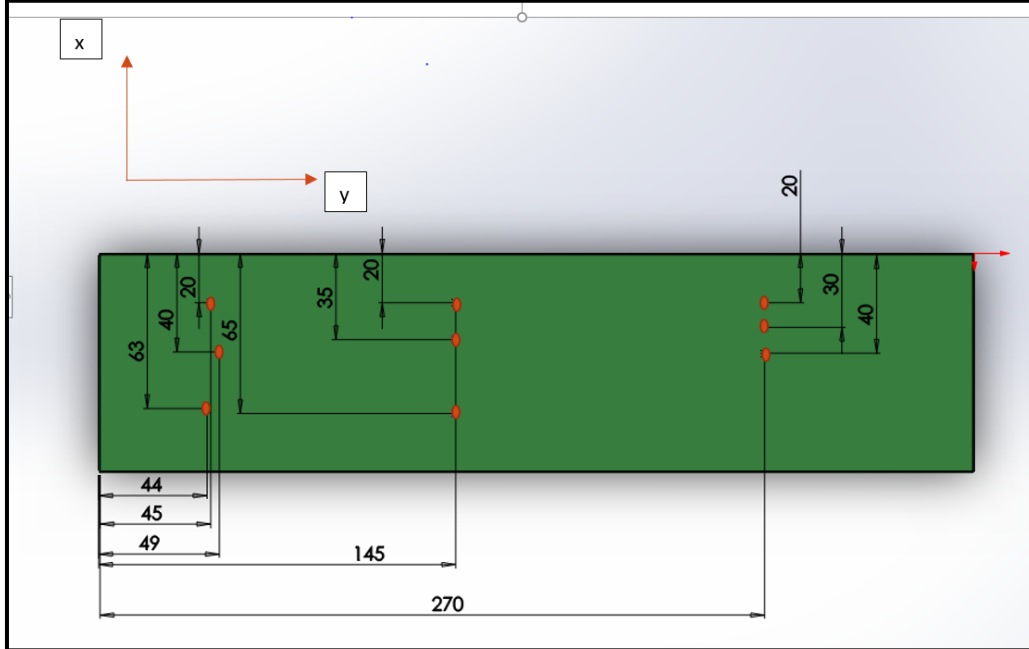


Figure 147 Shows the location of Surface roughness measurement micro areas for top surface

| Location (x , y) | RMS nm (μm) | Sa nm (μm) |
|-------------------------|--------------------------------------------|-------------------------------------------|
| (20,145) | 187 (0.187) | 215 (0.215) |
| (20, 45) | 221 (0.221) | 281 (0.281) |
| (40,49) | 191 (0.191) | 230 (0.230) |
| (63,44) | 167 (0.167) | 227 (0.227) |
| (65,145) | 198 (0.198) | 239 (0.239) |
| (35,145) | 171 (0.171) | 247 (0.247) |
| (30,270) | 272 (0.272) | 330 (0.330) |
| (40,270) | 284 (0.284) | 314 (0.314) |
| (15,270) | 277 (0.277) | 293 (0.293) |

Table 7 Shows the Values of corresponding Roughness values in micro areas

For lateral surface Measurements: Roughness measurements for Lateral side 1 was taken with the help of 4 measurement points, with the same length, width and height of micro area see *Figure 148 & Table 8*. For Lateral 2, Surface roughness measurement values were obtained from 2 measurement points with all the parameters being same See *Table 9 and Figure 149* .

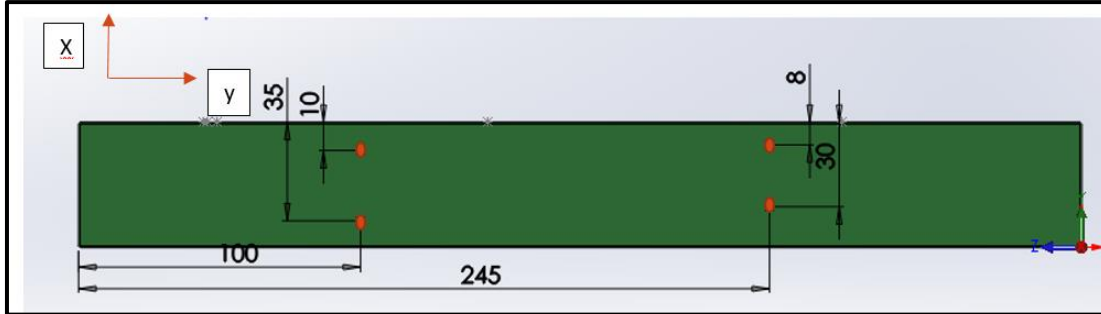


Figure 148 Shows the location of Surface roughness measurement micro areas for Lateral surface 1

Table 8 Shows the Values of corresponding Roughness values in micro areas for Lateral Surface

| <u>Location (x , y)</u> | <u>RMS nm (um)</u> | <u>Sa nm (um)</u> |
|-------------------------|----------------------|---------------------|
| (10,100) | 288 (0.288) | 338 (0.338) |
| (35,100) | 207(0.207) | 247 (0.247) |
| (30,245) | 255 (0.255) | 295 (0.295) |
| 8 ,245) | 332 (0.332) | 391 (0.391) |

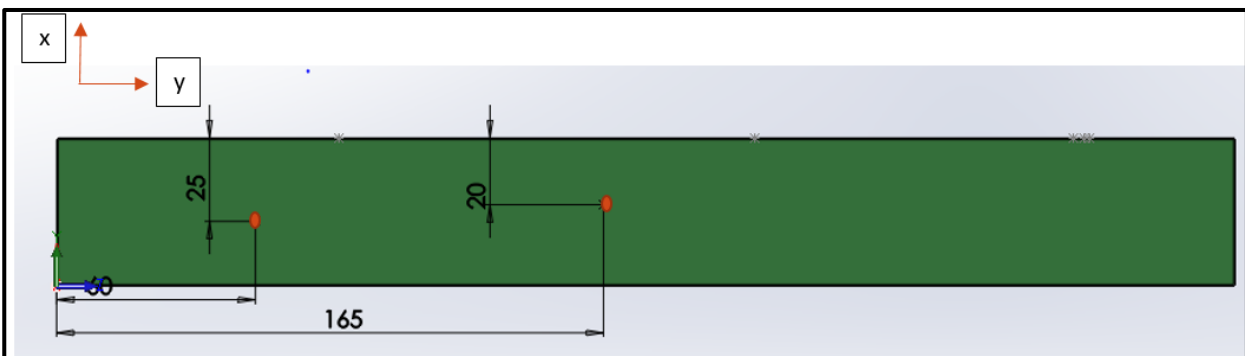


Figure 149 Shows the location of Surface roughness measurement micro areas for Lateral surface 2

| <u>Location (x , y)</u> | <u>RMS nm (um)</u> | <u>Sa nm (um)</u> |
|-------------------------|----------------------|---------------------|
| (20,165) | 212 (0.212) | 247(0.247) |
| (25, 6) | 215 (0.215) | 300 (0.300) |

Table 9 Shows the Values of corresponding Roughness values in micro areas for Lateral Surface

It can be seen that for the top surface the value for Rq or Rms ranges from 0.167um to 0.284 um which is within 0.41(um) RMS required for the air bearing surface. Hence, this proves that the guideway is coherent with the bearing surface roughness requirements. Furthermore, aerially root mean square height Sq ranges from 0.215 um to 0.33 um which is also under 0.41(um) RMS. See Figure 150 and Figure 151.

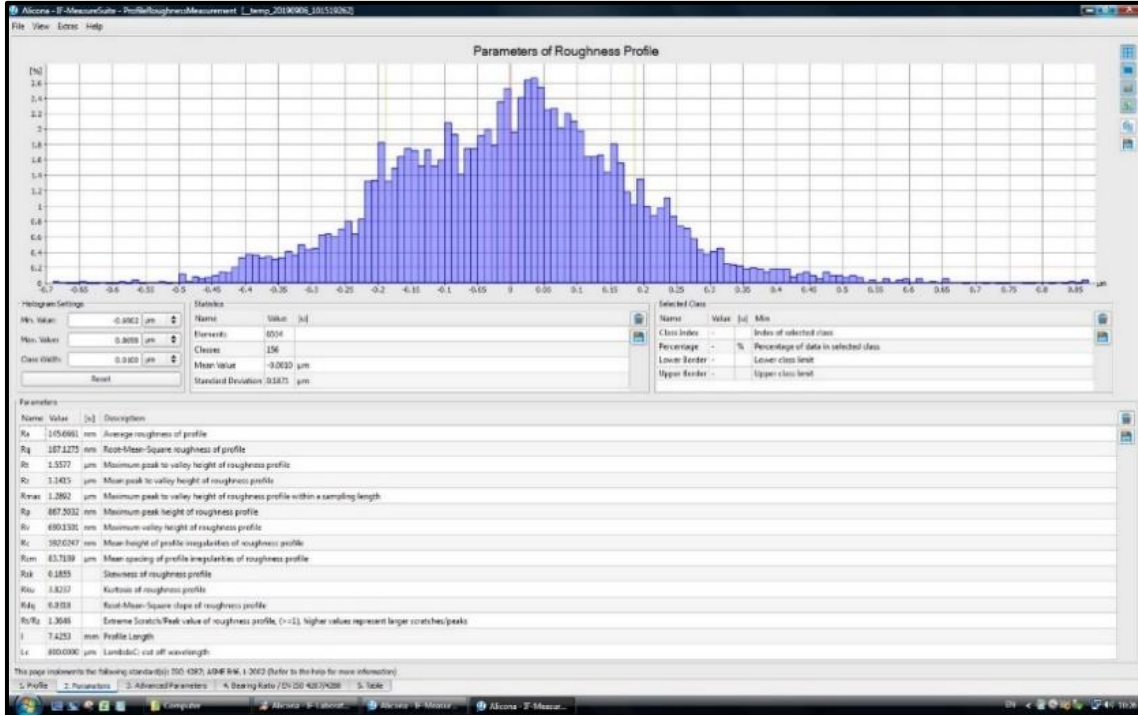


Figure 150 Shows all the parameters taken from Alcon

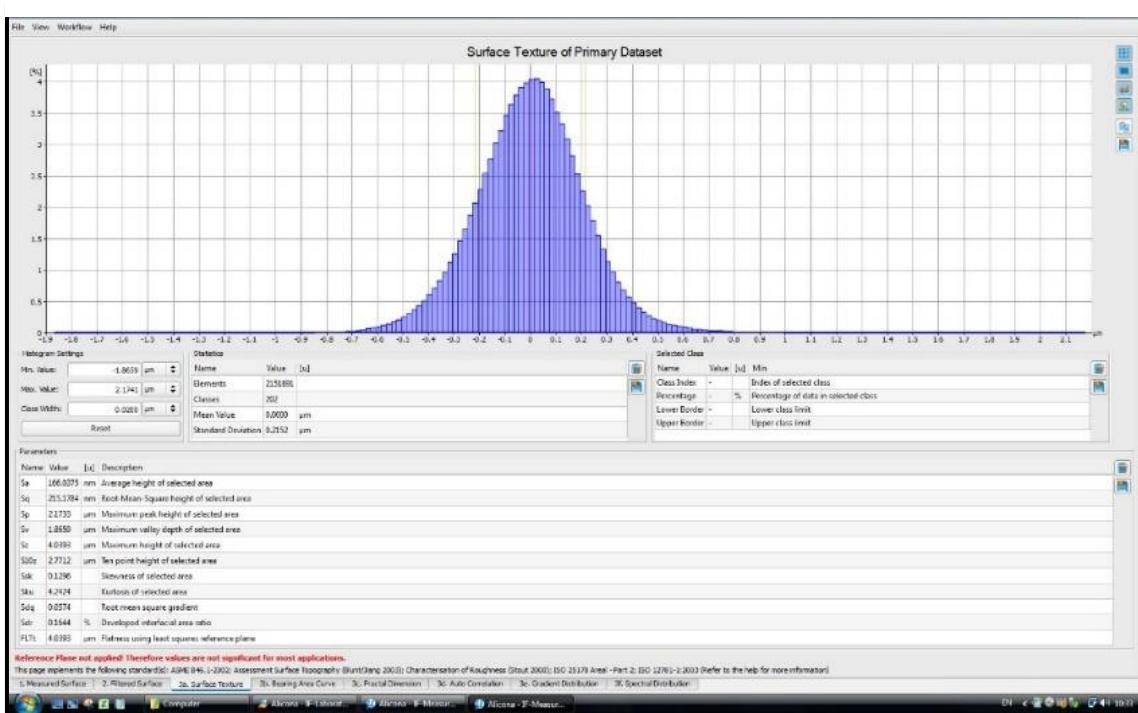


Figure 151 Shows all the aerial parameters taken on Alcon



Figure 152 the surface texture of the micro area

The *Figure 152 above* shows the surface texture of the micro area. The surface roughness within such a small surface is less and the texture is nearly smooth with the markings representing scratches, dirt and micro defects in the material.

Discussion fore Flatness

The local flatness of the bearing should be less than 50 % of the design air gap, it's the flatness under the bearing at a single time. Considering the $5 \mu\text{m}$ air gap as the ideal air gap , and the operating air gap to be $4 \mu\text{m}$. The requirement for flatness is $50 \% \times 4 \mu\text{m} = 2 \mu\text{m}$ The lose tolerances can then be specified as $1.8 \pm 0.2 \mu\text{m}'\text{s}$. This value is desired for the local flatness of the bearing area for all three surfaces.

Zeiss Primo Access CMM was used to determine the validity of the guideway in terms of its flatness for the use of air bearing. It can be seen that the Top bearing local surface of approx. 40×80 (The bearing surface area) has a flatness of 1.5 micro meters whereas the entire top surface flatness is 6.6 microns. *See Figure 153.*

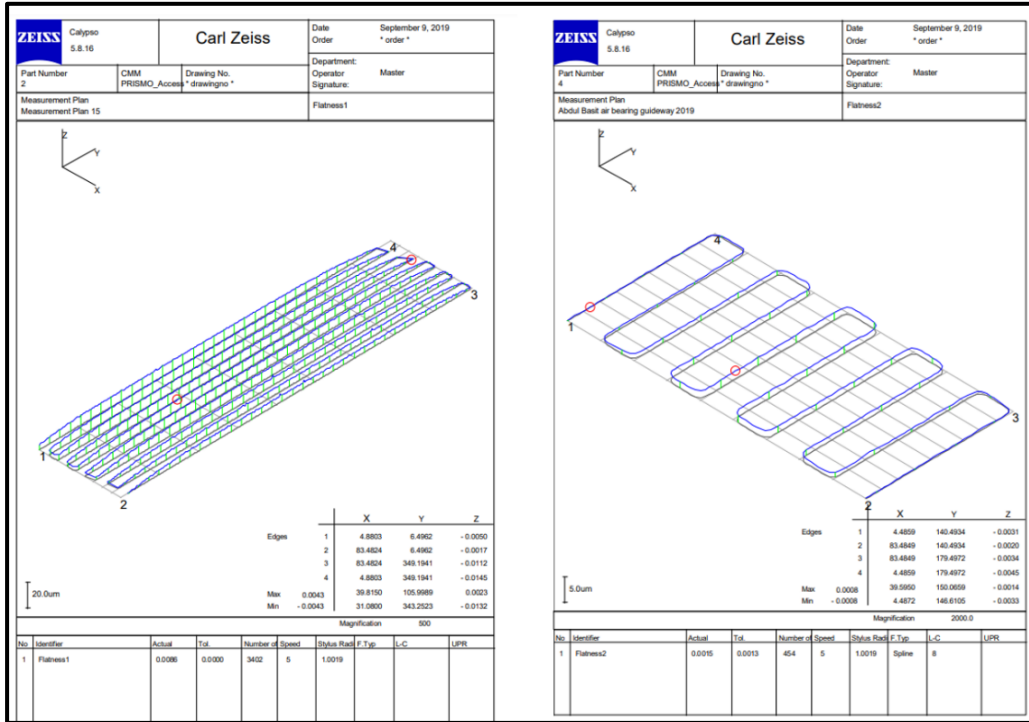


Figure 153 Local top surface flatness (right) Full top surface flatness (left)

Similarly, the local central flatness and full Surface flatness of Right and Left surfaces are 5.1 ,2.8 and 3.3, 1.7 microns respectively see *Figure 154 and Figure 155*. Four coordinate points were utilised for all 6 cases of flatness experiments, these coordinates can be seen for top, right and left surfaces respectively.

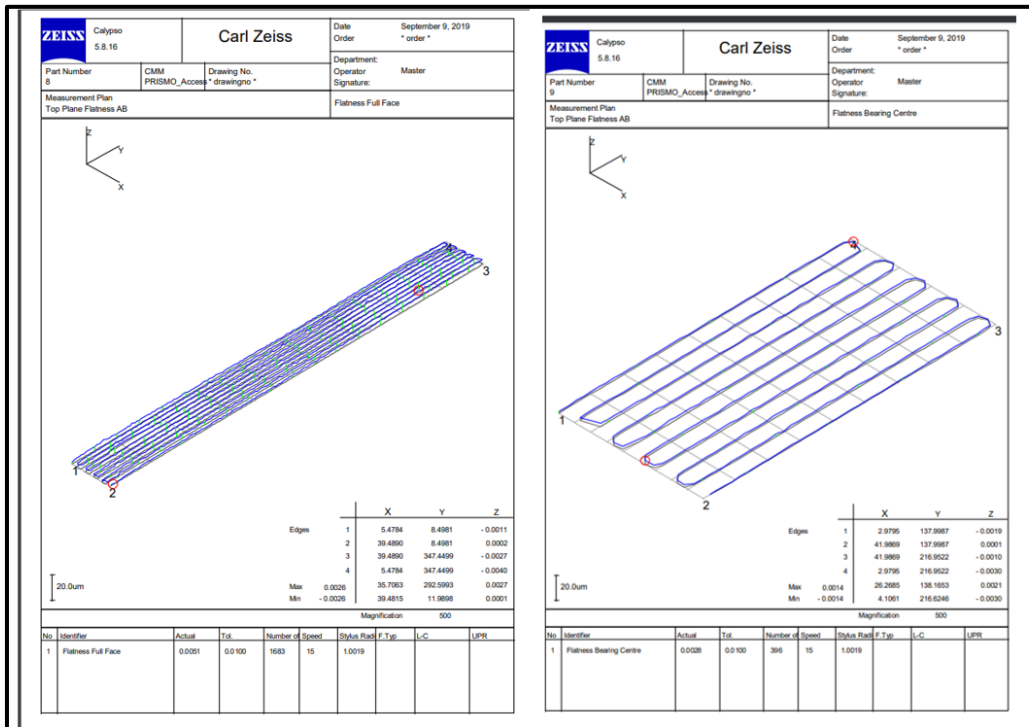


Figure 154 local central flatness and full Surface flatness of Right Surface

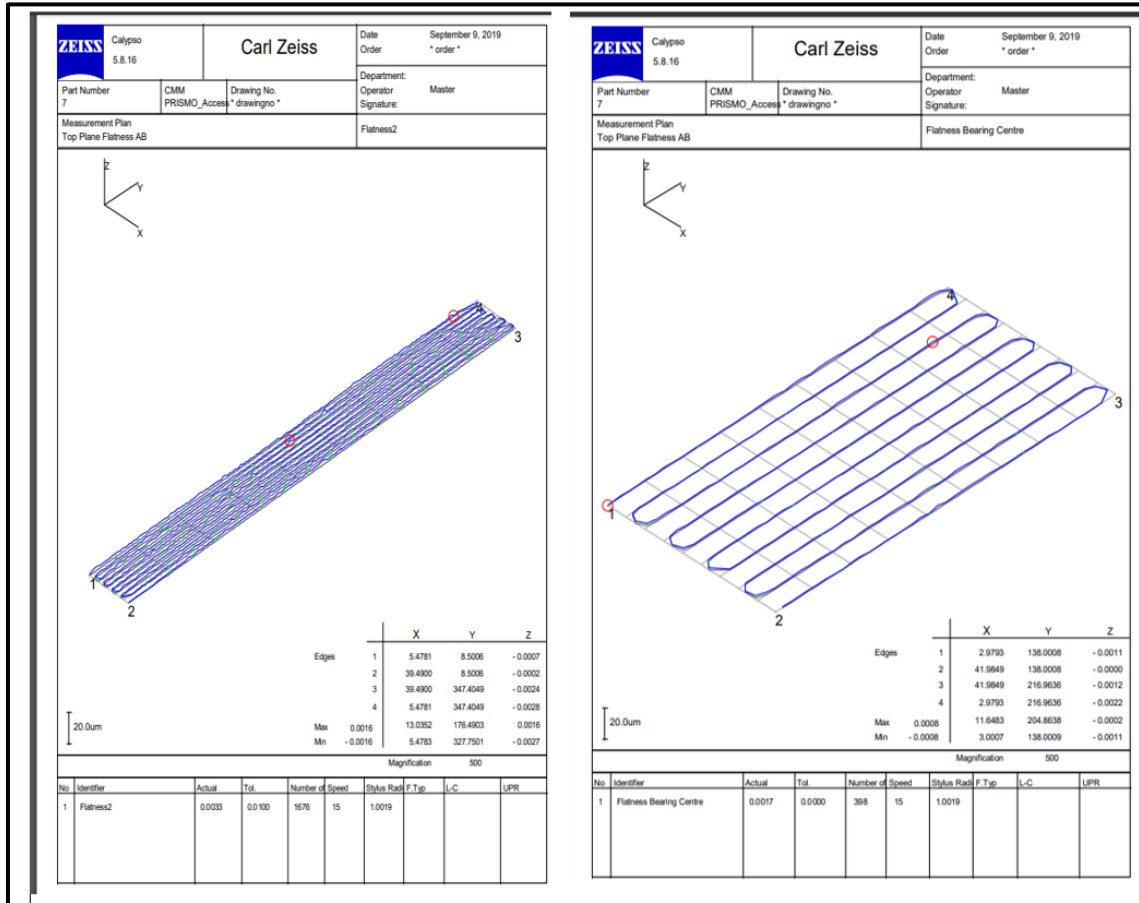


Figure 155 local central flatness and full Surface flatness of Left Surface

The local flatness of right Surface has a value of 1.7 microns and with the top local surface having 1.5 microns this meets the specifications required for the Air bearings as low tolerance values were set for a 4-micron gap. However, the local flatness value for left bearing surface is 2.8 microns which is 0.8 microns higher than the desired flatness. This can be due to the defect at the local site and other areas might have lesser defects this can be proven by the entire surface flatness value of left lateral surface (5.1 microns) which is only 1.8 microns higher than right surface value of 3.3 microns. Despite of this it can be problematic but since all the measurements strongly agree with the desired surface and geometrical tolerances the guideway can be used as an air bearing slide if it fails 5 Micron gap can be used which would accommodate for such flatness errors.

Justification of S Bracket Clamps:

The Guide way needs to be constrained in 6 DOFS in order to allow the air bearings and air bearing housing to slide on it. This therefore requires clamping of the Optical stainless-steel bar guideway. The Guideway is clamped with the help of 2× S shaped brackets. The S shaped brackets provide support to the Guideway by attaching it to the linear recirculating bearing guideway through 2 x (M12 x 80) hex head screws were chosen Based on measurements giving M12 x total length of 83mm (58mm shank length + 25mm (thread) length excluding head thickness), *See Figure 156*. A layer of epoxy to glue the lower surface of the polished guideway to the S shaped brackets.

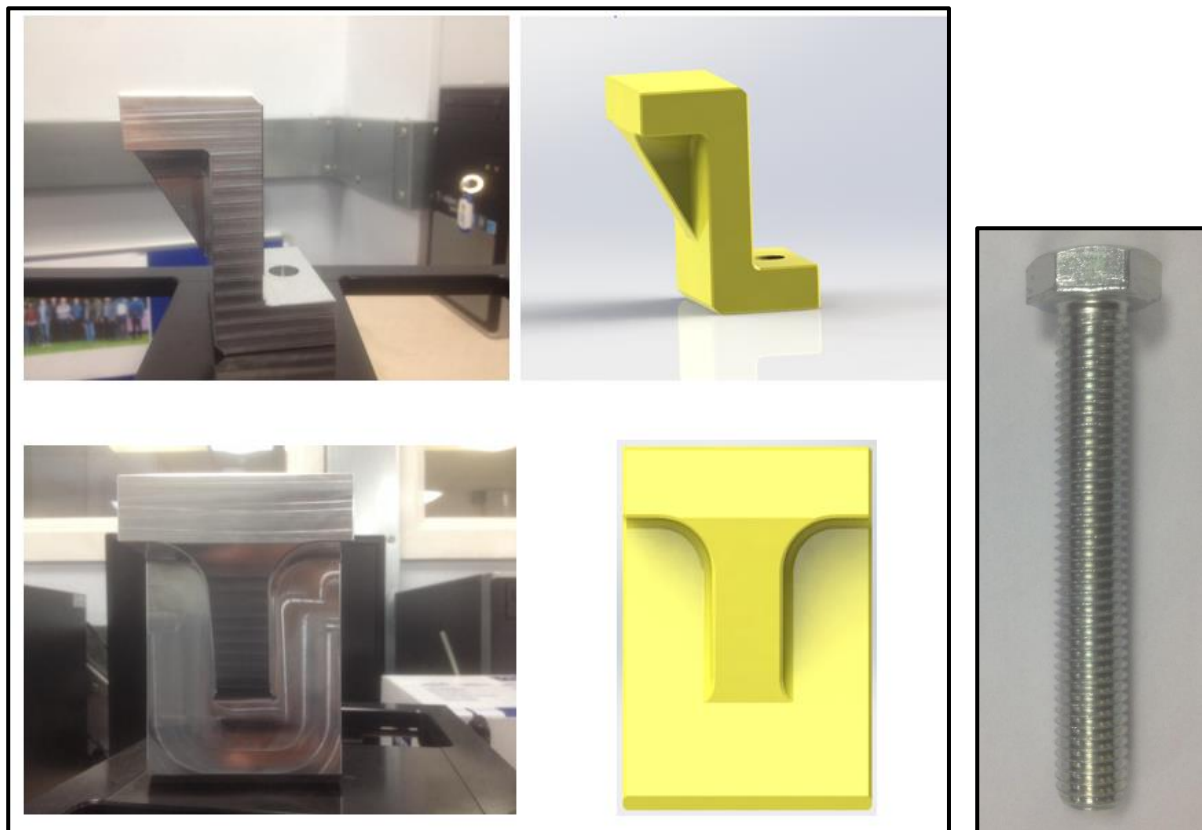


Figure 156 S Shaped Clamps (left) and M12 x 80 Bolt (Right)

The material used for S shaped brackets is 6082T6 Aluminium made from 2 square bars each with a dimension of 88.8 x 88.8 x 130.

The Design has a 20mm thick rib, with 60 mm slant and 30-degree angle and 3.05 fillets. To enhance the strength and to avoid any inclination of the bearing surface due to bending of the top surface of the S brackets. The material was glued to guideway with epoxy due to difficulty in cutting the optical surface for holes this also avoids any damage to the guideway surface during machining.

A 14mm clearance hole is used at the bottom of the S bracket for it to be attached to the guideway. The surface was chamfered and the 3mm fillets were used at the stress raisers.

In order to check if the inclination of the bearing surface due to bending of the top surface of the S brackets is acceptable a Finite element analysis was carried out.

The bending in the upper arm of the S clamping bracket is the main target area of the design as a slant created by the bending can make the Guideway to shift down to a certain extent this of course depends on the location of the applied external forces on the guideway which come from the air bearing and the shaker induced or Impact hammer induced forces in vertical direction. The change in location changes the normal reaction forces between the S clamping brackets for example the Normal reaction force or the force on the S shaped clamping bracket will be higher on the side where the air bearing housing is closer to it than the other bracket.

The Bending must be in microns, and the bending (in microns) should not be greater than 2 microns at the edge where a sufficient amount of area of the end of guideway touch.

Solving the 2D equilibrium equation to determine the Normal reactions when the Guide is closest one clamp and farthest to the other clamp gives:

$$W_g = \text{Weight of guideway} = 120 \text{ N}$$

$$L_C = \text{Load at the centre of the air bearing housing} = 1000 \text{ N}$$

$$L_C \text{ includes both weight of housing (11.2 kg) and air bearing force } 800 \text{ N} = 120 + 800 = 920 \text{ N or } 1000 \text{ N approximately}$$

$$a_1 = 90 \text{ mm}, a_2 = 155 \text{ mm}, a_3 = 312 \text{ mm}, a_4 = 210 \text{ mm}$$

Note: All the moments in counter clockwise are taken as positive. See Figure 157

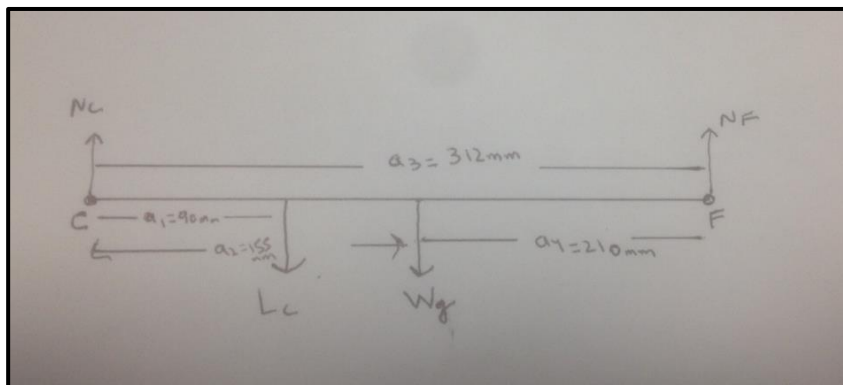


Figure 157 Free Body Diagram

$$\sum M_c = -(a_1 \times L_c) - W_g \times a_2 + N_F \times a_3 = 0$$

$$-(90\text{mm} \times 1000) - W_g \times 155\text{mm} + N_F \times 312\text{mm} = 0$$

$$N_F = 348.07 \text{ N}$$

$$\sum M_F - N_C \times a_3 + W_g \times a_2 + (L_c \times a_4) = 0$$

$$-N_C \times 312 + 120 \times 155\text{mm} + (210 \times 1000) = 0$$

$$N_C = 733 \text{ N}$$

FEA Results:

A very fine mesh with 366635 Nodes and 261179 elements was used to obtain the results *see Figure 158*

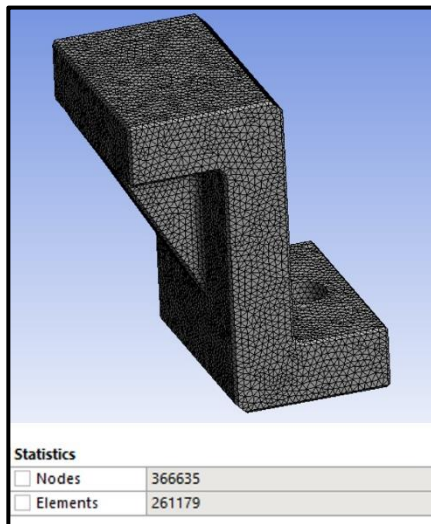


Figure 158 Meshed S bracket with given nodes and Elements

Boundary Conditions:

A force of 1000 N was applied on the top surface of the S shaped Bracket and the Bottom surface with constrained in 6 DOF'S with the help of a planar fixture. *See Figure 159.*

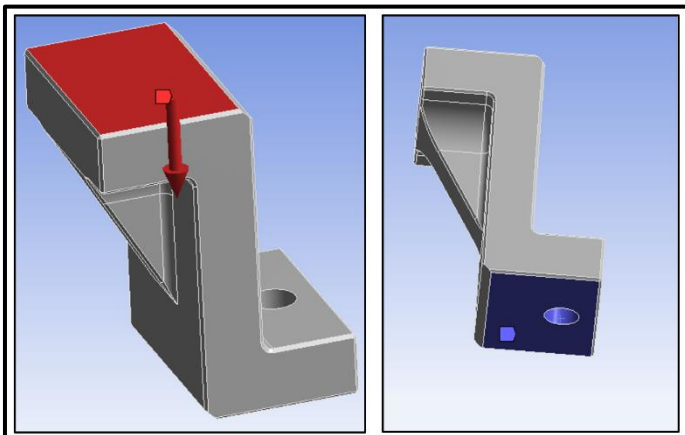


Figure 57 Boundary Conditions of S clamp

Results:

The Deflection at the given locations are (1.5909e-008) ,1.1246e-006 ,1.9192e-007 ,7.5643e-007 lesser than 2 microns. therefore, the slide won't shift down. See Figure 160.

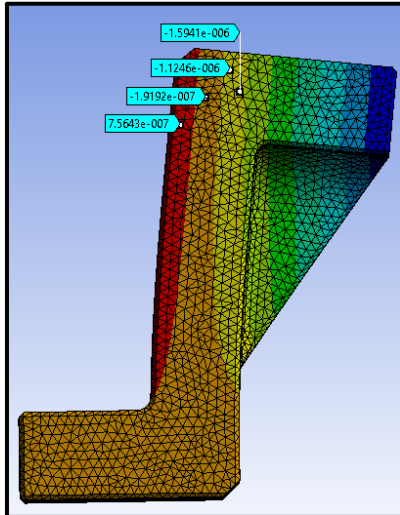


Figure 160 FEA Deflection results of the S Bracket

The epoxy has a shear strength enough to constraint any motion in the planar surface at the top of S clamping bracket.

Justification of Air bearing housing:

The Air bearings are housed in a 6082T6 Aluminium square envelop similar to as discussed in the section. Three (40 ×80) Flat rectangular air bearing pads are used one on the top and one on each side of guide. The Air bearings are attached to the housings via 13 mm Diameter /M10 ×0.75 ×54 mm lg ball mounting screws.

The 4 M6 threaded holes at the top will be used for mounting the shaker. The (M10 × 22 × 33.500) × 3 Counter bored clearance holes are used for the 13 mm Diameter /M10 ×0.75 ×54 mm lg ball mounting screws.

At the bottom four M10×18 threaded holes were drilled, this provides an attachment when the adaptor is connected to it. See Figure 161.

15 mm radius fillets were used at the most stress bearing corners which were the corners of the housing pocket. See Figure 161 .The size of the fillet was also dependent on the availability of the tooling.

The housing was made out of 6082T6 Aluminium square bar with dimensions 203.2 × 203.2 × 270

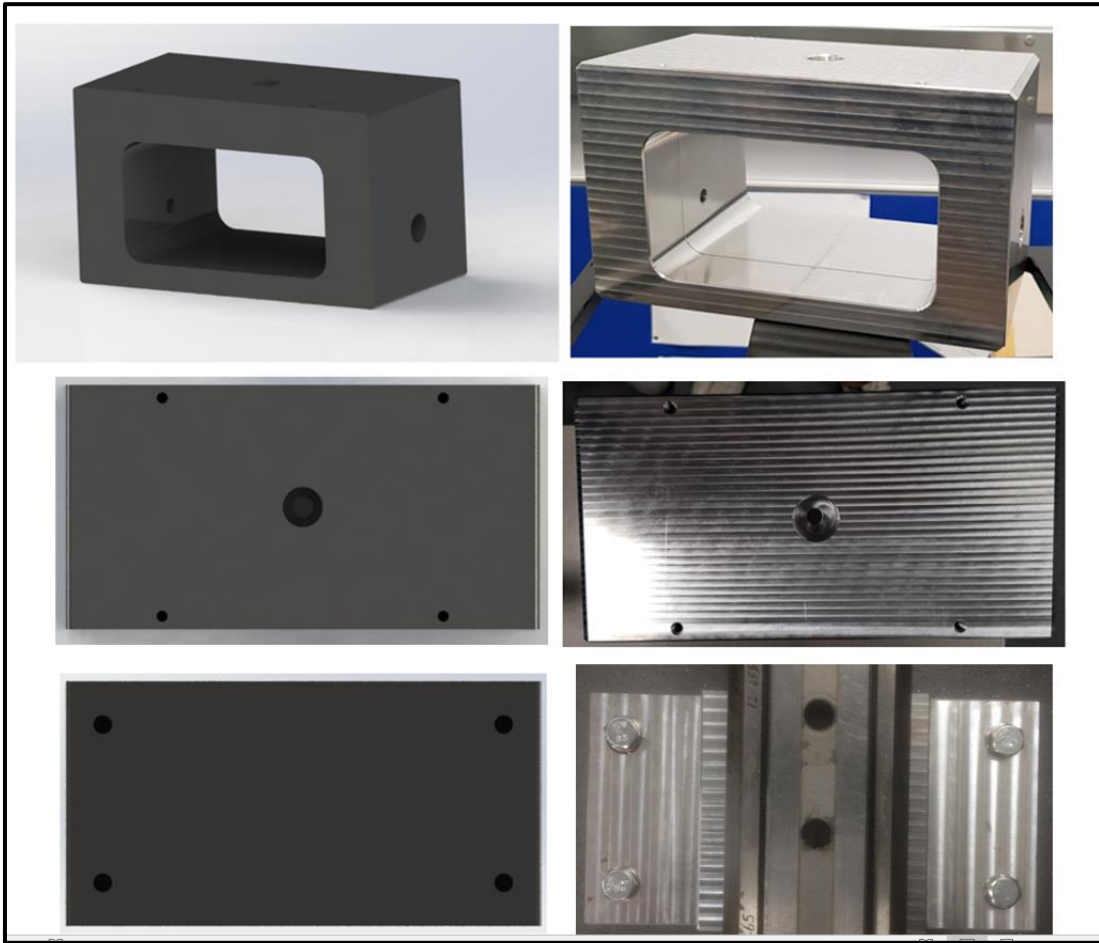


Figure 161 Aluminium Air Bearing housing

Aluminium 6082T6 was used, although Steel alloys could prove more robust in terms of rigidity for deflection but due to easy availability, lesser weight and easy machinability Aluminium 6082T6 square bar (203.2 x 203.2 x 270) was chosen to manufacture the housing *See Figure 162* . Aluminium has also been used in conventional Air bearing guideways as discussed with the new way air bearing company that use 6061-T6 Al for air bearing housing and the rail made of 2024-T351 Al.



Figure 162 Block of Aluminium 6082T6 square bar (203.2 x 203.2 x 270)

FEA: This design also behaves more like a pressure vessel; the housing walls are under a distributed force that is applied to them by the air bearings transferred evenly through the spacers. The area near the air bearing is sensitive to outward deflection. Similar to the case referred to in earlier section this causes change in the desired air gap. Therefore, the deflection in this area must be controlled within few microns.

Housing was tested with the help of FEA using Aluminium alloy in order to check for deflection.

The number of nodes and elements were set to a value of 1286647 and 922594 respectively. *See Figure 163.*

At this value mesh convergence can be approximated as the values do not change significantly by refining.

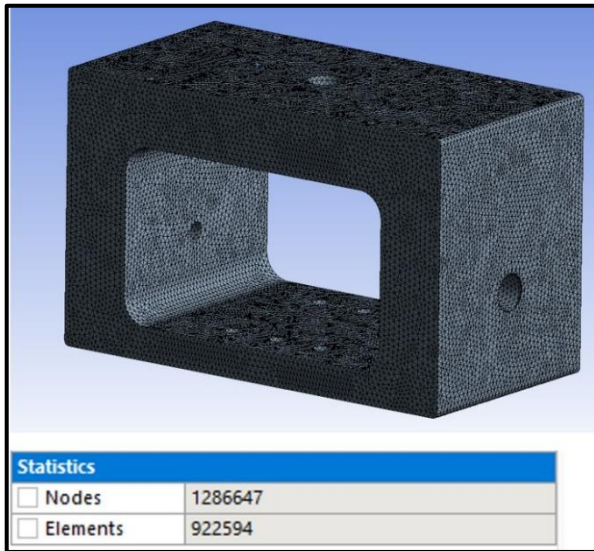


Figure 163 Shows the Meshed Air bearing housing with the nodal and element values

Boundary Condition:

The shaker applies a dynamic load at the top of the Air bearing housing, this was considered static as we are only considering the housing deflection. The maximum shaker load is 200 N, the Aluminium air bearing housing weighs 8 kg approximately which relates to 80 N of force. Applying 300 N force downwards

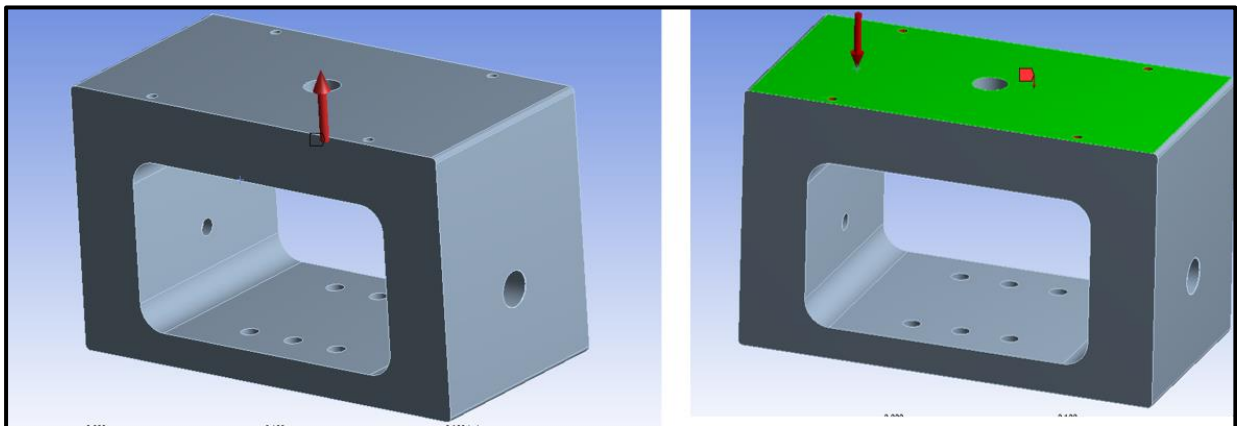


Figure 164 Shows Vertical boundary Conditions

replicates extreme conditions. The bearing ideal load is 600 N upwards at 60 psi, flying at 4.5 microns approximately but can reach up to 800 N upwards at 80 PSI at 4.5 microns approximately. Again, assuming the extreme condition, the bearing force of 800 N was applied at each bearing surface through the holes upwards for Top and leftwards for Left opposing the external load. See Figure 164 above.

In second case, everything similar expect now its assumed that the shaker or hammer is acting on left side. See Figure 165.

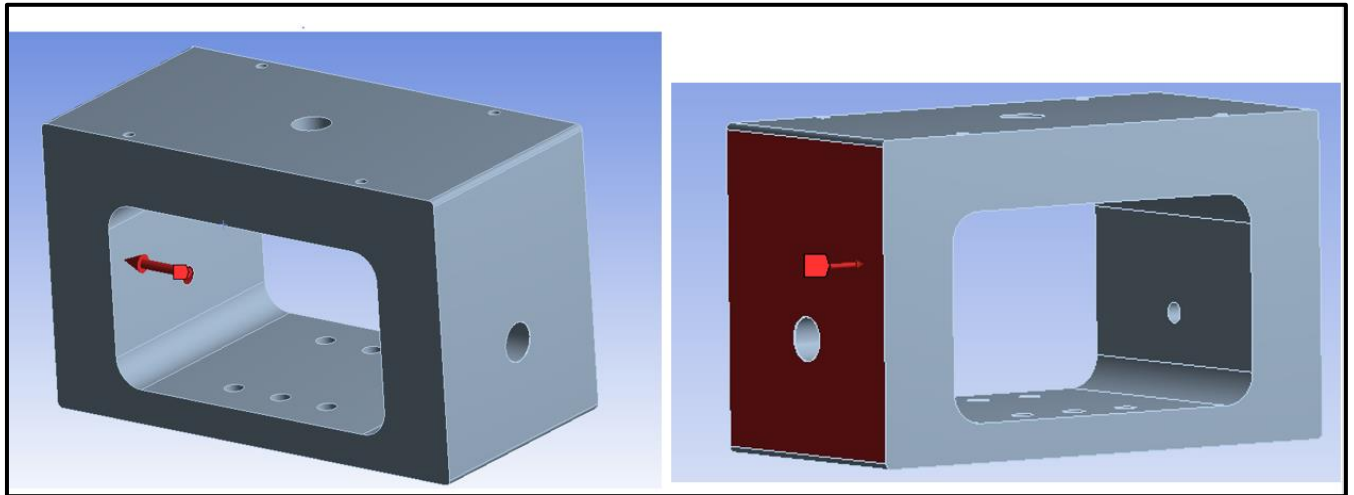


Figure 165 Horizontal boundary conditions of Air bearing housing

The Right face and the bottom face were constrained and fixed in 6 DOFS in order to attain the relative effects of load on other faces. See Figure 166.

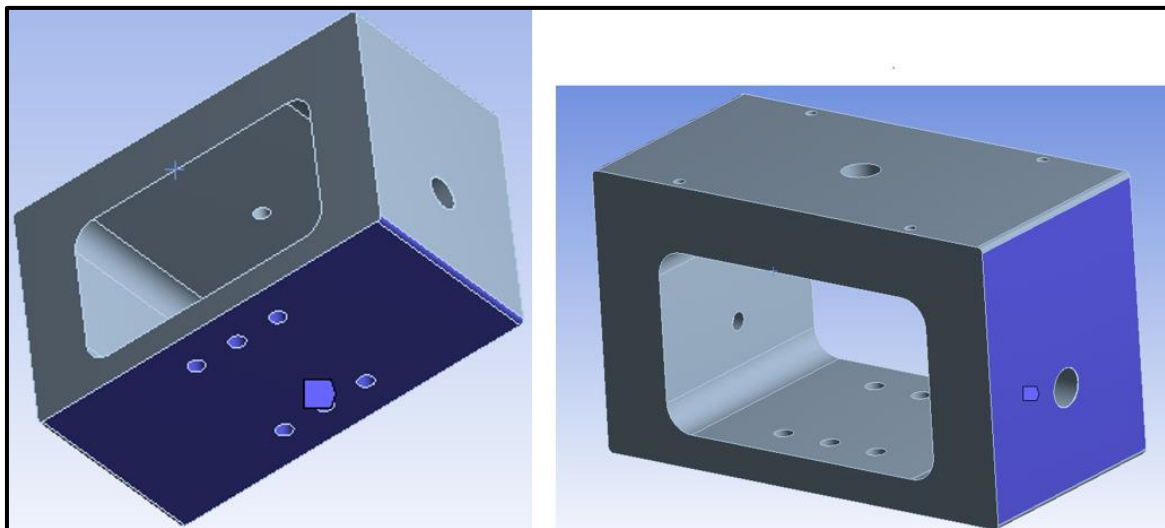


Figure 166 Fixed Constrains of Air Bearing Housing

The deflection near the bearing area in Y direction (Left hole) varies within a range of 8.172×10^{-7} to 2.3760×10^{-6} in the first case and 6.5879×10^{-7} to 2.511×10^{-6} in second case. The space plate spreads the load evenly therefore the average deflection is below 1.5 microns which justifies the structure. See Figure 167.

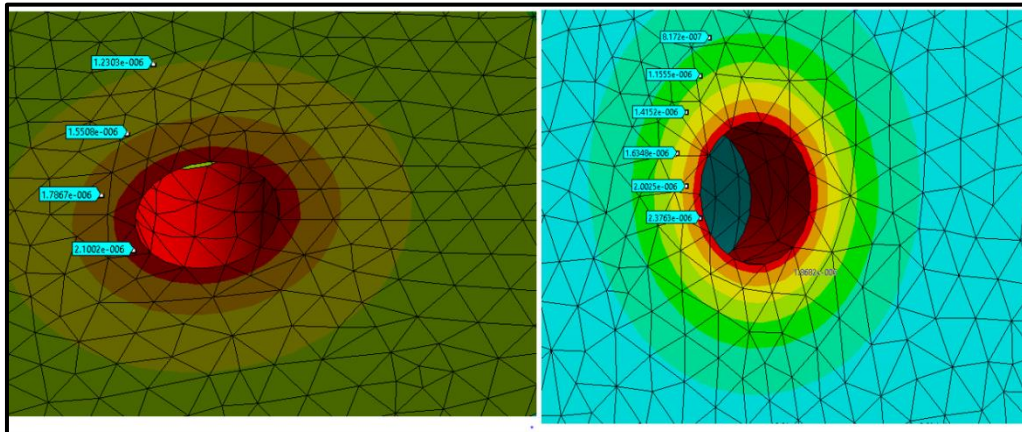


Figure 167 For y Direction load , top face (left) left face (right)

Similarly, the deflection near the bearing area in x direction (Top hole) varies within the range of 1.2303 e-006 to 2.1002 e-006 in first case and 1.7222 e-006 to 2.3573 e-006 in second.

Again, the average deflection is around 1.5 microns. See Figure 168

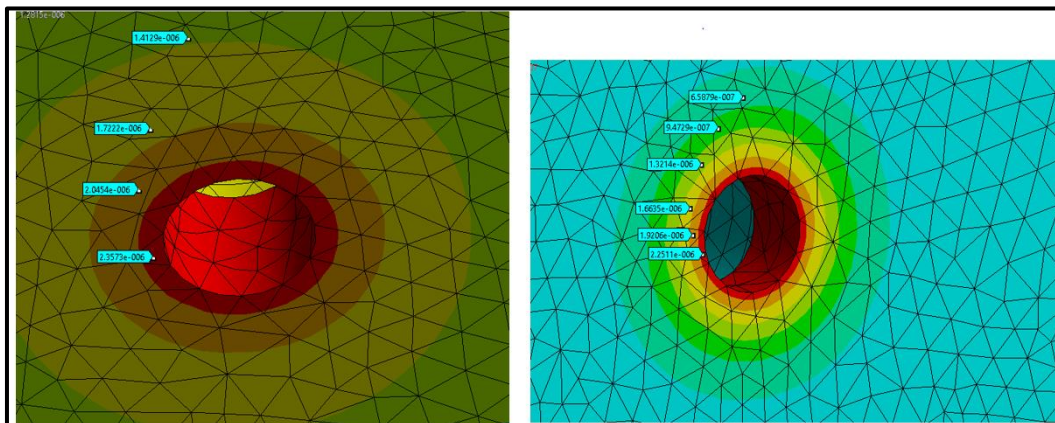


Figure 168 For x Direction load , top face (left) left face (right)

Justification of Air bearing Plumbing:

The bearing works on an air film that is free of particulates, water and oil. The quality class requirement recommended for New way air bearings is 3 but can be 4, 5, 6 as seen from chart below. Porous bearings are sensitive to oil contamination. they are also sensitive to water contamination but it can be avoided by supplying dry clean air. Insensitivity for Particulates like lineages shedding, Teflon tape and sealant can be found in porous bearings which are being used in prototype. (new way bearing design guide) .

The bearings need an air supply of 60 Psi or 80 Psi generally to match the data the graph provides. *See Figure 169.*

| | QUALITY CLASS | DIRT (Particle size in micron) | WATER Pressure Dew point > F (ppm. vol.) at 100psi g | OIL (including vapor mg/m ³) |
|----------------------|---------------|--------------------------------|------------------------------------------------------|------------------------------------------|
| | 1 | 0.1 | -94 (0.3) | 0.01 |
| | 2 | 1 | -40 (16) | 0.1 |
| RECOMMENDED | 3 | 5 | -4 (128) | 1.0 |
| MINIMUM SPECS | 4 | 15 | +37.4 (940) | 5 |
| | 5 | 40 | +44.6 (1240) | 25 |
| | 6 | - | +50 (1500) | - |



Figure 169 Bearing Air supply data taken from new way air bearing design guide

Figure 170 Polyurethane tube Amazon (2020)

A fresh air is supplied to the pressure regulator through a Pipe. The air at 60 psi is supplied to 8 mm Polyurethane Tube, which is connected to the 3 port 1/4 Bsp Manifold with 4 Outputs 3 x 6mm and 1 x 8mm. The 8mm tube is connected at one end and the 3 x 6mm tubes on the other three ends of the manifold. The 3 x 6mm Polyurethanes tubes are then connected to each of the air bearings separately through Straight Pneumatic Push to Quick Connect Fittings M5 Male x 6mm Union .*See Figure 170 and Figure 171.*

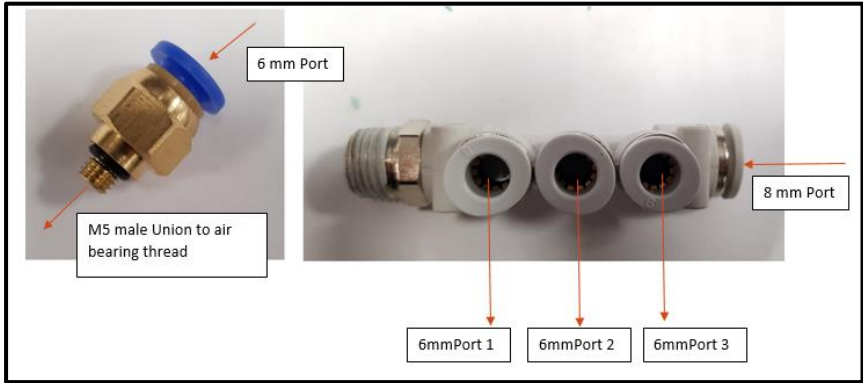


Figure 171 3 port 1/4 Bsp Manifold with 4 Outputs 3 x 6mm and 1 x 8mm (Right), Straight Pneumatic Push to Quick Connect Fittings M5 Male x 6mm Union (left)

Justification of Air Bearing Housing to Linear recirculating bearing Adaptor:

The Adaptor is a result of the manufacturing limits of the CNC machining centre HURCO VMX3001 that was used for manufacturing. Due to block size limitation of 6082T6 Aluminium square bar 203.2 x 203.2 x 270 that needed to be cut, the gap of 47.47 mm between the bearing and the housing was left, in order to fill this and attach the air bearing housing to the linear recirculating bearing an adaptor design was utilised.

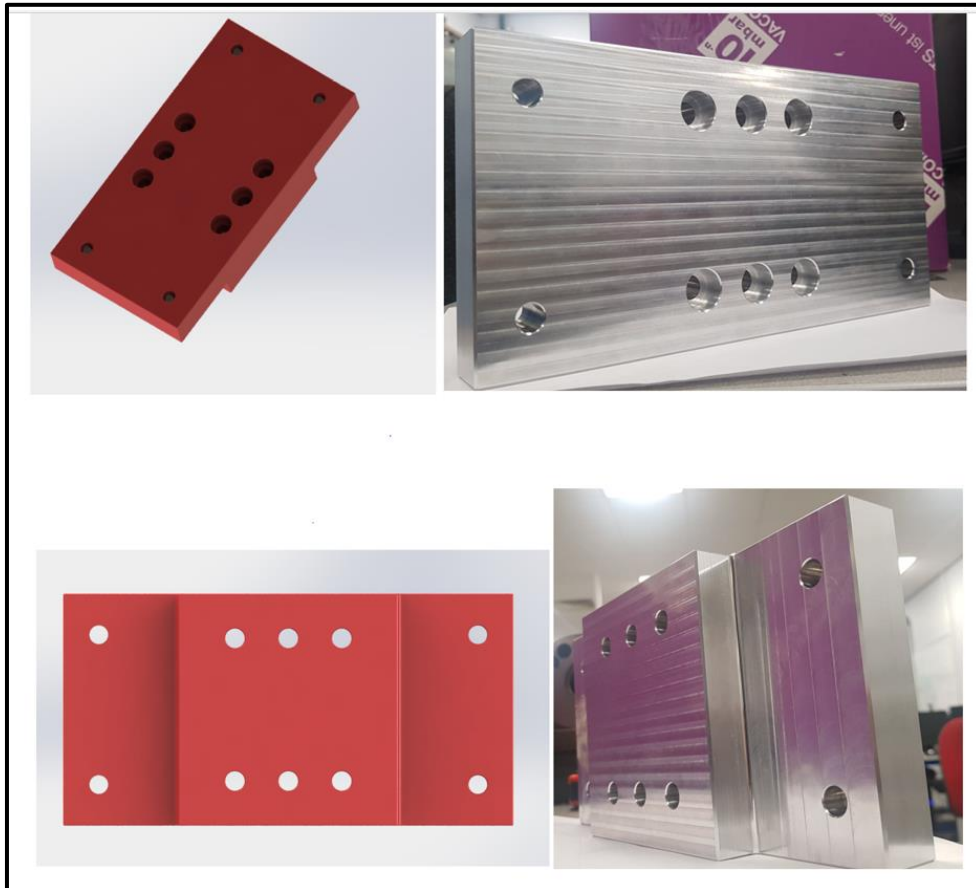


Figure 172 Air Bearing Housing to Linear recirculating bearing Adaptor Cad (left) , Manufactured Part (right)

The adaptor consists of 6 x (M10 x18 x12 x47.47) Counter bored clearance holes for linear recirculating bearing connection which uses a socket head. The nearest Metric size bolt 6 x (M10 x45 cap head screws) with hex Allan drive were used Based on a M10 hole with a Total length of 46.47mm (35.47 Shank length, 11max thread length excluding head thickness) . and for 4 x M10 drilled Clearance holes for air bearing housing connection M10 x40 hex head screws were used based on M10 hole with a Total length of 46.47mm (27.5 shank length, 14 thread length excluding head thickness). M10 Flat washers were used for even load distribution and to avoid damage to the surface. The plate is made of 6082T6 Aluminium square bar. See Figure 172.

Linear roller bearing guide:

The bearing used is a minimal quantity metering unit series SMDE-45-S by INA that uses rollers as bearing elements. The mechanical properties are given in the table above. The load capacity is of the guideway plus the linear bearing.

The guideway was shipped from MTT (Machine tool technologies LTD), it is assumed to be minimally preloaded. The Linear recirculating bearing has 6 × M10 Threaded holes which will be used to mate with the Air bearing to Linear recirculating bearing Adaptor. *See Figure 173.*



Figure 173 SMDE-45-S by INA Linear bearing guide

| Bearing Name | Basic Static Load rating (N) | Basic Dynamic Load rating (N) | Length (Containing linear recirculating rollers) mm | Height mm | Width mm | Mass bearing (Guide assem) kg | Stiffness N/um |
|---------------------------------------|------------------------------|-------------------------------|-----------------------------------------------------|-----------|----------|-------------------------------|----------------|
| INA-SMDE-45-S (Linear roller Bearing) | 205000 N | 92000 N | 137 mm | 51.2 mm | 81.7 mm | 0.2 (3.3-4.4) kg | 1560 /um |

Table 10 Characteristics of SMDE-45-S by INA Linear bearing guide

Details of mass of guideway, material used in bearing. and stiffness in all directions. See Figure 174, Figure 175 and Figure 176.

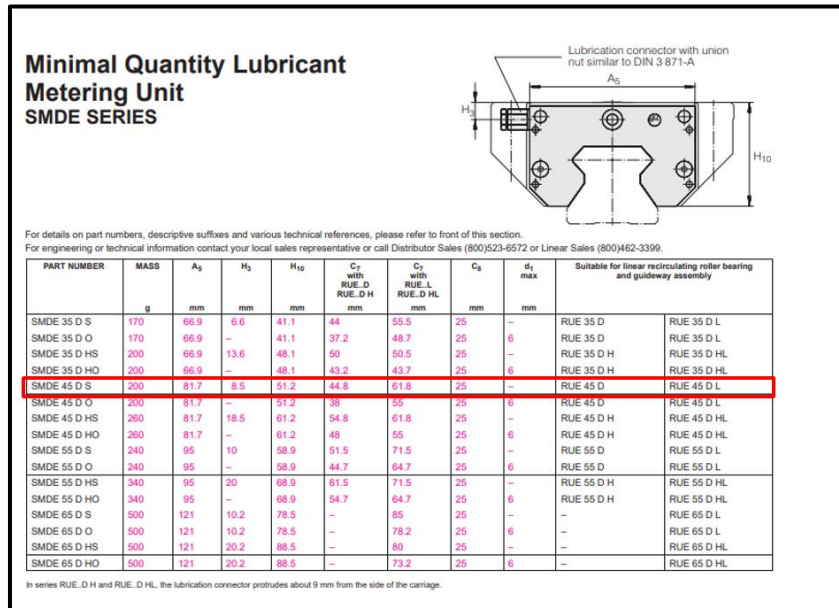


Figure 174 Table 10 Data of SMDE-45-S by INA Linear bearing

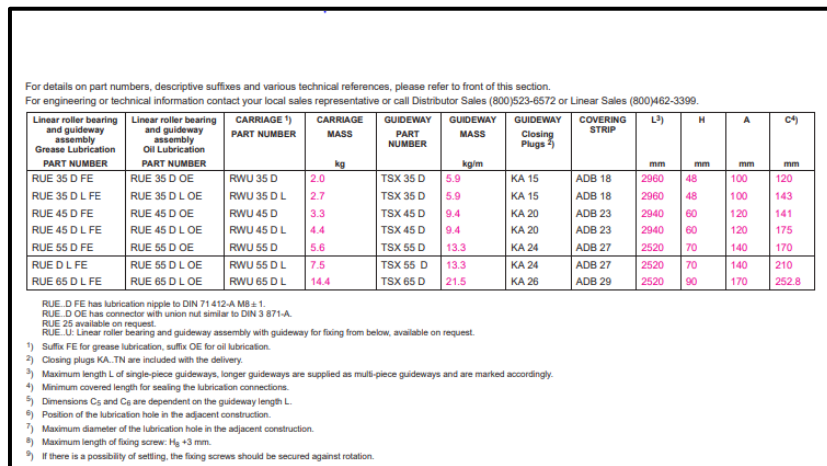


Figure 175 Table 10 Data of SMDE-45-S by INA Guide

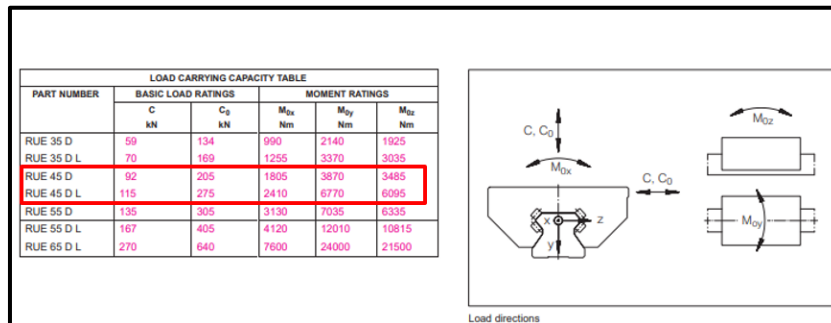


Figure 176 Table 10 Data of Load Capacity of SMDE-45-S by INA Linear bearing

CHAPTER 6: DISCUSSION

In this section of the report the Solution to the design problem is critically evaluated both in terms of the degree to which the objectives have been achieved and the performance of the design and its limitations. Also, the achievements in relation to the pre-set Aims and Objectives have been clearly defined.

Finally, Future recommendations are made to arrive at the desired solution. It must be noted that the discussions related to experimental and various Analyses have been carried out in their own section and this is only the overall discussion of the report.

6.1 ACHIEVEMENTS

The Project was technically demanding; The Scientific method of research was understood in great detail. The problem was understood and further explored by carrying out the Literature and Critical review in breadth as well as in depth. All methods of data extraction whether Analytical, experimental, or computational were carried out and understood in depth. Rigorous mathematical modelling was involved to arrive at a solution to various problems related to mechanics and dynamics. Besides this, the report proved to be a great source learning advanced CAD and Manufacturing techniques and Digital Signal Analyses.

6.1.1 Objectives Met and Delivered Solution.

6.1.1.1 Literature Review: To carry out the breadth and depth of the Literature review of already existing and developing new technologies relevant to feed drive systems. Various Scientific publications will be studied and critically reviewed.

Delivered Solution: Around 100 technical papers were studied, the problem was understood and further explored by carrying out market research followed by critical review. Most of the breadth as well as depth was in the field of Feed drive design was covered and documented in detail for further research. This section covered a broad spectrum of research and concluded a knowledge gap.

6.1.1.2 Novel Concept (Workable Solution): Brainstorming and Concept generation evaluation will be undertaken based on the knowledge gained through background research.

Delivered Solution: Various Novel Ideas were generated and rated on the basis of their viability leading to novel hybrid bearing design. Although other concepts also provide a viable solution Hybrid bearing proved to be the most efficient design with all the criterion mentioned in the section 4.4.3.

6.1.1.3 Preliminary Analysis: In order to Verify and Validate the Design various types of Analysis will be carried out during the design phase. Computational analysis including Finite element analysis and Vibrational Analysis using various software packages i: e Ansys, Solid works and MATLAB.

Delivered Solution: Most of the preliminary Analysis necessary for the validation and verification of Novel hybrid bearing original as well as the prototype design has been set for further validation This includes Computational Modal Analysis as well as the experimental benchmark tests. Furthermore, Force Analyses on the designed concept based on true machining forces was also evaluated through experimentation, bibliography and compilation of information from various research papers. This provides the basis for the Geometry and Material Selection.

In Addition, this section also contains a proof of why the piezo-electric actuators will not provide the viable solution.

6.1.1.4 Detailed Mechanical Design and Analysis: Includes the three-dimensional design, the space envelops, mechanics and dynamics.

Delivered Solution: Based on the Preliminary study the detailed design and Analysis of the Novel Hybrid bearing design and its close physical replica (prototype) was carried out with the help of CAD (Solid works) for Modelling and Ansys for Structural Analyses of the main frame housing. This section also includes the justification of selection of various components of the novel concept.

6.1.1.5 Prototype Design and development (for replication): A prototype will be designed and tested with the help of experimental modal analysis to obtain the desired parameters for the validation of the novel Hybrid bearing concept.

Delivered Solution: A prototype that can replicate the physics of the Novel hybrid bearing solution has been Design and Manufactured with all the plans of Experimental Analysis carried out for further research and development. This experiment is to be carried out if the desired outcome is validated, such a new technological advancement has a potential for a Patent.

In conclusion, the primary end result of the research is a Novel hybrid bearing Concept which is a crucial part of the feed drive system. The approach as well as the Design Concept has the following Advantages and Disadvantages.

Advantages:

The following problems are solved by choosing this Design.

Machining mode:

The Linear Bearings Modules and the Air bearings operate together to perform machining operations; this combination takes the advantage of High stiffness of Linear recirculating bearings (The Bearings allows for a stiff operation at high machining forces) whilst using damping from air bearings (with the help of squeeze film damping effect) to enhance the machining performance in order to achieve precise and accurately machined parts.

CMM (Coordinate measuring machine) Mode:

There is no need of Linear recirculating roller bearings in measurement mode as it doesn't demand a highly stiff structure (no machining forces are present), In addition to that linear roller bearings are major source of errors in precision measurement therefore the linear bearing modules are disconnected from the guide. This is done by releasing the force in the piezo electric actuators and then using the lead screw to detach and move the linear bearing modules away from the guideway grooves (see fig). In this way the machine runs on Air bearings stage only, enabling rapid, frictionless and vibration free motion ideal for measurements up to a nanometre accuracy level. (See Details) .

The following problems are solved by choosing this Approach.

Although the problem to arrive at the Novel feed drive system for ultra-low vibrations can vary from designing the Control system to Developing an existing drive train (e.g. Ball screws) or Coming up with new Drive train Idea or Developing Guideways. Even developing Workbench's can be a solution.

Focusing on Bearing Design has 2 reasons:

1. Bearing as well as the drive are the prime contributors and share almost equal contribution in inducing vibration.
2. Being a Mechanical Engineer enhancing the control system was not an efficient path to go through while as developing the remaining other areas the problem would have the same relative effect as that of focusing on the bearing or drive.

Disadvantages

The major Disadvantages of this Design and the Approach of solving the problem are:

- This is entirely new Concept with no work being done before, therefore it will take much longer for the Product to be fully developed and ready to be used on the Commercial scale.
- This Design needs a considerable amount of focus on its thermal shielding, as CNC Machining Centres Embedd higher temperatures as compared to CMM, due to which the air film can have a significant effect.
- The Novel hybrid bearing system also demands shielding from chips, coolants and other debris, even a small amount can lead to an Air Bearing failure.
- The size of the bearing will be larger than a regular linear bearing primarily due to the size of the air bearing required to cause a lift and withhold high machining forces.
- In terms of the approach, the Control system Design rather than the bearing system design may yield better results but this wasn't carried out due to lack of expertise and timescale.

Although the New hybrid bearing design promises a solid solution to the problem under consideration the success of the project is limited to the design phase only. In order to actually quantify the effect this new design more experiments need to be carried out on the prototype which is lacking in the project to confirm its validity. The prototype experiment was not carried out due to time constraints of the MSc therefore it will be referred for future work.

Besides this all other aims and objectives were met and can be evaluated in the next section.

6.2 FUTURE DIRECTION.

More areas need to be researched and developed in order to make the full use of the novel concept developed in this thesis, Moreover, this novel concept is only a component of the entire feed drive system that needs further exploration. Some of the future recommendations for the success of this project are as follows:

6.2.1 Experimental Vibrational analysis of the Prototype Design:

In order to determine the effectiveness of the Air bearings a highly accurate probe used on CNC versus the use of same probe on linear circulating bearings This Rig will be used for determination of the effects of scanning probe errors present in the CNC machining Centre, one of the sources of these errors are linear recirculating bearings therefore this prototype will allow to use a monorail with only linear bearing stage to quantify the effect of Vibration coming from the Linear roller bearing truck on the scanning probe parameters on Zeiss CMM with the advanced probe similar to CNC probe.

This will prove the requirement of the Air bearings during measurement operation rather than the conventional high accuracy probes operating on CNC feed drive that have Linear recirculating bearings. In short, this prototype can solve two Objectives stated as follows.

- Quantify the effect of hybrid bearing Stage on machining performance.
- Quantify the effect of using an Air bearing stage on CMM in terms of measurement accuracy compared to measuring with the same probe on conventional feed drive on CNC.

6.2.2 Errors due to roller bearings in measurement.

- Straightness without Air bearing mode, only linear roller bearing mode on.
- Straightness with air bearing and roller bearing mode on.
- Straightness without prototype.

6.2.3 Active vibration Suppression

As proven in this thesis Piezo actuators are not a viable option for a fine actuator or active vibration suppression new actuators need to be explored to achieve this goal.

6.2.4 ERF fluids.

Since damping of the air film is the primary cause of resolution of the novel concept, methods to enhance the squeeze film damping will be researched, for example the use of electrorheological fluids.

6.2.5 Reduce the bearing size:

The size of the entire Novel hybrid bearing is almost 3 times as big as the standard linear roller bearings, this is primarily due to air bearings as they pose the restriction on the air bearing housing, new design concepts to reduce the size must be undertaken.

6.2.6 Anti-debris guide:

In order to achieve better operational excellence on shop floor, methods to ward off metal chips and other debris from air bearing guide must be made available.

6.2.7 Novel feed drive elements:

This hybrid bearing is only a part of the feed drive; other components can also be enhanced to achieve the overall efficiency in the drive system.

6.2.8 Control Design:

Lastly, the algorithms and the architecture of the Control system design for Novel Hybrid bearing concept in a closed loop feedback is essential and will be investigated further.

6.2.9 Thermal Insulation Design

As discussed earlier the temperatures in the CNC are higher as Compared to CMM , in order to use the Air bearing efficiently a Thermal Insulation is must and can be achieved with the help of incorporating thermal cladding on main frame of the bearing and between the roller bearing and frame contact to avoid any further heat transfer to the air bearings.

The protrusions in the hybrid guideway can alter the flying gap of Air bearing and hence result in failure These protrusions are caused due to thermal expansion so it must also be considered and evaluated because of its applications in CNC. Usually Materials such as chromed steel., granite, stainless steel, hard-coated aluminium and ceramics, glass are recommended by the air bearing guide but its only for a small temperature rise range.

6.2.10 DFMA Considerations

In parallel with the detailed design process a detailed DFMA evaluation is must to ensure the parts can be produced commercially with ease and in cost effective ways. Although the initial manufacturing considerations in light of DFMA have been evaluated a lot of work needs to be done in terms of deciding whether the actuator housing will be used in the final design or should there be any type of shock absorber to be incorporated to further dampen the vibration in the vertical direction. This decision will have a significant impact on the entire assembly and the relative processes.

CHAPETR 7: REFERENCES AND BIBLIOGRAPHY

1. Sliding bearing with adjustable friction properties by Engel, T; Lechler, A; Verl, A CIRP Annals - Manufacturing Technology, 2016, Volume 65, Issue 1 Journal Article.
2. A rotary flexural bearing for micromanufacturing by Luo, H.P; Zhang, B; Zhou, Z.X CIRP Annals - Manufacturing Technology, 2008, Volume 57, Issue 1 Journal Article.
3. Rotary-axial spindles for ultra-precision machining by Lu, X.-D; Paone, M.P; Usman, I; CIRP Annals - Manufacturing Technology, 2009, Volume 58, Issue 1 Journal Article
4. Magnetic Bearing Stage for Photolithography by M.E.Williams;D.L.Trumper;R.Hocken; CIRP Annals - Manufacturing Technology, 1993, Volume 42, Issue 1 Journal Article
5. Machine Tool with Active Magnetic Guides by Denkena, B; Kallage, F; Ruskowski, M; CIRP Annals - Manufacturing Technology, 2004, Volume 53, Issue 1 Journal Article
6. Superconducting EMS feed drive system of NC machine tool by Jiang, Wenxue; Zhou, Kai; Lv, Jiangwei; The International Journal of Advanced Manufacturing Technology, 09/2014, Volume 74, Issue 5 Journal Article: Full Text Online
7. Dynamic characteristics of a direct-drive air-bearing slide system with squeeze film damping by Wardle, Frank P; Bond, C; Wilson, C; International Journal of Advanced Manufacturing Technology, 04/2010, Volume 47, Issue 9-12 Journal Article
8. Numerical and Experimental Analysis for the Small Vibration of Aerostatic Guideways by Aoyama, T; Kakinuma, Y; Kobayashi, Y CIRP Annals - Manufacturing Technology, 2006, Volume 55, Issue 1 Journal Article:

9. Cage Speed of Hydrodynamic Rolling Hybrid Bearings by Lu, Dun; Zhao, Wanhua; Lu, Bingheng; More... Tribology Letters, 09/2013, Volume 51, Issue 3 Journal Article.
10. Investigations on a permanent magnetic-hydrodynamic hybrid journal bearing by Tan, Qingchang; Li, Wei; Liu, Bo Tribology International, 2002, Volume 35, Issue 7 Journal Article
11. Santora, M. (2020). How to lower driving force and friction with hybrid linear bearings | Bearing Tips. Retrieved 10 January 2020, from <https://www.bearingtips.com/lower-driving-force-friction-hybrid-linear->
12. The 2:1 Rule and How to Define Fixed and Floating Bearings. (2020). Retrieved 10 January 2020, from <https://www.igus.com/info/linear-guides-the-2-1-rule-ca>
13. High precision linear slide. Part I: design and construction by Mekid, Samir International Journal of Machine Tools and Manufacture, 2000, Volume 40, Issue 7 Journal Article: Full Text Online
14. A Twist-Roller Friction Drive for Nanometer Positioning – Simplified Design Using Ball Be... by Mizumoto, H; Arii, S; Yoshimoto, A; More... CIRP Annals - Manufacturing Technology, 1996, Volume 45, Issue 1 Journal Article: Full Text Online
15. Nanometer Positioning of a Linear Motor-Driven Ultraprecision Aerostatic Table System with Electrorheological Fluid Dampers by Shinno, Hidenori; Hashizume, Hitoshi; Sato, Hisayoshi CIRP Annals - Manufacturing Technology, 1999, Volume 48, Issue 1 Journal Article.
16. Ultraprecision Feed System Based on Walking Drive by Moriwaki, Toshimichi; Shamoto, Eiji CIRP Annals - Manufacturing Technology, 1996, Volume 45, Issue 1 Journal Article:
17. Rigid XY θ Table for Ultraprecision Machine Tool Driven by Means of Walking Drive by Shamoto, Eiji; Moriwaki, Toshimichi CIRP Annals - Manufacturing Technology, 1997, Volume 46, Issue 1 Journal Article:

18. Electrohydraulic Active Damping System by Brecher, C; Schulz, A; Week, M CIRP Annals - Manufacturing Technology, 2005, Volume 54, Issue 1 Journal Article:
19. High Speed Nanometer Positioning Using a Hybrid Linear Motor by Shinno, H; Hashizume, H CIRP Annals - Manufacturing Technology, 2001, Volume 50, Issue 1 Journal Article: Full Text Online
20. Development of a 5-Axis Control Ultraprecision Milling Machine for Micromachining Based on Non-Friction Servomechanisms by Takeuchi, Y; Sakaida, Y; Sawada, K; More... CIRP Annals - Manufacturing Technology, 2000, Volume 49, Issue 1 Journal Article: Full Text Online
21. Adaptive preloading for rack-and-pinion drive systems by Verl, A; Engelberth, T CIRP Annals - Manufacturing Technology, 2018, Volume 67, Issue 1 Journal Article:
22. Kinematics, Frictional Characteristics and Wear Reduction by PVD Coating on Ball Screw Drives by Spath, D; Rosum, J; Haberkern, A; More... CIRP Annals - Manufacturing Technology, 1995, Volume 44, Issue 1 Journal Article:
23. A Study on the Drive at Center of Gravity (DCG) Feed Principle and Its Application for Development of High-Performance Machine Tool Systems by Hiramoto, K; Hansel, A; Ding, S; More... CIRP Annals - Manufacturing Technology, 2005, Volume 54, Issue 1 Journal Article:
24. Cost-efficient approach for impulse decoupled linear direct drives by Drossel, Welf-Guntram; Junker, Tom; Schmidt, Stefan; More... Production Engineering, 06/2016, Volume 10, Issue 3 Journal Article:
25. Energy optimized jerk-decoupling technology for translatory feed axes by Denkena, B; Hesse, P; Gümmer, O CIRP Annals - Manufacturing Technology, 2009, Volume 58, Issue 1 Journal Article: Full Text Online
26. Magnetically levitated six degree of freedom rotary table by Lu, Xiaodong; Dyck, Mark; Altintas, Yusuf CIRP Annals - Manufacturing Technology, 2015, Volume 64, Issue 1 Journal Article:

27. Control of a dual stage magneto strictive actuator and linear motor feed drive system by Tong, D; Tong, D; Veldhuis, S C; More... The International Journal of Advanced Manufacturing Technology, 06/2007, Volume 33, Issue 3 Journal Article:

28. Nexen Product Navigation. (2020). Retrieved 14 January 2020, from <https://www.nexengroup.com/nxn/products/prod-nav/lp/Roller+Pinion+System>

29. Magnetic bearings – Mc Nally Institute. (2020). Retrieved 16 January 2020, from <http://www.mcnallyinstitute.com/18-html/18-6.html>

30. Disadvantages of Magnetic Bearings. (2020). Retrieved 16 January 2020, from <http://todaywikimechanical.blogspot.com/2015/03/disadvantages-of-magnetic-bearings.html>(2020). Retrieved 17 January 2020, from <http://www.cinmac.com/VerticalMachCntrs/SMARTtVMCweb.pdf>

31. Cutting forces in the end milling of Inconel 718 by Alauddin, M; Mazid, M.A; El Baradi, M.A; More... Journal of Materials Processing Technology, 05/1998, Volume 300, Issue 3-4 Journal Article:

32. Conversation, C., Conversation, C., & profile, V. (2020). Take the Load Off Your Turning Tools. Retrieved 17 January 2020, from <http://cuttingedgeconversation.blogspot.com/2016/01/take-load-off-your-turning-tools.html>

33. Operation Safety and Performance of Milling Cutters with Shank Style Holders of Tool Inserts by Beňo, J; Maňková, I; Vrábek, M; More... Procedia Engineering, 2012, Volume 48 Journal Article:

34. Altin, A. (January 01, 2014). The effect of the cutting speed on the cutting forces and surface finish when milling chromium 210 Cr12 steel hardfacings with uncoated cutting tools =: Vpliv hitrosti rezanja na sile rezanja in kvaliteto površine pri rezkanju kromovih navarov 210 Cr12 z rezilnim orodjem brez prevleke. Materiali in Tehnologije, 48.)

35. Thk (2020). Retrieved 17 January 2020, from https://www.thk.com/sites/default/files/thkcom/eng/products/SNR_SNS_en.pdf

36. Collins, D. (2020). How to choose linear guide preload. Retrieved 17 January 2020, from <https://www.linearmotiontips.com/how-to-choose-linear-guide-preload/>

37. Construction and validation of a theoretical model of the stiffness matrix of a linear ball guide with consideration of carriage flexibility by Tong, Van-Canh; Khim, Gyungho; Hong, Seong-Wook; More... Mechanism and Machine Theory, 10/2019, Volume 140 Journal Article

38. McMaster-Carr.(2020).Retrieved 17 January 2020, from <https://www.mcmaster.com/99030a966>

39. McMaster-Carr. (2020). Retrieved 17 January 2020, from <https://www.mcmaster.com/95072a883>

40. Optmized, T. (2020). BN1010 - Lead Nut Only, BN, 1.0 in X 0.100 in, Non-Preloaded, RH, 1900 lbf Design Load. | Thomson. Retrieved 17 January 2020, from <https://www.thomsonlinear.com/en/product/BN1010>

41. Sun, Wei & Kong, Xiangxi & Wang, Bo & Li, Xingzhan. (2014). Statics modeling and analysis of linear rolling guideway considering rolling balls contact. Proceedings of the Institution of Mechanical Engineers, Part C: Journal of Mechanical Engineering Science. 229. 168-179. 10.1177/0954406214531943

42. PL55-2-6B - PL - LOCKED PL - Clamping Elements - Safety Products - Products - ACE Controls Inc. (2018). Retrieved from <https://www.acecontrols.com/us/products/safety-products/clamping-elements/locked-pl/pl/pl55-2-6b.html>

43. Air Bearings Application. (2018). Retrieved from <http://www.mager-ab.it/en/products/linear-systems/flat-air-bearings/air-bearing-application>

44. Collins, D. (2018). What are recirculating linear bearings? Retrieved from <https://www.linearmotiontips.com/faq-what-are-recirculating-linear-bearings/>

45. Hydrostatic linear guiding for standard design spaces. (2018). Retrieved from <https://www.machinedesign.com/linear-motion/hydrostatic-linear-guiding-standard-design-spaces>
46. Altintas, Yusuf & Verl, Alexander & Brecher, C & Uriarte, L & Pritschow, Guenter. (2011). Machine tool feed drives. *Cirp Annals-manufacturing Technology - CIRP ANN-MANUF TECHNOL.* 60. 779-796. 10.1016/j.cirp.2011.05.010.
47. Linear ball bearing and guideway assemblies. (2018). Retrieved from https://www.schaeffler.co.uk/content.schaeffler.co.uk/en/products-and-solutions/industrial/productportfolio/linear_guidance_systems/ball_mono_rail_guidance_systems/index.jsp
48. Advances in Mechanical Design. (2018). Retrieved from https://books.google.co.uk/books?id=kq4-DwAAQBAJ&pg=PA870&lpg=PA870&dq=anti+vibration+feed+drives&source=bl&ots=g1R_BkWwyc&s
49. Verl, S. Frey, (2012) Improvement of feed drive dynamics by means of semi-active damping, *CIRP Annals*, Volume 61, Issue 1, 2012, Pages 351-354, ISSN 0007-8506, <https://doi.org/10.1016/j.cirp.2012.03.135>. (<http://www.sciencedirect.com/science/article/pii/S0007850612001370>)
50. Chinedum Okwudire, Jason Rodgers, (2013) Design and control of a novel hybrid feed drive for high performance and energy efficient machining, *CIRP Annals*, Volume 62, Issue 1, 2013, Pages 391-394, ISSN 0007-8506, <https://doi.org/10.1016/j.cirp.2013.03.139>.
51. Hsieh, M. , Yao, W. and Hsu, C. (2012), Modeling and control of a feed drive with multiple mechanically coupled ball screws. *Asian Journal of Control*, 14: 1227-1238. doi:10.1002/asjc.400
52. Nexen Product Navigation. (2018). Retrieved from <https://www.nexengroup.com/nxn/products/prod-nav/lp/Roller+Pinion+System>

53. A.T. Elfizy, G.M. Bone, M.A. Elbestawi,(2005) Design and control of a dual-stage feed drive,International Journal of Machine Tools and Manufacture, Volume 45, Issue 2,2005,Pages 153-165,ISSN 0890-6955,<https://doi.org/10.1016/j.ijmachtools.2004.07.008>

54. Hendra Syahputra, Hyeon Yang, Byeong Chung, Tae Ko. Dual-Stage Feed Drive for Precision Positioning on Milling Machine. Svetan Ratchev. 6th International Precision Assembly Seminar (IPAS), Feb 2012, Chamonix, France. Springer, IFIP Advances in Information and Communication Technology, AICT-371, pp.81-88, 2012, Precision Assembly Technologies and Systems.

55. The History of the Coordinate Measuring Machine. (2018). Retrieved from <https://www.cmm-solutions.co.uk/contact-us/cmm-history/>

56. CNC.com. (2018). Retrieved from <http://www.cnc.com/the-history-of-computer-numerical-control-cn>

57. Accuracy in aerospace – Aerospace Manufacturing Magazine. (2018). Retrieved from <https://www.aero-mag.com/accuracy-in-aerospace/>

58. What is Metrology & Why is it Important in Manufacturing? (2018). Retrieved from <https://www.ptc.edu/news/what-metrology-why-it-important-in-manufacturing>

59. Friction guides made easy with Accuride’s engineering excellence - Automation. (2018). Retrieved from <https://www.connectingindustry.com/automation/friction-guides-made-easy-with-accurides-engineering-excellence.aspx>

60. High accuracy CMM - High accuracy 3D CMM - 3D COORDINATE MEASURING MACHINE|CMM SOFTWARE|XI'AN HIGH-TECH AEH INDUSTRIAL METROLOGY CO.,LTD. (2018). Retrieved from http://www.china-ah.com/en/html/2013/chaogaojd_0411/3.html

61. Delivery Time Crucial to Success to End User. (2018). Retrieved from <https://www.machinedesign.com/linear-motion/delivery-time-crucial-success-end-user>

62. LTD, M. (2020). SAE 660 Bronze - technical information. Retrieved 17 January 2020, from <https://www.metals4u.co.uk/sae-660-bronze.asp>

63. Development of an active clamping system for noise and vibration reduction by Hesselbach, J; Hoffmeister, H.-W; Schuller, B.-C; More... CIRP Annals - Manufacturing Technology, 2010, Volume 59, Issue 1 Journal Article:
64. VIBRATION OF LINEAR GUIDEWAY TYPE RECIRCULATING LINEAR BALL BEARINGS by OHTA, HIROYUKI; HAYASHI, EIJI Journal of Sound and Vibration, 08/2000, Volume 235, Issue 5 Journal Article
65. Calculate Required Tube Size Using Structural Properties | Allied Tube & Conduit | Mechanical Tube Division. (2020). Retrieved 17 January 2020, from <http://www.atc-mechanical.com/calculators/tube-size-using-structural-properties/>
66. (2020). Retrieved 17 January 2020, from <http://www.ibspe.com/public/uploads/content/files/Air-Bearing-Application-Design-Guide.pdf>
67. INA (2020). Retrieved 17 January 2020, from https://www.ahrinternational.com/PDF_catalogues/INA/LinearMonorailguidancesystems.pdf
68. Amazon (2020). Retrieved 17 January 2020, from <https://www.amazon.com/Uxcell-a12022700ux0184-32-8Ft-Pneumatic-Polyurethane/dp/B008MO66FO>
69.). Retrieved 17 January 2020, from https://en.wikipedia.org/wiki/Eigenvalues_and_eigenvectors#Vibration_analysis
70. Forced Oscillations and Resonance - College Physics. (2020). Retrieved 17 January 2020, from <https://opentextbc.ca/physicstestbook2/chapter/forced-oscillations-and-resonance>
71. Hanly, S. (2020). Vibration Analysis: FFT, PSD, and Spectrogram Basics [Free Download]. Retrieved 17 January 2020, from <https://blog.endaq.com/vibration-analysis-fft-psd-and-spectrogram>

72. en, H., & FFT, F. (2020). FFT. Retrieved 17 January 2020, from <https://www.nti-audio.com/en/support/know-how/fast-fourier-transform-fft>
73. Siemens PLM. (2020). Retrieved 17 January 2020, from <https://community.sw.siemens.com/s/article/digital-signal-processing-sampling-rates-bandwidth-spectral-lines-and-more>
74. Nasa (2020). Retrieved 17 January 2020, from <https://ntrs.nasa.gov/archive/nasa/casi.ntrs.nasa.gov/20170005173.pdf>
75. Damped free vibrations - All this. (2020). Retrieved 17 January 2020, from <https://leancrew.com/all-this/2014/04/damped-free-vibrations/>
76. Data acquisition and mathematical modelling: a case study September 2008 DOI: 10.13140/2.1.3838.6243 TIME2014At: Buffelspoort, South Africa Acm Bekker ,Stephan Victor Joubert Stephan Victor Joubert, Temple H. Fay
77. Porous Ceramic Water Hydrostatic Bearings for Improved for Accuracy Performance by Corbett, J; Almond, R.J; Stephenson, D.J; More... CIRP Annals - Manufacturing Technology, 1998, Volume 47, Issue 1 Journal Article
78. Porosity and the mechanical properties of aluminium welds. (2020). Retrieved 18 January 2020, from <https://www.twi-global.com/technical-knowledge/faqs/faq-what-is-the-influence-of-porosity-on-the-mechanical-properties-of-aluminium-welds>
79. Non-Contact Hydrostatic Fluid Bearings - ULS Innovation. (2020). Retrieved 18 January 2020, from <https://www.ulsinc.com/discover-uls-innovations/non-contact-hydrostatic-fluid-bearings>
80. The Engineering Design Process. (2020). Retrieved 18 January 2020, from <https://www.sciencebuddies.org/science-fair-projects/engineering-design-process/engineering-design-process-steps>

81. Li, Y., Su, D., Cai, X., Wu, W., Zhang, J., & Zhao, W. (2020). Temperature simulation and thermal equilibrium analysis of the ball screw feed drive system under various working conditions. *Proceedings of the Institution of Mechanical Engineers. Part C, Journal of Mechanical Engineering Science*, 234(24), 4844-4856. doi:10.1177/0954406220929051

82. Collins, D. (2020). What makes a linear guide suitable for high temperature use? Retrieved 12 December 2020, from <https://www.linearmotiontips.com/what-makes-linear-guide-suitable-for-high-temperature-use/>

83. Jang, S., Jang, S., Khim, G., Khim, G., Park, C., & Park, C. (2017). Estimation of friction heat in a linear motion bearing using Box-Behnken design. *International Journal of Advanced Manufacturing Technology*, 89(5), 2021-2029. doi:10.1007/s00170-016-9165-4

84. Hua, W., Zhou, W., Liu, B., Yu, S., & Wong, C. H. (2009). Effect of environment humidity and temperature on stationary and transient flying responses of air bearing slider. *Tribology International*, 42(8), 1125-1131. doi:10.1016/j.triboint.2008.09.010

85. Managing thermal loads in milling processes | Secotools.com. (2020). Retrieved 12 December 2020, from <https://www.secotools.com/article/21483?language=en>

CHAPTER 7: APPENDECIES

APPENDEX A

This Section contains the major Supporting Information, the Simulated and Experimental Modal Analysis Chapter including its Theory. It also contains some supporting Calculations.

RACK-AND-PINION VERSUS BALL SCREWS

- Compared to Rack and Pinion ball screws stiffness is lower and less constant. Rack and pinion can accelerate more than ball screws; Balls screws do not maintain the same speed as well.
- Ball screws are less efficient and have lower natural frequency than rack and pinion. Balls screws have higher mass moment of inertia compared to rack and pinion sets.
- Rack and pinion have less cumulative errors over total travel length, A two paired rack and pinion system has a cumulative error of 12 to 40 μm over four meters while as for a rolled screw drive there is a cumulative error of 300 μm to 1700 μm . In addition, there is a deviation between 30 μm to 110 μm in ground threaded ball screw drives.
- The efficiency of rack and pinion sets is 97 % compared to the preloaded ball screw efficiency that is 90%. Due to high mass moment of inertia during long travel lengths their critical speed is limited as well as their axial load capacity. Such long-stroke applications benefit from a switch to rack-and-pinion sets — with efficiency to 97%.
- There is a difficulty in achieving a stable system behaviour under dynamics due to the influence on rigidity by the bearings, housing bored and nut housing. Deviation of spindle stiffness depending on nut position over the spindle length compounds this problem.
- Only some balls circulate through the nut due to greasing demands and because of this reason are not suitable for short stroke applications. Balls screws also allow one carrier per linear axis. (Delivery Time Crucial to Success to End User. (2018).

•
This Concludes that rack and pinion is more efficient than ball screw drives especially in application where travel length of axis is above 4 foot and cost is of the major concern.

PROCEDURE TO SET UP AIR BEARINGS :

- Attach the top bearing close to the surface until it touches it.
- Keep the dial indicator at the back of bearing and set it to zero.
- Adjust the stud until the indicator reads 4 microns
- Do same for all sides.
- Turn the pressure on increase it slightly until 60 psi and check how much the dial indicator reads or varies, if it doesn't vary then compliance in bearings is 0, if it varies then compliance in air bearing is equal to the variance.
- If it above 4 microns due to compliance adjust the stud accordingly while the pressure is turned off.

Piezo Actuator Design Calculations:

PICA actuators are explored here,

Some physical behaviour and requires of Pica actuators are discussed as follows;

Operating voltage: 60 V for PICMA up to 1000 V for PICA actuators, the models are based on various layer thicknesses.

Electrical behaviour: The piezo behaves like a capacitor if they operate at frequencies that are lower than their natural frequency. The stored electrical charge varies with the first order estimate of actuator displacement. The thickness of the ceramic and the area determine the capacitance of the actuator. In stack actuators the layers of capacitance ceramics are connected in parallel. The More layer thicknesses the lesser capacitance.

Power Consumption: More the actuator capacitance and the frequency more the power consumption of the actuator (linear variation). Power consumption also depends on the load linearly at same freq and same displacement.

Blocking Force: The blocking force is generated by the piezo material to block an external force when external force compresses it to another value of free displacement from the initial value

In order to determine the max displacement travel of the piezo the displacement peak in machining operation or the Linear bearing operation or both need to be taken into consideration depending on the mode of vibration suppression we want to achieve.

In addition, the stiffness of the piezo has to be taken into consideration, the maximum blocking force resulting due to clamping should displace the piezo less to allow for more micro meter compensation for table or linear bearing displacement.

Heat generation: Maximum desired heat generation is 0.1 W/cm³ for Pica.

The charge and discharge currents in piezo increase with the operating frequency

The loss factor Tan alpha is of the order 0.01 to 0.02 meaning the heat generated out of electrical power flowing through actuator is 2% of electrical power for small signal conditions (1V, 1000Hz, 20 degrees Celsius, unloaded) meaning an unloaded piezo actuator. In case of large signal condition this can increase 30%.

Use 70 % of the small signal capacitance values added to the large signal conditions as a safety factor.

High frequency and High voltage demand cooling applications. More heat is generated with more voltage

Piezo Calculations:

$$f_0'(Hz) = f_0(Hz) \cdot \sqrt{\frac{m_{eff}(kg)}{m_{eff}'(kg)}}$$

f_0' = Resonant frequency of the system

f_0 = Resonant frequency of the actuator

m_{eff} = Effective mass of the actuator

m_{eff}' = effective mass of the system

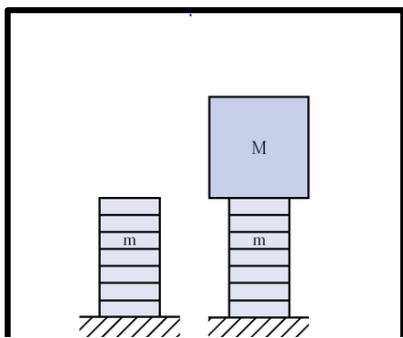


Figure 1 A Calculation of the effective mass of the unilaterally clamped piezo stack actuator with and without load

The piezo will operate below its loaded natural frequency effectively but at higher frequencies (still lower than loaded natural frequency) it has to compensate heat generation.

The frequency of the System that the actuator can control is again reduced due to the following factors.

Since the piezo is unilaterally clamped to the ball screw new value of frequency is half of the system frequency, See *Figure 1 A above*.

$$f_{uc} = \frac{f_0'(Hz)}{2} = \text{unilateral clamping frequency}$$

Control systems further reduce it down in the following manner,

$$f_{cl} = \frac{2}{3} f_{uc}(Hz) \text{ open loop}$$

$$f_{op} = \frac{1}{10} f_{uc}(Hz) \text{ the closed loop}$$

Dynamic forces should be lesser than the blocking way too less for a good operation. And they are calculated with the help of following equation.

$$F_{dyn}(N) = \pm 4\pi^2 \cdot m_{eff}(kg) \cdot \frac{\Delta L(m)}{2} \cdot f(Hz)^2$$

Corresponding active power P generated by the actuator is given as;

$$P(W) \approx \frac{\pi}{2} \cdot \tan\delta \cdot f(Hz) \cdot C(F) \cdot V(V)_{P-P}^2$$

Voltage of actuator ((V_{Opd})) is directly prop to force and displacement.

(V_{Opd}) can be calculated as;

$$\frac{D_{Req}}{\Delta L} \cdot V_{max} = V_{Opd}$$

D_{Req} = Displacement Required

ΔL = Max actuator displacement

V_{max} = Maximum actuator Voltage

Voltage required for Operating force ((V_{OpF})) can be calculated as;

$$\frac{F_{Req}}{F_{max}} \cdot V_{max} = V_{OpF}$$

V_{max} = Maximum actuator Voltage

F_{max} = Maximum Actuator Force

F_{Req} = Force Required

To get the total Voltage requirement, the two voltages are added;

$$V_{Op} = V_{Opd} + V_{OpF}$$

Note: The total voltage must not exceed the V_{max} if it exceeds the maximum operating voltage the system won't work.

Based on this the following calculations were carried out:

To damp the vibration coming from the linear guideway alone:

f_0 = Resonant frequency of the actuator = 59000 Hz

M= Mass of the system of the linear bearing module = 0.2 kg

M= Actuator mass (l×w×h , 1.7×1.6×1.6) (Cm)

m_{eff} = Effective mass of the actuator = $\frac{0.0339}{3} = 0.01132$ kg

m_{eff}' = effective mass of the system = $m_{eff} + M = 0.01132 + 0.2 = 0.21132$ kg

M= Mass of the system of the linear bearing module = 0.2 kg

$$f_0'(Hz) = f_0(Hz) \cdot \sqrt{\frac{m_{eff}(kg)}{m_{eff}'(kg)}} = 59000 \cdot \sqrt{\frac{0.01132}{0.21132}} = 13653 \text{ Hz}$$

f_0' = Resonant frequency of the system = 6826 hz

f_{uc} = unilateral clamping frequency = $\frac{f_0'(Hz)}{2} = \frac{13653}{2} = 6826$ Hz

$f_{op} = \frac{2}{3} f_{uc}(Hz) = \frac{2}{3} \times 6826(Hz)$ open loop = 4778 Hz

$$f_{cl} = \frac{1}{10} f_{uc} (\text{Hz}) \text{ the closed loop} = \frac{1}{10} \times 6826 = 683 \text{ Hz}$$

$$\begin{aligned} F_{dyn} (N) = \text{Dynamic forces} &= \pm 4\pi^2 \cdot m_{eff} (kg) \cdot \frac{\Delta L (m)}{2} \cdot f (\text{Hz})^2 \\ &= \pm 4\pi^2 \cdot 0.01132 \cdot \frac{15 \times 10^{-6}}{2} \cdot 600^2 = 22.52 \text{ N} \end{aligned}$$

Corresponding active power P generated by the actuator is given as:

$$P (W) \approx \frac{\pi}{2} \cdot \tan \delta \cdot f (\text{Hz}) \cdot C (F) \cdot V (V)_{P-P}^2 = \frac{\pi}{2} \cdot \tan(0.02) \cdot 1.8 \cdot 10^{-7} \cdot 666^2 = 0.0009 \text{ W}$$

$$P_d = \text{Power density} = \frac{P}{l \times w \times h} = \frac{0.0009}{1.7 \times 1.6 \times 1.6} = 0.00020172 \text{ w/cm}^3$$

Chapter A: Theory and Preliminary Study

In this Section, the theory behind Vibrations and Data acquisition has been clearly demonstrated, and the data preliminary to the design has been collected and analysed. Concept generation is also included here. This is Vital for the entire project into order to understand the behaviour of conventional rig to obtain benchmark tests of which theory is an integral part.

An experiment and computational Analysis of conventional test rig was carried out to collect the data for a reference as well as to Validate the finite element method that will later be employed to the Novel feed drive System.

A.1 BACKGROUND THEORY

Two Types of Analysis are carried out in Engineering one being the quasi static analysis and the other Dynamic Analysis. In Quasi-Static Analysis the load is applied at a very slow rate therefore acceleration can be neglected and is assumed to be zero in contrast Dynamic analyses cannot neglect the effect of acceleration. Modal Analysis comes under the category of Dynamic Analysis.

A.1.1 Modal Analysis:

The overview of the limits of the response of the system is given by Modal Analysis e.g. The determination of max displacement when a load of a certain frequency and amplitude is applied to a system. It is used to determine the natural frequencies or resonant frequencies of the system. At resonant frequency there is an asymptotical increase in the structure's amplitude of response to infinity thus the structure vibrates chaotically and is unstable. At such frequencies the transfer of energy happens with a minimum loss and is at its best.

In other words, the structure takes the frequency it likes, and its liking depends on the shape and constraints of the Mechanical Structure or a System.

When the driving frequency (of the driving force) matches the natural frequency, Resonance takes place and if the structure is less damped greatest response is observed.

The Mathematical equation used to extract modal frequencies is given by;

$$k \times x = y$$

The response of the system to the given input can therefore be written as:

$$[k][x] = \lambda [x]$$

Where $y = \text{input}$

$K = \text{Stiffness or } [k] = \text{stiffness matrix}$

$x = \text{eigenvector or } [x] = \text{eigenvector matrix}$

$\lambda = \text{eigenvalue or Eigen frequency}$

A.1.1.1 Eigenvectors:

The eigenvectors do not change direction when the stiffness matrix is raised to some power, they remain in constant direction however, the eigenvalue gets effected in magnitude for example if the stiffness matrix is squared the eigenvalue gets squared too.

$$[k]^2[x] = \lambda^2 [x]$$

It should be noted that all vectors are a combination of eigenvectors.

The eigenvalue is the natural frequency of the system also called eigenfrequency meaning "own frequency". Since it characterises the structures it is also called characteristic frequency as it is naturally embedded in it.

$$[k][x] = \omega^2 m[x]$$

$$\omega^2 m = \lambda$$

The Eigenvectors when transformed by stiffness matrix keep a constant direction (or has a constant line of action) Therefore, their magnitude may vary but direction is always constant. They can be written as

$$[k][x] = b$$

All the vectors when multiplied by K change direction except eigenvectors.

$$\lambda[x] = b$$

λ tells whether the special vector is shrunk or stretched or removed or left unchanged. When its multiplied by Stiffness Matrix. *See Figure 2A below.*

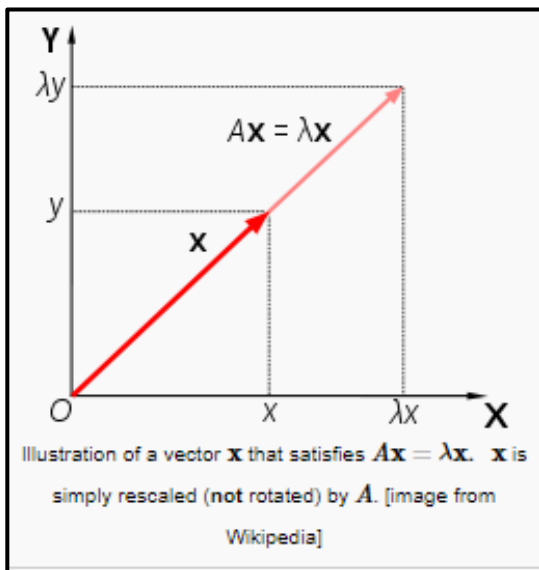


Figure 2A Eigenvector illustration, (Wikipedia (2020))

Different structures have different damping, the higher the peak at a certain natural frequency the less damped the system is. It can also be noted that the more damped structures have wide frequency range close to the natural frequency this means more frequencies must be avoided due to the nature of the high damped curve structure. See Figure 3A below.

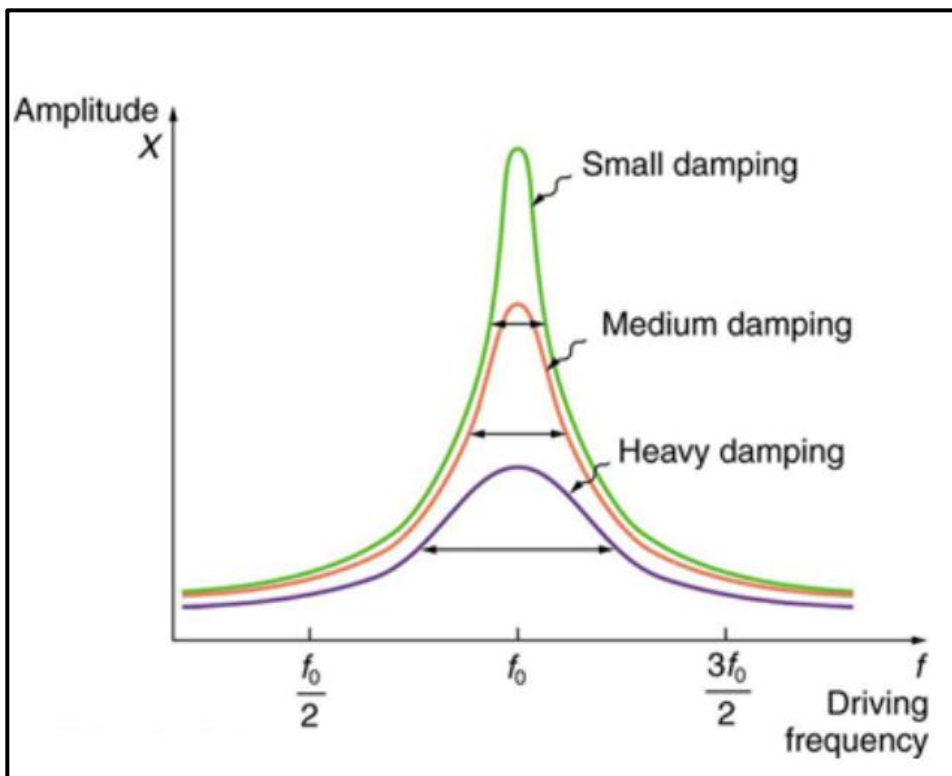


Figure 3A Driving frequency vs Amplitude (Forced Oscillations and Resonance – College Physics. (2020))

A.1.1.2 Fourier Transform:

Any wave form can be represented as a sum of sine waves with different frequencies, phases and amplitudes. A series that represents such wave forms is called Fourier series. This series helps to deconstruct the individual sine waves with their respective amplitudes and phases resulting in a frequency domain, frequency domain is more helpful as it helps to analyse vibrations in depth and with ease. DFT (Discrete Fourier Transform) multiplies the raw wave form with its discrete frequency sin waves for matching and knowing what their corresponding amplitudes and phases are. FFT is simply DFT but is faster than DFT. FFT requires a single length that are powers of 2. Such an algorithm is faster but for today's modern computers this effect is less significant. The sine waves are symmetrical such symmetry is used by FFT.

The mathematical Model of Fourier Series in continuous time form can be written as:

$$F\{x(t)\} = X(\xi) = \int_{-\infty}^{\infty} x(t)e^{-j2\pi\xi t} \delta t$$

The inverse of the above equation can be written as , $X(t) = \int_{-\infty}^{\infty} X(\xi)e^{j2\pi\xi t} \delta t$

$\xi = \text{Frequency}$

$X = \text{Amplitude of a frequency}$

The mathematical Model of Fourier Series in discrete time form can be written as:

$$F\{x(n)\} = X(m) = \sum_{n=0}^{N-1} x(n) e^{\frac{-j2\pi nm}{N}} \int_{-\infty}^{\infty} x(t)e^{-j2\pi\xi t} \delta t$$

N

= total number of points included in the equation, m is the input to the transformed function.

To increase the resolution of frequency (Δf) one must increase recording time to get more samples. Also, the frequency bin has an interval, to decrease this one must reduce the sample rate or increase the number of samples which is possible if we increase the total time refer to next section.

In DFT the number of samples in the original waveform have direct proportional relation with the discrete frequencies tested as a part of Fourier transform.

FFT is used to determine the cause of vibration in the signal by looking at various frequencies clearly in frequency domain. See Figure 4A ,Figure 5A below.

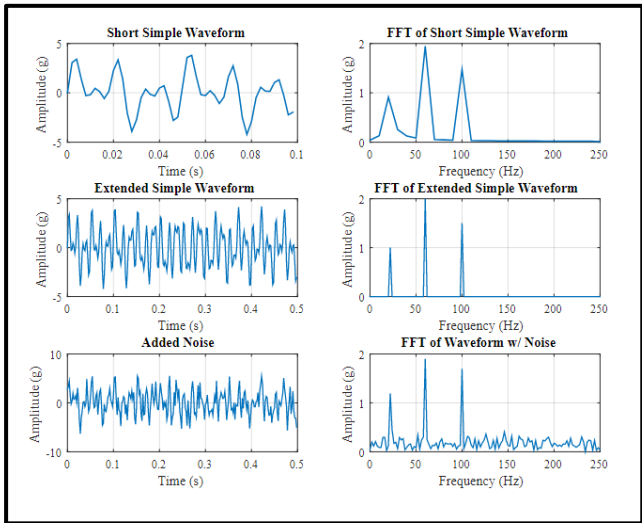


Figure 59 Amplitude time domain (left) , Amplitude frequency domain (right) Hanly, S. (2020).

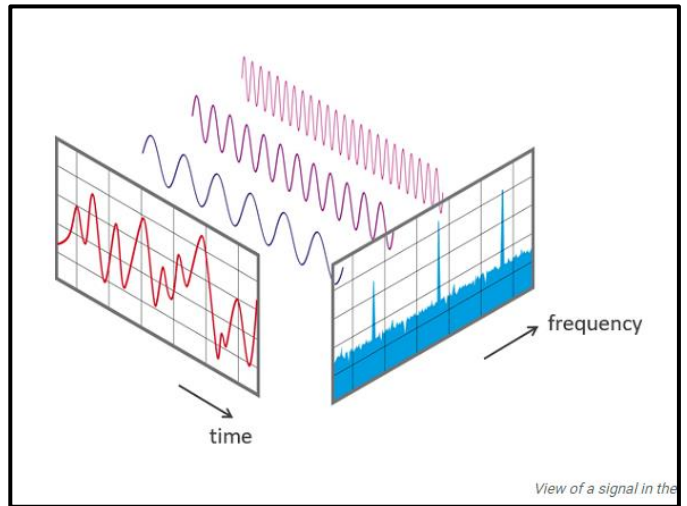


Figure 60 Shows FFT Visually (en, H., & FFT, F. (2020).)

A.1.2 Digital Signal Processing Theory:

Transducers output analogue signals which have a continuous time frame, the computers cannot take these continuous time frame signals therefore a digital data acquisition is carried out by breaking the continuous signal in discrete pieces or samples to store them.

Initially, a discrete-time domain data is recorded and later if FFT is required to perform frequency analysis unique terms are used for this digitalised data during undertaking FFT.

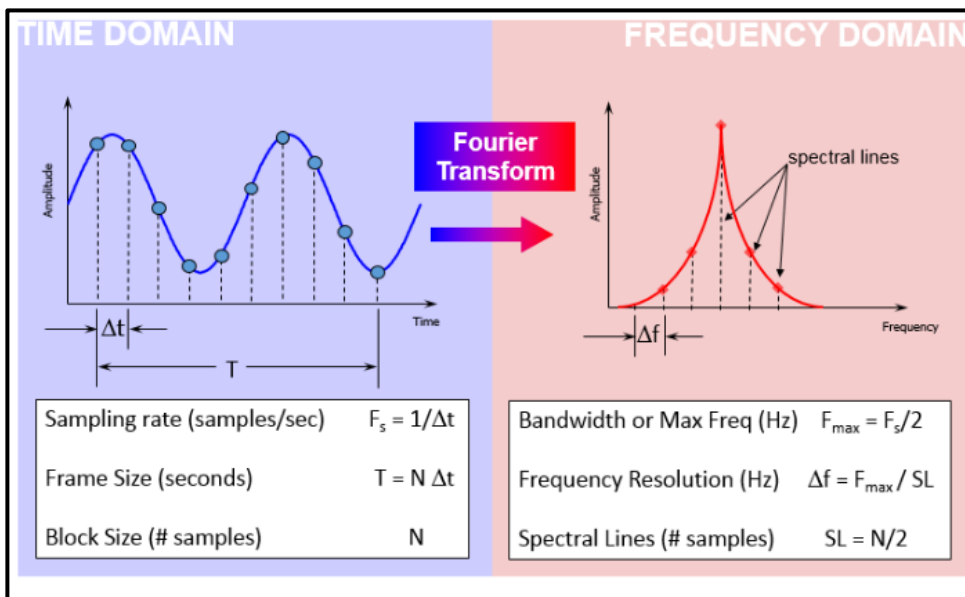


Figure 6A Frequency Domain and Time Domain terms used in performing Digital Fourier Transform

The quality of final analysis depends on understanding certain important terms which are defined as follows refer to *Figure 6A above*.

A.1.2.1 Time Domain Terms:

Sampling rate (F_s): The acquired number of samples or data samples per second.

Frame Size (T span): In order to perform FFT some time is taken to collect data from time domain this is called frame size or T span.

Block size (N): In order to obtain two points (Frequency and phase) that a spectral line in frequency domain contains, samples are collected from time domain number of these samples collected in one-time frame is block size.

A.1.2.2 Frequency Domain Terms:

Bandwidth (F_{max}): The highest frequency that is captured in FFT.

Spectral lines (SI): Lines containing number of frequency domain samples.

Frequency resolution (Δf): The spectral lines have spaces in between them in frequency domain these spaces are delta Δf or frequency resolution.

A.1.2.3 Digital Signal Processing Parametric Relations:

$$\text{Sampling rate, } F_s = \frac{1}{\Delta t}$$

$$\text{Block size relation : } T = \frac{N}{F_s} \text{ or } F_s = \frac{N}{T}$$

Example: With the block size containing 2000 data points at 1000 Hz sampling frequency, T (frame size) = 2 secs is required to obtain one data block.

Also $T = N \times \Delta t$

Bandwidth = $F_{max} = \frac{1}{2} F_s$ (because Nyquist sampling criterion requires $F_s = 2 F_{max}$).

Many times, when 80 % of the bandwidth is reached the signals preceding from that point have a reduced amplitude due to anti aliasing filter to avoid this and to get a usable frequency bandwidth F_{span} is used.

Span means the actual usable bandwidth which stops the analyses at 80% because above 80% amplitude of the signal is reduced. Therefore, using Fspan is desired as all the frequencies falling in this range will have the original amplitude. See Figure 7A below.

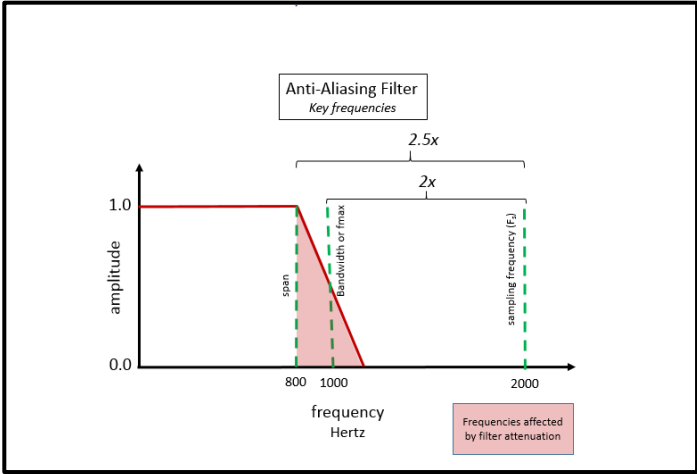


Figure 7A Shows the Anti Aliasing Filter Characteristics

Spectral Lines (SL), analogous to N have a relation: $Sl = N/2$,For 2000 N there are 1000 SL.

Frequency resolution relation: $\Delta f = \frac{Bandwidth}{Spectral\ lines}$

For example, in figure the bandwidth is 16 Hz and Spectral lines are 8 therefore, the spaces between spectral lines are given as $\Delta f = \frac{16}{8} = 2Hz$

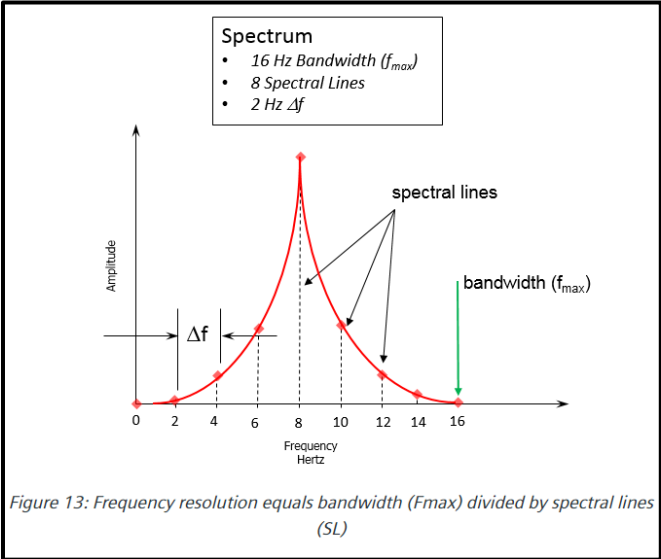


Figure 13: Frequency resolution equals bandwidth (Fmax) divided by spectral lines (SL)

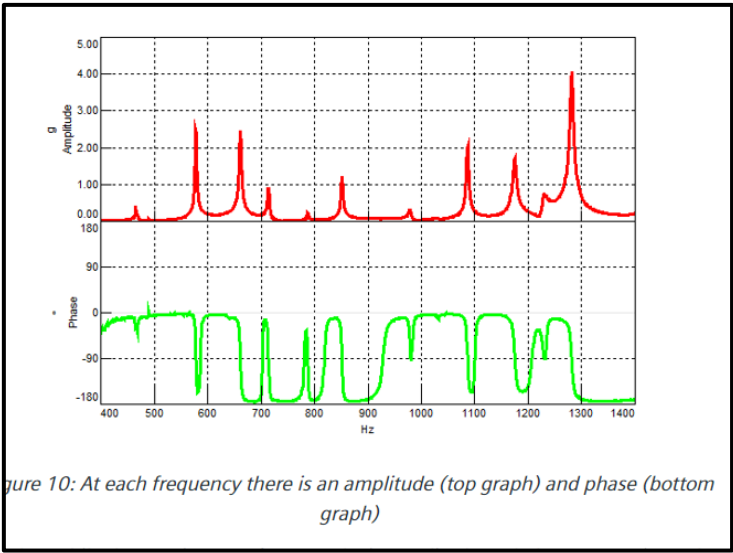


Figure 10: At each frequency there is an amplitude (top graph) and phase (bottom graph)

Figure 61A Shows Resolution frequency equates to bandwidth divided by spectral lines

Figure 9A shows Amplitude (top graph) phase (bottom) graph is present at each frequency

A constant amplitude DC offset happens when SI is at 0 and therefore it's not included. See Figure 8A and Figure 9A above.

$$\frac{1}{T} = \frac{\text{Bandwidth}}{\text{Spectral lines}} = \frac{\text{Sampling Frequency}}{\text{Blocksize}} = \Delta f$$

This gives a golden equation:

$$\frac{1}{T} = \Delta f$$

Recommendations for Experiment:

In time domain; $F_s = 10 \times F_{span}$

In frequency domain; $F_s = 2 \times F_{span}$ or $F_s = 2.5 * F_{max}$ (if anti aliasing filter is used and maximum frequency is taken as F_{max}). (Siemens PLM. (2020).

A.1.3 Methods of Extracting Damping:

A.1.3.1 Db Method:

The 3 Db Method is used to calculate damping at a resonance in FRF or transfer function

The width of the resonant peak is proportional to damping about the centre of the peak. The damping can be obtained by going 3db down the resonant peak. The lesser the width the lesser the damping.

An important parameter in damping extraction is the quality factor Q or the damping factor this can be then evaluated using the equation, $Q = \frac{f}{(f_2 - f_1)}$, where f_2 is the point 3 db down on right of resonant frequency and f_1 is frequency 3 db down on left of resonant peak. See Figure 10A below. (Siemens PLM. (2020)). (Nasa (2020)).

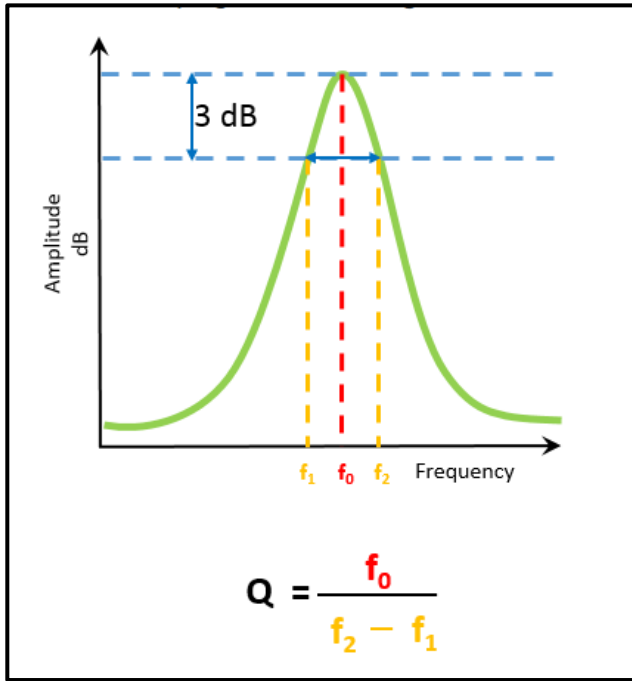


Figure 10 A Shows 3 Db Method , (Siemens PLM. (2020))

Lesser damping on a system means more time to stop moving or more settling time and vice versa. With no damping, a system moves forever as there is no mechanism of energy dissipation for that motion.

Quality factor form is mainly used to understand the differences very clearly because by using percentage critical damping the use of long number with a small decimal difference is neglected.

The quality factor decreases with more damping while as percentage critical damping and loss factor increases with damping. Both are the measures of damping and quantify it.

Using a 3b method can be problematic in case of less resolution as there are frequency spaces in between each value where there is no data, so we are forced to take the values that don't fall exactly 3b below this can give bad results.

One must not use windowing that exponentially multiplies the original signal to decay faster in order to avoid leakage effects to an accelerometer. this can give higher damping values than what is actual, thereby, 3 db can't be used as the width changes.

Mode Spacing: Where 2 resonant peaks are close together, the 3 db method is useless and modal curve fitter should be used. (Nasa (2020)).

A.1.3.2 Half Power Method:

Half power method is same as 3 db method but it can be used without dbs. for example, the maximum peak (with maximum power) times $\frac{1}{\sqrt{2}}$ gives the base line to select the two frequencies up and down the x axis at a half power level. The relationship to compute the quality factor ($Q = \frac{f}{(f_2-f_1)}$), is same but its only valid if the systems $\xi < 0.05$

$$\xi = \frac{(f_2-f_1)}{2f}$$

It should be noted this is only for Fourier transform and is only valid for low ξ values.

Its major drawback can be attributed to the fact that the maximum power exists at undamped vibrations therefore the peak value is an assumption and may not be the highest-powered peak. (See next section.) (Nasa (2020)).

A.1.3.3 Half quadratic Gain method:

Here the square of frequency response function is used directly in estimating damping equation rather than approximating the power curve like in the half power method, in half power method the values of upper and lower frequencies change as the zeta gets above 0.5. But in reality, the power curve upper and lower bond values of frequencies is always constant hence such an assumption can give wrong value of damping *Figure 11A* shows the deviation of half power frequency values as damping coefficient increases. Power curve is always constant. Also, see *Figure 12A* for upper and lower

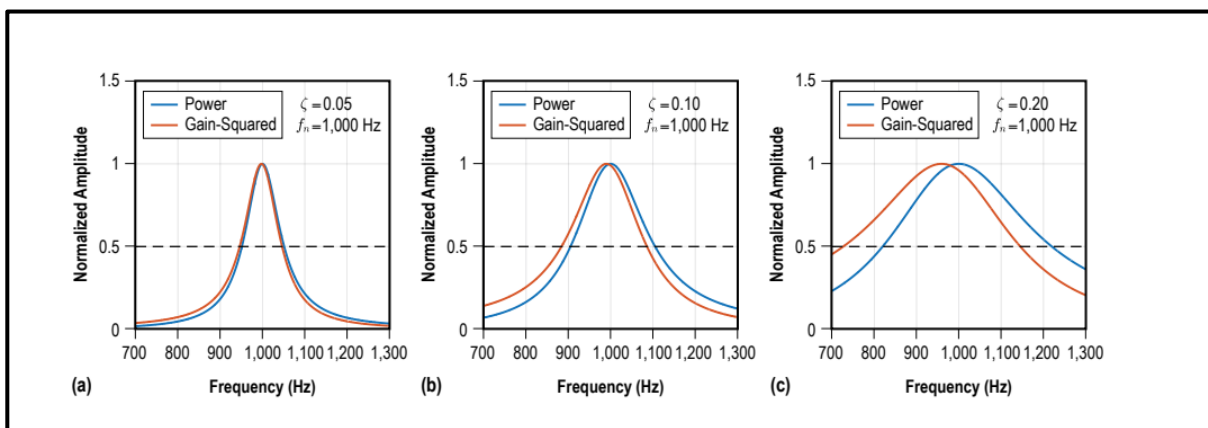


Figure 11A Normalised Amplitude vs frequency of Power and gain squared curve at damping ratio of 0.05, 0.10 and 0.20

frequency values.

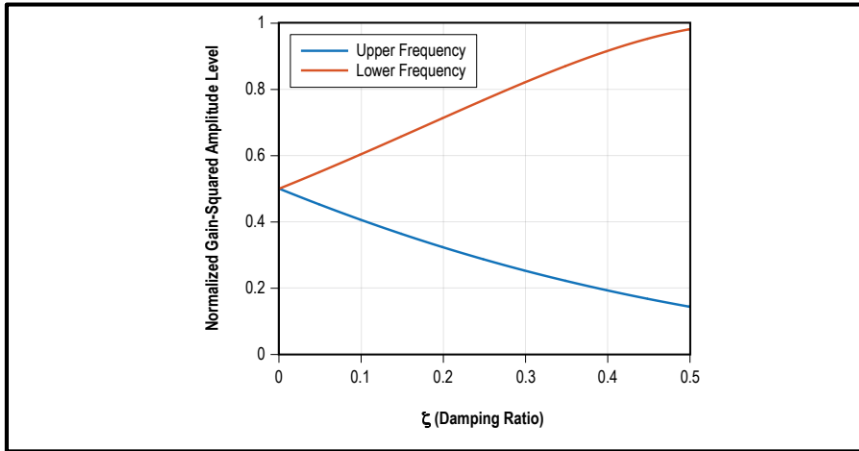


Figure 12A Expected Amplitude level of the normalised quadratic gain at half-power point

The error is given by a derived equation, with its power being normalised by dividing it to maximum power and square of the frequency response function is also normalised by dividing it with the squaring of maximum frequency response. The following equation results:

$$\varepsilon = P_{norm} - |H(f)|_{norm}^2 = \frac{(2\xi f/f_n)^2 + 4\xi^2(\xi^2 - 1)}{((1 - (f/f_n)^2)^2 + (2\xi f/f_n)^2)}$$

In order to reduce this error, using the frequency response function to derive actual relation rather than assuming it's relation to be squared to power curve is beneficial and this method provides more accurate damping data as the peak amplitude response frequency for a single degree of freedom is equal to the frequency at the centre of the peak measured during the experiment. To obtain lower and upper frequency values for FFT $\frac{1}{\sqrt{2}}$ times maximum peak and for PSD $\frac{1}{2}$ of maximum peak is used. (Nasa (2020)).

$$\xi = \sqrt{\left(4 + 4\left(\frac{f_2 - f_1}{f_p}\right)^2 - \left(\frac{f_2 - f_1}{f_p}\right)^4\right)^{-1}}$$

A.1.3.4 Logarithmic Decrement Method:

The rate of decay of the amplitude of the signal determines the damping and is proportional to it. The larger decay rates the more the damping. This rate of decay can be known with the help of logarithmic decrement method. Two successive amplitudes are selected and their ratio is determined on the same side of the mean after this their natural log is taken. The formula that relates it to the damping coefficient or ratio zeta can then be used for extracting and evaluating damping.

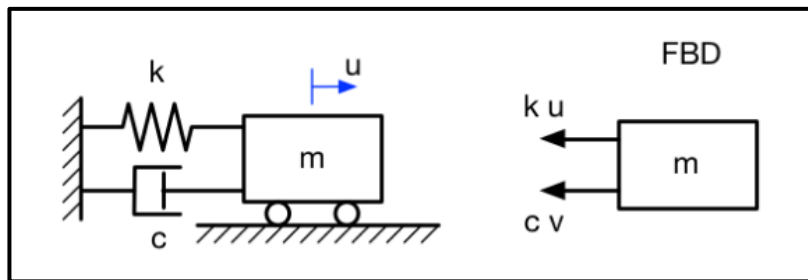


Figure 13A Mass Spring damper system with single degree of freedom (Damped free vibrations - All this. (2020)).

The Linear Differential equation for a system with single degree of freedom See 13A , above can be written as:

$$m\ddot{x} + c\dot{x} + kx = 0$$

Diving by m on both sides gives new variables:

$$\ddot{x} + 2\xi\omega_n\dot{x} + \omega_n^2x = 0$$

Where $\omega_n = \sqrt{\frac{k}{m}}$ = undamped Natural Frequency of the System,

$$\xi = \frac{c}{2m\omega_n} = \frac{c}{2\sqrt{km}}$$

ξ = damping coefficient

$c_c = 2m\omega_n$ = critically damped constant

The damping coefficient can also be written as the ratio.

$$\xi = \frac{c}{c_c}$$

Change in the nature of the solution of a differential equation in mathematical terms is represented by critical damping, or critical damping in physical terms represents a boundary between an oscillatory and non-

oscillatory behaviour. An oscillatory behaviour happens only when the critical damping is greater than the damping. $c < c_c$ and $\xi < 1$.

The solution to the differential equation above can be written as:

$$x = e^{-\xi\omega_n t} \left(x_0 \cos\omega_d t + \frac{\dot{x}_0 + \xi\omega_n x_0}{\omega_d} \sin\omega_d t \right)$$

At $t=0$, $x = x_0$, $\dot{x} = \dot{x}_0$,

$$\omega_d = \sqrt{1 - \xi^2} \omega_n$$

$\omega_d =$ damped natural frequency

The solution to LDE can be rewritten in a compact form as:

$$x = Ae^{-\xi\omega_n t} \cos(\omega_d t - \Phi)$$

$\Phi =$ Phase angle

The phase angle has an arbitrary value and is determine at $t=0$, at any chosen arbitrary (t) Φ can be made 0.

In order to explain the logarithmic decrement, the solution at $\Phi = 0$ and $\xi = 0.1$ can be visualised as follows:

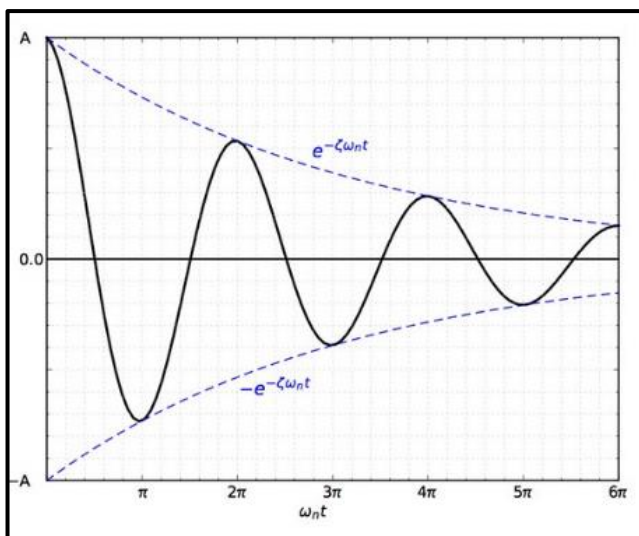


Figure 62 Shows the decay in Exponential envelop

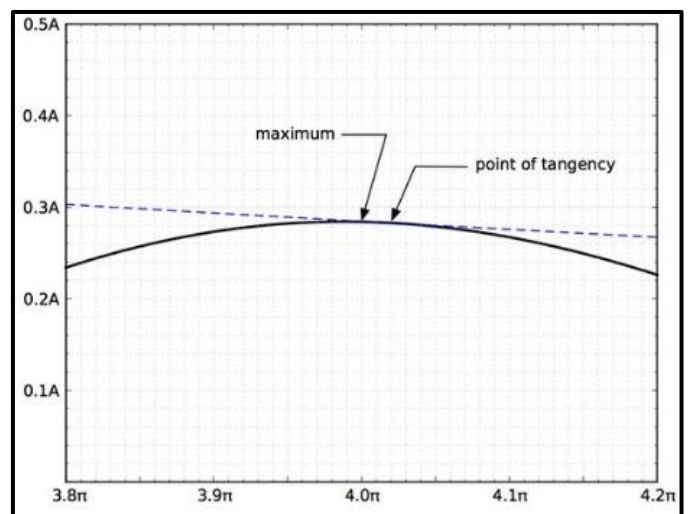


Figure 15 A Shows the Maximum point and the point of tangency

As time proceeds the amplitude of oscillation is lowered by the envelop that is generated by the exponential term. When the dashed blue solution curve touches the black oscillation curve a point of tangency is determined. And there is a space between the consecutive points of tangencies both lower and upper. At this point $\cos\omega_d t = 1$ See Figure 14 A above.

$$T_d = \frac{2\pi}{\omega_d} = \frac{2\pi}{\sqrt{1 - \xi^2}\omega_n}$$

$T_d =$ damped period of the system

$T_d = T_n$ and $\omega_d = \omega_n$ (For small values of damping coefficient)

The points of tangency and the maxima and minima are not coincident on the curve. Despite this the difference between successive points of tangency and difference between successive maxima and successive minima points is same and its already proved. During the experiment, this will be used to determine the maxima and minima points. See Figure 15 A above.

The relation can be written as:

$$\frac{x_m}{x_{m+1}} = \frac{e^{-\xi\omega_n t}}{e^{-\xi\omega_n(t+2\pi/\omega_d)}} = e^{2\pi\xi\omega_n/\omega_d}$$

Taking natural log on both sides gives:

$$\delta = \ln \left[\frac{x_m}{x_{m+1}} \right] = \frac{1}{m} \left[\frac{x_m}{x_{m+1}} \right] = \frac{2\pi\xi\omega_n}{\omega_d} = \frac{2\pi\xi}{\sqrt{1 - \xi^2}}$$

$\delta =$ logarithmic decrement

After getting the successive peak displacement values and taking their natural log the following equation gives damping coefficient:

$$\xi = \frac{\delta}{\sqrt{4\pi^2 + \delta^2}}$$

This method can be applied to Single degree of freedom time harmonic oscillator and exponentially decaying data that is underdamped See *Figure 16A below*.

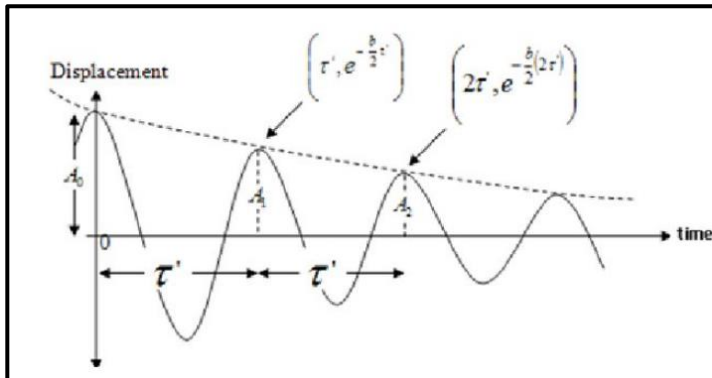


Figure 16A Coordinates required to evaluate logarithmic decrement (Acm Bekker, Stephan Victor Joubert Stephan Victor Joubert, Temple H. Fay (2008))

Exponential envelope needs to be fitted for the response where peaks are not smoothly decaying.

$$\xi = \frac{\ln\left(\frac{A_{t1}}{A_{t2}}\right)}{\sqrt{(2\pi f_1 \tau)^2 + \ln\left(\frac{A_{t1}}{A_{t2}}\right)^2}}$$

Use the equation from the link and then deduce the curve. the curve gives damping values. The first amplitude is always there in the calculations. (Nasa (2020)), (Damped free vibrations - All this. (2020)). (Acm Bekker, Stephan Victor Joubert Stephan Victor Joubert, Temple H. Fay (2008))

A.2 SIMULATED MODAL ANALYSIS OF THE BRIDGEPORT BALL SCREW FEED DRIVE SYSTEM DESIGN.

A.2.1 Rig design Schematic

The Bridgeport Ball screw feed drive system was used to evaluate the response of the feed drive system and to validate the FEA (Finite Element Analyses) on the basis of modal analysis. The rig is shown as follows refer to *Figure 17A below*.

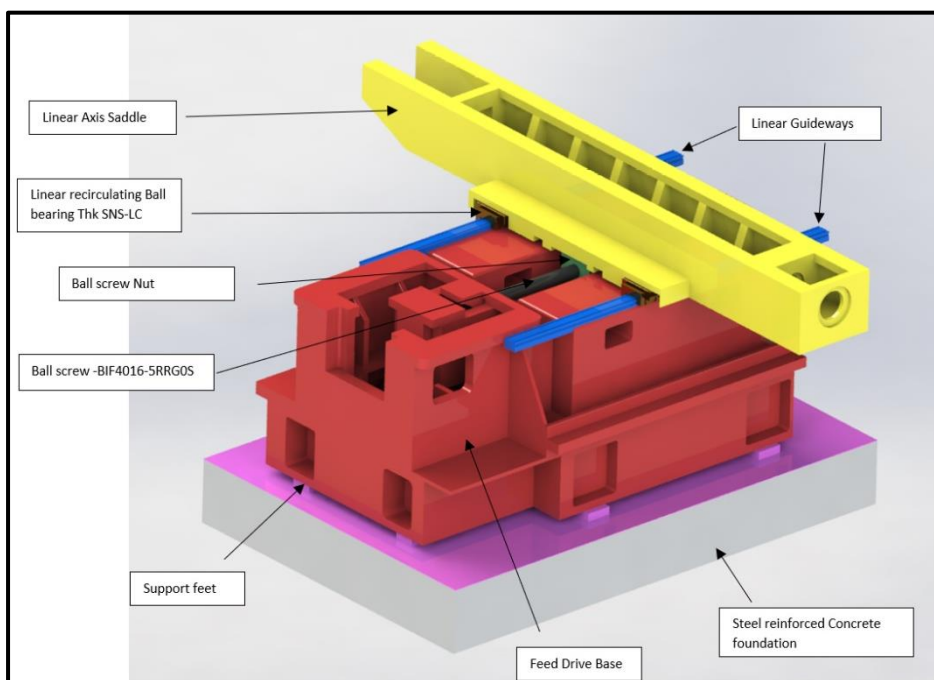


Figure 17A Schematic of the Bridgeport Ball screw feed drive system.

A.2.2 Importance of Computational Analysis and Introduction to Finite Element Analysis:

In order to Understand the Physical behaviour i: e to understand the physics of a certain component or a system and to derive its characteristic's, three methods can be utilised, Experimental method, Analytical method and Computational method. Experimental methods are the most accurate as they directly interfere with the object under consideration but like everything they have their drawback. One of the major drawbacks is the setup time and the cost.

On other hand Analytical methods are derived from experimental methods and can be used correctly to analyse a problem but the level of difficulty to solve a highly complex problem for example doing modal analysis on an engine with the help of hand calculations only, is extremely difficult and can involve a lot of human errors. In order to solve this issue, an alternative method is referred to as a computational method where governing equations of the problem in hand are mathematically modelled in the computer with some assumptions and discretised with the help of certain numeric solution. One of such computational methods used to solve problems related to the physics of an object or system is called finite element method. Such a method saves Costs and Time associated with the experimental setup and eradicates any errors resulting due to the analytical method (hand calculations). In order to solve a given problem finite element method uses tiny elements of a definite shape made by nodes and uses the applied boundary conditions to generate data at nodes which is then averaged over the element. (H. Shih, 2016).

The Finite Element analysis is performed by the Machine in the schematic manner as Shown in *Figure 18A below*.

The solver in Finite element method uses a mathematical model that is based on assumptions applied to real physical principles, which involve governing equations. These assumptions are important for example when converting continuous time equations into discrete forms. The mathematical model is then solved with the help of some numerical strategy of selected variables at selected points. These variables or the data at selected points can then be used to extract more information with the help of post processing to give coloured pictures used for analysis.

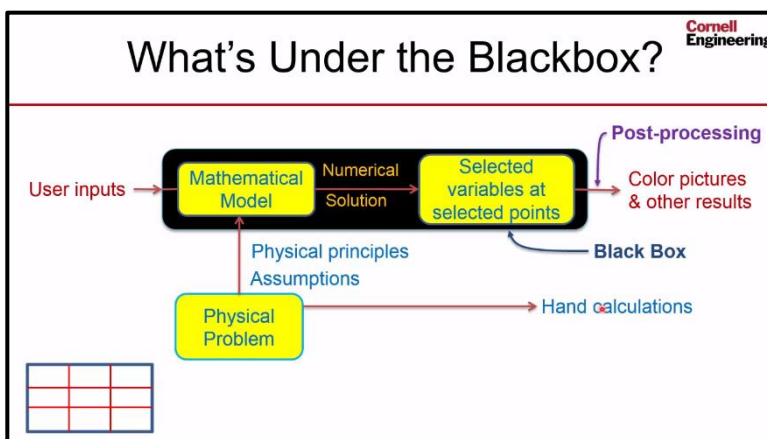


Figure 18 An Algorithm of Finite Element Analysis. (Cornell Engineering ,(2020)).

Ansys workbench 18.2 was utilised to model the boundary conditions and Ansys workbench 19.2 was used to perform the modal Analysis. Solid model of the Bridgeport Feed drive system was transferred from solid works to space claim and saved as .scdoc file.

A.2.3 Materials Assigned:

Following materials were assigned to each part:

- Ball screw-BIF4016-5RRG0S - AISI 4150 H Steel (Standard low alloy) Stainless Steel
- Ball screw Nut- BIF4016-5RRG0S- SAE 8620 (Common carburising steel) SS
- INA -ZKLF 3080.2RS- Angular contact thrust ball bearing: Stainless Steel
- THK SNS-LC Linear Recirculation Ball bearing: Stainless Steel
- Feed Drive Base: Grey Cast Iron
- Guideway: Stainless Steel
- Support Feet: Stainless Steel
- Rig Floor: Steel -reinforced Concrete: 250Gn/m^2 , 0.2 Poisons ratio.
- Linear axis Saddle: Grey Cast Iron
- Sub Soil: Weathered over consolidated Clay: 50 Mpa

A.2.4 Mesh quality and Convergence:

The more the number of elements, the more acute data can be achieved at the nodes as there is less averaging within the element.

Number of Nodes and Elements were monitored in order to attain mesh convergence (where the resulting modes do not change considerably on mesh refinement)

Behaviour is set to Soft, this enables the mesh to adjust close to the element value near curvature, proximity or local remeshing (Ansys). The mesh used constitutes the element size of 0.03 which was adequate for the solver time and accuracy required as proved by mesh convergence. The elements used were program controlled, it can be seen in *Figure 19 A below*, the elements are tetrahedrons except at the concrete base where shells have been applied.

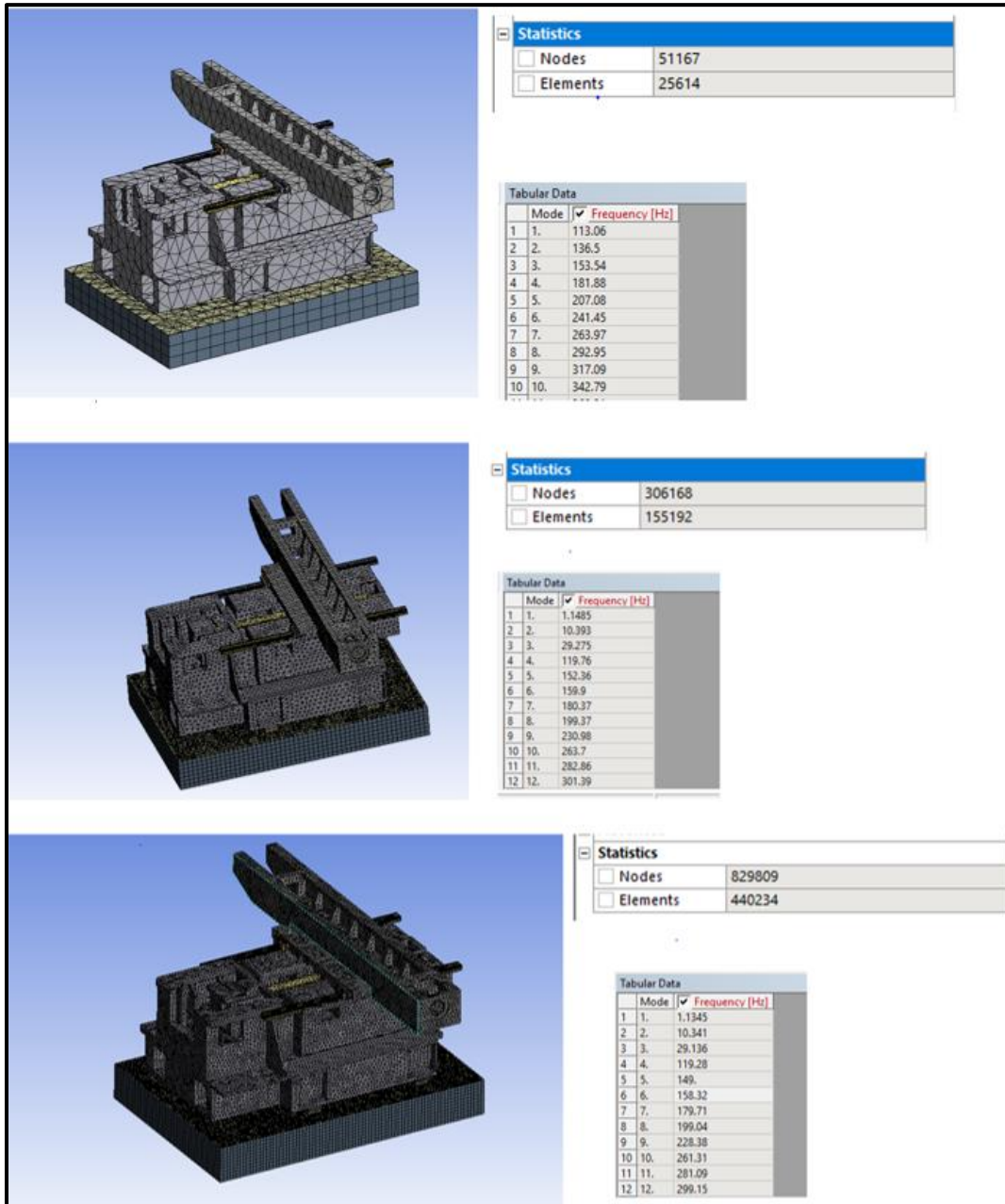


Figure 63 Shows the mesh convergence process and the relative Modes

A.2.5 Mechanical Contacts:

Ansys Comes with various contacts between mating surfaces(shells), this assigns the boundary conditions between mating parts which are essential for modal analysis as modal analysis depends highly on the degree of freedom, the stiffness and damping between contacts.

Contact generation demands a pair to be involved (a target and contact) , this pair can either be a point-surface or a surface- surface. The surface is the target and the point are the contact in point-surface connection while as in surface to surface, the contact and target are both surfaces however, in this case concave is chosen as target and convex is chosen as the contact. If there is a size difference between two bodies, the large body is treated as the target and the small body as contact. *See Figure 20A below.*

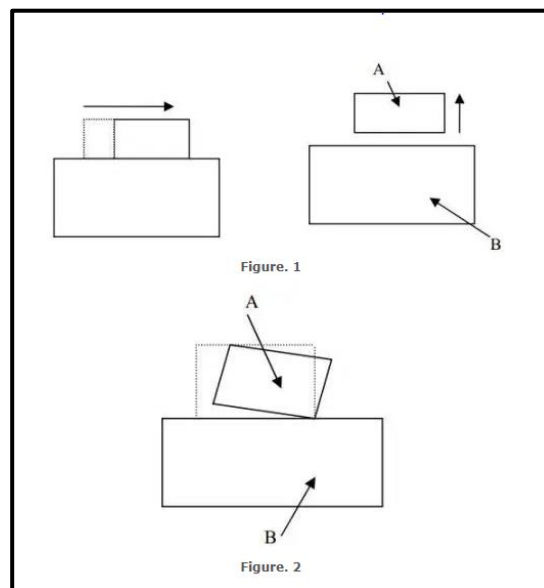


Figure 20A Mechanical Contact characteristics

Depending on the characteristics of the contact they can be categorised as follows.

Bonded Contact: In bonded connection the contact surfaces can be constrained in both normal and tangential direction they can neither slide tangentially nor move vertically.

Rough Contact: This can be used when no motion in the tangential direction is desired i: e in order to avoid any sliding the nodes are tied on the target body; the surface assumes the coefficient of friction to be infinite. Nodes in contact are glued on the target surface in tangential direction.

Frictional Contact: Both the tangential and the vertical degree of freedom is allowed with this type of contact. Sliding is allowed on target surface, the coefficient of friction in tangential direction can be adjusted to a desired value.

No separation Contact: Allows translational motion or sliding in tangential direction but a bonded contact between the target and contact surface is generated in normal direction i: e in the normal direction the nodes are tied up.

A.2.6 Boundary Conditions:

Boundary conditions are an important part of the analysis without which it's not possible. In Solid-mechanics all the data is generated by assigning the known boundary conditions.

In order to provide Modal Analysis of a mechanical system the physical nature of each contact needs to be determined and assigned.

Based on this, Contacts with proper numeric values were assigned to each mating surface in the model as follows:

Ball screw to Nut: The axial rigidity of the balls screws to nut connection can be assumed to be highly stiff and therefore the connection can be assumed to be a bonded connection. *See Figure 21A below.*

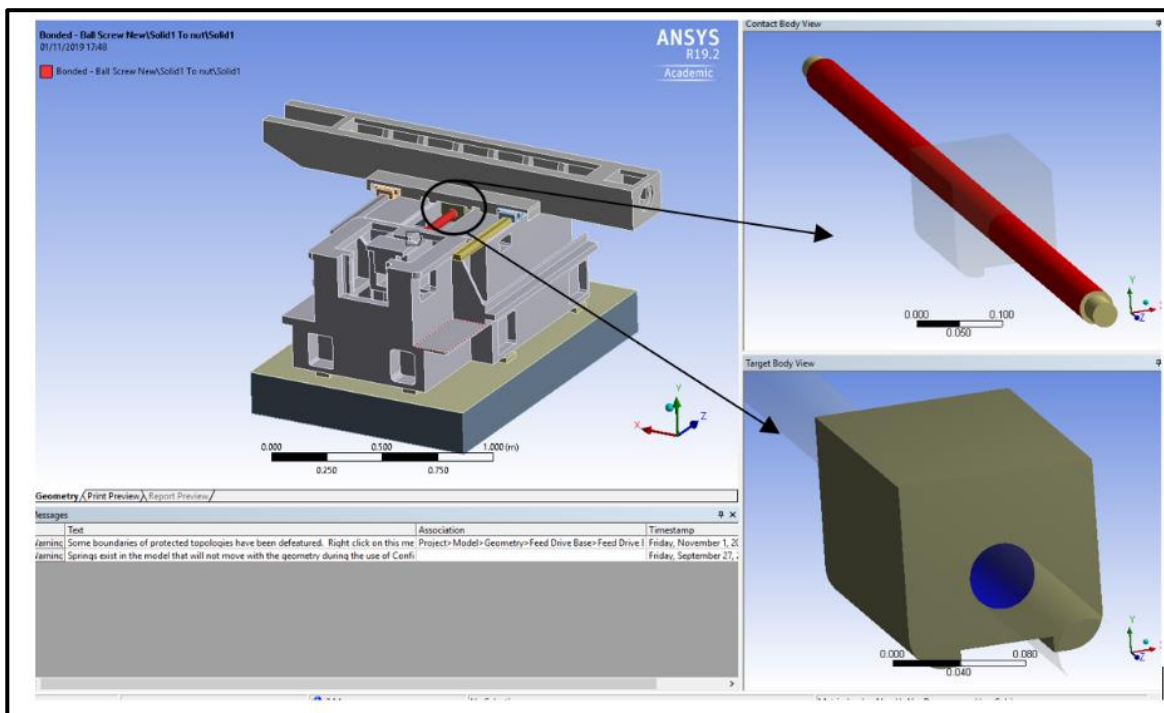


Figure 21A Ball to nut Boundary condition

THK SNR-LC Linear roller bearing to Saddle: The Saddle is rigidly attached to the four Linear bearings with the help of cap screws, this connection can be treated as a bonded connection as all 6 DOFs are restricted. See Figure 22A below.

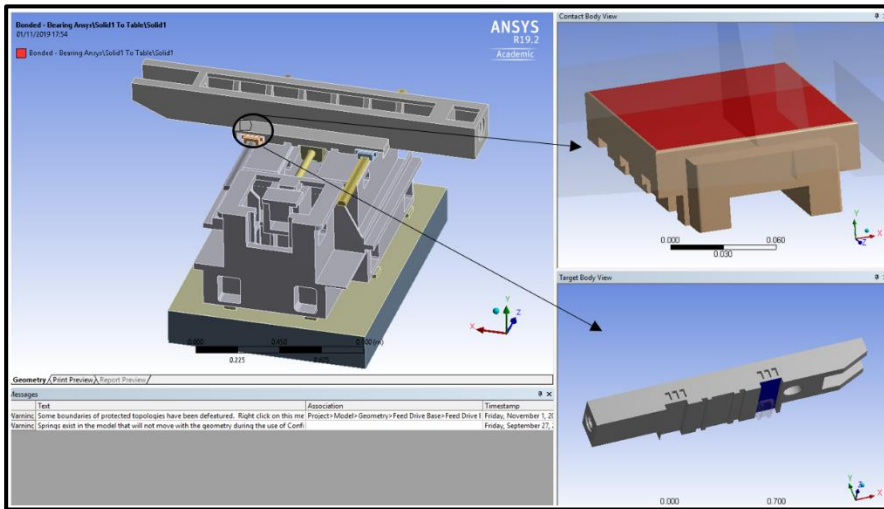


Figure 22A THK SNR-LC Linear roller bearing to Saddle boundary condition

Feed drive base to ball screw stiffness (Axial rigidity of ball Bearing):

The axial rigidity of the ball bearings INA -ZKLF 3080.2RS play an important role in the bucking of the ball screw and other parameters involved in the modal analysis. The axial rigidity of the angular contact thrust bearing was 850N/um. This was set using a spring connection between the ball screw and the ball bearing mounting. The procedure was applied in the same manner to the other side of ball screw. See Figure 23A below.

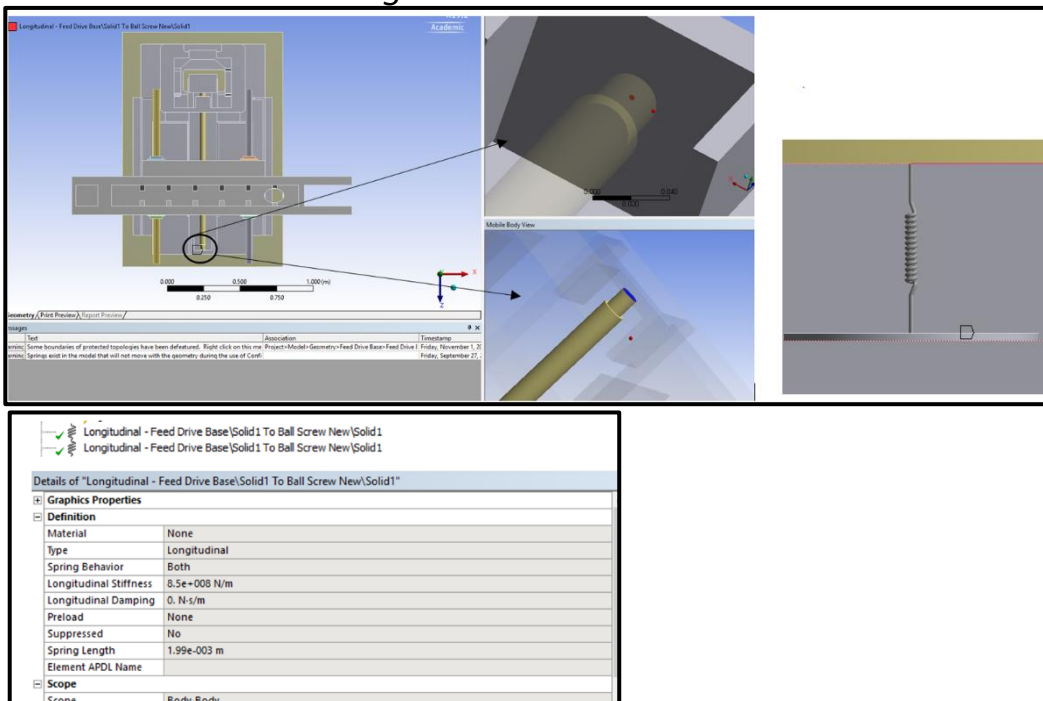


Figure 23A Shows Feed drive base to ball screw stiffness (Axial rigidity of ball Bearing) Boundary condition

Radial rigidity of ball bearing: The radial rigidity of the ball screw is also important, in order to apply this a bearing joint was utilised where two radial stiffness values were assigned a value of 850N/um (Note: this value was assumed to be similar to axial rigidity). See Figure 24A below.

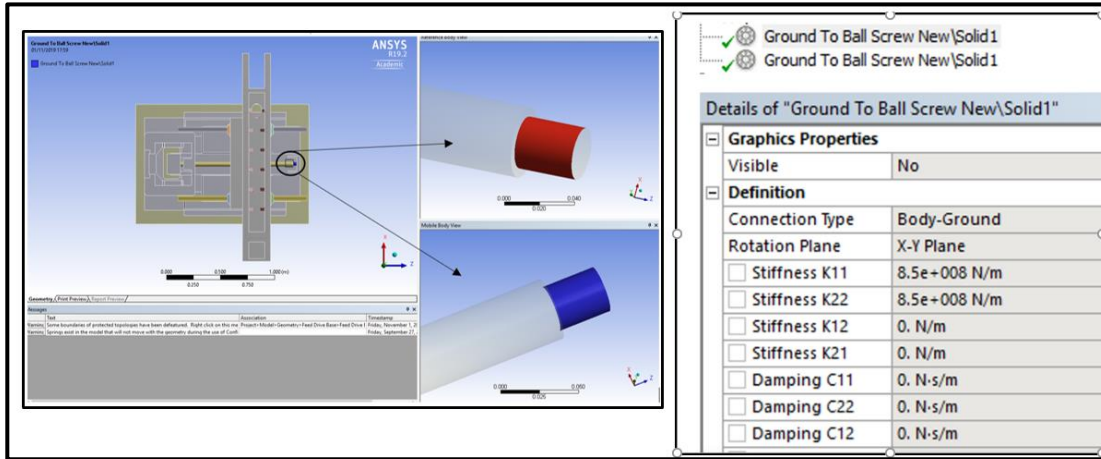


Figure 24A Radial rigidity of ball bearing boundary condition

THK SNR-LC to Linear Stainless-steel guideway:

The joint is translational and the friction between rolling elements (rollers) and the guideway has a known value therefore, the bond can be set frictional and the joint as translational, the joint only allows one degree of freedom along the assigned axis, this was first taken into consideration but later removed as Modal Analysis in Ansys is a linear Analysis and hence will not include friction which is nonlinear in nature.

A no separation joint was used instead of a combination of translational and frictionless contact because it does not allow the mating parts to separate in normal direction and simultaneously allows for sliding of Linear bearing on the guide rail.

The stiffness between THK SNR-LC bearings and Guideway is 1.20 kN/um approximately but it is negligible and does not affect the results as the modes go higher. See Figure 25A below.

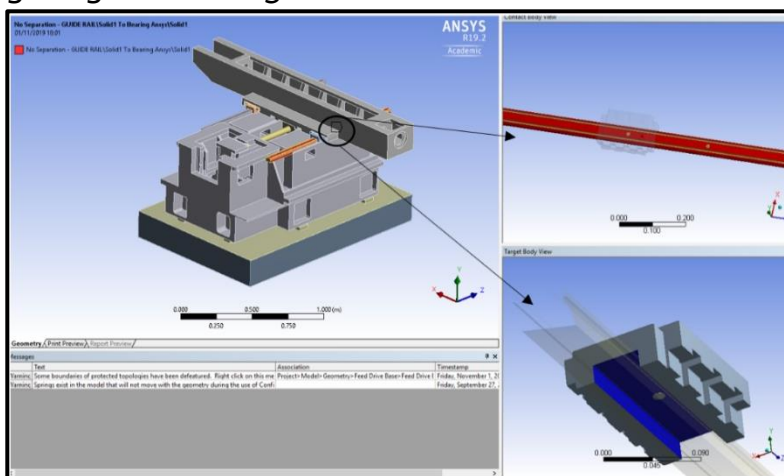


Figure 25A THK SNR-LC to Linear Stainless-steel guideway Boundary Condition

Feed drive Base to Support feet: The connection was set to bonded as the feed drive base is connected to the support feet through a bolts. See Figure 26A below.

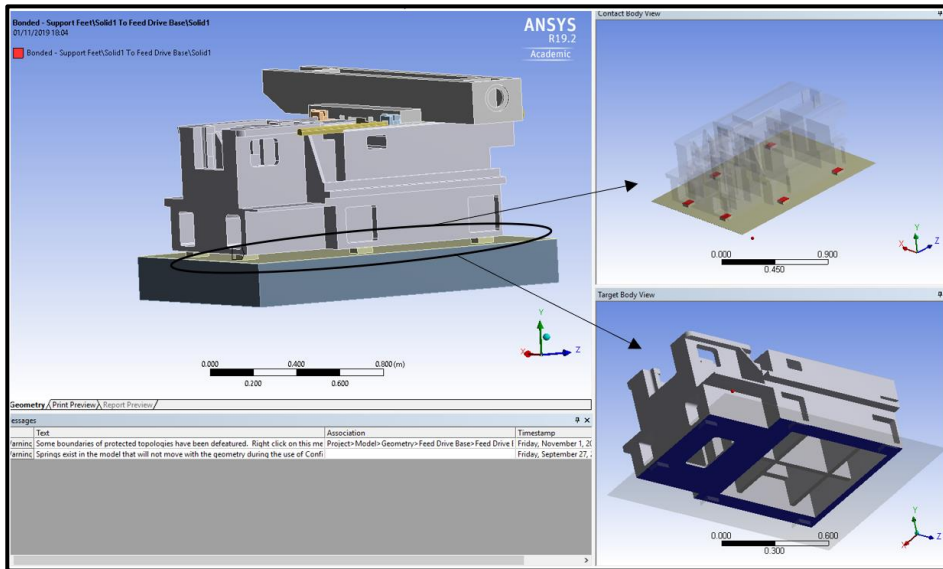


Figure 26A Feed drive Base to Support feet: Boundary Condition

Support Feet to concrete floor: The support feet sit on a concrete; this connection is frictional and the coefficient between the steel feet and the concrete is 0.1. See Figure 27A below.

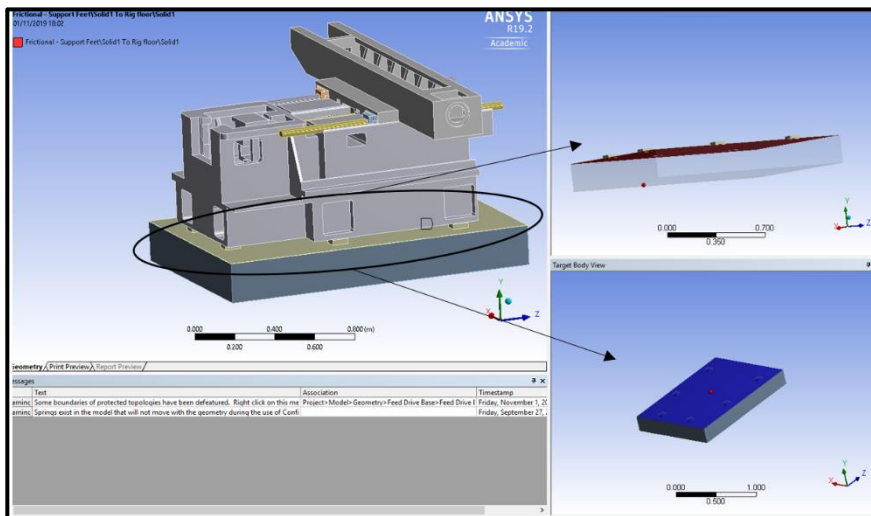


Figure 27A Support Feet to concrete floor Boundary Condition

Fixture: In order to extract the Modes, the concrete base was assumed to be fixed to the soil underneath, which in reality is not the case. The soil is elastically support on the walls by the neighbouring layers of soil and it has its own stiffness and damping in all directions. This was neglected as the modes would be of a very low frequency which are not of interest. See Figure 28A below.

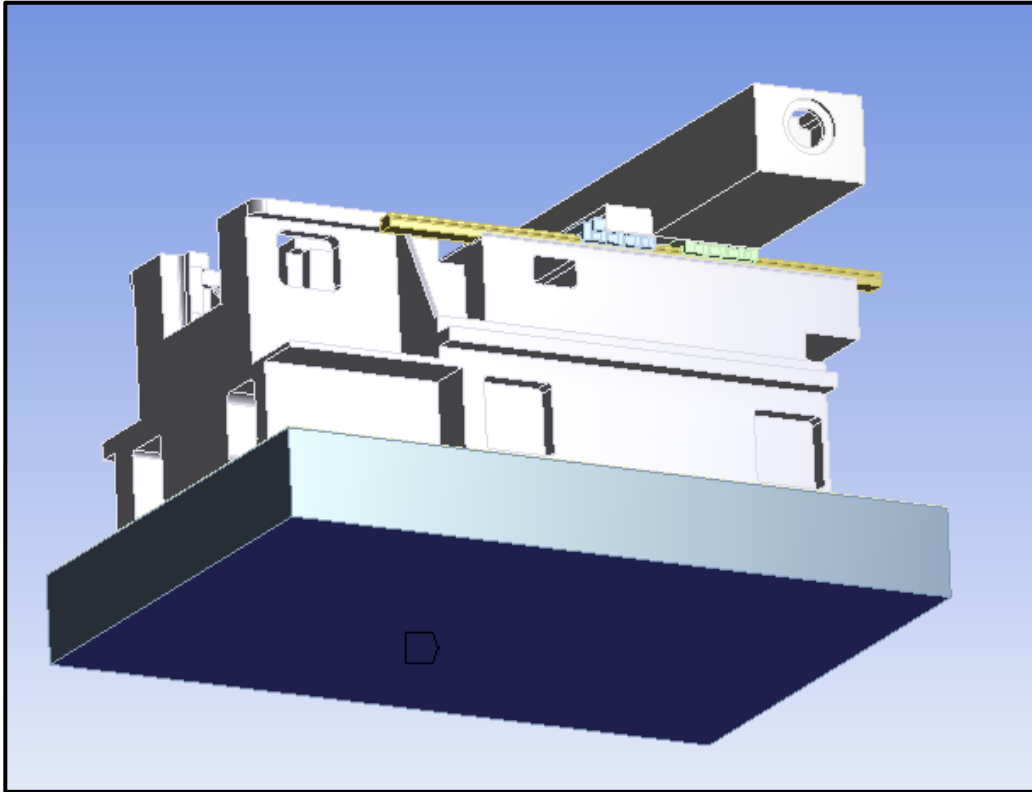


Figure 28A Fixture Applied

A.3 EXPERIMENTAL MODAL ANALYSIS OF THE SCREW DRIVE.

The main Aim of the experiment was to validate the computational Modal Analysis with the help of Experimental Modal Analysis. The main Aim is to prove the validity of applying the devised Finite Element Method strategy on the new bearing design to carry out its structural response as compared to Conventional linear recirculating bearings.

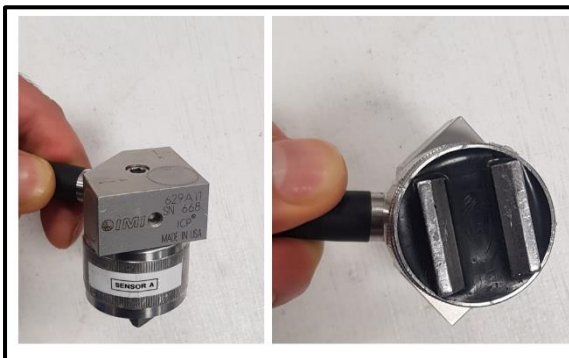
In order to compare the Modes of the feed drive test rig with the modes of the computational modal analysis. Following steps were carried out.

A.3 .1 Apparatus Used:

The vibration sensor used to capture the signal was a triaxial accelerometer (IMI-629A11 SN668 ICP) with the following specifications See Table 1 and See Figure 29A below.

| | |
|--------------------------|---------------------------------------------------|
| Sensitivity | (±5%) 100mV/g (10.2 mV/(m/s²)) |
| Sensing Element | Ceramic |
| Measurement Range | ± 50g (±490 m/s²) |
| Frequency range | (± 3dB) 48 to 480000 cpm (0.8 to 8000 Hz) |
| Weight | 139 gm |

Table 1A triaxial accelerometer (IMI-629A11 SN668 ICP) specifications



| Model Number | INDUSTRIAL ICP® ACCELEROMETER | | Revision: B ECN #: 48136 |
|--------------------------------------------------------------------------------------------------------------------------------------------------------------------------------------------------------------------------------------------------------------------------------------------------------------------------------------------------------------------------------------------------------------------------------------------------------------------------|-------------------------------|--------------------------------|-----------------------------------------------------------------|
| 629A11 | | | |
| Performance | ENGLISH | SI | OPTIONAL VERSIONS |
| Sensitivity (± 5%) | 100 mV/g | 10.2 mV/(m/s ²) | [2] |
| Measurement Range | ± 50 g | ± 490 m/s ² | [3][4] |
| Frequency Range(± 5%) | 144 to 120,000 cpm | 2.4 to 2000 Hz | |
| Frequency Range(± 10%) | 102 to 300,000 cpm | 1.7 to 5000 Hz | |
| Frequency Range(± 3 dB) | 48 to 480,000 cpm | 0.8 to 8000 Hz | |
| Resonant Frequency | 1200 kcpm | 20 Hz | [1] |
| Bandwidth Resolution(1 to 10,000 Hz) | ± 1% | ± 1% | [5] |
| Non-Linearity | ± 1% | ± 1% | [6] |
| Transverse Sensitivity | ± 5% | ± 5% | |
| Environmental | | | |
| Overload Limit(Shock) | 5000 g pk | 49,050 m/s ² pk | |
| Temperature Range | -65 to +250 °F | -54 to +121 °C | [1] |
| Temperature Response | See Graph | See Graph | |
| Electrical | | | |
| Settling Time(within 1% of bias) | ≤ 3.0 sec | ≤ 3.0 sec | |
| Discharge Time Constant | ± 0.2 sec | ± 0.2 sec | |
| Excitation Voltage | 18 to 28 VDC | 18 to 28 VDC | |
| Constant Current Excitation | 2 to 20 mA | 2 to 20 mA | |
| Output Impedance | <100 Ohm | <100 Ohm | |
| Output Bias Voltage | 8 to 12 VDC | 8 to 12 VDC | |
| Spectral Noise(10 Hz) | 7.0 µg/√Hz | 68.7 (µmsec ²)/√Hz | [1] |
| Spectral Noise(100 Hz) | 2.8 µg/√Hz | 27.5 (µmsec ²)/√Hz | [1] |
| Spectral Noise(1 kHz) | 1.0 µg/√Hz | 9.8 (µmsec ²)/√Hz | [1] |
| Electrical Protection | RFI/ESD | RFI/ESD | |
| Electrical Isolation(Case) | ≥ 10 ⁸ Ohm | ≥ 10 ⁸ Ohm | |
| Physical | | | |
| Size (Length x Width x Height) | 1.5 in x 1.5 in x 0.82 in | 38.1 mm x 38.1 mm x 20.8 mm | |
| Weight(without cable) | 4.9 oz | 139 gm | |
| Mounting Thread | 1/4-28 Male | No Metric Equivalent | [6] |
| Mounting Torque | 2 to 5 lbf | 2.7 to 6.8 Nm | |
| Sensing Element | Ceramic | Ceramic | |
| Sensing Geometry | Shear | Shear | |
| Housing Material | Stainless Steel | Stainless Steel | |
| Sealing | Welded Hermetic | Welded Hermetic | |
| Electrical Connector | Sealed Integral Cable | Sealed Integral Cable | |
| Electrical Connection Position | Side | Side | |
| Electrical Connections(Red) | X axis | X axis | |
| Electrical Connections(Green) | Y axis | Y axis | |
| Electrical Connections(White) | Z axis | Z axis | |
| Electrical Connections(Black) | Ground | Ground | |
| Electrical Connections(Shield) | NC | NC | |
| Cable Length | 10 ft | 3.0 m | |
| Cable Type | Polyurethane | Polyurethane | [7] |
| Typical Sensitivity Deviation vs Temperature | | | |
| | | | |
| <p>NOTES:</p> <p>[1] Typical.</p> <p>[2] Conversion Factor 1g = 9.81 m/s².</p> <p>[3] The high frequency tolerance is accurate within ±10% of the specified frequency.</p> <p>[4] 1Hz = 60 cpm (cycles per minute).</p> <p>[5] Zero-based, least-squares, straight line method.</p> <p>[6] 1/4-28 has no equivalent in S.I. units.</p> <p>[7] Twisted shielded 4-conductor cable.</p> <p>[8] See PCB Declaration of Conformance PS022 for details.</p> | | | |
| <p>SUPPLIED ACCESSORIES:</p> <p>Model 081A59 Captive mounting bolt: 1/4-28 x .75"</p> <p>Model ICS-1 NIST-traceable single-axis amplitude response calibration from 600 cpm (10 Hz) to upper 5% frequency</p> | | | |
| Entered: LK | Engineer: BAM | Sales: MC | Approved: BAM |
| Date: 4/26/2018 | Date: 4/26/2018 | Date: 4/26/2018 | Date: 4/26/2018 |
| | | | Spec Number: 8316 |
| <p>IMI SENSORS A PCB PIEZOTRONICS DIV 3425 Walden Avenue, Depew, NY 14043</p> | | | Phone: 800-959-4464 Fax: 716-684-3823 E-Mail: imi@pcb.com |

Figure 29A T f triaxial accelerometer (IMI-629A11 SN668 ICP) picture and Data Sheet

Impact Hammer: External force excitation was carried out with the help of an Impact hammer (PCB-086D20 SN14930) and its characteristics are tabulated below. See Table 2 and Figure 30 A below.

| | |
|--------------------------|------------------------------------|
| Sensitivity | (±15%) 1mV/lbf (0.23 mV/N) |
| Measurement Range | ± 5000 lbf pk (±22240 N pk) |
| Hammer Mass | 1.1 kg |

Table 2 An Impact hammer (PCB-086D20 SN14930) Data.

| Model Number 086D20 | ICP® IMPACT HAMMER | | | Revision: H ECN #: 44362 |
|--------------------------------------------------------------------------------------------------------------------------------------------------------------------------------------------------------------------------------------------------------------------------------------------------------------------------------------------|---------------------------|------------------|--------------------------------------------------------------------------------------------------------------------------------------------------------------|-----------------------------|
| Performance | ENGLISH | SI | OPTIONAL VERSIONS | |
| Sensitivity(± 15 %) | 1 mV/lbf | 0.23 mV/N | Optional versions have identical specifications and accessories as listed for the standard model except where noted below. More than one option may be used. | |
| Measurement Range | ± 5000 lbf pk | ± 22,240 N pk | T - TEDS Capable of Digital Memory and Communication Compliant with IEEE P1451.4 | |
| Resonant Frequency | ≥ 12 kHz | ≥ 12 kHz | TLD - TEDS Capable of Digital Memory and Communication Compliant with IEEE 1451.4 | |
| Non-Linearity | ≤ 1 % | ≤ 1 % | Output Bias Voltage 8.5 to 15 VDC 8.5 to 15 VDC | |
| Electrical | | | NOTES: | |
| Excitation Voltage | 20 to 30 VDC | 20 to 30 VDC | [1]Typical. | |
| Constant Current Excitation | 2 to 20 mA | 2 to 20 mA | [2]See PCB Declaration of Conformance PS136 for details. | |
| Output Impedance | <100 Ohm | <100 Ohm | SUPPLIED ACCESSORIES: | |
| Output Bias Voltage | 8 to 14 VDC | 8 to 14 VDC | Model 084A60 Tip - super soft plastic, gray (1) | |
| Discharge Time Constant | ≥ 1400 sec | ≥ 1400 sec | Model 084A61 Tip - soft plastic, brown (1) | |
| Physical | | | Model 084A62 Tip - medium plastic, red (1) | |
| Sensing Element | Quartz | Quartz | Model 084A63 Tip - hard plastic, black (1) | |
| Sealing | Hermetic | Hermetic | Model HCS-2 Calibration of Series 086 instrumented impact hammers (1) | |
| Hammer Mass | 2.4 lb | 1.1 kg | Entered: JM Engineer: NJF Sales: RWM Approved: NJF Spec Number: | |
| Head Diameter | 2.0 in | 5.1 cm | Date: 6/29/2015 Date: 6/29/2015 Date: 6/29/2015 Date: 6/29/2015 12923 | |
| Tip Diameter | 2.0 in | 5.1 cm | | |
| Hammer Length | 14.5 in | 37 cm | | |
| Electrical Connection Position | Bottom of Handle | Bottom of Handle | | |
| Electrical Connector | BNC Jack | BNC Jack | | |
|  <p>All specifications are at room temperature unless otherwise specified. In the interest of constant product improvement, we reserve the right to change specifications without notice. ICP® is a registered trademark of PCB Group, Inc.</p> | | | | |
| | | |  <p>3425 Walden Avenue, Depew, NY 14043</p> | |
| | | | <p>Phone: 716-684-0001 Fax: 716-684-0987 E-Mail: info@pcb.com</p> | |



Figure 30A Impact hammer (PCB-086D20 SN14930) and Data Sheet

Hammer tip: The Impact hammer comes with various hammer tips ranging from hard to super soft a brown soft plastic 0.84A61 Tip was used to excite the required medium frequency range of 0 to 600 Hz. *See Figure 31A below.*



Figure 64 Shows brown soft plastic 0.84A61 Tip

Data acquisition unit: Sampling of the frequency was carried out with the help of a SignalCalc Mobilyser by Data Physics. *See Figure 32A below.*



Figure 32A SignalCalc Mobilyser by Data Physics

Software: SignalCalc Mobilyser dynamic signal analyser version 4.0.070.

Laptop: Samsung Electronics: *See Figure 33A below.*

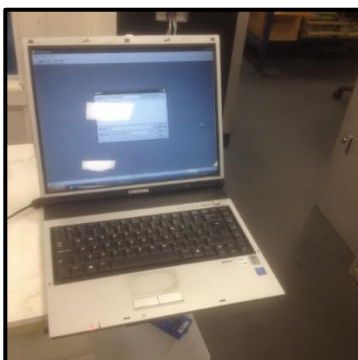


Figure 33A Machine used Samsung Electronics

Rig: A bridge port Linear feed drive was used for experimentation.

A.3 .2 Methodology:

As mentioned Earlier, the main aim of the experiment was to validate the computational Modal Analysis with the help of Experimental Modal Analysis. The main Aim is to prove the validity of applying the devised Finite Element Method strategy on the new bearing design to carry out its structural response as compared to Conventional linear recirculating bearings.

In order to compare the Modes of the feed drive test rig with the modes of the computational modal analysis. Following steps were carried out.

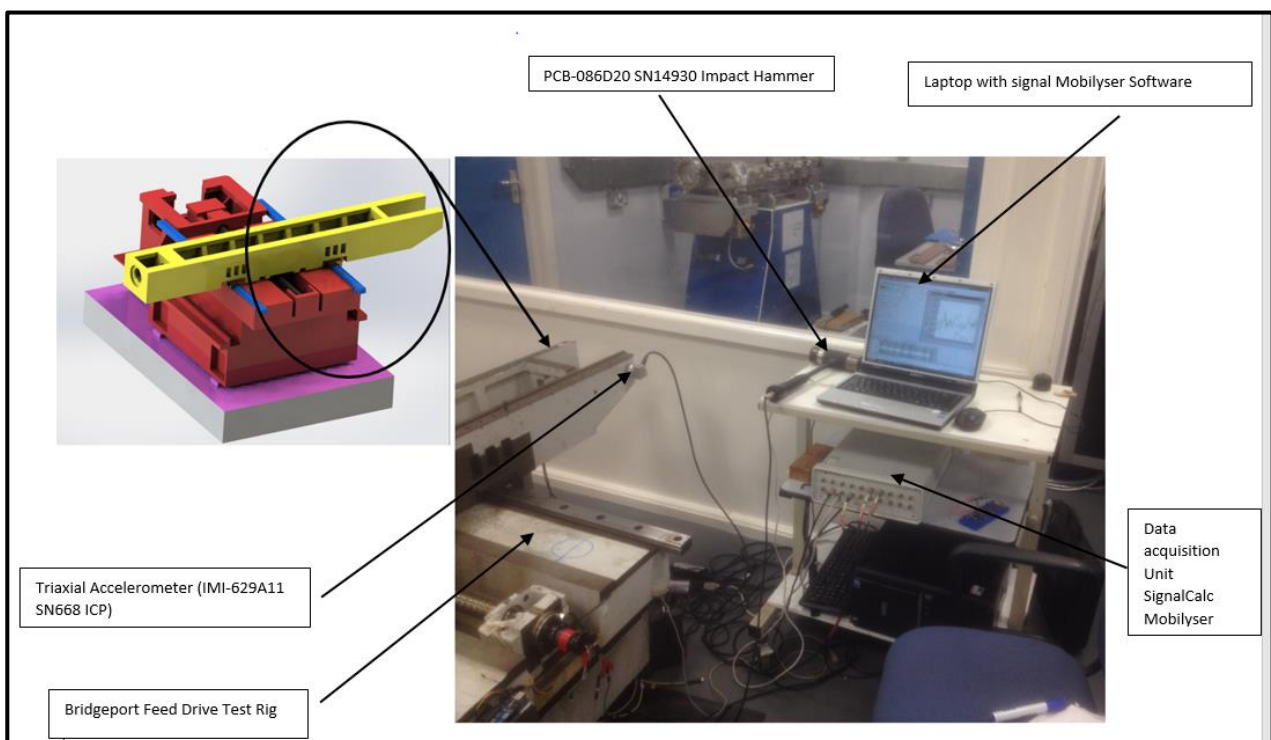


Figure 34A Shows Experimental Modal Analysis Setup

A Triaxial accelerometer was connected to data ports of the data box in Channel 4, 5 , and 10 representing captured data in X, Y and Z axis with the hammer being connected in channel 8. See Figure 35A below.



Figure 35A Triaxial accelerometer was connected to data ports of the data box

1. Signal Analyser was set to capture Transfer function (Fast Fourier Transform) to obtain the frequency spectrum.
2. All the ICP 4Ma channels were set according to their ports with their sensitivity being in accordance with the data specifications as mention in section earlier. *See Figure 36A below.*

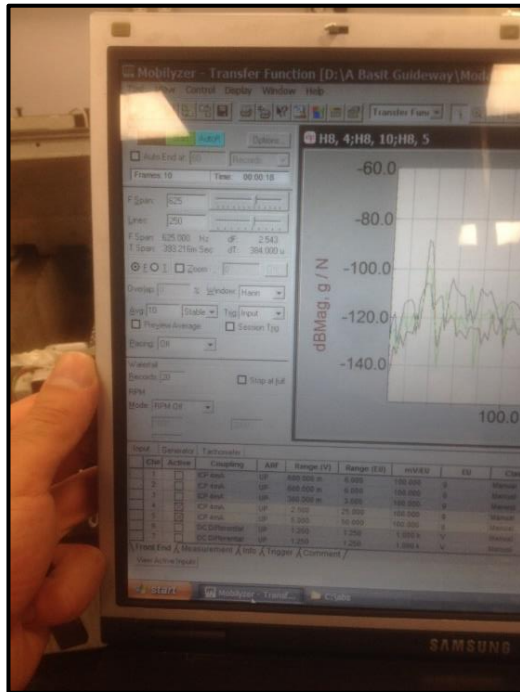


Figure 36A ICP 4 Ma channels set according to their ports

3. The sampling parameters were set, F span was set to 625 Hz and the number of lines to 250, this results in a frequency bin dF of 2.543, T span of 393.216 msec, dT 384 usec and the bandwidth to. This given a frequency resolution. *See Figure 37A below.*

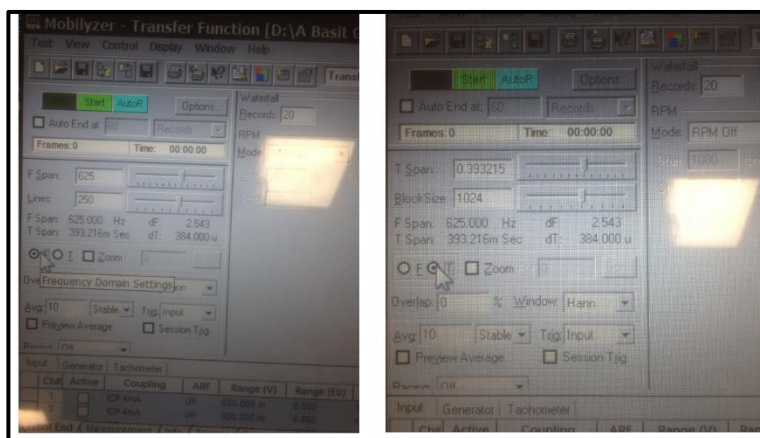


Figure 65 Sampling frequency parameters.

4. Three Hitting points were selected at 3 different locations. Point was having the direction - Y axis, point 2 +Z axis and point 3 +X axis as shown in *Figure 38A . below.*

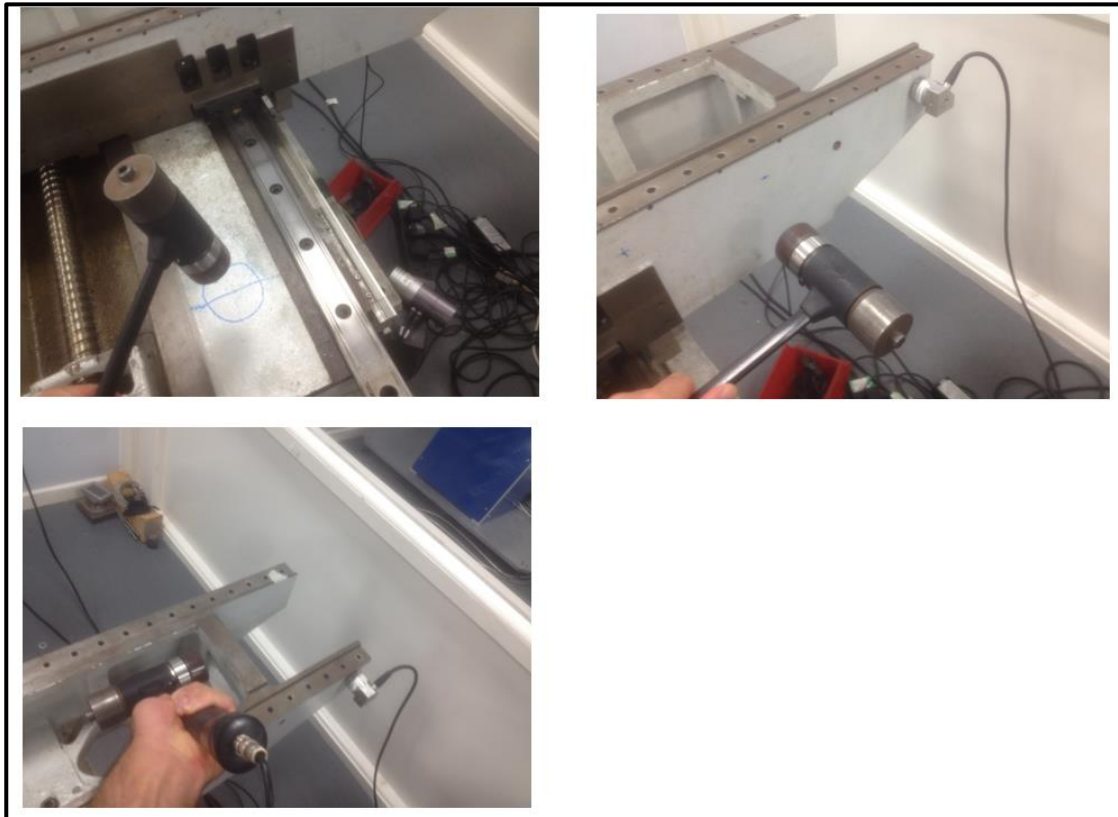


Figure 38A Three Hitting points selected at 3 different locations

5. The accelerometer was roved for each Hit point to 3 different locations on the saddle, these locations were selected because it's easy to analyse the mode shapes here due to large deflection resembling a simple beam like structure.
6. The FFT obtained for each Hit point including 3 different accelerometer position was saved and later post processed in MATLAB.
7. The main peaks were compared with the main peaks obtained from Simulations.

A.3 .3 Validation

Validation of the computational Modal Analysis was carried out by utilising the mode shapes of the experiment already performed by Dr. Simon Fletcher as a reference data . The Analyses of the acceleration values gained from the experimental Modal analysis on Bridgeport drive was carried out followed by comparison with similar mode shapes obtained from Computational Modal Analysis.

Three mode shapes were selected to validate the simulation performed with the help of finite element method technique. The table below shows the Mode values (Natural frequencies) of the reference Mode shape experimental result, its corresponding guess in experimental Modal analysis on Bridgeport drive and the suspected Computational Modal Value. $Z > Y > X$. See Table 3 and figure 39A below.

| Reference Mode Shape Experiment | Experimental Modal Analysis | Computational Modal Analysis | % M/E | %E/C | Acceleration Amplitude Relation |
|---------------------------------|-----------------------------|------------------------------|-------|-------|---------------------------------|
| 249 | 295 | 263.7 | 15% | 10.6% | Z>X>Y |
| 139 | 122 | 119.37 | 12% | 2.45% | Z>X>Y (Z>Y>X) |
| 207 | 203 | 199.37 | 2% | 2% | Y>X>Z (Y>Z>X) |

Table 3 table below shows the Mode values (Natural frequencies) of the reference Mode shape experimental result, its corresponding guess in experimental Modal analysis on Bridgeport drive and the suspected Computational Modal Value. $Z > Y > X$.

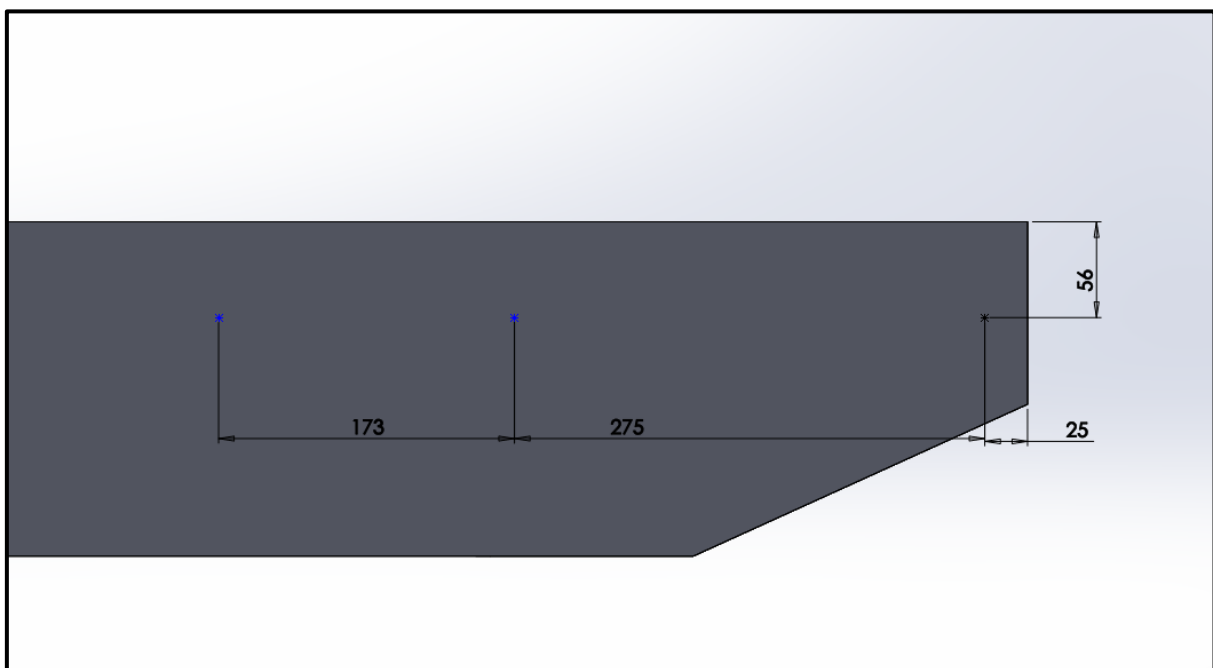


Figure 39A Location of Accelerometer

A.3.3.1 Yaw Moment about the Y axis at 139 Hz mode shape:

At 139 Hz it can be noted that the experimental analysis of 114-122 Hz closely resembles this mode where Z is always dominating. $Z > X > Y$ in first 2 excitation points but $Z > Y > X$ in case of 3rd excitation point, but difference between Y and X is quite low. This in computational Modal Analysis relates to 119.37 value. See Figure 40A and Figure 41A respectively.

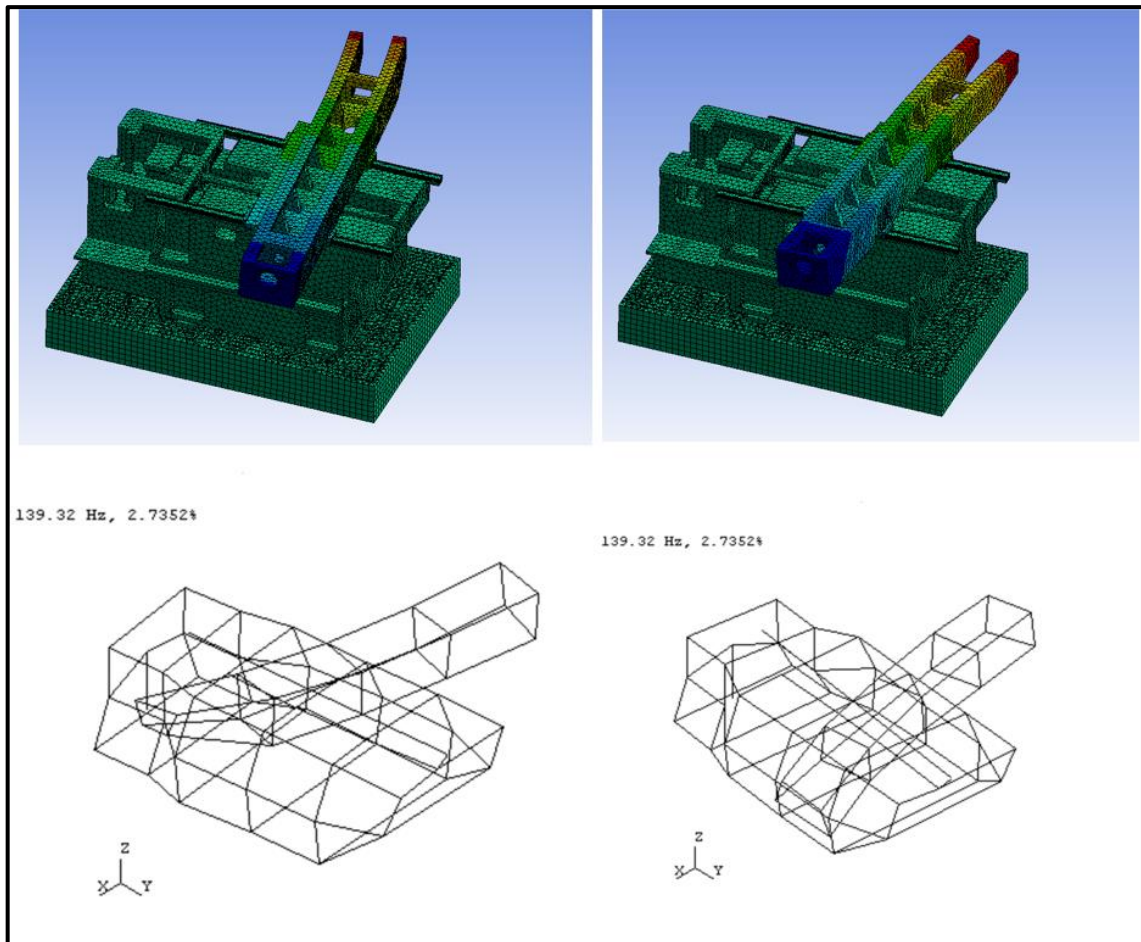


Figure 40A FEA Mode shape (top), Experimental Mode Shape (bottom).

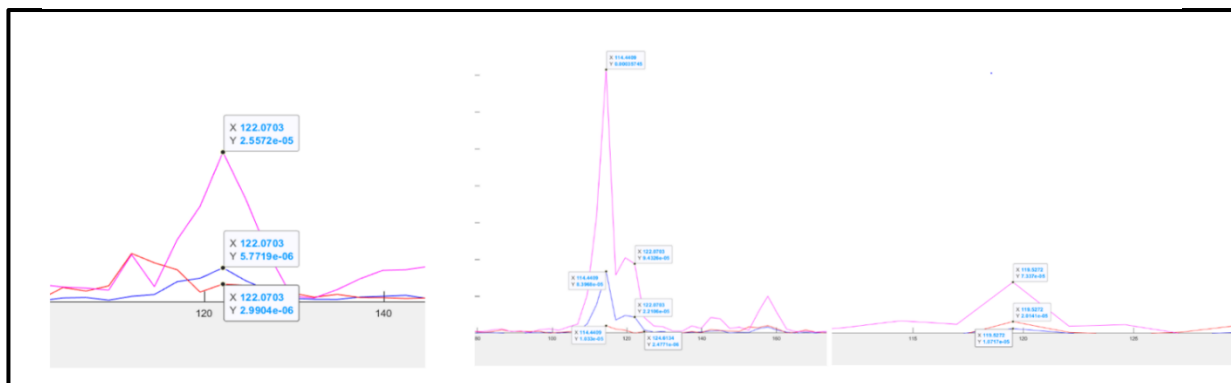


Figure 66 MATLAB Peak results FFT

A.3.3.2 Torsion About X axis at 207 Hz:

Similarly, at 207 Hz mode Shape value, the closest experimental natural frequency is given by 203 Hz peak corresponding to 199.27 Computational Modal Analysis. Here the experiment shows Y Amplitude is Dominant and follows $y > x > z$. This mode may also be the next following peak around 216 Hz where $y > z > x$ in first two excitation points (which is evident from visual inspection and $y > x > z$ for excitation point 3. See Figure 42A and Figure 43A below.

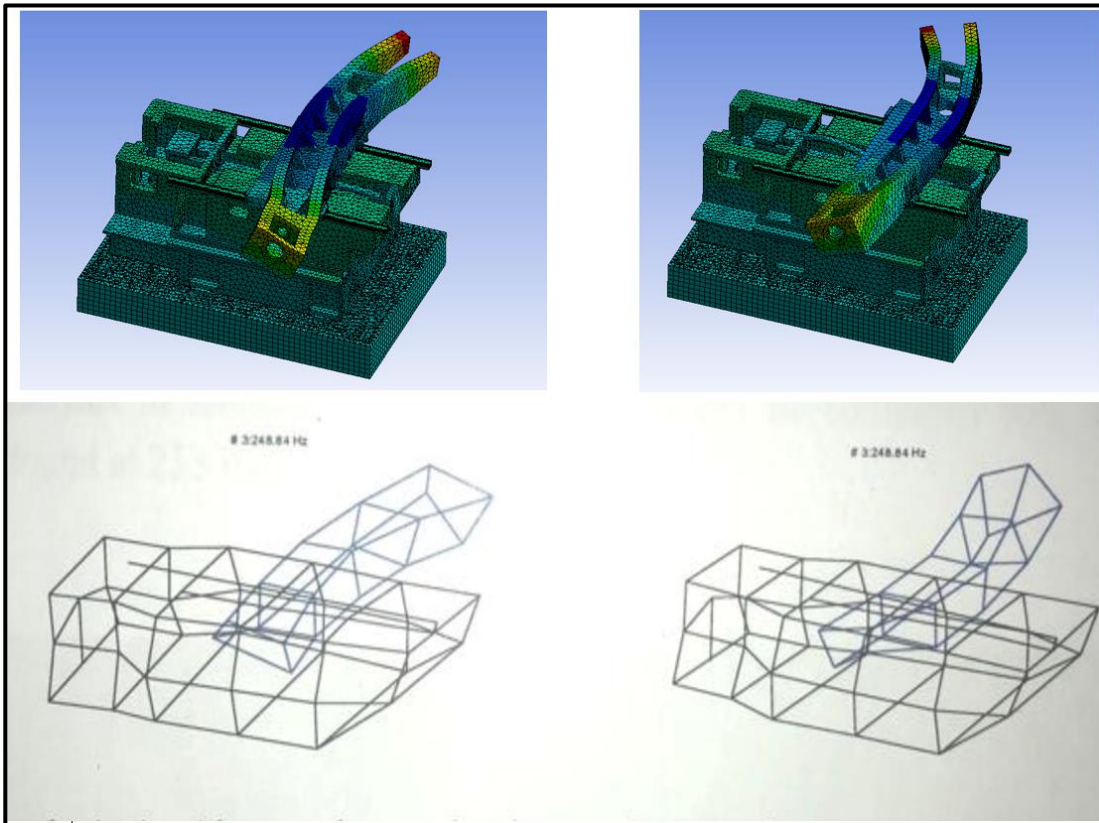


Figure 43A FEA Mode shape (top) , Experimental Mode Shape (bottom).

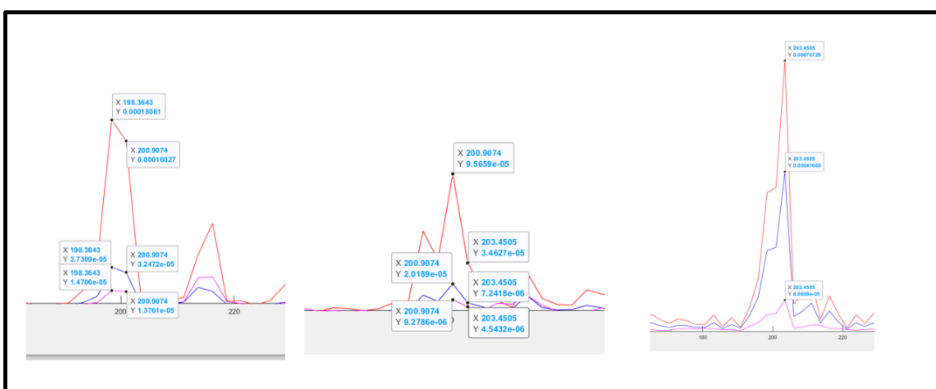


Figure 42A MATLAB Peak results FFT

A.3.3.3 Bi-directional bending About Z axis (Flapping) at 249 Hz:

Similarly, at 249 Hz mode Shape is similar to the experimental natural frequency given by 295 Hz, the closest peak value in Computational Modal Analysis is 263.7 Hz. This is a Flapping Mode where Y Acceleration Amplitude Dominates. X is always lesser. But it can be noted when the Rig is Hit at excitation point 3 Z>X>Y which is not true, this may be related to more freedom in X as now most of the energy is imparted in X direction (excitation point 3) or this can be due to errors as mentioned in earlier section, See Figure 44A and Figure 45A below.

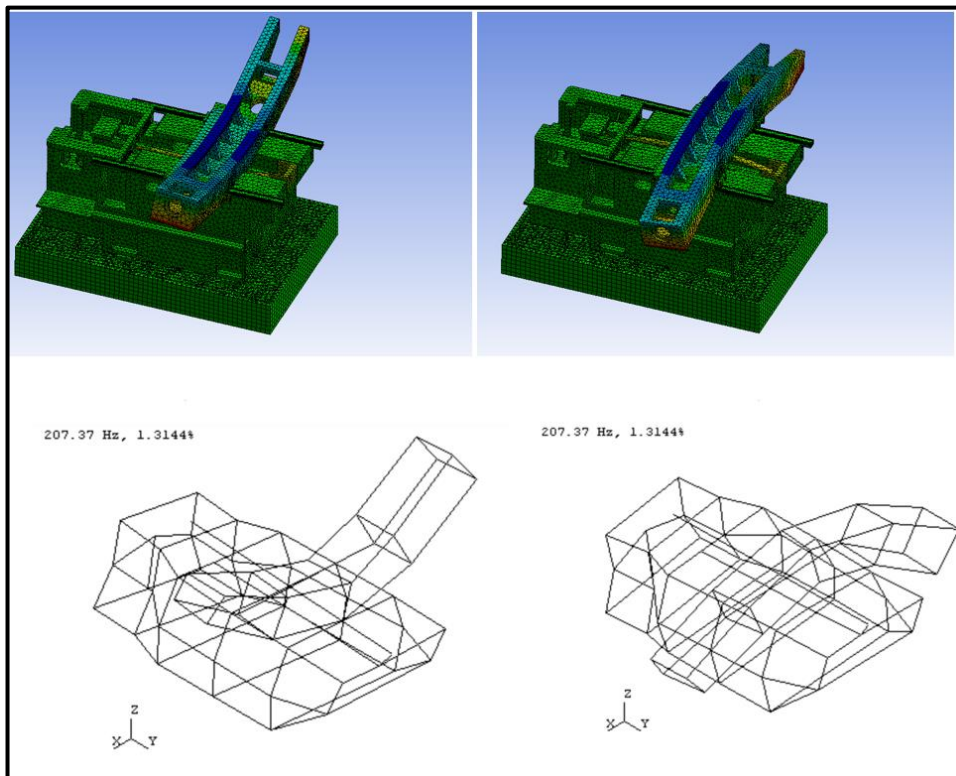


Figure 45A FEA Mode shape (top) , Experimental Mode Shape (bottom).

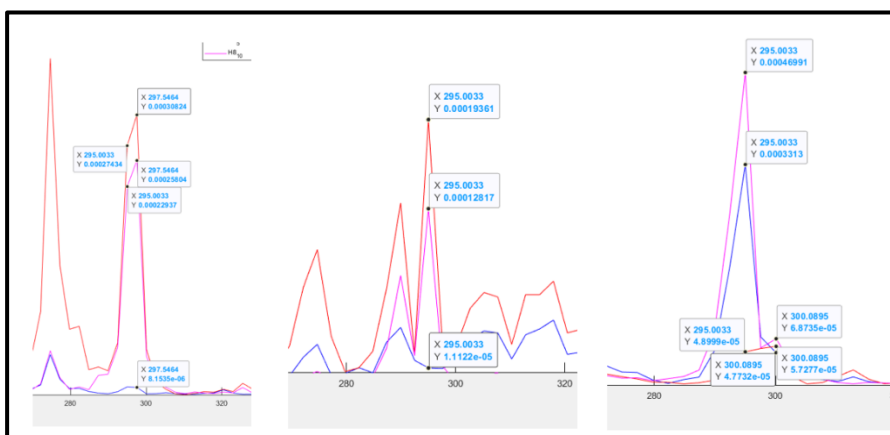


Figure 67 MATLAB Peak results FFT

A.3.4 Discussion of Results:

Three mode shapes were analysed and mode shapes were similar to the existing modal analysis experiment. The presence of percentage difference in terms of acceleration amplitudes and frequency difference between the 3 experiments as shown in table 3, may be attributed to one of the following reasons:

For Finite Element Analysis:

- The Effect of un weathered over consolidated soil on the lower frequency spectrum which was neglected due to low frequency problems.
- The absence of Motor, coupling and other parts that may have additional joints.
- Absence of detailed Bulk Material properties of each component.
- Assuming the axial stiffness of ball bearing to be equivalent to radial bearing Stiffness.
- Assumption of Bonded contact between Ball screw and Nut. In reality the axial stiffness may be important.

For Experimental Modal Analysis:

- Data Taken only with the help of three hammer locations and 3 accelerometer locations.
- No filters used to get rid of blunt peaks (PSD may be used)
- Acceleration Data Compared with the reference Modal experimental data that might have different boundary conditions.
- The accelerometer may not have been firmly fixed giving over populated peaks as is evident from the data.

A.3.5 Conclusion:

A well-defined Finite Element Model was Simulated with boundary conditions that are very close to actual boundary conditions of the rig. The mode shapes are satisfactory but the frequency at which they occur may not be accurate as compared with the experimental modal Analysis. The Comparison was done by inspecting and guessing the evident dominant displacement directions (mode shapes) in FEA for each mode to be analysed while as in experimental modal analysis case it was carried out with the help of manual graphical analysis. Such an approach can lead to many errors and therefore demands a Spatial Modal Analysis where the Mode shapes and their natural frequency data can be experimentally visualised and compared with the Finite element model to attain better results. Such a model has been prepared for the novel rig design.

7.1 APPENDIX B

This Section contains the pictures that are being referenced.

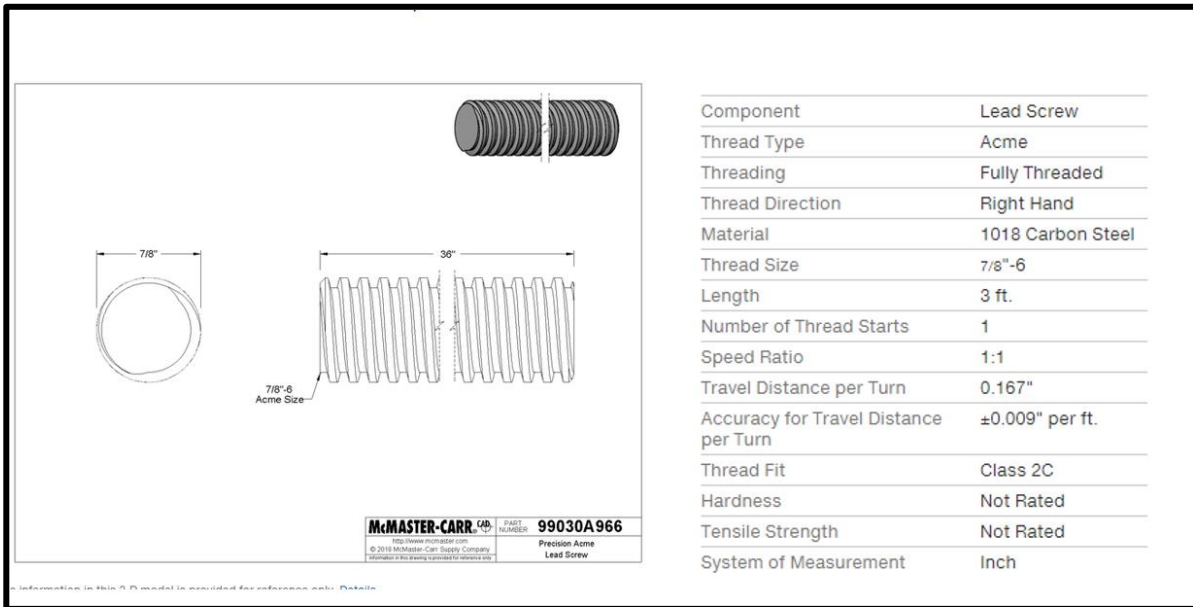


Figure 1 B Lead Screw used in the drive

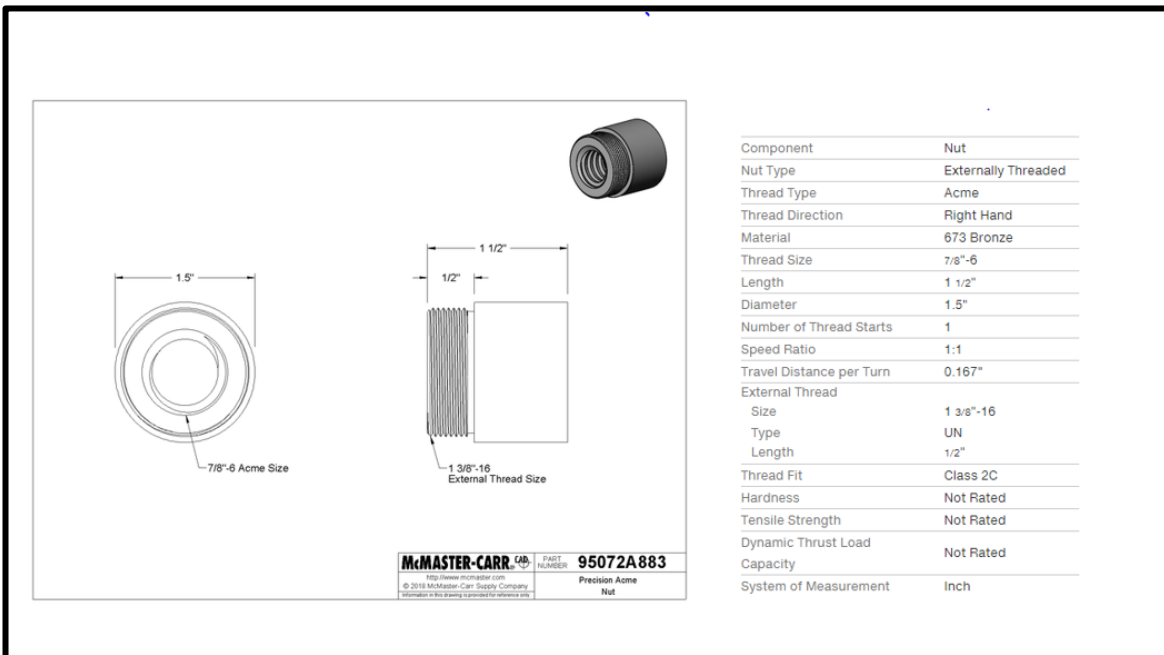


Figure 2 B Threaded nut for Lead screw

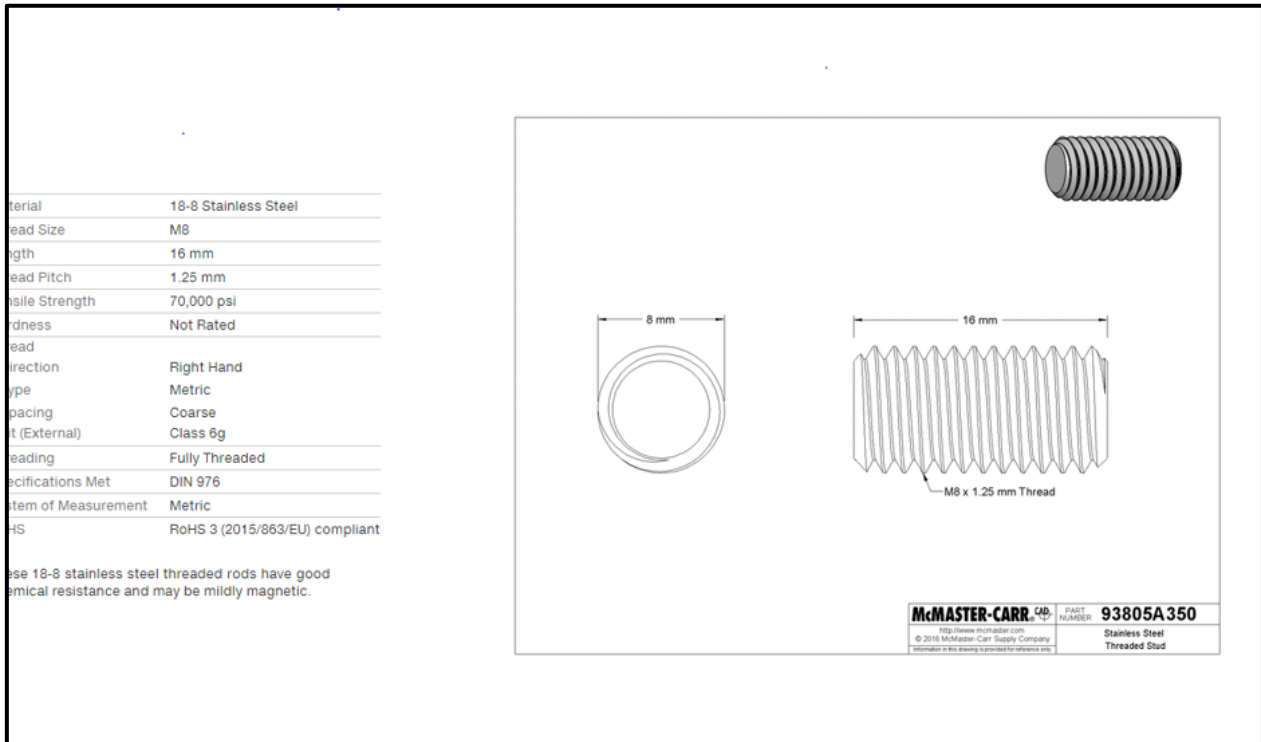


Figure 3B M8 *16 threaded rod

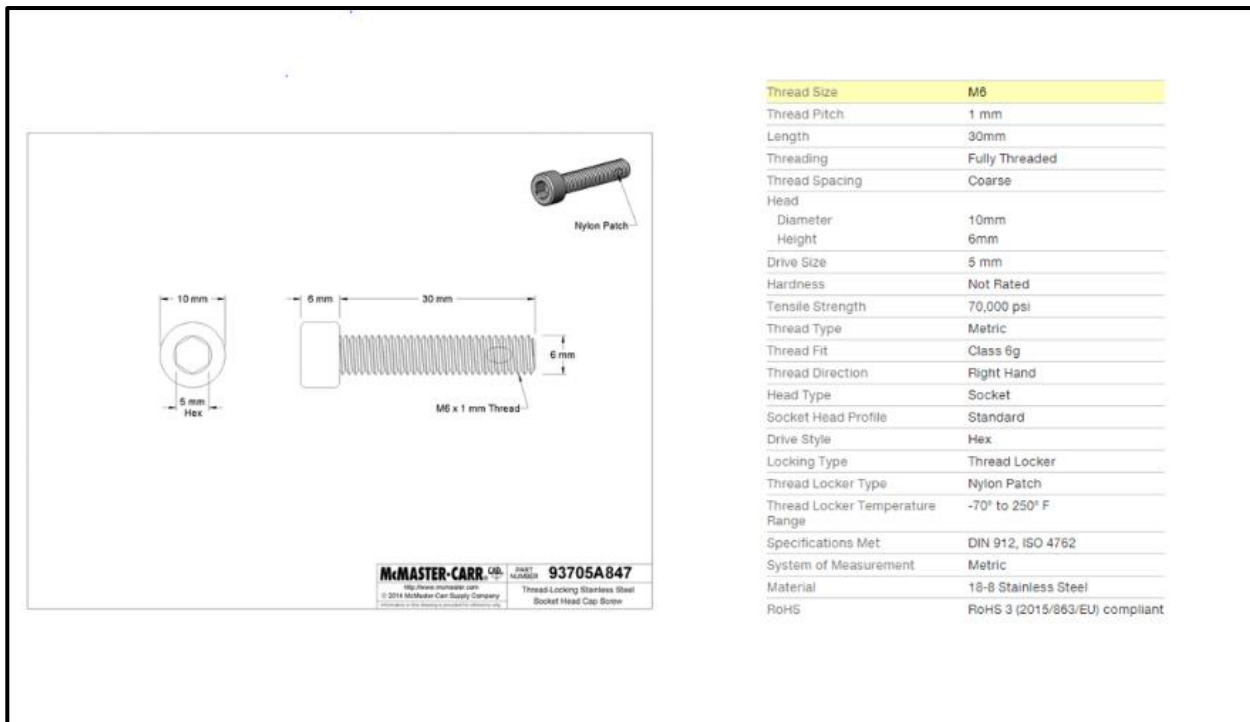


Figure 4B Shows 4 x M6 18-8 stainless steel thread locking socket head Screw

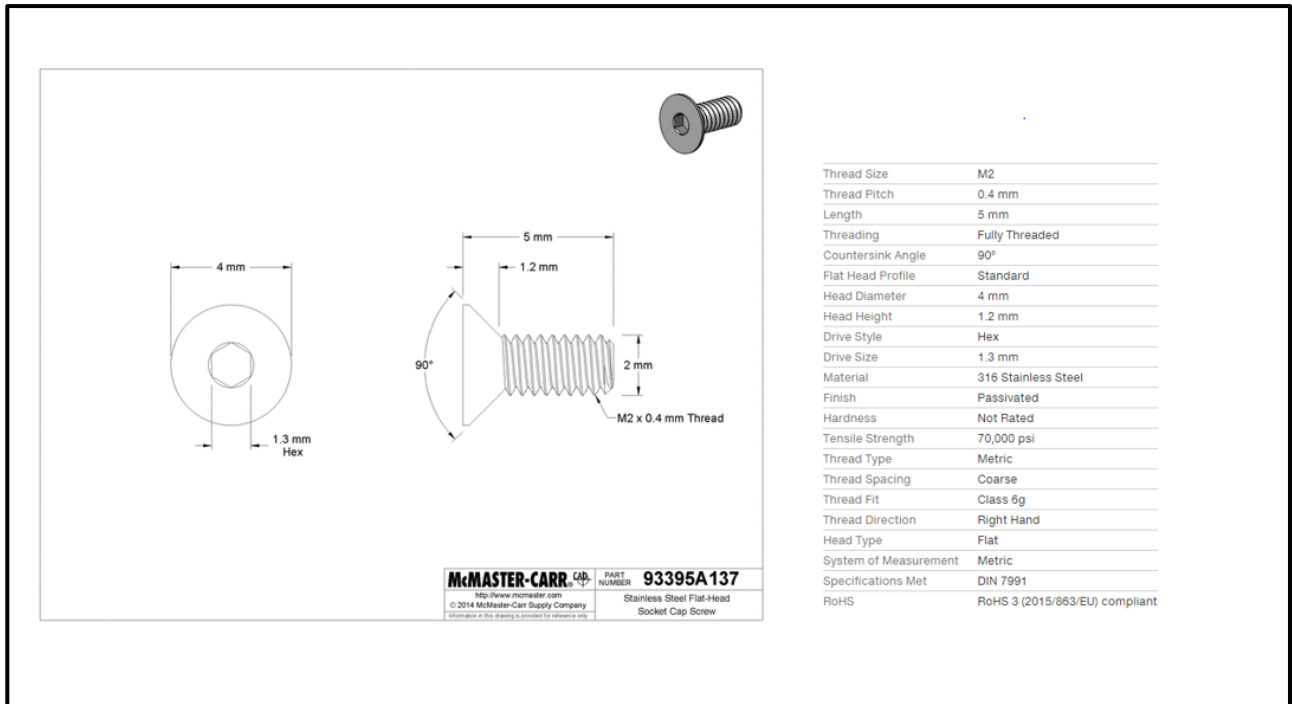


Figure 68 Shows the M2 0.4 316 Stainless Steel Hex Drive Head Screws